

The University of Alberta

**HOSK CHANNEL:
FROM DISCOVERY TO DESCRIPTION**

by

Rohit Moudgil



A thesis submitted to the Faculty of Graduate Studies and Research in partial
fulfillment of the requirements for the degree of
Doctor of Philosophy

Department of Physiology

Edmonton, Alberta

Spring 2007



Library and
Archives Canada

Bibliothèque et
Archives Canada

Published Heritage
Branch

Direction du
Patrimoine de l'édition

395 Wellington Street
Ottawa ON K1A 0N4
Canada

395, rue Wellington
Ottawa ON K1A 0N4
Canada

Your file *Votre référence*
ISBN: 978-0-494-29717-9
Our file *Notre référence*
ISBN: 978-0-494-29717-9

NOTICE:

The author has granted a non-exclusive license allowing Library and Archives Canada to reproduce, publish, archive, preserve, conserve, communicate to the public by telecommunication or on the Internet, loan, distribute and sell theses worldwide, for commercial or non-commercial purposes, in microform, paper, electronic and/or any other formats.

The author retains copyright ownership and moral rights in this thesis. Neither the thesis nor substantial extracts from it may be printed or otherwise reproduced without the author's permission.

AVIS:

L'auteur a accordé une licence non exclusive permettant à la Bibliothèque et Archives Canada de reproduire, publier, archiver, sauvegarder, conserver, transmettre au public par télécommunication ou par l'Internet, prêter, distribuer et vendre des thèses partout dans le monde, à des fins commerciales ou autres, sur support microforme, papier, électronique et/ou autres formats.

L'auteur conserve la propriété du droit d'auteur et des droits moraux qui protègent cette thèse. Ni la thèse ni des extraits substantiels de celle-ci ne doivent être imprimés ou autrement reproduits sans son autorisation.

In compliance with the Canadian Privacy Act some supporting forms may have been removed from this thesis.

Conformément à la loi canadienne sur la protection de la vie privée, quelques formulaires secondaires ont été enlevés de cette thèse.

While these forms may be included in the document page count, their removal does not represent any loss of content from the thesis.

Bien que ces formulaires aient inclus dans la pagination, il n'y aura aucun contenu manquant.


Canada

DEDICATION

This thesis is dedicated to my beloved uncle Mr. Rajinder Sharma who passed away in August 2005. He was a man of great honor and integrity. He was a true embodiment of what perseverance and hard work is. In times of peril he provided for us when he did not have anything for himself. In every essence of the word he was a wonderful human being. I aspire to be half a human being that he was.

He will be greatly missed in my life...

ABSTRACT

The mammalian, specialized, oxygen-sensing system, comprised of the pulmonary artery, carotid body and ductus arteriosus (DA), initiates adaptive response to changes in PO_2 by inhibition of a heterogeneous group of K^+ channels, including O_2 -sensitive, voltage-gated (Kv) channels. We report the discovery of a novel K^+ channel; Human Oxygen-Sensitive K^+ channel (HOSK). HOSK cDNA, isolated from human DA, corresponds to a 3.0 kb neuronal, expressed sequence tag (EST).

Heterologously expressed HOSK creates a voltage-gated current that displays K^+ specificity ($Rb > K >> Cs > Na$) and is inhibited by 4-aminopyridine and the Kv1.x inhibitor, correolide. HOSK is active at the resting membrane potential of human DA smooth muscle cells (DASMC) and, consistent with its role in O_2 -sensing, the open-state probability of this 19pS channel is increased by hypoxia and decreased by oxygen or H_2O_2 . Anti-HOSK antibodies or HOSK siRNA inhibit human DASMC K^+ current, consistent with endogenous activity of HOSK.

In silico modeling suggests that HOSK has four hydrophobic domains (HD) with a unique K^+ selectivity filter, established by GVL, rather than the typical GYG amino acid sequence. Its putative voltage-sensing domain lies within HD1, and is comprised of 2 arginine and 2 lysine residues, separated by 2 non-cationic amino acids. This configuration has similarities to the S4 region (voltage sensor) of typical Kv channels, however HOSK's voltage sensor differs

in length and in the properties of residues interposed between the cationic amino acids.

HOSK has an unusual coding mechanism. It is translated from an alternative open reading frame within the collagen $\alpha 2(I)$ mRNA transcript. Phylogenetic analysis indicates that HOSK is only present in amniotes.

HOSK channel, hidden by its complex “gene within a gene” encoding mechanism and unique structure, is a novel K^+ channel, arising independent of the canonical K^+ channel family.

ACKNOWLEDGEMENTS

- I would like to acknowledge my Mom, my Dad and my brothers Mohit and Navodit Moudgil without whom nothing would have been possible. They have their motivating me all their lives and I am truly indebted to them.
- I would also like to acknowledge my beautiful wife, Harmina who I met and got married during my PhD. She has been there to listen to my rants at the end of the day and has been tremendous in helping me through this degree. I owe her my sanity and everything!
- I would like to acknowledge Dr. Archer. He has been a true mentor in every sense of the word. We had agreements and disagreements during the thesis but the end result has always been nothing less than SPECTACULAR! I learned a lot and hopefully I can come close to being a clinician scientist as good as him.
- Dr. Jason Dyck-who has been my co-supervisor, my research therapist and mostly a friend to me. Any problem I had I would go to him and he would always have a solution. I am truly honored to have worked under him.
- Dr. Evangelos Michelakis – For being the skeptic of the team and friend outside of the research confines
- Dr. Bernard Thebaud – For being Bernard
- Dr. Sebatién Bonnet – For being just like a college roommate-everything together. Thanks for wonderful times and for patch-clamping
- Dr. Xichen Wu – For patch-clamping, fishing stories and laughs.
- Kyoko Hashimoto – For having an answer to every question pertaining to the lab.
- Gwyneth Harris – For being Gwyneth
- Sandra Bonnet – For always laughing at my jokes
- Alois Haromy – For confocal and everything in between
- Dr. Barbara Wieland – For SELDI-TOF and putting up with my music taste.
- Dr. Hidemi Kajimoto - For being a sweetheart of the lab
- Bronwyn Lewis – For her ideas, her laughs, and smiling face in the morning
- Tim Van Haften - For being a companion in the quest of finishing our respective degrees,
- Farah Eaton - For good times
- Jason Iden – For being the best friend anybody could ask for!
- Jay Jaswal – For being the best brown and a true friend anybody could ask for!
- Ken Strynadka – For discussion of life and the people involved in it.
- Ray Kozak – For being a good (although little) friend.
- AND EVERYBODY IN CARDIOVASCULAR REASERCH GROUP AND DEPT. OF PHARMACOLOGY...YOU GUYS HAVE BEEN GREAT
THANK YOU FOR EVERYTHING!!!

TABLE OF CONTENT

	Page
1 INTRODUCTION	1
1.1 INTRODUCTION	1
1.2 EVOLUTION OF K_v CHANNELS	4
1.2.1 Prokaryotes	4
1.2.2 Eukaryotes	7
1.3 K_v CHANNELS-OVERVIEW	9
1.4 STRUCTURAL BASIS OF K_v CHANNELS	10
1.4.1 Ion Selectivity and Conduction	10
1.4.2 Gating	12
1.4.2.1 <i>Activation</i>	12
1.4.2.2 <i>Inactivation</i>	14
1.4.2.3 <i>Deactivation</i>	16
1.4.3 Voltage Sensing	17
1.4.3.1 <i>The Canonical model</i>	18
1.4.3.2 <i>The Transporter model</i>	18
1.4.3.3 <i>The Paddle model</i>	18
1.4.3.4 <i>The Twisted S4 Model</i>	18
1.5 K_v CHANNELS IN VASCULAR SMOOTH MUSCLE	20
1.6 DUCTUS ARTERIOSUS	21
1.6.1 Endothelial contribution to DA constriction	22
1.6.2 K ⁺ channels and constriction of the DA	23
1.6.3 K _v channels as an effector	24
1.6.4 K _v Diversity and O ₂ Sensing	26
1.7 HYPOTHESIS	27
1.8 THESIS OBJECTIVES	28
1.9 REFERENCES	29
2 MOLECULAR BIOLOGICAL DETERMINATION OF THE HOSK CHANNEL	50
2.1 INTRODUCTION	50
2.2 DIVERSIFICATION OF K_v CHANNEL IN MAMMALS	53
2.3 ALTERNATIVE SPLICING AND HOSK CHANNEL	54
2.4 MATERIALS AND METHODS	55
2.4.1 Human DA cDNA	55
2.4.2 Plasmids	55
2.4.3 Northern Blots	56
2.4.4 Immunoblot	57
2.4.5 Fluorescence in situ hybridization	57
2.4.6 In silico Analysis	58

2.5 RESULTS	59
2.6 DISCUSSION	62
2.6.1 Transcriptional regulation of COL1A2	63
2.6.2 Putative mechanism involved in translation of HOSK channel	68
2.6.3 Other features of HOSK channel sequence	71
2.6.4 Summary	73
2.7 REFERENCES	74

3 PROTEOMIC IDENTIFICATION AND ISOLATION OF THE HOSK CHANNEL 96

3.1 INTRODUCTION	96
3.2 MATERIALS AND METHODS	99
3.2.1 Generation of a HOSK Antibody	99
3.2.2 Immunoblot	99
3.2.3 Plasmids	99
3.2.4 Protein analysis with SELDI-TOF MS	100
3.2.5 In silico analysis	101
3.3 RESULTS	102
3.3.1 Analysis of the protein sequence	102
3.3.2 Expression of HOSK channel	103
3.3.3 Isolation of HOSK with SELDI-TOF MS	104
3.3.4 Evolutionary origination of HOSK	104
3.4 DISCUSSION	105
3.4.1 Structural Biology of the HOSK Channel	107
3.4.1.1 <i>Putative hydrophobic domains</i>	107
3.4.1.2 <i>Voltage Sensing</i>	108
3.4.1.3 <i>Gating of K⁺ channels</i>	109
3.4.1.4 <i>Selectivity Filter</i>	113
3.4.2 Evolutionary Perspective	115
3.4.3 Summary	117
3.5 REFERENCES	118

4 ELECTROPHYSIOLOGICAL CHARACTERIZATION OF THE HOSK CHANNEL 136

4.1 INTRODUCTION	136
4.1.1 Voltage Dependence	138
4.1.2 Functional Properties of Kv Channels	139
4.1.3 Physiological role of Kv channels in vasculature	139
4.1.3.1 <i>Repolarization of the action potential</i>	139

4.1.3.2	<i>Regulation of membrane potential</i>	140
4.1.4	Hypoxic Pulmonary Vasoconstriction	142
4.1.5	Closure of DA	144
4.2	MATERIALS AND METHODS	146
4.2.1	Transfection of Chinese Hamster Ovary cells and Monkey Kidney (COS) cells	146
4.2.2	Whole cell patch clamp solutions	146
4.2.3	Single channel patch clamp	147
4.2.4	Immunoelectrophysiology	147
4.2.5	Site-directed mutagenesis	148
4.2.6	Quantitative real-time polymerase chain reaction	148
4.2.7	Immunoblot	149
4.2.8	Generation of a HOSK siRNA	149
4.2.9	Statistics	149
4.3	RESULTS	150
4.4	DISCUSSION	154
4.4.1	Electrophysiology	154
4.4.2	Pharmacology	155
4.4.3	Oxygen sensitivity	156
4.4.4	Pore sequence	157
4.4.5	Endogenous HOSK channel activity in hDASMC	158
4.4.6	Caveats	159
4.4.7	Lessons from the minK story	159
4.4.8	HOSK channel gene sequence	162
4.4.9	Summary	163
4.5	REFERENCES	164

5 SUMMARY AND DISCUSSIONS ON THE HOSK CHANNEL

5.1	INTRODUCTION	202
5.1.1	Hypothesis	203
5.1.2	Biophysical characterization of HOSK channel	204
5.1.3	Oxygen sensitivity of the HOSK channel	205
5.1.4	Identification of HOSK's Pore	206
5.1.5	Is endogenous HOSK active in human DASMC?	207
5.1.6	In silico modeling of HOSK structure	208
5.2	HOSK AS A NEW TYPE OF K⁺ CHANNEL	210
5.2.1	Similarities and differences	210
5.2.2	The HOSK voltage sensor	211
5.3	PHYSIOLOGICAL IMPLICATIONS OF HOSK	214
5.3.1	Closure of DA during pregnancy	214
5.3.2	Mitochondria as an oxygen sensor	215
5.3.3	Reactive Oxygen Species (ROS) as a mediator of O ₂ -induced DA constriction	217

5.4 POTENTIAL PATHOLOGICAL RAMIFICATION OF HOSK	219
5.4.1 Speculations	219
5.4.2 Patent DA	220
5.5 STUDY LIMITATIONS AND FUTURE DIRECTIONS	220
5.6 CONCLUSION	223
5.7 REFERENCES	225

LIST OF TABLES

Table 3.1: The variations of filter sequence (GYGD) among the prokaryotic K⁺ channels.

LIST OF FIGURES

Figure 1.1: A universal phylogenetic tree based on *ssrRNA* sequences, showing the three domains of life.

Figure 1.2: Schematic representations of the *KcsA* folds and pore.

Figure 1.3: Generalized topology of a voltage-gated potassium channel.

Figure 1.4: Phylogenetic tree of prokaryotic and eukaryotic K^+ channel genes.

Figure 1.5: Structure of *KcsA* in the presence of high K^+ concentration.

Figure 1.6: The Hodgkin–Huxley (HH) model of independently gating subunits and predicted ionic and gating currents.

Figure 1.7: Models of topology and voltage sensor movement.

Figure 1.8. Opposite Regulation of Potassium Channels by Oxygen in pulmonary artery as compared with ductus arteriosus smooth-muscle cells.

Figure 2.1: Full nucleotide sequence of HOSK.

Figure 2.2: PCR isolation of 1.4 fragment with *Kv1.5* from human ductus arteriosus.

Figure 2.3: Primers of sense complement human *Kv1.5* primers aligned with the HOSK sequence.

Figure 2.4: Schematic of DNA exons alignment of Collagen $1\alpha 2$ with HOSK gene.

Figure 2.5: Location of COL1A2 on human chromosome 7 as published in NCBI database.

Figure 2.6: Immunoblotting of collagen protein in CHO cells transfected with either empty vector (pTracer-CMV) or HOSK channel.

Figure 2.7: cDNA sequence of collagen $1\alpha 2$.

Figure 2.8: Full cDNA nucleotide sequence of HOSK channel.

Figure 2.9: MFOLD of RNA structure of collagen $1\alpha 2$ gene.

Figure 2.10: Fluorescent in-situ Hybridization (FISH) on human chromosomes arrested in metaphase

Figure 2.11: Northern Blot analysis on a panel of human tissues with HOSK and Collagen probes.

Figure 2.12: Northern Blot of hDASMC incubated for 48 hrs in either hypoxia or normoxia.

Figure 3.1: Amino acid sequence of the HOSK channel.

Figure 3.2: Kyte-Doolittle hydrophilicity plot of the HOSK channel.

Figure 3.3: Amino acid sequence of the HOSK channel with potential sites of posttranslational modifications

Figure 3.4: In silico analysis of 5' extension of collagen $\alpha 2(I)$ transcript from HOSK translational site

Figure 3.5: Immunoblot of various tissues show presence of HOSK in human DASMC, human PASMC and DA.

Figure 3.6: Isolation of HOSK channel using SELDI-TOF.

Figure 3.7: On-chip antibody capture of HOSK and SELDI-TOF MS analysis.

Figure 3.8: Species alignment of HOSK protein sequence using the open reading frame generated from the point where HOSK gene coincides with collagen $\alpha 2(I)$.

Figure 3.9: Schematic representation of evolution of nervous system.

Figure 4.1: Sketch of ductus arteriosus present in the human body.

Figure 4.2: Oxygen-sensing pathway in ductus arteriosus.

Figure 4.3: Representative traces and current-voltage (I-V) plots showing that HOSK-transfection produces a voltage-dependent current in CHO cells.

Figure 4.4: Current-voltage relationship of dose-dependent increase in HOSK cDNA.

Figure 4.5: Logarithm curve shows that progressive increase in $[K^+]_{out}$ results in reversal potential approaching zero.

Figure 4.6: Ionic substitution experiments show that HOSK channel cannot conduct cesium chloride (CsCl) and sodium chloride (NaCl). However, it is permeable for rubidium chloride.

Figure 4.7: Ionic substitution experiments show that HOSK channel can be inhibited by cesium chloride (CsCl) in a dose-dependent manner.

Figure 4.8: Ionic substitution experiments show that HOSK channel can be inhibited by barium chloride (BaCl₂) in a dose-dependent manner.

Figure 4.9: Activation protocol entailed measurement of tail current after the stepwise increase in voltage was brought down to -60 mV.

Figure 4.10: Inactivation protocol entailed measurement of tail current after inactivating the HOSK channel by holding it at +80 mV for 10 seconds.

Figure 4.11: Inhibition of HOSK channel by the Kv blocker 4-aminopyridine (4-AP)

Figure 4.12: Inhibition of HOSK channel by the Kv1.x blocker correolide

Figure 4.13: HOSK channel is not inhibited by big conductance calcium sensitive K⁺ channel inhibitor, Iberitoxin (IBTX) in transfected CHO cells.

Figure 4.14: HOSK channel is not inhibited by small conductance calcium sensitive K⁺ channel inhibitor, Charybdotoxin in transfected CHO cells.

Figure 4.15: HOSK channel is not inhibited by Kv1.2 and Kv2.1 channel inhibitor, rtitystoxin in transfected CHO cells.

Figure 4.16: HOSK channel is not inhibited by Kv4.2 channel inhibitor, E 4031 in transfected CHO cells.

Figure 4.17: HOSK channel is sensitive to Kv1.3 channel inhibitor, margatoxin.

Figure 4.18: Current-voltage relationship of CHO cells transfected with HOSK show that HOSK current is activated by hypoxia.

Figure 4.19: Current-voltage relationship of CHO cells transfected with HOSK show that HOSK current is inhibited by H₂O₂.

Figure 4.20: Single channel conductance by HOSK in the inside-out configuration.

Figure 4.21: Mutagenesis of the HOSK pore (substitution of GVL with AAA) eliminates the voltage-dependent current and 4-aminopyridine sensitivity.

Figure 4.22: Immunoelectropharmacology was performed in HOSK expressing CHO cells. HOSK opening is (at 1.5 pA amplitude) reversibly inhibited by anti-HOSK antibody.

Figure 4.23: Immunoelectropharmacology was performed in HOSK expressing CHO cells. HOSK opening (at 1.5 pA amplitude) is unaffected by a cocktail of Kv antibodies.

Figure 4.24: Immunoblot of various channels shows no change HOSK transfected CHO cells.

Figure 4.25: The HOSK antibody, when dialyzed into the DASMC via the patch pipette, inhibited K⁺ current.

Figure 4.26: HOSK siRNA attenuates whole-cell K⁺ current in hypoxic human DASMCs.

Figure 4.27: Transfection of pTracer-CMV carrying 1.4 kb fragment in CHO cells resulted in a current that was virtually identical to that created by expressing the EST clone.

Figure 4.28: Immunoelectropharmacology was performed in 1.4 kb expressing CHO cells.

Figure 4.29: K⁺ current in HOSK transfected CHO cells was not inhibited by Iberitoxin, rTityustoxin, and E 4031. However, margatoxin, inhibited K⁺ current in HOSK transfected CHO cells.

Figure 5.1: Human ductus arteriosus constricts with increasing amount of oxygen, an effect is mimicked by hydrogen peroxide (H₂O₂).

Figure 5.2: Electrophysiological characterization of HOSK channel.

Figure 5.3: Regulation of HOSK channel.

Figure 5.4: Molecular Biological determination of HOSK channel.

Figure 5.5: Proteomic isolation and identification of HOSK channel.

Figure 5.6: Formation of funnel like structure by re-entrant loop of K⁺ channels.

LIST OF ABBREVIATIONS

4-AP	4-aminopyridine
α	Alpha
AAA	Alanine-Alanine-Alanine
ANOVA	Analysis of variance
AREs	AU-rich elements
ASCOL1A2	Alternatively spliced collagen a2(I)
ATP	Adenosine triphosphate
AU	Adenine-uracil (nucleosides)
AUAP	Abridged universal amplification primer
AUG	Adenine-uracil-guanosine
β	Beta
Ba^{2+}	Barium
BKCa	Big conductance calcium sensitive potassium channel
BLAST	Basic local alignment search tool
bp	Base pairs
Ca^{2+}	Calcium
Cav	Voltage-gated calcium channels
CDD	Conservative domain database
cDNA	Complementary Deoxyribonucleic acid
cGMP	Cyclic guanosine monophosphate
CHO	Chinese Hamster Ovary
CK2	Casein Kinase 2
CMV	Cytomeglovirus
COL1A2	Collagen a2(I)
COS	Monkey Kidney Cells
Cs^{+}	Cesium
Ct	Cycle time
C-type	Carboxyl terminus type
DA	Ductus arteriosus
DAPI	4, 6 diamidino-2-phenylindole dihydrochloride
DASMC	Ductus arteriosus smooth muscle cell
DIDS	Diisothiocyano-2,2, disulfonic acid stilbene
DLAD	DNase II-like acid DNase
DLG	Disc-large-related gene
DNA	Deoxyribonucleic acid
E.coli	Escherichia Coli
E°	Standard Equilibrium
EPR	Electron paramagnetic resonance
EST	Expressed Sequence Tag
ETC	Electron Transport Chain
FADH	Flavin adenine dinucleotide
Fe-S	Iron-Sulfur center
FISH	Fluorescence In situ Hybridization

g	Gamma
GFG	Glycine-Phenylalanine-Glycine
GFP	Glycine-Phenylalanine-Proline
GFQE	Glycine-Phenylalanine-Glutamine-Glutamic acid
GLE	Glycine-Leucine-Glutamic acid
GLYA	Glycine-Leucine-Tyrosine-Alanine
GLYS	Glycine-Leucine-Tyrosine-Serine
GVL	Glycine-Valine-Leucine
GYSD	Glycine-Tyrosine-Serine-Aspartate
GYSI	Glycine-Tyrosine-Serine-Isoleucine
H ₂ O ₂	Hydrogen peroxide
HCN	Hyperpolarizing-activated cyclic nucleotide potassium channels
HD	Hydrophobic domain
HERG	Human <i>ether-a-go-go</i> channels
HOSK	Human Oxygen Sensitive potassium channel
HPV	Hypoxic Vasoconstriction
IBTx	Iberitoxin
IRES	Internal ribosomal entry site
K ⁺	Potassium
K2P	Two-pore potassium channel
Kb	Kilobase
Kca	Calcium-sensitive potassium channel
KcsA	Potassium channel in <i>Streptomyces lividans</i>
kDa	Kilodalton
Kir	inward rectifying potassium channels
KLH	Ket-limpet hemocyanine
Kv	Voltage-gated potassium channel
KvAP	Voltage-gated potassium channel in <i>Aeropyrum pernix</i>
KvLQT1	Voltage-gated long QT potassium channel
Mg ²⁺	Magnesium
minK	Minimal potassium channel
MNTB	Medial nucleus of trapezoid body
mRNA	messenger RNA
MthK	Calcium-gated potassium channel in <i>Methanobacterium autotrophicum</i>
MS	Mass Spectrometry
Na	Sodium
NADH	Nicotinamide dinucleotide dehydrogenase
Nav	Voltage-gated sodium channels
NCRs	Non-coding regions
NFAT	Nuclear Factor alpha T-lymphocytes
NF-E1	Nuclear Factor E1
NF-IL6	Nuclear Factor IL-6
NMPG	N-mercaptopropionylglycerine
NO	Nitric oxide
N-type	Amino terminus

O	Oxygen
ORF	Open reading frame
P	Pore
P_0	Opening probability
pOCAT	Plamid with chloramphenicol acetyltransferase
PA	Pulmonary artery
P_{act}	Propotion of channel in activated state
PAH	Pulmonary arterial hypertension
PASMC	Pulmonary artery smooth muscle cell
PCR	Polymerase chain reaction
PDA	Patent ductus arteriosus
pI	Isoelectric point (-log)
PO_2	Partial pressure of oxygen
pT	pTracer-CMV
P-type	Pore-type
PxG	Proline-(amino acid)-Glycine
PXP	Proline-(amino acid)-Proline
Q	Equilibrium quotient
qRT-PCR	Quantitative reverse transcriptase- polymerase chain reaction
Rb+	Rubidium
RCK	regulatory component of potassium channel
RNA	Ribonucleic acid
ROS	Reactive Oxygen Species
RT	Reverse Transcriptase
S	Segment or Site
SDS-PAGE	Sodium dodecyl sulphate Polyacryl gel electrophoresis
SELDI-TOF	Surface enhance laser desorption/ionization time of flight
SEM	Standard error of mean
siRNA	small interfering RNA
SKCa	Small conductance calcium sensitive potassium channel
SMC	smooth muscle cells
SOD	Superoxide dismutase
TASK	Two-pore acid sensitive potassium channel
TCF	T-cell factor
TEA	Tetraethylammonium
TM	Transmembrane
TRAAK	Arachidonic acid sensitive two-pore potassium channel
TRP	Transient receptor potential channel
TVGYGD	Threonine-Valine-Glycine-Valine-Glycine-Aspartate
TWIK	Two-pore weak inward rectifying channel
Uox	Urate Oxidase
UTP	5-(3-aminoallyl) uridine trisphospate
UTR	Untranslated region
UV	Ultraviolet
VLCAD	Very long chain acyl-CoA
VSMC	Vascular smooth muscle cell

Chapter 1: Introduction

1.1 INTRODUCTION

The fascination of evolutionary biologists, structural biologists and physician-scientists for potassium (K^+) channels stems from their ancient origins, elegant structure and their broad implication in health and diseases. Since Hodgkin and Huxley proved that K^+ channels existed, in classical experiments studying nerve conduction in the squid axon, ^{1, 2} crucial roles for these channels have been identified in diverse cellular activities, ranging from oxygen sensing to cardiac repolarization. In addition, it has been recognized that the K^+ channels is a diverse family as roughly 80 different genes encode various subgroups of K^+ channels in the body. Some K^+ channels, i.e., voltage-gated K^+ (K_v) channels, are activated in response to a change in membrane potential. These channels act to counter depolarizing influences on the cell and are important in repolarizing action potentials. Other K^+ channels are activated by elevations in intracellular Ca^{2+} (Ca^{2+} -activated K^+ channels). These channels prevent excessive Ca^{2+} entry and are involved in muscle relaxation and inhibition of neurotransmitter release. Another class of K^+ channels, the inward rectifiers, passes current primarily over a hyperpolarized voltage range. They show a pronounced polyamine and Mg^{2+} -induced block at depolarized potentials. As a result, these channels play an important role in the maintenance of resting membrane potential in many cells. Other inward rectifying K^+ channels are tightly regulated by intracellular ATP levels (ATP-sensitive K^+ channels), and thus provide a link between cellular metabolism and membrane potential. These channels play important roles in the metabolic control of insulin secretion and muscle contraction. Other members of the inward rectifier family are activated by G-proteins (G-protein-activated K^+ channels) following ligand or neurotransmitter activation of G-

protein-coupled receptors. G-protein-activated K⁺ channels are key to the control of heart rate and neuronal function. Many central neurons also express a class of K⁺ channels that show little or no rectification that may give rise to the so-called “background” or “leak” currents. These channels are also regulated by neurotransmitters and intracellular messengers and they participate in controlling membrane potential and cellular excitability in the CNS. Therefore, understanding the structure and function of these diverse groups of K⁺ channels offers a paradigm to explore intricate mechanism involved in regulation of K⁺ channels or by extension in other ionic channels. Recently, crystallographic studies of K⁺ channel structure have been especially exciting, revealing the 3-dimensional structure of a prokaryotic Kv channel, work for which Rod McKinnon won the Nobel Prize in Chemistry in 2003³. More recently, similar techniques have revealed the structure of the eukaryotic voltage-gated (Kv) channel, Kv1.2⁴. The subsequent section will discuss exclusively the workings of Kv channels.

The main function of Kv channels is to regulate membrane potential and thereby cell excitability, ion content and the activity of many other types of ion channels. In excitable cells, this is achieved by altering action potential frequency and duration (during repolarization phase) or the rate at which the threshold for action potential is achieved (via their contribution to pacemaker potentials). In vascular cells, K⁺ channels regulate tone by establishing the resting membrane potential. Any external stimulus that can modulate Kv channel activity and/or expression will, therefore, have a profound effect on cell function. This is particularly true for cellular functions that are dependent on Ca²⁺ influx through voltage-gated Ca²⁺ channels.

While it is accepted that Kv channels control membrane potential and vascular

tone, recent work indicates that inhibition of the activity and expression of Kv channels also promotes cell proliferation and inhibits apoptosis, contributing to the pathology of various vascular diseases, including pulmonary arterial hypertension (PAH)⁵⁻⁷. By altering membrane potential, Kv channels control the activation of L-type calcium channels and thus influence the level of cytosolic calcium, a key regulator of contractility, exocytosis and the activity of many calcium-dependent factors involved in cell proliferation and transcriptional control (e.g. calcineurin, nuclear factor activated T-lymphocytes (NFAT) etc). Studies done in various PAH models have shown that acute and chronic downregulation of Kv activity and protein precipitates hypertrophy of smooth muscle cells and hyperplasia of adventitia and also suppresses apoptosis, thereby promoting pathological vascular remodeling⁸. Kv channel downregulation has also been implicated in cancer. Restoration of Kv channel expression can make the cancerous cell undergo apoptosis⁵. Similarly, in PAH, restoring Kv channel expression directly⁹ or indirectly⁵⁻⁷ reduces pulmonary hypertension and reduces vascular remodeling. Conversely, increasing intracellular K⁺ (which accompanies Kv inhibition or downregulation) inhibits caspases and suppresses apoptosis. Likewise the rise in cytosolic calcium activates proliferative pathways, such as the calcineurin pathway and also activates transcription factors, such as NFAT, which reinforce the pathology by further inhibiting Kv transcription¹⁰. Thus, the original view of K⁺ channels as regulators of membrane potential has been expanded to acknowledge their role as regulators of apoptosis and proliferation. This chapter will summarize the evolution of K⁺ channels and describe the structural basis of ion selectivity, gating and voltage-sensing. This will be followed by a discussion focused on molecular regulation of Kv channels.

Furthermore, the role of Kv channels in ductus arteriosus (DA) with special emphasis on oxygen-sensitive Kv channels and their contribution to the regulation of DA tone will be highlighted.

1.2 EVOLUTION OF K_v CHANNELS

1.2.1 Prokaryotes

Potassium channels appear to have emerged some 3 billion years ago before present day bacteria and archaeobacteria diverged. The cytoplasm of all primitive organisms is rich in K⁺, where it serves as a major osmolyte. Given the central role of K⁺ in controlling the primordial cell's osmotic balance, the early appearance of a selective K⁺ filter in cellular evolution (separating the cytoplasm from the outside environment) is not surprising¹¹. The concept of an ancient ancestry for K⁺ channels, supported by DNA sequence analysis, is bolstered further by the fact that even the most primitive bacteria, (e.g. hyperthermophiles that thrive at 90 °C, in some cases without oxygen, under conditions similar to those in which life first appeared) contain K⁺ channel genes. *Aquifex aeolicus*, considered to be among the earliest bacteria genus (based on its 16S-rRNA) has two K⁺-channel genes in its genome¹². *Thermotoga maritima*, another ancient bacteria¹³, has one K⁺-channel gene¹¹. (Figure1).

The electric activities of prokaryotic K⁺ channels have been successfully recorded in six cases by expressing the channel proteins heterologously in *E. coli*, yeast, *Xenopus* oocyte, cultured mammalian cells or reconstituting them into artificial lipid membranes¹¹. Perhaps the major stride made in characterization of primordial prokaryotic K⁺ channels was the crystallization of a KcsA channel^{3, 14}.

Studies with X-ray crystallography showed that KcsA channels are tetramers, comprised of helices that assemble and enclose an aqueous central pathway. The KcsA channel narrows from the outside mouth (3.2 angstrom) into a selectivity filter of 2.0 angstrom diameter near the periplasmic surface^{3, 15}. The amino-acid sequence, TVGYGD of each subunit, contributes carbonyl oxygens which are distributed on a horizontal plane. The subunit tetramerizes and the carbonyl oxygen line the filter, thereby determining the K⁺ ion selectivity. The removed hydration shell of K⁺ ion (as it goes through the channel pore) is replaced by the carbonyl oxygen. Ionic specificity depends, in large part, on the crucial bond length (i.e., Na⁺ is too small to coordinate). Several K⁺ ions occupy different positions in the channel at a time and they are moved through the pore by electrostatic repulsion. In the 3-dimensional structure, the central filter is supported by the four pore helices in a form of an inverted teepee. Beneath the teepee is a water-filled cavity, which is sealed off at the bottom near the cytoplasmic side by the convergence of the rest of the four transmembrane domain from the two-domain tetramer forming the gate¹⁶. Thus, the first crystallized K⁺ channel, KcsA, had characteristics similar to the empirically derived theoretical model of K⁺ channel (Figure 2).

Although, the Nobel Prize winning structure describes an archetypical form of K⁺ channel, substantial variation in the number of reentrant loops, number of transmembrane domains and even the K⁺ filter sequence exists amongst species and phyla. To date numerous K⁺ structures have been elucidated including, channels with two transmembrane helices (TM) with a single pore (P) (TM1-P-TM2), channels with two-pore domains K⁺ channel (TM1-P1-TM2-TM3-P2-TM4), channels with a Shaker motif (in these channels the nomenclature changes and transmembrane domains are abbreviated

as “S”) (S1-S2-S3-S4-S5-P-S6), a 12 TM domain K⁺ channel found in *Paramecium* (S1-S2-S3-S4-S5-P-S6-S7-S8-S9-S10-S11-P2-S12)¹¹ and finally a 8TM motif found in fungi (S1-S2-S3-S4-S5-P-S6-S7-P-S8)¹⁷.

The K⁺ channel filter sequence is relatively well conserved. To date most eukaryotic and prokaryotic K⁺ channels have GYG or GFG K⁺ filter sequences. Since the HOSK channel has a variant putative filter, it is useful to examine the known variability in the filter amongst conventional K⁺ channels. However, in depth research of prokaryotic and eukaryotic realm does show variations in the K⁺ recognition sequence. For example, *Thermotoga maritime* uses GYSI as a K⁺ filter sequence¹³. Likewise, the filter sequences of two other hyperthermophilic and acidophilic organisms from the genus *Sulfolobus* have alternative pore sequences. Both *Sulfolobus solfataricus* and *Sulfolobus tokodaii*, encode a 2TM RCK (regulatory component of K⁺) type channel with putative pore sequence of GLYS and GLYA, respectively^{18,19}. These K⁺ specificity sequences are not found among eukaryotes. These putative filter sequences are not likely adaptations to high temperatures, since other hyperthermophilic archeabacterium or bacteria have conventional filters. Another variant (GYSD is found in one of the five K⁺ channels of *Synechocystis* sp. PCC6803, a fresh water cyanobacterium. Other species with variant filter sequences include a GFQE in *Desulfovibrio desulfuricans* and a GFKE in *Geobacter metallireducens*, both subterranean bacteria associated with iron corrosion. A GYQE is found in *Magnetococcus* sp. MC-1 as well¹¹. Recently in eukaryotes, Salinas et al has cloned a subunit named KCNK7, which requires another unidentified subunit to form a functional channel, employs GLE as its selectivity filter²⁰. However, the true frequency of filter sequence variation amongst eukaryotes, although thought to be low, is

unknown as is its evolutionary basis.

1.2.2 Eukaryotes

Since the HOSK channel has a unique topology with little structural homology to known K⁺ channels, it is useful to review the structural variability amongst conventional K⁺ channels. The most ancient K⁺ channel family, the inward rectifying K⁺ (Kir) channels, form 2-TM proteins. Within the eukaryotic lineage, particularly in vertebrates, these 2-TM K⁺ channels have undergone extensive divergence. Different sequences that have evolved within this family result in diversity in the channels' strength of rectification, single-channel conductance, and response to modulating factors²¹⁻²³.

The ancestor of most Kv channel proteins appears to have arisen by the addition of four TM segments to the N-terminus of a 2-TM precursor, yielding a channel with six TM helices (S1-S6). The theory of independent evolution of voltage sensing domain has been recently strengthened by discovery of a novel protein in *Ciona intestinalis* that has a transmembrane voltage-sensing domain, homologous to the S1-S4 segments of Kv channels, and a cytoplasmic domain similar to phosphatase and tensin homologue²⁴. This protein, named *C. intestinalis* voltage-sensor-containing phosphatase (Ci-VSP), displays channel-like 'gating' currents and directly translates changes in membrane potential into the turnover of phosphoinositides. Perhaps the S1-S4 domains underwent independent evolution before joining the K⁺ channel to exist as a signature *Shaker* motif. This concept is strengthened by the Kv1.2 crystallization data which shows that the voltage sensor of one subunit regulates the gating of another subunit, suggesting independence of the S1-S4 domains.

The Shaker channels have two general features that distinguish them from the 2-

TM channels. First, they have intrinsic gating regulators, as opposed to the Kir inward rectifiers, which are gated by extrinsic cytoplasmic factors, Mg^{2+} ions, and /or polyamines²³. Second, the fourth transmembrane helix (S4) of Shaker channels has positively charged residues (either lysine or arginine) at every third position, producing an α -helical cylinder with a single row of positive charge. This charged cylinder confers intrinsic voltage sensitivity (independent of soluble cytoplasmic factors) to the channels by providing a charged element in the protein that moves in response to changes in membrane potential. The S2 and S3 segments also contribute to voltage sensitivity through charged amino acid residues and hydrophobic residues that interact with the S4 segment, stabilizing the open or closed conformation of the channel²⁵. A 6-TM K^+ channel was probably ancestral to the voltage-gated Ca^{2+} and Na^+ channels, which consists of four 6-TM modules²⁶ (Figure 3).

The *Shaker* subtype, or Kv1 family, of voltage-gated K^+ channels has been found in diverse nonvertebrate multicellular animals from Cnidarian to Chordata. Within the vertebrate lineage, there are at least twelve subfamilies of the Kv1 family of channels, each encoded by a distinct gene. However, the origination of functional Kv1.x- channels in nonvertebrate taxa seems to be independent and perhaps may be due to the divergence of the various phyla. In some cases, for example, *Drosophila melanogaster*, there is a single Kv1-type gene that yields a variety of channel proteins by alternative splicing. Conversely, in *Polyorchis penicillatus*, a cnidarian (jellyfish), there are at least two different Shaker-type channel genes, but these appeared to have diverged from an ancestral channel gene after the separation of the cnidarian lineage from the other metazoans²⁷. Thus, it appears that ancestral members of the Kv1, Kv2, Kv3, and Kv4

families of K⁺ channels originated in multicellular animals and then evolved independently in different phyla²⁸ (figure 4).

1.3 Kv CHANNELS-OVERVIEW

The Kv channels are a highly diverse superfamily whose members share K⁺ selectivity and intrinsic voltage-dependent activation, a property conferred by a series of positively charged arginines in the S4 subunit as discussed below. The nomenclature for the 38 known Kv channels has recently been revised by the International Union of Pharmacology to account for architectural similarities and phylogenetic relationships between different channel families (47). The Kv family consists of 3 groupings: Kv1-6 and 8-9, Kv7.1-7.4 and Kv10-12. Kv channels are proteins consisting of four transmembrane-bound α subunits, sometimes associated with four regulatory β subunits. The potassium channel pore is conferred by the formation of tetramers of α subunits that determines the intrinsic conductance and voltage sensitivity of the channel. β -subunits, on the other hand, are small cytosolic subunits (with some homology to NADH oxidase) that associate with many K⁺ channel α subunits and alter their activation and inactivation kinetics. Kv1-4 channels can form homotetrameric channels or heterotetramers, although tetramerization primarily occurs within a family. Kv channels (Kv5-12) are often referred to as gamma subunits. They do not themselves form conducting channels when assembled as homotetramers, but can interact with Kv1-4 subunits, particularly Kv2.x alpha subunits, to alter their gating.

1.4 STRUCTURAL BASIS OF K_v CHANNELS

There are three major questions concerning the structure that are central to understanding the molecular functioning of a K_v channel: (1) the stereochemical and thermodynamic basis of ion selectivity; (2) the mechanism of channel gating between open and closed conformations; and (3) the regulation of channel electrical activity by voltage-sensing and resulting protein-protein interactions.

1.4.1 Ion Selectivity and Conduction

The main task of the tetrameric structure of K_v channels is to conduct K⁺ ions out of the channel while excluding Na⁺ ions from entering the cell. This degree of selectivity is invoked by the geometry of the pore and the energetics of ionic interaction with hydrated K⁺ ion and with the residues of the pore. Series of substitution studies of amino acids done for determination of the pore size found that the pore narrows to an opening of only 3.0 angstrom^{29, 30}. The signature sequence (GYG) is thought to be the heart of the selectivity filter³¹. This selectivity filter across the membrane has been identified as the site that is physically responsible for the ion-selection process³². Computational biology suggested that several successive layers of four oxygen atoms occupying corners of a square, which are provided by the carbonyl oxygen of the main chains of the four subunits, can act as surrogate for water, to co-ordinate the passing of dehydrated cations³³. The centers of these squares are excellent binding pockets for K⁺, yet the proximity of successive layers of squares provides a means to facilitate ion flow through the pore, giving a near diffusion rate of permeation. The proposed model supports the

idea that the rigidity of the selective filter, made up by four “main chain” atoms, accounts for the energetic preference for a K^+ over the physically smaller Na^+ by coordinating the short-range interaction between the pore-lining protein atoms and the cations passing through the filter^{34, 35}.

The direct proof of channel structure came from the crystallization of KcsA. In the lower (3.2 angstrom) resolution X-ray structure of KcsA, four ion binding sites within the filter were identified (sites S1 to S4). It was therefore suggested that ion permeation through the narrow filter region of a K^+ channel required the K^+ ion to be stripped of its hydration shell. Thus, when a K^+ ion is within the filter, its hydration shell is replaced by eight oxygen (O) atoms of the backbone carbonyl groups or by (at site S4) four carbonyl O atoms and four hydroxyl O atoms of threonine side chains³. The 2.0 angstrom resolution crystal structure revealed details of both hydration and coordination within the filter. The coordination of K^+ ions within the filter at each of the four sites S1 to S4 is made up of eight O atoms from the protein arranged at the corners of a distorted cube (at site S4), with a K^+ ion at its center. The higher resolution structure reveals two further K^+ ion sites not observed in the earlier structure, namely S0 and S_{EXT}. S0 is formed by four oxygen atoms with the remaining interactions provided by water molecules. Thus, the K^+ ion's hydration shell has been half-replaced by interactions with the protein. S_{EXT} is on the extracellular side of site S0, and an ion at this site remains surrounded by eight waters. The higher resolution structure also resolves a single K^+ ion within the central cavity, solvated by eight water molecules in a square anti-prism arrangement^{15, 36}. Thus, the structure supports the suggestion that KcsA (and by extension other K^+ channels) is a multi-ion pore, with a succession of up to six sites in a row capable of binding K^+ ions.

The mechanism of rapid permeation is envisaged in terms of rapid shuttling between two configurations: one with K⁺ ions at sites S1 and S3 and another with ions at sites S2 and S4. Approximately equal probabilities of occurrence of these two configurations results in equal average occupancies of sites S1 to S4. A cycle of permeation is initiated whereby individual sites are occupied and the directional motion of the ions is achieved by the chemical gradient. Since these sites exist in a close proximity, electrostatic repulsion between ions provides the means for rapid directional permeation of K⁺ ions at a near diffusion constant³⁶⁻⁴¹. Thus, K⁺ channels achieve high conduction rates by exploiting electrostatic repulsion between closely spaced ions and by coupling the conformation of the selectivity filter to ion binding within the filter (Figure 5).

1.4.2 Gating

K⁺ channel pores undergo a conformational change to open and close (a phenomenon termed “gating”) in response to activating or inactivating stimuli. The following section deals with how the activation and inactivation of Kv channels is achieved.

1.4.2.1 Activation

The opening of the channel pore requires stimulation that results in the rotation of S6 helices, the so called “activation gate”. Specific to Kv channels, depolarization acts as such a stimulus.

In response to a depolarization, the S4 helix moves in a manner such that there is net movement of S4 charged residues, resulting in an outward capacitive current⁴². The

current is also known as the gating current and has an on-phase (outward current upon depolarization) and off-phase (inward currents upon repolarization). These gating currents can provide valuable information about the activation gating mechanism because they reflect transitions which are generally not observable simply by measuring ionic currents⁴³. Schoppa et al⁴⁴, using fluctuation analysis, determined the number of gating charges per Shaker channel quantitatively and this gave a value between 12 and 13 elementary charges. Since it was believed that the S4 helix carry 3-4 elementary charge, this was in agreement with the fact that Kv channels are tetramer⁴⁵.

When Hodgkin and Huxley plotted the conductance-voltage relationship from the K⁺ current of the squid giant axon, it was found that it was reasonably well modeled with a Boltzmann function raised to the fourth power. For this reason, they proposed a model in which four identical and independent gating transitions must occur prior to channel opening i.e, each S4 helix from the tetramer moves individually to achieve activation of Kv channel². For simplicity these transitions were considered identical. Subsequently, Cole and Moore⁴⁶ observed that the delay between individual S4 helix movements is lessened through the conditioning of the channel with varying holding potentials. The more depolarized the holding potential, the less delay was noted for channel activation elicited by a subsequent depolarization, the so-called Cole-Moore shift. In order to explain this dependence of the activation rate upon the conditioning stimulus, Cole and Moore postulated that 26 independent transitions were required prior to channel opening. This model was subsequently simplified with the assumption that a transitional state exists between open and closed state. The Zagotta-Hoshi-Aldrich (ZHA) model simplified the model to 15 states in which a *Shaker* channel can exist⁴⁷(Figure 6). A more

recent model of *Shaker* channel gating has built upon the ideas of Hoshi et al⁴⁸ and Zagotta et al⁴⁹, but examined *Shaker* gating over a wider range of voltage range and employed new protocols to study these transitions in more detail. This approach has identified new transitions not apparent over the voltage-ranges studied previously and consequently led to a more refined model. This Schoppa-Sigworth (SS)⁵⁰⁻⁵² model of *Shaker* channel activation involves gating which proceeds first through three sequential transitions (S_0 - S_3) in each of the four subunits independently but occur as a single concerted transition among all the subunits at the end.



Overall, the model, closely predicts many features of *Shaker* channel gating such as the voltage dependence of channel opening and gating charge movement, the sigmoidicity of activation as well as slow tail currents and off-gating currents with slow kinetics and a prominent rising phase. This model predicts that from very negative potentials, the channel must undergo 14 transition prior to opening. The first 12 transitions (three per subunit) are largely independent (except for a small amount of positive cooperativity in the first transition), and the final two transitions represent the concerted action of all four subunits and are heavily biased towards the open state⁵⁰⁻⁵². Cooperativity likely explains the steep voltage dependence of the probability of opening and charge movement⁵³.

1.4.2.2 Inactivation

There are three established mechanisms by which the Kv channels can close. The first mechanism involves conditional plugging of the pore by an auto-inhibitory part of the channel (N-type inactivation). Second mechanism involves conformational

constriction of the permeation pathway (C-type inactivation).

Ball-and-chain gating

The N-terminus of *Shaker* K⁺ channels can act as a channel blocker by interacting directly with the channel cavity. Because this interaction occurs only after the S6 gate has opened, some Kv channels conduct only transiently, during the brief period after the S6 gate opens and before the N-terminal peptide blocks the channels, hence N-type inactivation^{54,55}. N-type inactivation (also called the ball-and-chain mechanism because it involves a tethered blocker, initially imagined to be a ball) occurs in several known voltage-gated K⁺ channels, and can involve either the N terminus of the principal α -subunit of the channel⁵⁶ or the N-terminus of an associated β -subunit⁵⁷. N-type inactivation can be disrupted by enzymatic or genetic removal of the N-terminal truncation, and restored by addition of soluble peptide of the same sequence to the intracellular bathing solution⁵⁸.

Gating at the selectivity filter

A second mechanism for closing the pore is to pinch shut at the narrow selectivity filter itself- a selectivity filter or pore gate. This mechanism was recognized in the form of C-type inactivation, an alternative to N-type inactivation for producing transient K⁺ conductance by closing the channels in spite of a maintained stimulus⁵⁹. C-type inactivation persists in *Shaker* channels when the inactivation ball is deleted, and it is quite sensitive to extracellular K⁺ concentrations and to mutations at the extracellular entryway to the pore⁶⁰.

1.4.2.3 Deactivation

This mechanism entails a gate at the intracellular entrance (P-type inactivation).

Gating by S6 domain

A mechanism that can cause deactivation is the shutting of an intracellular gate at the entrance. This intracellular or S6 gate obstructs entrance from the cytoplasmic surface to the water-filled “cavity” in the center of the channel protein. This gate corresponds to a functionally determined closure point of at least some of the voltage-gated K⁺ channels^{61, 62}. The S6 transmembrane region and its intracellular extension show very high sequence conservation within principal Kv1.x families, and at the bundle crossing there is a strongly conserved proline sequence (PxP or PxG) that is not found in the bacterial K⁺ channels. Studies of this region indicate that it is likely bend of the S6 that initially determines the opening or closing of the channel⁶²⁻⁶⁴.

The probable nature of the S6 opening motion has now been made apparent by determining the structure of a second bacterial K⁺ channel, MthK¹⁶, tetrameric 2-TM that can be opened by intracellular Ca²⁺. The MthK channel in the open state, has no bundle crossing: instead, the homologues of the S6 helices are splayed wide open with no constriction between the intracellular solution and the selectivity filter. Comparing this with the presumably closed structure of KcsA gives a plausible picture for the gating motion: the S6 helices swing open from an apparent hinge located at a highly conserved glycine residue⁶⁵.

Recently, crystallization of Kv1.2 structure also suggests a mechanism of

conformational change involving the kinked helix⁴. The sequences of the pore-lining S6 helices in these mammalian Kv channels contain a conserved PxP motif. This motif disrupts the hydrogen bond network of the alpha-helix and introduces a flexible kink into the S6 helix^{63, 66-69}. The Kv1.2 structure confirms that in the open state, the S6 helix is indeed kinked in the vicinity of the PxP. In Kv1.2, the gate is linked indirectly to the voltage sensor via an alpha-helical S4-S5 linker which is in contact with the S6 helix. This linker couples the conformation of the gate to movement of the sensor^{4, 70}. Thus, it seems that there is a general model for K⁺ channel gating in which a structural hinge at PxP forms intracellular gating. Overall, it seems probable that the basic functioning of the S6 gate and the selectivity filter gate are conserved among different channels: the S6 gate moves in response to a transmembrane voltage sensor or intracellular sensor domain, and the selectivity filter may react to the change in S6 by opening or closing.

1.4.3 Voltage Sensing

Voltage-dependent ion channels are exquisitely sensitive to membrane potential, so much so that a depolarization of only 10 mV can cause a 100-fold increase of open probability^{44, 71}. This feat requires the energetic coupling of channel opening to the movement of at least 12 elementary charges across the membrane electric field, as previously discussed. These charges reside in specialized structures of the ion channel protein known as voltage sensors, located in S4 segment⁷². This is the only domain that is appreciably charged in voltage-gated ion channels; S4 segments contain from two to eight position charged residues, typically separated from one another by two neutral residues⁷³. Despite the functional knowledge of S4 being a sensor, how the movement of

sensor translates into gating is still elusive. Years of experimentation have resulted in evolution of a number of competing models that have attempted to explain the conformational changes resulting from depolarization (described below)

1.4.3.1 The Canonical Model

The canonical, or sliding-helix model, of Kv channel gating is derived from studies of S4 residue accessibility using cysteine scanning mutagenesis and thiol-reactive compounds, and from changes in fluorescence of probes attached to S4 upon channel activation. Upon membrane depolarization, each S4 helix is proposed to slide or screw outwards toward the extracellular surface through a narrow vestibule, or ‘canaliculus’. The canaliculi are proposed to provide an aqueous environment for most of the length of the S4 helices, with hydrophobic ‘seal’ midway along⁷⁴.

1.4.3.2 The Transporter Model

The transporter model is similar to the canonical model in that the S4 helix is thought to be buried within a canaliculus between the pore domain (S5-P-S6) and the S1-S3 helices. In this case, however, the movement of S4 upon depolarization is suggested to be quite subtle, so that, although the S4 helices do not undergo any substantial movement, they change the exposure of the gating charges from the intracellular aqueous solution to the extracellular solution. Thus, gating charges move across the entire transmembrane electric field, even though no large scale motion of S4 occurs^{75, 76} (Figure 7a)

1.4.3.3 The Paddle Model

The paddle model is derived from comparison of the crystal structures of the voltage sensor domain of the bacterial channel KvAP^{77, 78}, and of intact KvAP channel⁷⁹.

The critical component of the model is a paddle-like structure formed by S4 and carboxy-terminal half of the S3 helix. The paddles are attached to the channel through flexible S3 loops and S4-S5 linkers and, with the exception of the critical S4 arginine residues, have an amino acid composition that is mainly hydrophobic.

In this model, the paddles are positioned loosely around the periphery of the channels and are exposed to the membrane environment. In the full-length crystal structure, the paddles are located close to the intracellular surface; biophysical studies, however, indicate that the paddles can also be exposed to the extracellular solution⁸⁰. From these findings it was inferred that the paddles translocate their cargo of gating charge across the entire bilayer in response to changes in the membrane potential (Figure 7b).

1.4.3.4 The Twisted S4 Model

The result of recent site-directed spin labeling experiments of KvAP in a lipid bilayer environment indicates that the S4 helices are at the protein-lipid interface, rather than buried within a canaliculus. This is an apparent agreement with the paddle model, but more detailed examination of spin label accessibility data indicates that most of the arginine sidechains are shielded from the lipid environment. These data can be explained by a modification to the structure of the voltage-sensor, whereby there is flexible linker or hinge in the middle of S4, enabling one half of S4 to rotate relative to other⁸¹.

Recently the crystallization shone more light on apparent movement of voltage sensor. The Kv1.2 crystal structure is compatible with the old description of S4 segment acting in accordance to the transporter model but also has properties similar to voltage paddle model. Using molecular dynamics simulation, the movement of voltage-sensing

domain of Kv1.2 was modeled. Studies suggest that Kv1.2 voltage-sensing domain agrees with the transporter model, however instead of a vertical movement, a lateral displacement of S4 is observed. In conclusion, further experimentation is clearly warranted to reach a complete understanding of the structural mechanisms of voltage-sensing and voltage-gating of Kv channels. More importantly the question remains of how this mechanistic change in Kv channel subunits translates into a functional role at the tissue level.

1.5 Kv CHANNELS IN VASCULAR SMOOTH MUSCLE CELLS

Kv channels are important determinants of resting membrane potential (E_m) of vascular smooth muscle cells (VSMC). The resting potential is determined by the Nernst equation; $E = E^0 - 0.059/n \log_{10}Q$, where E^0 is standard equilibrium and Q is the reaction quotient and for VSMC the resting membrane potential at -55 mV. When Kv channels close and the tonic efflux of potassium are decreased, the interior of the cell becomes relatively more positive (depolarized). At these more positive potentials (i.e, -30 to 10 mV) the opening probability of L-type calcium channels (which are voltage-gated) increases. This increases intracellular calcium influx (down a $10,000/1$ gradient) and activates calcium-induced calcium release, effectively increasing total calcium levels inside the cell. Thus, regulation of potassium channel activity, specifically Kv channels, and the subsequent regulation of Ca^{2+} plays an important role in maintaining vascular tone⁸².

There has been controversy as to whether Kv channels are open at sufficiently negative potentials to establish resting membrane potential. However, when patch clamp

studies are conducted carefully, avoiding prolonged depolarizations that inactivate the channels, one can see Kv1.x activity at or near resting membrane potential in pulmonary artery smooth muscle cell (PASMC) from resistance arteries⁸³. In addition to inactivation by depolarization, the impression that Kv channels do not set membrane potential may result from the fact that many investigators study cultured cells (in which membrane potential is depolarized due to loss of Kv1.x channels)⁸⁴. An additional factor which can obscure the role of Kv channels in setting resting membrane potential is the fact that VSMCs have a high input resistance; therefore, even a small change in Kv activity (which may be difficult to measure at very negative potential) can have a significant effect on membrane potential and, consequently, vascular tone^{85, 86}. Inhibition of VSMC Kv channel leads to depolarization, due to inhibition of K⁺ ion movement down its concentration gradient (140/5mM). This leads to inhibition of voltage-gated Ca²⁺ channels, and vasodilation.

1.6 DUCTUS ARTERIOSUS

Ductus arteriosus (DA) is a fetal shunt vessel that connects the left pulmonary artery and the aorta. The DA shunts deoxygenated blood to the descending aorta, bypassing the unexpanded fetal lung. Over half of the blood flow in the descending aorta is diverted to the umbilico-placental circulation⁸⁷, where gaseous exchange takes place. As PO₂ increases with the first breath, the DA constricts and the pulmonary vascular resistance decreases. The resulting cessation of a right to left shunt and the increase in pulmonary blood flow initiates the transition to the newborn circulation. Constriction of the DA rarely fails in term infants but is common in low birth weight, premature infants.

Within days, cell proliferation anatomically obliterates the DA lumen. Numerous mechanism(s) have been postulated for the acute increase in ductal constriction in response to the increased PO_2 , one of which is acute inhibition of O_2 -sensitive Kv channels, including the newly discovered HOSK channel. These mechanisms of DA constriction are outlined below.

1.6.1 Endothelial contribution to DA constriction

Although O_2 -induced DA constriction in human and rabbit is intrinsic to the ductus arteriosus smooth muscle cell (DASMC) ⁸⁸; it is significantly modulated by the endothelium (endothelin⁸⁹ increases constriction while prostaglandins ⁹⁰⁻⁹² and nitric oxide ⁹³ inhibits constriction). The prostaglandin pathway has been effectively exploited in clinical management of the DA. Prostaglandin E infusion is useful in sustaining DA patency in infants with complex congenital heart disease, such as hypoplastic left heart syndrome, as a bridge to surgery ⁹⁴. Conversely, Prostaglandin H synthase inhibitors (e.g. indomethacin or ibuprofen) treat or prevent 70% of cases of persistent DA ⁹⁰, by promoting DA constriction ^{91, 92}. However, these agents fail in almost half of preterm infants born before 28 weeks ⁹⁰, necessitating surgical closure.

O_2 mediated vasoconstriction have two stages. The acute phase is characterized by rapid increase in PO_2 resulting in functional closure of DA. Subsequently the second phase entails synthesis of various factors that facilitate the prolonged closure and anatomical obliteration of DA. Numerous empirical evidences exist in favor of the acute phase. The O_2 -induced constriction persists even after removal of the endothelium or inhibition of prostaglandin H and nitric oxide synthases. While O_2 induces endothelin

synthesis and exogenous endothelin does elicit prolonged DA constriction^{95, 96}, endothelin receptor blockade does not impair acute O₂-constriction in vivo⁹⁷. Moreover, in term human DA, inhibition of endothelin-A receptors and endothelin converting enzyme fails to attenuate acute O₂ constriction⁹⁸. Finally, mice lacking endothelin-A receptors achieve normal rates of DA closure (although the intensity of acute O₂ constrictor response is reduced)⁹⁹. O₂-induced endothelin synthesis (first detectable ~30 minutes after increased PO₂) lags behind onset of O₂ constriction (onset <10 minutes). Thus, it appears that although endothelin may reinforce later phases of O₂ constriction, it is not essential to initial functional closure.

1.6.2 K⁺ channels and constriction of the DA

Initial experimentation found that the oxygen-induced contraction of the guinea pig DA was associated with smooth muscle cell depolarization¹⁰⁰. In an elegant experiment done by Roulet and Coburn, they found that stepwise increase in PO₂ resulted in: (1) progressive development of tension coupled to action potentials and (2) sustained membrane depolarization associated with tonic contraction. Subsequently, it was observed that glibenclamide, a blocker of ATP-sensitive potassium channels, contracted the hypoxic isolated rabbit ductus and had little effect on the oxygen-contracted ductus¹⁰¹. Conversely, cromakalim, an ATP-sensitive potassium channel activator, relaxed the ductus contracted by oxygen, but had much less of an effect on the vessel precontracted with 10 μM norepinephrine¹⁰¹. These authors suggested that oxygen depolarized the ductus by closing ATP-sensitive potassium channels.

Further in depth analysis on smooth muscle cells from the rabbit ductus using patch clamp techniques confirmed that increasing oxygen tension inhibited whole cell potassium current¹⁰². However, when the effects of antagonists of potassium channels were studied using isolated ring preparations, it was found that 1 mM 4-aminopyridine (AP) (an inhibitor of Kv channels) caused a much greater contraction of the rabbit ductus exposed to fetal oxygen tension than glibenclamide (10 μ M)¹⁰². Furthermore, 4-AP (in ductal smooth muscle cells exposed to fetal oxygen tension) suppressed whole cell potassium current and depolarized ductal smooth muscle cells; a response that was not duplicated by glibenclamide. Finally, single channel recordings demonstrated a 58-pS channel that was closed both by 4-AP and increasing oxygen tension¹⁰². These observations suggested that increasing oxygen contracts the ductus at least in part by closing oxygen-sensitive Kv channels.

The first direct evidence that Kv channels mediated the O₂-induced DA in the human DA resulted from our groups demonstration that: (1) 4-aminopyridine, but not glyburide (K_{ATP} channel inhibitor) or charybdotoxin (Ca²⁺-sensitive K⁺ channel inhibitor), constricts the human DA, suggesting that Kv channels are important in the regulation of basal tone in the hypoxic human DA; (2) the magnitude of the constrictions to 4-aminopyridine and oxygen are similar and not additive, suggesting that they share a common mechanism of action—i.e, Kv channel inhibition; (3) an L-type Ca²⁺ channel inhibitor) significantly inhibits the response to both oxygen and 4-aminopyridine. (4) The human DASMC expresses several putative O₂-sensitive Kv channels, including Kv1.5 and Kv2.1. These findings suggest that O₂-mediated DA vasoconstriction involves Kv channels.

1.6.3 Kv channels as an effector

The human DA expresses: Kv1.2, Kv1.4, Kv1.5, Kv2.1, Kv3.1, Kv4.3, Kv9.3 Kir2.1, Kir6.1, TASK and the large conductance, calcium sensitive K⁺ channel, BK_{Ca})^{98, 103, 104}. Thus, DAs express several putative O₂ sensitive channels - Kv1.5^{105, 106}, Kv2.1/9.3^{105, 107, 108} (a heterotetrameric association of Kv2.1 and Kv9.3) & Kv3.1b¹⁰⁹.

Initial data suggested that perhaps Kv1.5 and Kv2.1 were the main effector of O₂-mediated DA constriction. In ionically remodeled DAs (DAs incubated in normoxic chamber for 48 hrs), a condition mimicking first few days after birth, a significant decrease in K⁺ current (I_K) as well as O₂-mediated vasoconstriction was noted. This was correlated to decreased Kv1.5 and Kv2.1 gene expression. Adenoviral mediated gene delivery of Kv2.1 reversed ionic remodeling and partially restored both the electrophysiological and vasoconstrictor responses to 4-AP and O₂. Furthermore, in preterm rabbit DA, which typically have an impaired response to O₂, targeted increase in gene expression of Kv1.5 driven under the smooth muscle cell promoter restored the oxygen sensitivity in preterm DA. In addition, a similar effect is achieved in human DA. Thus, the Kv1.5 and perhaps to some extent Kv2.1 contributes to the O₂-mediated vasoconstriction in DA. Despite the implications of Kv2.1 and Kv1.5 channels in physiological and adaptive response in PA and DA, the question remains as to how a stimulus such as hypoxia dilates DA and constricts PA (Figure 8).

The central mechanism of oxygen sensing involves a redox-based O₂-sensor (e.g. mitochondria) which during normoxia, tonically generates a diffusible redox mediator (e.g. H₂O₂). Therefore under normoxic conditions, H₂O₂ increases in I_k of PASMC¹¹⁰ whilst in DASMC the I_k is decreased¹¹¹. In the DASMC, removal of endogenous H₂O₂, via intracellular catalase, increases normoxic I_k and hyperpolarizes DAMSC membrane potential (E_M); whereas intracellular H₂O₂ decreases I_k and depolarizes E_M¹¹¹. Likewise, reducing agents such as duroquinone and dithiothreitol dilated normoxic-constricted DA rings¹¹¹ while constriction was observed in PA rings¹¹⁰. Conversely, oxidants such as 5,5'-dithiobis-(2-nitrobenzoic acid) dilate PA rings and lower pulmonary vascular resistance, oxidants such as constricted hypoxia-dilated DA rings¹¹¹.

1.6.4 Kv Diversity and O₂ Sensing

We hypothesize that a form of reverse redox regulation (in DA vs PA) resulted, at least in part, from diversity in the K⁺ channels in the respective arteries. Various K⁺ channels have been known to undergo alternative splicing of mRNA transcripts to create diverse electrophysiological relevant K⁺ channels. Furthermore, at the translational level also K⁺ channel seems to display diversity by having ribosomes bind to these unique internal ribosomal entry site and thus providing two diverse protein products. Moreover, K⁺ channel also utilize diverse modular assembly of proteins to create heterotetramers with functional properties reflecting their heterogeneous subunit composition. For Kv1.5, numerous reports exist of splice variants causing functional diversity. For example, a longer form encodes a 602-amino acid protein, while in a short form (Kv1.5 delta 5'), the first 200 amino acids lying upstream the transmembrane segment S1 were deleted¹¹².

Moreover, an additional short cDNA clone (Kv1.5 delta 3') that codes for a carboxyl-terminal truncated protein has been isolated. It appears that the short mRNA fragments arose by an unusual splicing event within the exonic sequence. Expression in *Xenopus* oocytes revealed that the long (Kv1.5) and the amino-terminal deleted (Kv1.5 delta 5') isoforms elicited similar K⁺ currents. The carboxyl-terminal truncated Kv1.5 delta 3' clone was not functional but inhibited the expression of the long isoform. Kurata et al found that truncated cardiac isoforms of Kv1.5 can be expressed *in vivo* and provided evidence that absence of the NH₂ terminus can accelerate inactivation from closed states, relative to full-length Kv1.5. They speculated that “differential expression of isoforms of Kv1.5 may contribute to K⁺ current diversity in human heart and many other tissues.”¹¹³. Moreover, Kv 1.5 in colonic smooth muscle cells (SMCs) differs slightly from cardiac Kv1.5¹¹⁴. The highly conserved inter-tissue homology of Kv1.5 in transmembrane segments, S1-S6, decreases to 74-82% at the intracellular NH₂ and COOH termini¹¹⁴. Thus given the evidence, it is possible that the opposing O₂-sensitivity of certain Kv channels in the DA and adjacent PA relates to tissue-specific splice variants with opposing redox properties.

1.7 HYPOTHESIS

Since the pathway of oxygen mediated vascular response in two contiguous vessels PA and DA appeared to diverge at the level of the Kv channel response to a common stimulus at birth (increased mitochondrial derived H₂O₂ in the SMC), the original goal was to determine the role of diversity in expression of O₂-sensitive K⁺ channels, specifically Kv1.5 splice variants, in the DA of humans and rabbits. To that

end, human DA harvested from neonates suffering from congenital heart defects and undergoing palliative surgical repair involving aortic arch were used to synthesize total cDNA. A polymerase chain reaction (PCR) was performed with sense complement Kv1.5 primers on a DA cDNA. Serendipitously, this also led to isolation of a single smaller PCR, a product which was present in 4 of 7 human DAs, but in 0 of 7 human PAs.

We inserted this PCR product in pTracer-CMV mammalian expression vector and transfected Chinese Hamster Ovary (CHO) cells. This resulted in a voltage-dependent current. On sequencing and further *in silico* analysis suggested that, rather than encoding for a splice variant of Kv1.5, this 1.4 kb product encodes a novel voltage-gated human oxygen-sensitive K⁺ channel (HOSK). **We hypothesized that HOSK, a novel class of K⁺ channel, contributes to the oxygen-sensitivity in DA.**

1.8 THESIS OBJECTIVES

This thesis delineates three different aspects of HOSK channel:

1. Molecular Biological determination of HOSK channel
2. Proteomic identification and isolation of HOSK channel
3. Electrophysiological characterization of HOSK channel

Through these objectives, this thesis will provide the first examination of HOSK channel as it pertains to its identification, isolation and characterization. Together, these studies will set a foundation for further description of HOSK from its current discovery.

1.9 REFERENCES

1. Hodgkin, A. L. & Huxley, A. F. A quantitative description of membrane current and its application to conduction and excitation in nerve. 1952. *Bull Math Biol* 52, 25-71; discussion 5-23 (1990).
2. Hodgkin, A. L. & Huxley, A. F. A quantitative description of membrane current and its application to conduction and excitation in nerve. 1952. *J. Physiol* 117, 500-544 (1990).
3. Doyle, D. A. et al. The structure of the potassium channel: molecular basis of K⁺ conduction and selectivity. *Science* 280, 69-77 (1998).
4. Long, S. B., Campbell, E. B. & Mackinnon, R. Crystal structure of a mammalian voltage-dependent Shaker family K⁺ channel. *Science* 309, 897-903 (2005).
5. McMurtry, M. S. et al. Gene therapy targeting survivin selectively induces pulmonary vascular apoptosis and reverses pulmonary arterial hypertension. *J Clin Invest* 115, 1479-91 (2005).
6. Michelakis, E. D. et al. Dichloroacetate, a metabolic modulator, prevents and reverses chronic hypoxic pulmonary hypertension in rats: role of increased expression and activity of voltage-gated potassium channels. *Circulation* 105, 244-50 (2002).
7. Bonnet, S. et al. An abnormal mitochondrial-HIF-1-Kv channel pathway disrupts oxygen-sensing and triggers pulmonary arterial hypertension (PAH) in fawn-hooded rats: similarities to human PAH. *Circulation* (in press) (2006).
8. Archer, S. & Rich, S. Primary pulmonary hypertension: a vascular biology and translational research "Work in progress". *Circulation* 102, 2781-91 (2000).

9. Pozeg, Z. I. et al. In vivo gene transfer of the O₂-sensitive potassium channel Kv1.5 reduces pulmonary hypertension and restores hypoxic pulmonary vasoconstriction in chronically hypoxic rats. *Circulation* 107, 2037-44 (2003).
10. Bonnet, S. et al. NFAT regulates Kv1.5, a voltage-gated K⁺ channel which is downregulated in both human and animal pulmonary hypertension. (abstract). *Canadian Journal of Cardiology* 21, 57 (2005).
11. Kuo, M. M., Haynes, W. J., Loukin, S. H., Kung, C. & Saimi, Y. Prokaryotic K(+) channels: from crystal structures to diversity. *FEMS Microbiol Rev* 29, 961-85 (2005).
12. Deckert, G. et al. The complete genome of the hyperthermophilic bacterium *Aquifex aeolicus*. *Nature* 392, 353-8 (1998).
13. Nelson, K. E. et al. Evidence for lateral gene transfer between Archaea and bacteria from genome sequence of *Thermotoga maritima*. *Nature* 399, 323-9 (1999).
14. MacKinnon, R. Nobel Lecture. Potassium channels and the atomic basis of selective ion conduction. *Biosci Rep* 24, 75-100 (2004).
15. Zhou, Y., Morais-Cabral, J. H., Kaufman, A. & MacKinnon, R. Chemistry of ion coordination and hydration revealed by a K⁺ channel-Fab complex at 2.0 Å resolution. *Nature* 414, 43-8 (2001).
16. Jiang, Y. et al. The open pore conformation of potassium channels. *Nature* 417, 523-6 (2002).

17. Ketchum, K. A., Joiner, W. J., Sellers, A. J., Kaczmarek, L. K. & Goldstein, S. A. A new family of outwardly rectifying potassium channel proteins with two pore domains in tandem. *Nature* 376, 690-5 (1995).
18. Kawarabayasi, Y. et al. Complete genome sequence of an aerobic thermoacidophilic crenarchaeon, *Sulfolobus tokodaii* strain 7. *DNA Res* 8, 123-40 (2001).
19. She, Q. et al. The complete genome of the crenarchaeon *Sulfolobus solfataricus* P2. *Proc Natl Acad Sci U S A* 98, 7835-40 (2001).
20. Salinas, M. et al. Cloning of a new mouse two-P domain channel subunit and a human homologue with a unique pore structure. *J Biol Chem* 274, 11751-60 (1999).
21. Fakler, B., Brandle, U., Glowatzki, E., Zenner, H. P. & Ruppersberg, J. P. Kir2.1 inward rectifier K⁺ channels are regulated independently by protein kinases and ATP hydrolysis. *Neuron* 13, 1413-20 (1994).
22. Krapivinsky, G. et al. A novel inward rectifier K⁺ channel with unique pore properties. *Neuron* 20, 995-1005 (1998).
23. Lopatin, A. N., Makhina, E. N. & Nichols, C. G. Potassium channel block by cytoplasmic polyamines as the mechanism of intrinsic rectification. *Nature* 372, 366-9 (1994).
24. Murata, Y., Iwasaki, H., Sasaki, M., Inaba, K. & Okamura, Y. Phosphoinositide phosphatase activity coupled to an intrinsic voltage sensor. *Nature* 435, 1239-43 (2005).

25. Papazian, D. M. et al. Electrostatic interactions of S4 voltage sensor in Shaker K⁺ channel. *Neuron* 14, 1293-301 (1995).
26. Strong, M., Chandy, K. G. & Gutman, G. A. Molecular evolution of voltage-sensitive ion channel genes: on the origins of electrical excitability. *Mol Biol Evol* 10, 221-42 (1993).
27. Jegla, T., Grigoriev, N., Gallin, W. J., Salkoff, L. & Spencer, A. N. Multiple Shaker potassium channels in a primitive metazoan. *J Neurosci* 15, 7989-99 (1995).
28. Derst, C. & Karschin, A. Evolutionary link between prokaryotic and eukaryotic K⁺ channels. *J Exp Biol* 201, 2791-9 (1998).
29. Armstrong, C. M. & Hille, B. The inner quaternary ammonium ion receptor in potassium channels of the node of Ranvier. *J Gen Physiol* 59, 388-400 (1972).
30. Hille, B. Potassium channels in myelinated nerve. Selective permeability to small cations. *J Gen Physiol* 61, 669-86 (1973).
31. Heginbotham, L., Lu, Z., Abramson, T. & MacKinnon, R. Mutations in the K⁺ channel signature sequence. *Biophys J* 66, 1061-7 (1994).
32. Hille, B. & Schwarz, W. Potassium channels as multi-ion single-file pores. *J Gen Physiol* 72, 409-42 (1978).
33. Roux, B. Theoretical and computational models of ion channels. *Curr Opin Struct Biol* 12, 182-9 (2002).
34. Antz, C. et al. NMR structure of inactivation gates from mammalian voltage-dependent potassium channels. *Nature* 385, 272-5 (1997).

35. Kreusch, A., Pfaffinger, P. J., Stevens, C. F. & Choe, S. Crystal structure of the tetramerization domain of the Shaker potassium channel. *Nature* 392, 945-8 (1998).
36. Morais-Cabral, J. H., Zhou, Y. & MacKinnon, R. Energetic optimization of ion conduction rate by the K⁺ selectivity filter. *Nature* 414, 37-42 (2001).
37. Guidoni, L., Torre, V. & Carloni, P. Potassium and sodium binding to the outer mouth of the K⁺ channel. *Biochemistry* 38, 8599-604 (1999).
38. Shrivastava, I. H. & Sansom, M. S. Simulations of ion permeation through a potassium channel: molecular dynamics of KcsA in a phospholipid bilayer. *Biophys J* 78, 557-70 (2000).
39. Berneche, S. & Roux, B. Molecular dynamics of the KcsA K(+) channel in a bilayer membrane. *Biophys J* 78, 2900-17 (2000).
40. Berneche, S. & Roux, B. Energetics of ion conduction through the K⁺ channel. *Nature* 414, 73-7 (2001).
41. Aqvist, J. & Luzhkov, V. Ion permeation mechanism of the potassium channel. *Nature* 404, 881-4 (2000).
42. Armstrong, C. M. & Bezanilla, F. Currents related to movement of the gating particles of the sodium channels. *Nature* 242, 459-61 (1973).
43. Aggarwal, S. K. & MacKinnon, R. Contribution of the S4 segment to gating charge in the Shaker K⁺ channel. *Neuron* 16, 1169-77 (1996).
44. Schoppa, N. E., McCormack, K., Tanouye, M. A. & Sigworth, F. J. The size of gating charge in wild-type and mutant Shaker potassium channels. *Science* 255, 1712-5 (1992).

45. MacKinnon, R. Determination of the subunit stoichiometry of a voltage-activated potassium channel. *Nature* 350, 232-5 (1991).
46. Cole, K. S. & Moore, J. W. Potassium ion current in the squid giant axon: dynamic characteristic. *Biophys J* 1, 1-14 (1960).
47. Zagotta, W. N., Hoshi, T. & Aldrich, R. W. Shaker potassium channel gating. III: Evaluation of kinetic models for activation. *J Gen Physiol* 103, 321-62 (1994).
48. Hoshi, T., Zagotta, W. N. & Aldrich, R. W. Shaker potassium channel gating. I: Transitions near the open state. *J Gen Physiol* 103, 249-78 (1994).
49. Zagotta, W. N., Hoshi, T., Dittman, J. & Aldrich, R. W. Shaker potassium channel gating. II: Transitions in the activation pathway. *J Gen Physiol* 103, 279-319 (1994).
50. Schoppa, N. E. & Sigworth, F. J. Activation of Shaker potassium channels. III. An activation gating model for wild-type and V2 mutant channels. *J Gen Physiol* 111, 313-42 (1998).
51. Schoppa, N. E. & Sigworth, F. J. Activation of Shaker potassium channels. II. Kinetics of the V2 mutant channel. *J Gen Physiol* 111, 295-311 (1998).
52. Schoppa, N. E. & Sigworth, F. J. Activation of shaker potassium channels. I. Characterization of voltage-dependent transitions. *J Gen Physiol* 111, 271-94 (1998).
53. Sigworth, F. J. Voltage gating of ion channels. *Q Rev Biophys* 27, 1-40 (1994).
54. Armstrong, C. M. Nineteenth Bowditch lecture. Ionic pores and gates in nerve membranes. *Physiologist* 18, 93-8 (1975).

55. Armstrong, C. M. Interaction of tetraethylammonium ion derivatives with the potassium channels of giant axons. *J Gen Physiol* 58, 413-37 (1971).
56. Hoshi, T., Zagotta, W. N. & Aldrich, R. W. Biophysical and molecular mechanisms of Shaker potassium channel inactivation. *Science* 250, 533-8 (1990).
57. Rettig, J. et al. Inactivation properties of voltage-gated K⁺ channels altered by presence of beta-subunit. *Nature* 369, 289-94 (1994).
58. Zagotta, W. N., Hoshi, T. & Aldrich, R. W. Restoration of inactivation in mutants of Shaker potassium channels by a peptide derived from ShB. *Science* 250, 568-71 (1990).
59. Hoshi, T., Zagotta, W. N. & Aldrich, R. W. Two types of inactivation in Shaker K⁺ channels: effects of alterations in the carboxy-terminal region. *Neuron* 7, 547-56 (1991).
60. Lopez-Barneo, J., Hoshi, T., Heinemann, S. H. & Aldrich, R. W. Effects of external cations and mutations in the pore region on C-type inactivation of Shaker potassium channels. *Receptors Channels* 1, 61-71 (1993).
61. Liu, Y., Holmgren, M., Jurman, M. E. & Yellen, G. Gated access to the pore of a voltage-dependent K⁺ channel. *Neuron* 19, 175-84 (1997).
62. del Camino, D. & Yellen, G. Tight steric closure at the intracellular activation gate of a voltage-gated K(+) channel. *Neuron* 32, 649-56 (2001).
63. del Camino, D., Holmgren, M., Liu, Y. & Yellen, G. Blocker protection in the pore of a voltage-gated K⁺ channel and its structural implications. *Nature* 403, 321-5 (2000).

64. Holmgren, M., Shin, K. S. & Yellen, G. The activation gate of a voltage-gated K⁺ channel can be trapped in the open state by an intersubunit metal bridge. *Neuron* 21, 617-21 (1998).
65. Perozo, E., Cortes, D. M. & Cuello, L. G. Structural rearrangements underlying K⁺-channel activation gating. *Science* 285, 73-8 (1999).
66. Labro, A. J., Raes, A. L., Bellens, I., Ottschytsch, N. & Snyders, D. J. Gating of shaker-type channels requires the flexibility of S6 caused by prolines. *J Biol Chem* 278, 50724-31 (2003).
67. Webster, S. M., Del Camino, D., Dekker, J. P. & Yellen, G. Intracellular gate opening in Shaker K⁺ channels defined by high-affinity metal bridges. *Nature* 428, 864-8 (2004).
68. Bright, J. N., Shrivastava, I. H., Cordes, F. S. & Sansom, M. S. Conformational dynamics of helix S6 from Shaker potassium channel: simulation studies. *Biopolymers* 64, 303-13 (2002).
69. Beckstein, O. et al. Ion channel gating: insights via molecular simulations. *FEBS Lett* 555, 85-90 (2003).
70. Long, S. B., Campbell, E. B. & Mackinnon, R. Voltage sensor of Kv1.2: structural basis of electromechanical coupling. *Science* 309, 903-8 (2005).
71. Hirschberg, B., Rovner, A., Lieberman, M. & Patlak, J. Transfer of twelve charges is needed to open skeletal muscle Na⁺ channels. *J Gen Physiol* 106, 1053-68 (1995).

72. Schneider, M. F. & Chandler, W. K. Voltage dependent charge movement of skeletal muscle: a possible step in excitation-contraction coupling. *Nature* 242, 244-6 (1973).
73. Bezanilla, F. The voltage sensor in voltage-dependent ion channels. *Physiol Rev* 80, 555-92 (2000).
74. Gandhi, C. S. & Isacoff, E. Y. Molecular models of voltage sensing. *J Gen Physiol* 120, 455-63 (2002).
75. Cha, A., Snyder, G. E., Selvin, P. R. & Bezanilla, F. Atomic scale movement of the voltage-sensing region in a potassium channel measured via spectroscopy. *Nature* 402, 809-13 (1999).
76. Glauner, K. S., Mannuzzu, L. M., Gandhi, C. S. & Isacoff, E. Y. Spectroscopic mapping of voltage sensor movement in the Shaker potassium channel. *Nature* 402, 813-7 (1999).
77. Jiang, Y. et al. X-ray structure of a voltage-dependent K⁺ channel. *Nature* 423, 33-41 (2003).
78. Jiang, Y., Ruta, V., Chen, J., Lee, A. & MacKinnon, R. The principle of gating charge movement in a voltage-dependent K⁺ channel. *Nature* 423, 42-8 (2003).
79. Ruta, V., Jiang, Y., Lee, A., Chen, J. & MacKinnon, R. Functional analysis of an archaeobacterial voltage-dependent K⁺ channel. *Nature* 422, 180-5 (2003).
80. Jiang, Q. X., Wang, D. N. & MacKinnon, R. Electron microscopic analysis of KvAP voltage-dependent K⁺ channels in an open conformation. *Nature* 430, 806-10 (2004).

81. Cuello, L. G., Cortes, D. M. & Perozo, E. Molecular architecture of the KvAP voltage-dependent K⁺ channel in a lipid bilayer. *Science* 306, 491-5 (2004).
82. Michelakis, E. D. & Weir, E. K. The pathobiology of pulmonary hypertension. Smooth muscle cells and ion channels. *Clin Chest Med* 22, 419-32 (2001).
83. Archer, S. L. et al. Preferential expression and function of voltage-gated, O₂-sensitive K⁺ channels in resistance pulmonary arteries explains regional heterogeneity in hypoxic pulmonary vasoconstriction: ionic diversity in smooth muscle cells. *Circ Res* 95, 308-18 (2004).
84. Navarro-Antolin, J., Levitsky, K. L., Calderon, E., Ordonez, A. & Lopez-Barneo, J. Decreased expression of maxi-K⁺ channel beta1-subunit and altered vasoregulation in hypoxia. *Circulation* 112, 1309-15 (2005).
85. Jackson, W. F. Ion channels and vascular tone. *Hypertension* 35, 173-8 (2000).
86. Standen, N. B. & Quayle, J. M. K⁺ channel modulation in arterial smooth muscle. *Acta Physiol Scand* 164, 549-57 (1998).
87. Heyman, M. A. & Rudolph, A. Control of the ductus arteriosus. *Physiol Rev* 55, 62-78 (1975).
88. Tristani-Firouzi, M., Reeve, H. L., Tolarova, S., Weir, E. K. & Archer, S. L. Oxygen-induced constriction of the rabbit ductus arteriosus occurs via inhibition of a 4-aminopyridine-sensitive potassium channel. *J. Clin. Investigation* 98, 1959-1965 (1996).
89. Coceani, F., Armstrong, C. & Kelsey, L. Endothelin is a potent constrictor of the lamb ductus arteriosus. *Can J Physiol Pharmacol* 67, 902-4 (1989).

90. Casalaz, D. Ibuprofen versus indomethacin for closure of patent ductus arteriosus. *N Engl J Med* 344, 457-8. (2001).
91. Heymann, M. A., Rudolph, A. M. & Silverman, N. H. Closure of the ductus arteriosus in premature infants by inhibition of prostaglandin synthesis. *N. Engl. J. Med.* 295, 530-533 (1976).
92. De Carolis, M. P. et al. Prophylactic ibuprofen therapy of patent ductus arteriosus in preterm infants. *Eur J Pediatr* 159, 364-8 (2000).
93. Momma, K. & Toyono, M. The role of nitric oxide in dilating the fetal ductus arteriosus in rats. *Pediatr Res* 46, 311-5 (1999).
94. Coceani, F. & Olley, P. M. The response of the ductus arteriosus to prostaglandins. *Can. J. Physiol.* 51, 220-223 (1973).
95. Coceani, F. & Kelsey, L. Endothelin-1 release from lamb ductus arteriosus: relevance to postnatal closure of the vessel. *Can. J. Physiol. Pharmacol.* 69, 218-221 (1991).
96. Coceani, F., Kelsey, L. & Seidiltz, E. Evidence of an effector role of endothelin in closure of the ductus arteriosus at birth. *Can J Physiol Pharmacol* 70, 1061-1064 (1992).
97. Fineman, J., Takahashi, Y., Roman, C. & Clyman, R. Endothelin-receptor blockade does not alter closure of the ductus arteriosus. *Am J Physiol* 44, H1620-H1626 (1998).
98. Michelakis, E. et al. Voltage-gated potassium channels in human ductus arteriosus. *Lancet* 356, 134-7. (2000).

99. Coceani, F. et al. Deletion of the endothelin-A-receptor suppresses oxygen-induced constriction but not postnatal closure of the ductus arteriosus. *J Cardiovasc Pharmacol* 36, S75-7. (2000).
100. Roulet, M. J. & Coburn, R. F. Oxygen-induced contraction in guinea pig neonatal ductus arteriosus. *Circ. Res.* 49, 997-1002 (1981).
101. Nakanishi, T., Gu, H., Hagiwara, N. & Momma, K. Mechanisms of oxygen-induced contraction of ductus arteriosus isolated from the fetal rabbit. *Circ. Res.* 72, 1218-1228 (1993).
102. Tristani-Firouzi, M., Reeve, H. L., Tolarova, S., Weir, E. K. & Archer, S. L. Oxygen-induced constriction of rabbit ductus arteriosus occurs via inhibition of a 4-aminopyridine-, voltage-sensitive potassium channel. *J Clin Invest* 98, 1959-65 (1996).
103. Michelakis, E. D. et al. O₂ sensing in the human ductus arteriosus: regulation of voltage-gated K⁺ channels in smooth muscle cells by a mitochondrial redox sensor. *Circ Res* 91, 478-86. (2002).
104. Thebaud, B. et al. Sildenafil reverses O₂ constriction of the rabbit ductus arteriosus by inhibiting type 5 phosphodiesterase and activating BK(Ca) channels. *Pediatr Res* 52, 19-24 (2002).
105. Archer, S. L. et al. Molecular identification of the role of voltage-gated K⁺ channels, Kv1.5 and Kv2.1, in hypoxic pulmonary vasoconstriction and control of resting membrane potential in rat pulmonary artery myocytes. *J Clin Invest* 101, 2319-30 (1998).

106. Archer, S. L. et al. Impairment of hypoxic pulmonary vasoconstriction in mice lacking the voltage-gated potassium channel Kv1.5. *FASEB J* 15, 1801-3. (2001).
107. Patel, A. J., Lazdunski, M. & Honore, E. Kv2.1/Kv9.3, a novel ATP-dependent delayed-rectifier K⁺ channel in oxygen-sensitive pulmonary artery myocytes. *EMBO J* 16, 6615-25 (1997).
108. Hulme, J. T., Coppock, E. A., Felipe, A., Martens, J. R. & Tamkun, M. M. Oxygen sensitivity of cloned voltage-gated K(+) channels expressed in the pulmonary vasculature. *Circ Res* 85, 489-97 (1999).
109. Osipenko, O. N., Tate, R. J. & Gurney, A. M. Potential role for kv3.1b channels as oxygen sensors. *Circ Res* 86, 534-40 (2000).
110. Reeve, H. L., Weir, E. K., Nelson, D. P., Peterson, D. A. & Archer, S. L. Opposing Effects of Oxidants and Antioxidants on K⁺ Channel Activity and Tone in Vascular Tissue. *Exp. Physiol.* 80, 825-834 (1995).
111. Reeve, H. L., Tolarova, S., Nelson, D. P., Archer, S. & Weir, E. K. Redox control of oxygen sensing in the rabbit ductus arteriosus. *J Physiol* 533, 253-61. (2001).
112. Attali, B. et al. Multiple mRNA isoforms encoding the mouse cardiac Kv1-5 delayed rectifier K⁺ channel. *J Biol Chem* 268, 24283-9 (1993).
113. Kurata, H. T., Soon, G. S. & Fedida, D. Altered state dependence of c-type inactivation in the long and short forms of human Kv1.5. *J Gen Physiol* 118, 315-32 (2001).
114. Overturf, K. E. et al. Cloning and characterization of a Kv1.5 delayed rectifier K⁺ channel from vascular and visceral smooth muscles. *Am J Physiol* 267, C1231-8 (1994).

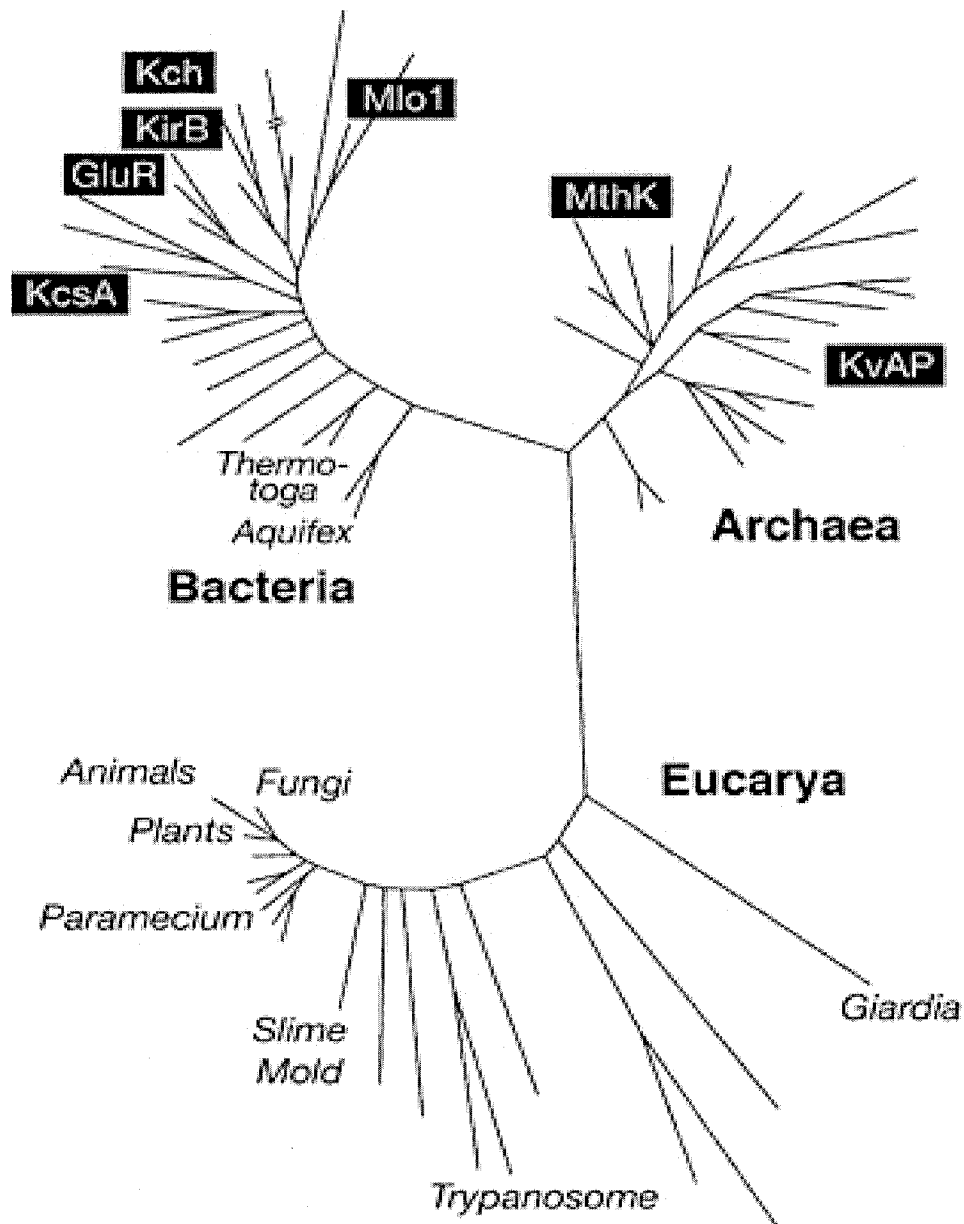


Figure 1: A universal phylogenetic tree based on ssrRNA sequences, showing the three domains of life. Marked are also the K⁺ channels, the crystal structures of which have been fully or partially solved: KvAP (6TM, voltage sensitive) from *Aeropyrum pernix*, a thermophilic archaeon, member of *Crenarchaeota*; MthK (2TM + RCK, Ca²⁺ binding, with a gating ring) from the methanogen *Methanobacterium thermoautotrophicum*, a member of *Euarchaeota*; Mlo1 (6TM + cyclic nucleotide-binding domain) from the soil bacterium *Mesorhizobium loti*, an α -proteobacterium (Gram negative); Kch (6TM + RCK) from *Escherichia coli*, a γ -proteobacterium; KirB (KirBAC1.1) a 2TM inward rectifier from *Burkholderia pseudomalli*, a rice pathogen of the β proteobacterium subdivision; GluR (GluR0) from the photosynthetic bacterium *Synechocystis sp* (cyanobacterium); KcsA (2TM) from *Streptomyces lividans*, an actinobactium (Gram positive). Lengths of the branches indicate differences in the nucleotide sequence of the small subunit ribosomal RNAs as a measure of the relatedness of different organisms. (Adapted from ref 6)

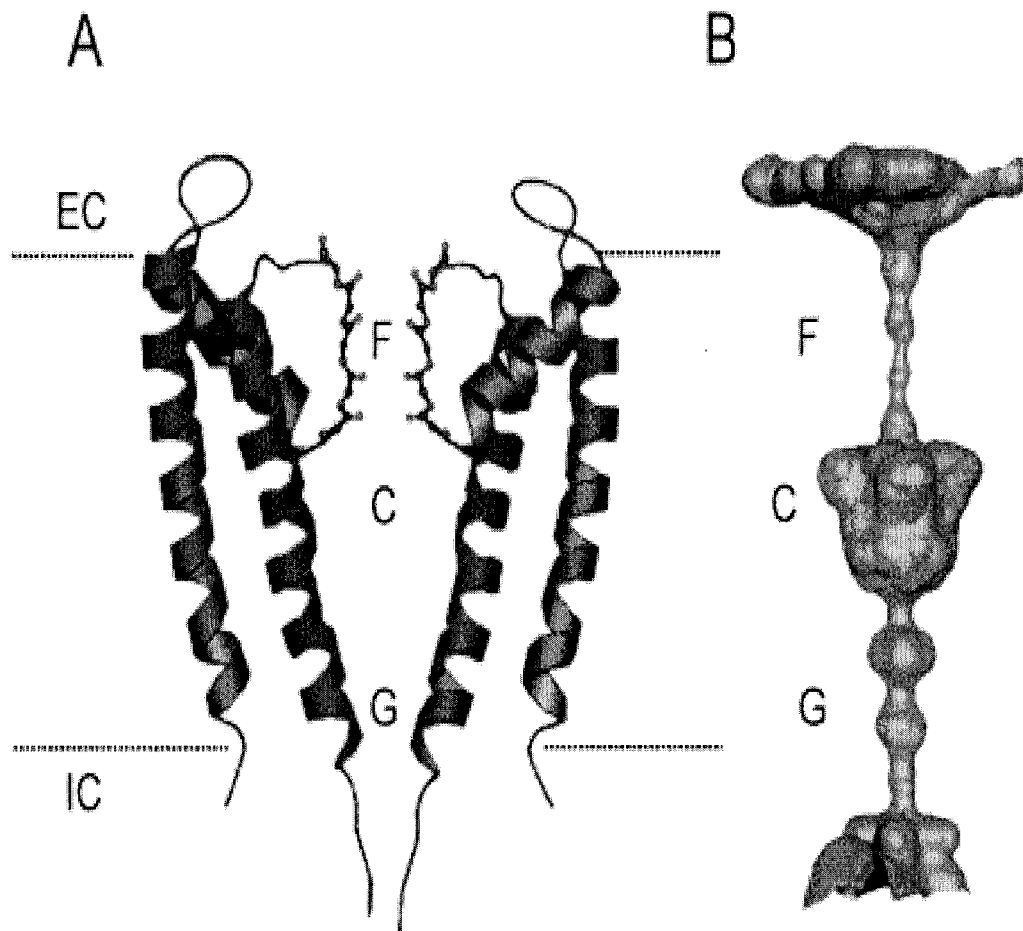


Figure 2: KcsA fold and pore. (A) Two of the four subunits of KcsA, viewed down a perpendicular to the pore axis. The helices are shown as ribbons; all backbone atoms of the selectivity filter are shown in ball-and-stick format. The lipid bilayer is indicated by the horizontal dotted lines. IC=intracellular; EC=extracellular. (B) The pore-lining surface of KcsA showing the filter (F), cavity (C) and gate (G) regions. (Adapted from ref 13)

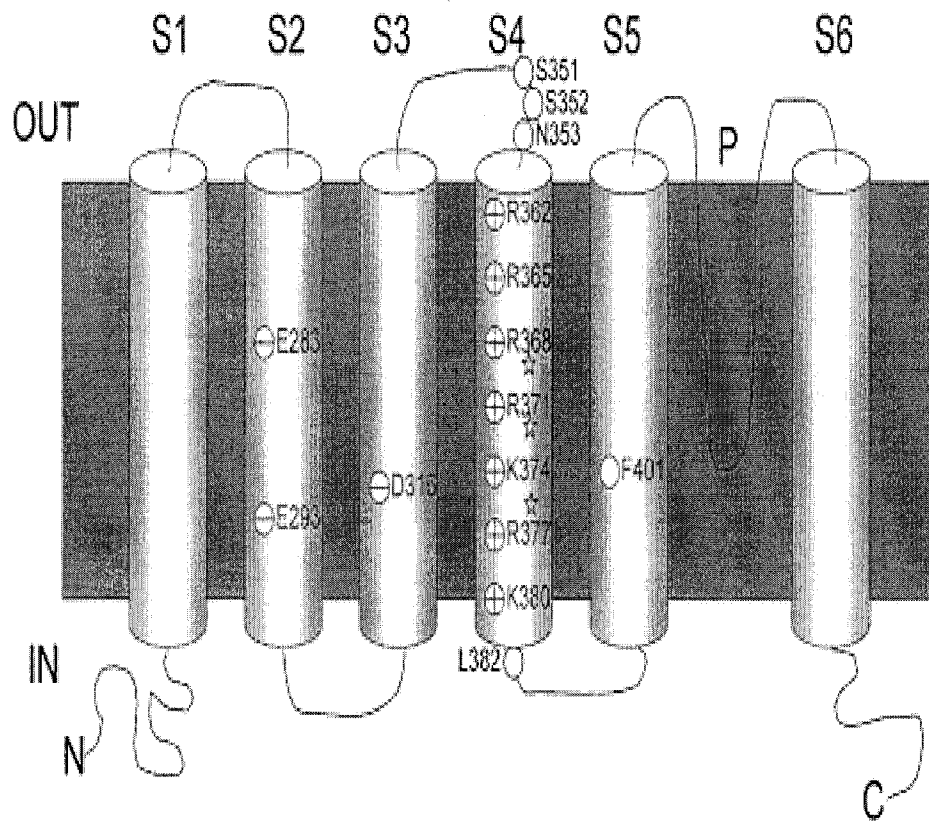


Figure 3: Generalized topology of a voltage-gated potassium channel. The transmembrane helices are labelled S1–S6, P indicates the conduction pore while N and C indicate the N-terminal and C-terminal ends of the channel respectively. Residues indicated correspond to Shaker residues and are denoted by the amino acid single-letter abbreviation followed by the position of the residue in the Shaker amino acid sequence. Positively charged residues are indicated by a "plus sign", negatively charged residues are indicated by a "minus sign" and neutral residues are indicated by an empty circle. The stars within the S4 transmembrane helix denote the positions of the Shaker ILT mutant. Each channel is composed of four of these single transcripts. (Adapted from ref 43)

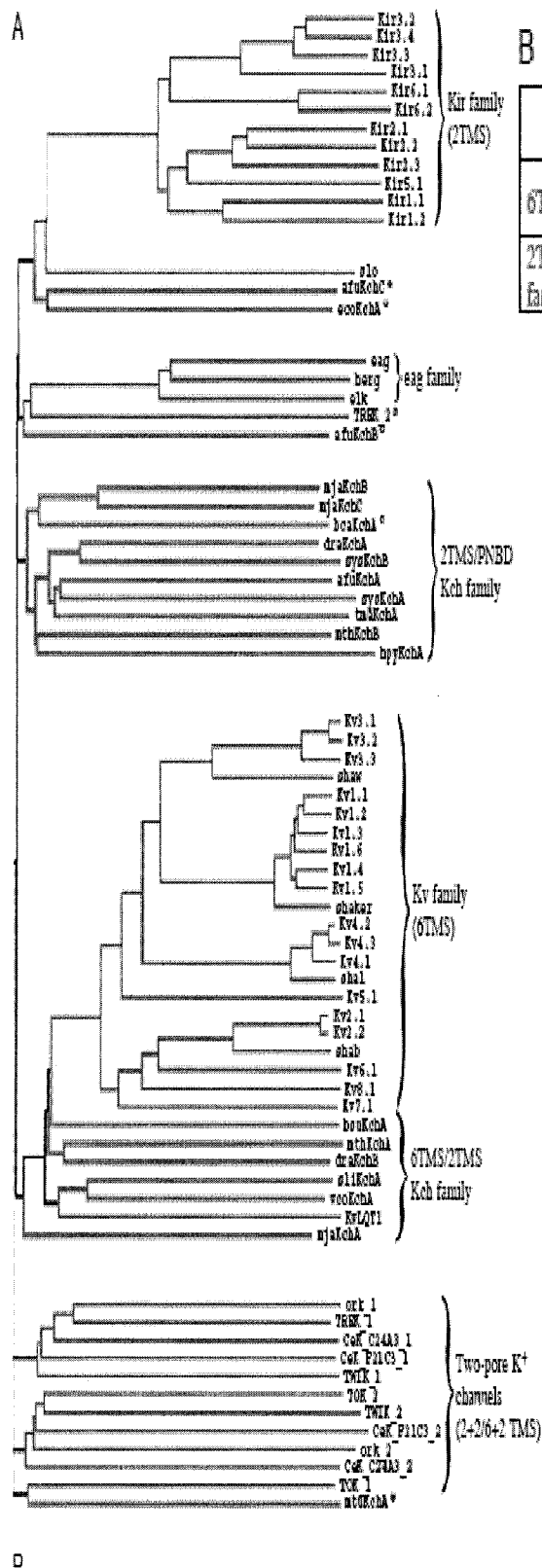


Figure 4: (A) Phylogenetic tree of prokaryotic and eukaryotic K⁺ channel genes. Prokaryotic sequences are in red and eukaryotic sequences in blue. (B) The table shows the percent homology between different channels in prokaryotes and eukaryotes. (Adapted from ref 23)

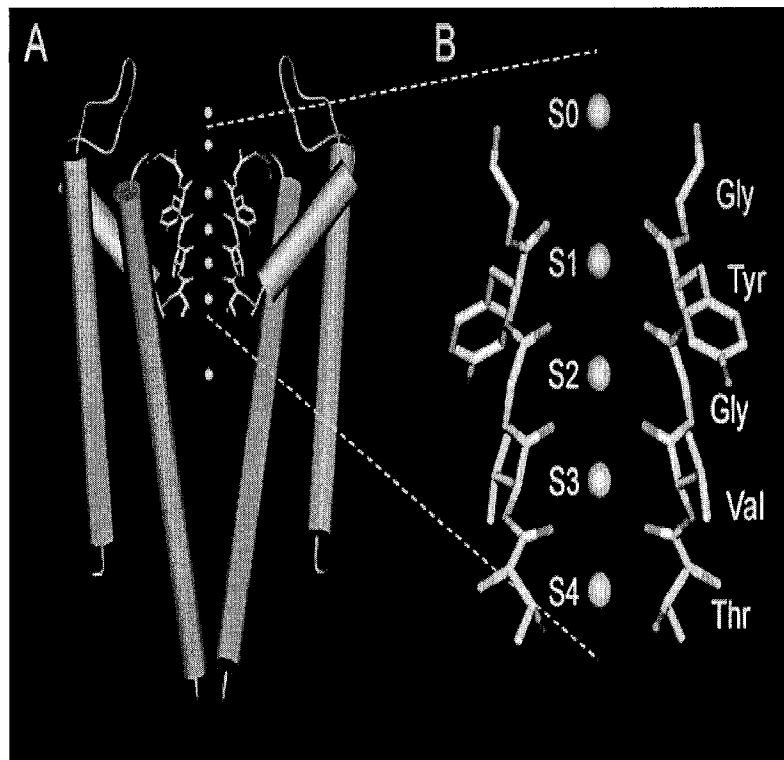


Figure 5: Structure of KcsA in the presence of high $[K^+]$. (A) Two subunits of the four are shown (blue), plus the seven locations of K^+ ions revealed in the X-ray structure. These are (from top to bottom): the external mouth, the five sites (S0–S4) in the filter, and the central cavity. (B) A more detailed view of the selectivity filter, again showing two of the four subunits. Ions at sites S0 to S4 are shown. (C) Schematic diagram of the alternating patterns of occupancy of the selectivity filter by K^+ ions (●) and water molecules (○) that are proposed to underlie rapid permeation of K^+ ions through the KcsA channel. (Adapted from ref 13)

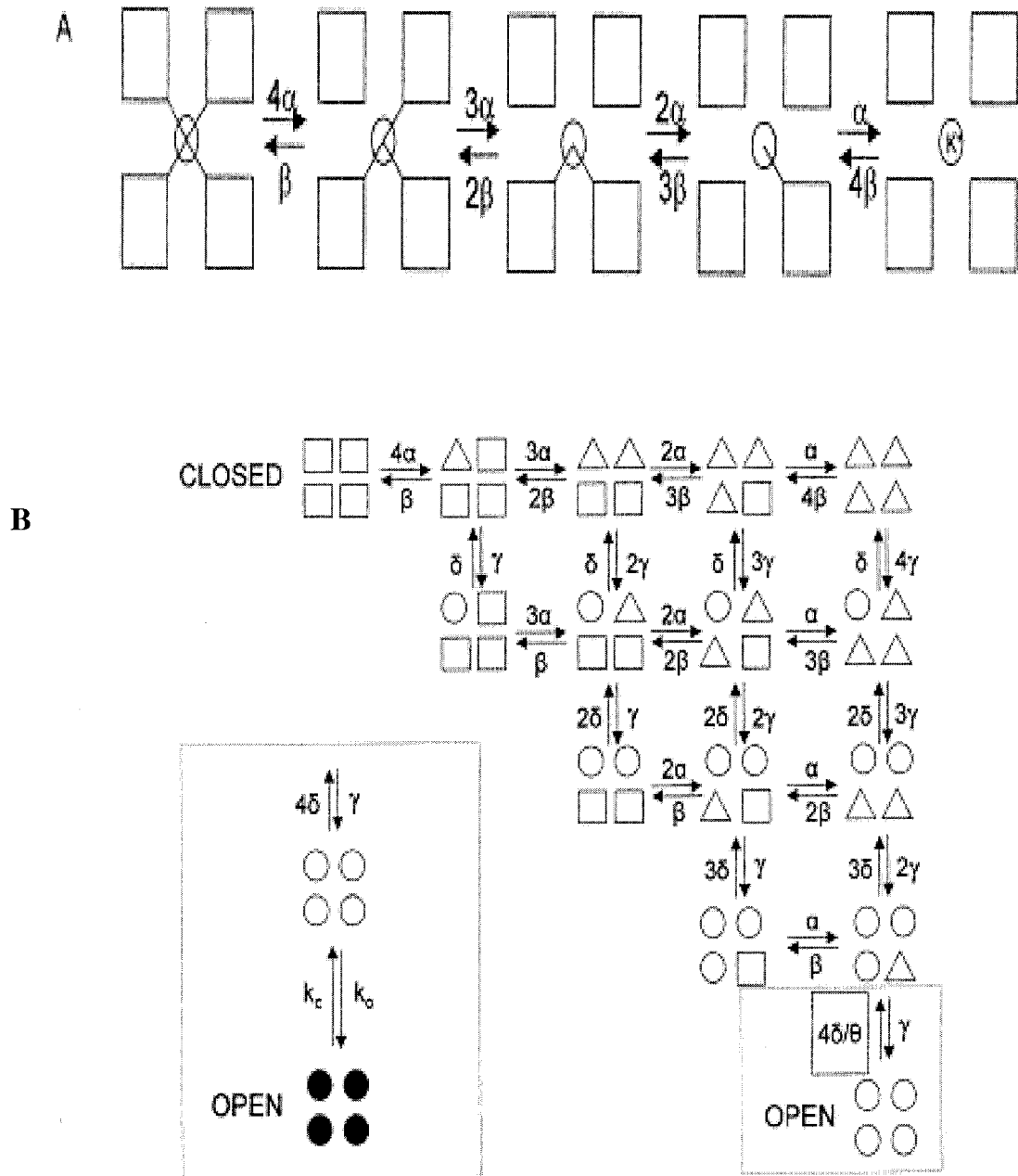


Figure 6: The Hodgkin–Huxley (HH) model of independently gating subunits and predicted ionic and gating currents. (A) Each transition represents the movement of one of the four activation gates. The forwards rate constant, α , and backwards rate constant, β , are scaled as indicated. The final gating state represents the open channel. (B) The Zagotta-Hoshi-Aldrich (ZHA) model of *Shaker* channel activation. Channels progress in a sequential fashion from an initial closed state (denoted by squares) to an intermediate state (denoted by triangles) to a final gating state (denoted by circles). Progression within these gating states is assumed to be independent. (Adapted from ref 43)

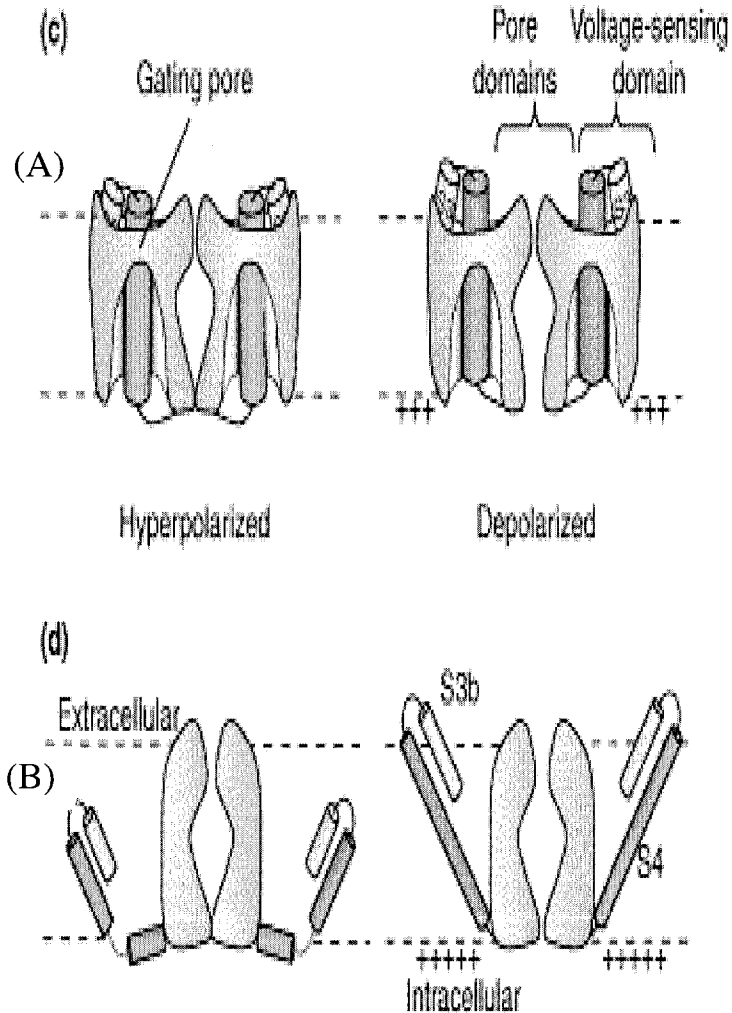


Figure 7: Models of topology and voltage sensor movement. **(A)** Conventional model of voltage sensor movement. Two opposing subunits are shown with the ion permeation pathway between them. Depolarization (right panel) moves the extracellular portion of the S4 segment outwards through a short gating pore, opening the permeation pathway. Most of the S4 segment is surrounded by hydrophilic crevices or vestibules. The transmembrane electric field falls mainly across the short gating pore. **(B)** Paddle model Two opposing subunits are shown. Depolarization (right panel) moves the paddle, the S3b helix and extracellular end of the S4 segment, outwards through lipid, pulling the cytoplasmic activation gate open. (Adapted from ref 78)

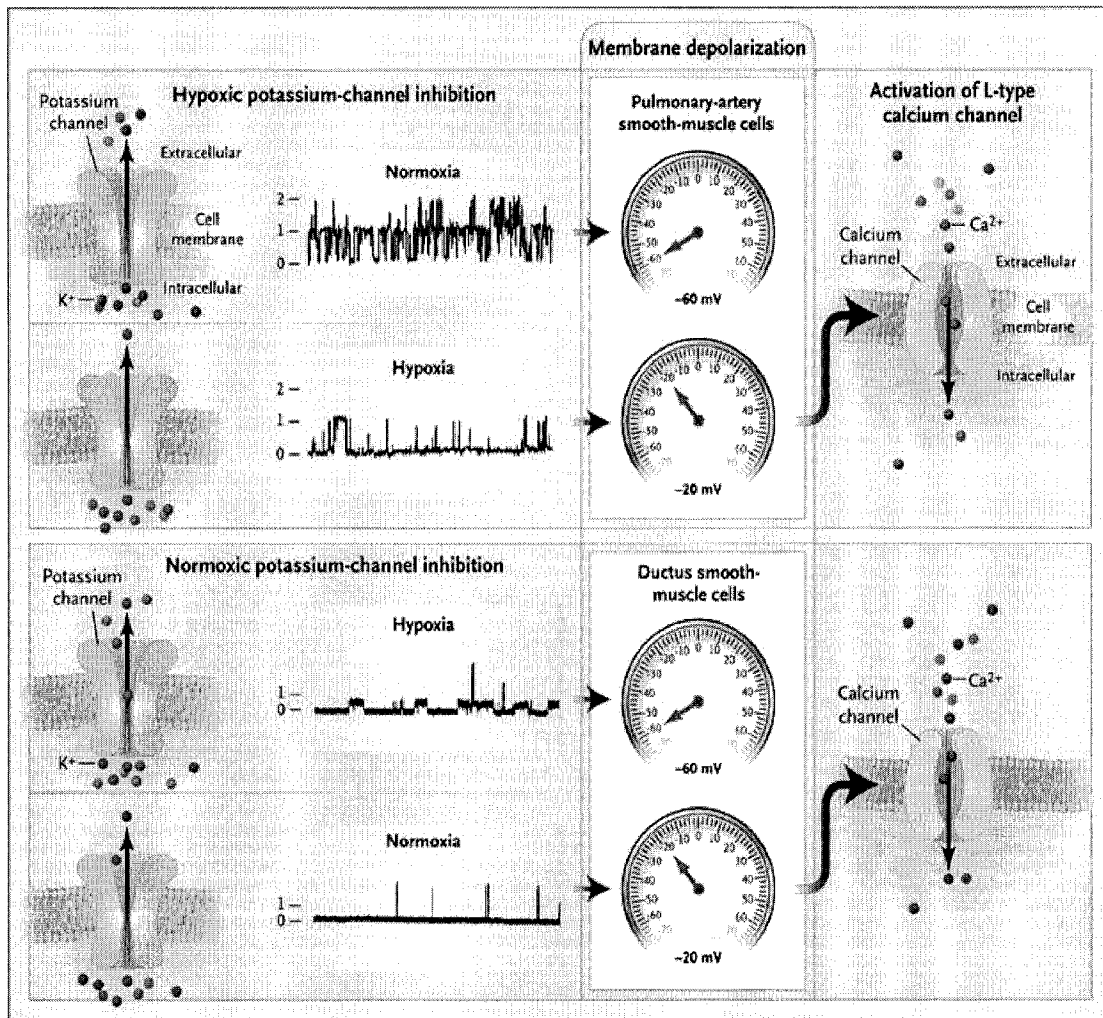


Figure 8. Opposite Regulation of Potassium Channels by Oxygen in Pulmonary-Artery as Compared with Ductus Smooth-Muscle Cells. In the pulmonary-artery smooth-muscle cell (shown in the upper half of the figure) during normoxia, an outward potassium (K^+) current, illustrated by the single channel trace that shows steplike opening and closing, keeps the membrane potential at about -50 mV or -60 mV. This hyperpolarization prevents calcium from entering the cell through the voltage-gated L-type calcium channel. Hypoxia inhibits potassium-channel activity and depolarizes the membrane to about -20 mV, permitting calcium entry. In the ductus smooth-muscle cell (lower half of the figure), by contrast, the outward potassium current is maintained during hypoxia and is inhibited by normoxia. A rise in oxygen, as at birth, then causes membrane depolarization and calcium entry. (Adapted from ref 100)

2.1 INTRODUCTION

Comparative genomic analysis indicates that increases in gene number do not account for rise in morphological and behavioural complexity. For example, the simple nematode worm, *Caenorhabditis elegans*, possesses nearly 20,000 genes¹ but lacks the full range of cell types and tissues seen in the fruit fly, *Drosophila sp*, which contains fewer than 14,000 genes². Indeed, the revelation that the human genome contains only 30,000 protein-coding genes^{3, 4} ignited speculation regarding the molecular basis of organism complexity in light of the lack of its correlation with apparent number of genes.

In principle, there are many ways in which a relatively small number of genes could be utilized to generate progressively more complex organisms over time, at least on an evolutionary timescale. There are a number of mechanisms to confer diversity in proteins with fewer genes such as alternative start sites and different promoters. However, two mechanisms which have been an important source of complexity: (1) DNA rearrangement, where genes themselves are rearranged and (2) alternative splicing (the production of different mRNA species from a given gene during mRNA splicing).

DNA rearrangement or a transposition event (movement of a segment of DNA from one position in the genome to another position (or to a different genome)), creates new mRNA transcripts and thereby produces new proteins within the existing sequence. This involves specialized proteins which translocate introns and exons between loci of the same or different chromosomes. This mechanism is heavily utilized by the mammalian immune system. The multitude of permutations and combinations achieved by gene rearrangement enables the immune system genes to generate a staggering

number of antibodies against diverse array of pathogens, allergens and other foreign bodies. Thus, transposition of genes facilitates the creation of a highly efficient immune system seen in eukaryotes while only relying on a relatively small number of genes⁵.

Another process of creating diversity in genes is by alternative splicing. This process is more of a rule than an exception as it affects the expression of 60% of human genes and it is the predominant mechanism by which mammalian proteomic complexity is achieved with a limited number of genes⁶. Regulation of alternative splicing not only depends on the interaction of splicing factors with their target sequences in the pre-mRNA but is also coupled to transcription. It appears that alternative splicing involves three processing reactions (capping, splicing and cleavage/polyadenylation) which are tightly coupled to RNA polymerase II transcription⁷. The combination of the intrinsic sequence specific signals, the presence of enhancers, silencers and *cis*- and *trans*-acting elements, individually or together, can contribute to alternative splicing⁷. Membrane-associated cytokine receptors are an example of an important family of mammalian proteins that utilize this phenomenon to generate diversity⁸.

Alternative splicing results in production of different mRNA transcripts that can be used to synthesize proteins with similar or different properties than the original transcript. Alternative splicing exposes alternative translation sites within an mRNA transcript that can be utilized to synthesize novel proteins^{9,10}. Initiation of translation on a subset of eukaryotic mRNAs occurs by a 5'-end-independent process of ribosomal attachment that is mediated by an internal ribosomal entry site (IRES) in the mRNA. IRESs, initially described in RNA viruses, are functionally defined by their ability to promote translation of the downstream cistron in a dicistronic mRNA, independent of

translation of the upstream cistron, thus producing a variant of the original protein or a new protein⁹. IRES regions bind the ribosomal translation initiation complex thereby promoting translation without requiring the conventional mechanism (association with the 5'-terminal 7mG cap structure). Whether the attractiveness of an IRES for the initiation complex reflects a conserved sequence versus a common secondary structure remains controversial. This phenomenon involves binding of the 40S ribosomal subunit at or near the authentic start codon (AUG), thereby eliminating the requirement for the presence of a 5' cap structure^{9,11}.

One of the main features required for IRES is the existence of large mRNA (> 4kb) sequence. The large mRNA sequence enables the folding of mRNA into stems and loops thus creating an energetically stable mRNA secondary structure¹². This secondary structure facilitates binding of ribosomes at various sites along the mRNA transcript and thereby producing different proteins in prokaryotes and eukaryotes⁹. Some of the viruses such as hepatitis C virus¹³, cricket paralysis virus^{14, 15} and encephalomyocarditis virus^{15, 16} employ this technique to generate increased proteomic diversity. Mammalian proteins such as c-myc¹⁷ (an important transcriptional factor) and Tie-2 receptor¹⁸ also utilize this mechanism.

In the context of Kv channels, mRNA species contain extensive 5' and 3' - noncoding regions (NCRs) and while these alter mRNA stability (and thus gene expression) their role in Kv expression was unknown. However, a recent paper by Jang et al¹⁹, stimulated by the fact that Kv channels have unusually long 5' -NCRs found that Kv1.4 expression is mediated through a complex interplay between many distinct RNA regions which form IRESs. A list of all known IRES identified within humans and other

animals can be found at (www.iresite.org). This site lists 55 viruses and 78 eukaryotic cellular mRNAs reported to be translated using IRES.

2.2 DIVERSIFICATION OF Kv CHANNEL IN MAMMALS

In *Drosophila*, diversity of the K⁺ channels within a given class arises, in part, from the alternative splicing of the RNA encoding the channels²⁰⁻²⁵. In humans these different Kv channels were initially divided into four distinct classes by virtue of their sequence homology to channels encoded at the *Drosophila* *Shaker* (Kv1), *Shab* (Kv2), *Shaw* (Kv3) and *Shal* (Kv4) loci²⁰⁻²⁵. Despite the nomenclature based on the alternative splicing in *Drosophila*, mammalian K⁺ channels were thought to be result in an expression from an intronless coding region and therefore diversity among the Kv channel was attributed to gene duplication and divergence²⁶⁻²⁸. However, subsequent studies showed the alternative splicing did occur in Kv channels, primarily in 5' and 3' untranslated regions^{29, 30}. More specifically, studies with Kv3.1 showed that two different transcripts were produced by alternative splicing named, α and β , which differed in their regulation during development³¹. The Kv3.1 α transcript was primarily found in the neurons of adult rat brain while the β isoform predominated in embryonic and perinatal neurons³¹. Alternative splicing is also utilized to produce two different isoforms of Kv4.3 which not only differ in the location in which they are expressed (smooth muscle vs cardiac muscle) but in the sequence of the expressed protein (the smooth muscle cell variant has an extra 19 amino acids that confer more sensitivity to the inhibitory effects of arachidonic acid³²). In other channels such as Kv1.5³³ and Kv3.4³⁴, splicing creates channel with different electrophysiological properties.

2.3 ALTERNATIVE SPLICING AND HOSK CHANNEL

This chapter highlights that the mammalian system employs diverse molecular tactics to create HOSK channel, like previously mentioned Kv channels. Our data indicate that the HOSK is produced from the collagen $\alpha 2(I)$ (COL1A2) transcript. We postulate that COL1A2 mRNA undergoes alternative splicing and the resulting transcript exposes putative IRES sites. These IRES sites provide template for HOSK protein synthesis. This chapter outlines the current understanding of HOSK from a molecular biology perspective and provides some insights into its regulation at the transcriptional and post-transcriptional level.

2.4 MATERIAL AND METHODS

2.4.1 Human DA cDNA

All the procedures and the practices were conducted in accordance to the guidelines set by Animal Welfare Committee and Human Ethics Committee of University of Alberta, Edmonton. DAs excised from 11 neonates suffering from congenital heart defect and undergoing palliative surgical repair were used for our studies. Freshly isolated DA that had not been used for other experiments and which had been maintained in -80°C were used for RNA isolation. Total RNA (RNeasy, Qiagen, Mississauga, Ontario) was isolated from human DA as per manufacturer's protocol. Reverse transcription was performed by Omniscript RT Kit (Qiagen, Mississauga, Ontario).

2.4.2 Plasmids

In an attempt to isolate splice variants of Kv1.5 from DA cDNA using low stringency PCR, control primers (Kv1.5 sense complement primer 5'...TACCTCTAGCGGGACCAC...3') resulted in serendipitous isolation of a 1.4 kb fragment, which yielded an unidentified clone corresponding in sequence to the expressed sequence tag (EST) library clone (BU 838453; dEST Id: 14311426; Clone Id: IMAGE: 6177087). This clone was purchased from Open Biosystems Huntsville, Alabama. To verify if the EST clone was a full transcript, rapid amplification of 5' complementary DNA (cDNA) ends were carried on human DA cDNA according to the

manufacturer's specification (Roche, Indianapolis, Indiana). The gene-specific antisense oligonucleotide for the EST was designed and used in conjunction with abridged universal amplification primer (AUAP) as an anchoring primer. Although at that time we thought that we had a complete clone (as determined by presence of new methionine upstream), subsequent *in silico* analysis highlighted that the clone was partial and the starting methionine was ~100 amino acid upstream; discussed in chapter 3. The resulting clone was digested with Not I and Sal I and inserted in pTracer-CMV (Invitrogen, Burlington, Ontario). pTracer-CMV is a vector that requires the presence of kozak sequence and putative start codon in the cDNA insert for the successful expression of the protein. The directional cloning was confirmed by Nru I restriction digest. Transfection in CHO cells and COS cells was performed with Fugene 6 transfection reagent (Roche, Indianapolis, Indiana) following the manufacturer's specifications.

2.4.3 Northern Blot

Total RNA was extracted from DA, PA, DASMC and PASMCM using RNeasy Mini Kit (Qiagen, Mississauga, Canada) and quantified with UV spectrophotometry. Northern blots were performed using formaldehyde agarose gel electrophoresis under reducing conditions. The gel was transferred to Hybond-N nylon membrane (Amersham Biosciences, Piscataway, New Jersey USA) and ultraviolet crosslinking (Fisher Scientific, Nepean, Ontario) was used for binding RNA to the membrane. Probes were synthesized by PCR, purified with PCR purification kit (Qiaquick PCR purification kit, Mississauga, Ontario) and radiolabelled with ³²P by ready-to-go DNA labeling beads (Amersham Biosciences, Piscataway, New Jersey USA). The radiolabelled probe was

isolated with G25 microspin columns (Amersham Biosciences, Piscataway, New Jersey USA). The blot was hybridized in Express Hyb (BD Biosciences, Mississauga, Ontario). After sequential washing, the blots were exposed to autoradiography. For human mRNA expression screening of non-PA and DA tissues, a human 12-lane multiple tissue blot (MTN; BD Biosciences, Mississauga, Ontario) was used.

2.4.4 Immunoblot

Immunoblotting was performed on transfected CHO cells, primary cultures of DASMCs and the proteins isolated from human heart. Briefly, equal amounts of protein from clear homogenate (as determined by Bradford protein assay) were resolved by sodium dodecyl sulphate-polyacrylamide gel electrophoresis (SDS-PAGE) and transferred to nitrocellulose membrane. Membrane was probed first with collagen 1 alpha 2 antibody (Abcam, Cambridge, MA). Blots were then probed with a horseradish peroxidase-coupled goat anti-rabbit secondary antibody (MP Biomedicals, Aurora, Ohio). All the aforementioned antibodies were used at a concentrations recommended by the manufacturer. Blots were developed using enhanced chemiluminescence's reagent (PerkinElmer Life Sciences, Boston, MA).

2.4.5 Fluorescence In Situ Hybridization

Human chromosome arrested in metaphase was generous gift from the University of Alberta Cytogenetic laboratory. The chromosomes were arrested by adding 0.5 μ g of colcemide to 5ml of blood cell culture. The human chromosomes were counterstained with 4', 6 diamidino-2-phenylindole, dihydrochloride (DAPI; Invitrogen, Burlington,

Ontario). The cDNA probe was prepared by ARES DNA labeling kit (Invitrogen, Burlington, Ontario) according to manufacturer's specifications. Briefly, amine-modified UTP (5-(3-aminoallyl) deoxy-uridine triphosphate) was incorporated in the cDNA probe. The amine-modified cDNA was purified and incubated with reactive Alexa Fluor 488 dye. For hybridizations, PerfectHyb (Sigma, Oakville, Ontario) hybridizing solution was used and the probe was incubated with the slides containing human chromosomes in the humidifying chamber at 68⁰C for 2 hours. The localization of the probe on the chromosome was captured by 2-photon confocal Microscopy (Carl Zeiss, Jena, Germany). For the identification of chromosome 7, CEP7 (D7Z1; Abbott laboratories, Downers Grove, Illinois, USA) a highly specific probe against centromeric region was used.

2.4.6 *In silico* analysis

In silico analysis such as nucleotide NCBI-Basic Local Alignment Search Tool (BLAST) was performed. For IRES analysis, DNA Strider 1.2.1 was used. MFOLD analysis was also performed on the COL1A2 transcript. MacVector (Accelrys San Diego, CA, USA) was used to align the COL1A2 mRNA sequences from various species.

2.5 RESULTS

We report the characterization of a novel human K⁺ channel, HOSK. The full length cDNA, and the 1.4 kb sequence originally isolated from the DA, are shown in Figure 1 with the coding regions of HOSK channel. The isolation of this cDNA was a serendipitous finding as in the course of searching for Kv1.5 splice variants, we isolated a 1.4 kb fragment from term human DAs (Figure 2) with a sense complement primer of Kv1.5. The sense primer was intended as a “negative control” but we noted that it consistently yielded a 1.4kb band in DA but not in PAs. Subsequent analysis showed that the complement sense primer sequences of Kv1.5 matched with HOSK cDNA sequence at 5' and 3' end outside of the protein-coding region (Figure 3) signifying that a single primer attached itself to the 5' and 3' ends of the HOSK. To further substantiate that the sequence isolated is not Kv1.5, qRT-PCR with human and rat Kv1.5 probe were used to detect Kv1.5 mRNA transcript in CHO cells transfected with HOSK. As expected both human and rat Kv1.5 isotype were significantly low (background) in HOSK transfected CHO cells, however, as a positive control for our qRT-PCR, Kv1.5 was detected in CHO cells infected with human Kv1.5 adenovirus and rat PSMCs (data not shown). The full length HOSK cDNA corresponds to a 3.0 kb expressed sequence tag (EST) isolated from the dorsal root ganglia of a 36 years old adult male.

Surprisingly, the sequence of HOSK shares 100% identity with the C-terminus of COL1A2. The HOSK cDNA corresponds to the mRNA sequence of COL1A2 in the region of +1973 to +4842 bp (Figure 5). This represents the last 29 exons out of 58 exons used to encode collagen 1A2 protein. A nucleotide BLAST search shows the presence of numerous predicted genes at the 3' end of collagen gene. This suggests that COL1A2 is a

hotspot for overlapping genes. The histogram on the scale signifies the putative number of genes present at that location (Figure 6). The deduced amino acid sequence of the transcript sequence of HOSK bears no similarity to the collagen or any other known protein as determined by NCBI-BLAST. Furthermore, immunoblotting of cell lysates from CHO cells transfected with either empty vector, pTracer-CMV or with HOSK channel and DASC shows no collagen protein (Figure 7). Protein isolated from human heart was used as a positive control. Moreover, in silico analysis of 5' untranslated regions suggest the presence of four IRES (-628, -539, 163 and -93) upstream of HOSK cDNA sequence (Figure 8). The 3' untranslated region showed the presence of an AU rich region (Figure 9). Modified MFOLD analysis suggests that COL1A2 transcript exists as a secondary structure with the Gibbs free energy of -1323.7 kcal/mol (Figure 10). Importance of folding of mRNA is that it exposes IRES and thus encodes on new protein and in our case it is HOSK channel.

The HOSK gene is located on chromosome 7, as confirmed by fluorescence in-situ hybridization (Figure 4). Northern blots on a panel of human tissues, performed with the 1.4 kb HOSK and COL1A2 probe, detected two bands in human DA, and placenta (Figure 11), whereas in other tissues such as heart, skeletal muscle, colon, thymus, spleen, kidney, liver, and lung only a single transcript was present. No transcripts were found in brain and white blood cells (Figure 11). Furthermore, we looked at qRT-PCR of different tissues with COL1A2 probe and HOSK channel. We found that collagen transcript was present in human DA, hDASC and placenta. Not surprisingly, a similar profile was shown with HOSK probe since the cDNA is identical to COL1A2. In utero the DA is hypoxic ($PO_2 < 40\text{mmHg}$); incubation of human DASCs for 48 hrs at PO_2

(120 mmHg) decreased HOSK transcript levels, signifying the oxygen-sensitivity of its expression (Figure 12).

2.6 DISCUSSION

The HOSK channel has a mRNA sequence of 510 bps originally isolated with complement sense primer of human Kv1.5. The nucleotide NCBI-BLAST showed a near identity with COL1A2, which was later confirmed by the identification of HOSK gene on chromosome 7 using fluorescent in situ hybridization. Northern blot analysis, using 1.4 kb probe for HOSK channel and 1.0 kb fragment of COL1A2 cDNA, identified two mRNA transcripts in DA, placenta and to a lesser extent in small intestine. However, other adult human tissues such as heart, skeletal muscle, colon, thymus, spleen, kidney, liver, and lung showed one transcript and brain and white blood cells did not express any transcripts. Normoxia (PO_2 120 mmHg) resulted in downregulation of the transcript signifying the oxygen-sensitive regulation of the HOSK mRNA. Moreover, to determine if transfection of HOSK produced collagen protein, immunoblotting was performed with antibody against the C-terminus of the collagen. Immunoblots showed no expression collagen protein in the transfected CHO cells with HOSK or in the human DASMCS, while COL1A2 was expressed in human hearts, which we used as a positive control. Prior studies have shown that transcriptional regulation of COL1A2 produces two different transcripts (one a full length transcript generating collagen; the other an alternatively spliced transcript yielding a new protein-which the authors did not characterize)³⁵⁻³⁷. Our contention is that the alternatively spliced COL1A2 mRNA serves as a template for HOSK protein, likely by exposing IRES sites. A brief description of this regulation is outlined below.

2.6.1 Transcriptional regulation of COL1A2

Early studies revealed that chondrogenesis, the differentiation of mesenchyme into cartilage, involves the synthesis of COL1A2³⁸. However, dissociation existed between the fibroblasts and the chondroblasts as the latter cell type showed the presence of COL1A2 mRNA but lacked the associated protein synthesis³⁹⁻⁴¹. This observation resulted in studies to identify pathways which would explain the tissue-specific expression of COL1A2 protein. Studies demonstrated that COL1A2 has two transcripts: a full length transcript that encodes COL1A2 protein and an alternatively splice variant that produces various noncollagenous proteins^{35, 36, 42}. The alternative splice variant uses a transcriptional start site within intron 2 of the COL1A2 gene, replacing exons 1 and exons 2 with exon A^{36, 37}. Exon 1 and 2 contain a 5'-untranslated region and the first 27 amino acids of the encoded COL1A2 subunit (the signal peptide and the beginning of the amino terminal propeptide)^{36, 37}. This omission of the first intron in COL1A2 has also been documented to occur in humans⁴³. The presence of two different transcripts is due to the utilization of two different promoters³⁶.

There is precedent for genes having two promoters that are utilized in a tissue-specific manner. Both α -amylase^{44, 45} and dihydrofolate reductase⁴⁶ have more than one promoter and these promoters reside in the 5'-flanking portion of these genes, and as a consequence of differential promoter activation the genes (which do not differ within the coding regions), yield different mRNA products. Examples in which the second promoter occurs in an intron are of two types. One type, such as occurs in the acetyl-CoA carboxylase⁴⁷ and carbonic anhydrase I genes⁴⁸, results in changes to the 5'-untranslated region of the mRNAs, but does not alter the structure of the resulting proteins. The other

type, however, produces multiple forms of the protein, as occurs with tropomyosin⁴⁹ and the myosin light chain 1 and 3 genes⁵⁰ in *Drosophila*.

In COL1A2, there are two promoter sites. The COL1A2 predominates in fibroblasts while chondrocytes have both the parent COL1A2 and alternatively spliced COL1A2. For alternatively spliced COL1A2, the major transcription initiation site in chondrocytes (at +2353) is preceded by an imperfect TATA box (TGTAAG) and a CCAAT box, located 25 and 73 nucleotides, respectively, upstream from the major start site³⁶. To determine whether this is a functional promoter in chondrocytes, a 2266-bp DNA fragment extending from +130 in exon 1 through +2397 in exon A was introduced into the multiple cloning site of the plasmid p0CAT (plasmid with chloramphenicol acetyltransferase as a reporter gene) to create the plasmid C1⁴². This plasmid directed a significant level of CAT activity in cultured chondrocytes, 5.2 times higher than a construct containing the same DNA fragment in the reverse orientation. These results indicate that this DNA fragment constitutes a functional promoter and appears to contain most or all of the sequences that are necessary for expression in these cells⁴². Furthermore, a successive cleavage of promoter regions narrowed down a 179-bp subdomain that essential for alternatively spliced COL1A2 mRNA synthesis. This subdomain lies 152 bp upstream from the major internal transcription start site at the beginning of exon A⁴². It contains potential binding sites for numerous transcription factors, which may play a role in the chondrocyte-specific activation of this internal promoter. For example, there are three potential binding sites for the basic/helix-loop-helix class of transcription factors, which play important roles during myogenesis⁵¹, and five sites for binding of GATA-1⁵² and NF-E1⁵³, members of the GATA class of

transcription factors, which regulate hematopoiesis⁵⁴, as well as other developmental programs. In addition, there is a binding site for NF-IL6⁵⁵, which plays a role in adipogenesis⁵⁶ and transactivates the mouse 1(I) collagen gene⁵⁷, as well as two binding sites for TCF1⁵⁸, a member of the *Ets* family of transcription factors⁵⁹. The clustering in this relatively small region of binding sites for several transcription factors known to be involved in other cell differentiation pathways suggests that some of these proteins may be involved in the developmental control of the internal promoter of the COL1A2 gene. Thus, it was demonstrated that the presumptive internal promoter of the COL1A2 gene is not only functional, but is also more active in chondrocytes than in fibroblasts, suggesting that its function is cell type-specific.

This preferential activity of a second promoter in chondrocytes results in the replacement of first two exons with exon A, producing a transcript that does not encode COL1A2^{35, 36}. Instead, the alternatively spliced COL1A2 mRNA contains at least four open reading frames that are out of frame with the collagen coding sequence. Studies have shown that the alternative transcript of COL1A2 mRNA is present in cartilage and associates with chondrocytes ribosomes³⁵. In elegant experiments using puromycin (an aminoacyl tRNA analogue⁶⁰, which serves as an acceptor of nascent peptide chain⁶¹ causing it to be prematurely released from the polysomes⁶²), it was shown that this alternatively spliced COL1A2 mRNA indeed forms a template for active protein synthesis. The polysomes attached to COL1A2 form peptide bonds with puromycin, suggesting that they are actively engaged in protein synthesis³⁵. Thus, inhibition of elongating peptide in presence of puromycin suggests that the alternatively spliced COL1A2 mRNA transcript is involved in active protein synthesis. However, the protein

product from alternatively spliced COL1A2 has never been identified or the predicted sequences not been analyzed.

In addition, studies were carried out to identify the number of ribosomes associated with the translation of alternatively spliced COL1A2 mRNA transcript. To that end, low concentration of cycloheximide was used to reduce the rate of the peptide chain elongation so that elongation rather than initiation⁶³, becomes the rate-limiting step for translation of cellular RNA molecules^{64, 65}. Under these conditions most ribosome-associated RNA molecules, no matter at what speed the polymerase initiate translation which will accumulate ribosomes. This accumulation of ribosomes onto the RNAs can be detected in sucrose gradients by a shift of the RNAs from their original position to a region containing heavier polysomes. The number of ribosomes (three or four) that associate with the alternatively spliced COL1A2 mRNA in chondrocytes is small for a large mRNA (approx 4400-4900 bases prior to polyadenylation)^{37, 66}. However, this small number of ribosomes is consistent with the translation of the 71-amino acid peptide which these investigators identified during the experiments. In fact, polysomes with an average size of four or five ribosomes associate with the β -globin mRNA (146 amino acid) in rabbit reticulocytes⁶³. Thus, a putative 71-amino acid protein encoded for by the cartilage COL1A2 mRNA may well be synthesized in chondrocytes. In depth analysis of the 71-amino acid, produced by the second open reading frame (ORF) of the cartilage alternatively spliced COL1A2 mRNA, has a number of interesting characteristics³⁶. First, the protein is completely unrelated to collagen in amino acid sequence since the coding sequence is out of frame with the collagen. Second, the protein appears to be very basic (predicted pI of 10.33) and with basic-loop-helix structure it suggests a possible role of

this protein in nucleus. Furthermore, this variant of COL1A2 mRNA is also present during chicken embryogenesis. Studies have shown that this variant is present in neuroectoderm; at a time when chondrogenesis has not been developmentally initiated (and thus when collagen protein synthesis is not expected)⁶⁷. This implies that perhaps alternatively spliced COL1A2 transcript might act as a template for synthesis of other proteins. Thus, alternatively spliced COL1A2 mRNA transcript provides a template for translation of another protein and we believe a similar mechanism is occurring to generate HOSK.

We postulate that HOSK channel is also a translational derivative of alternatively spliced COL1A2 mRNA transcript. We refer to this concept as a “gene within a gene” and it explains how HOSK remained hidden. Our finding of a HOSK gene within a gene is consistent with the discovery that the genome contains almost 800 overlapping genes⁶⁸ of which ~100 are present on chromosome 7⁶⁹. In fact region of 7q21-22 (the locus of the collagen and HOSK genes) is a hotspot for overlapping genes, as determined by NCBI BLAST-2-Seq.

There are numerous examples of eukaryotic proteins being produced by virtue of a gene within gene. Isolation of genomic fragments have shown that calcium camodulin (CaM) kinase are present in the cerebellar granule cells and caldesmon mRNAs are derived from the same genetic sequence through alternative splicing of exons, and through alternative transcription initiation sites⁷⁰. This highlights the concept of gene within a gene, and shows how two proteins with different functions and amino acid sequences can derive from a single gene⁷⁰. Other examples include very-long-chain acyl-CoA dehydrogenase (VLCAD), an enzyme catalyzing the first step in mitochondrial beta-

oxidation of long-chain fatty acids⁷¹. During analysis of the VLCAD promoter, it was discovered that another gene, discs-large-related 4 (DLG4)⁷², overlaps VLCAD but is transcribed in the opposite direction. Furthermore, a novel DNA endonuclease named DLAD (DNase II-Like Acid DNase) was identified in humans. Interestingly, sequence analysis of DLAD showed that the 1st exon of the urate oxidase gene, UOX, is located on the opposite strand in its 5'-flanking region of DLAD. Promoter analysis revealed that the intergenic region between DLAD and UOX has bidirectional promoter activity⁷³, i.e., activation of a promoter induce mRNA expression of both DLAD and UOX. Thus, ample precedent exists that multiple proteins can be produced from one gene, as we have found with HOSK and the COL1A2 gene.

2.6.2 Putative mechanism involved in translation of HOSK channel

Repression of COL1A2 synthesis involves partial suppression of the upstream promoter of the COL1A2 gene and activation of an internal promoter, resulting in production of an alternative transcript that does not encode collagen due to the change in the translational reading frame. There are two unusual structural features in the 5'-untranslated region of chondroblast COL1A2 mRNA that suggest the capacity to produce two types of protein, as a result of translational regulation. This region contains two short open reading frames upstream from the major translation start site, as well as an inverted repeat sequence with the potential for forming a the stem loop structure. Both the major translation start site and the AUG codon for the second open reading frame appear in the stem of this potential secondary structure in a cell-type specific manner. This secondary structure could prevent synthesis of COL1A2 during chondrogenesis⁷⁴.

Additional evidence suggests that COL1A2 mRNA has secondary structure that regulates the resulting protein produced. The 5' untranslated region (UTR) of zebrafish COL1A2 shares some characteristics seen in mammals: a highly conserved region, with three ATG codons corresponding to three independent open reading frames, each being ended by stop codons⁷⁵. The two ATG codons upstream of the initiation ATG severely depress initiation of translation of the authentic start codon. A second feature of the 5' UTR suggests that sequences surrounding the start codon are folded into a stem-loop structure consisting of a lower stem, a first loop and an upper stem closed with a short loop⁷⁵. This stem-loop structure plays a regulatory role in the mRNA translation⁷⁶. Such regulation could be tissue specific, as suggested by the ubiquitous presence of COL1A2 mRNAs in various tissues, although selective in the protein expression. Thus, a similar mechanism might exist in mammalian system

To further assess this possibility, we used MFOLD on alternatively spliced COL1A2 mRNA's secondary structure. MFOLD utilizes an empirical based algorithms that estimates the thermodynamic existence of stable conformation of long mRNAs in vivo^{77, 78}. MFOLD analysis suggests a secondary structure characterized by stems and loops with the Gibbs free energy of -1323.7 kcal/mol signifying a stable configuration of COL1A2 secondary structure. This is consistent with the probable occurrence of a secondary structure within COL1A2 mRNA. This structure may be involved in the regulation of expression of HOSK and COL1A2 in vivo. The most interesting feature is that the sequence of HOSK is present at the base of the stem of one of the loops and hence, is not hindered from the interaction with the translational machinery (as it would have been had it appeared within the loop itself). Studies have shown that the three

dimensional RNA fold, rather than its primary sequence, is the major determinant of IRES function⁹. To operate as an IRES, an RNA should form a structural scaffold in which precisely positioned RNA tertiary structures contact the 40S ribosomal subunit through a number of specific intermolecular interactions¹². Although IRES activity was originally thought to be conferred by the 3' 208 nucleotides of some genes¹⁹, it has been also proven to be conferred by the upstream 1.0 kb¹⁹.

Given the fact that Gibbs free energy shows a very stable conformation of alternatively spliced COL1A2 mRNA, the presence of putative IRES might trigger HOSK synthesis, perhaps allowing for its synthesis only in a specific tissue or at specific times in development. Therefore, we performed in silico analysis for the IRES. Genomic analysis showed presence of four putative IRES sequences⁷⁹⁻⁸¹ upstream of the HOSK channel coding region. We found four putative IRES sequence that can initiate the translation of HOSK channel on the COL1A2 template while no IRES putative sequence was detected downstream of the HOSK start codon. This is important as it suggests that COL1A2 transcript might act as a template for the internal ribosomal binding site and thereby produces HOSK channel. Together, our data suggests that COL1A2 mRNA transcript exists as a secondary structure that exposes putative IRES that starts the RNA translation that produces HOSK, independent of the conventional 5' stimulated mechanism.

Similar to the HOSK channel, Kv1.4 also employs IRES for its protein synthesis. It seems that the mammalian Kv1.4 voltage-gated potassium channel mRNA contains an unusually long (1.2 kilobases) 5'- UTR and includes 18 AUG codons upstream of the authentic site of translation initiation⁸². Computer-predicted secondary structures of this

region reveal complex stem-loop structures that would serve as barriers to 5' to 3' ribosomal scanning¹⁹. These features suggested that translation initiation in Kv1.4 also occurs by the internal ribosomal entry, a mode of initiation employed by a variety of RNA viruses but only a limited number of vertebrate genes and potentially to HOSK¹⁹.

2.6.3 Other features of HOSK channel sequence

In addition to the 5' IRES, another interesting feature of the HOSK sequence is its 3' AU-rich region. AU-rich elements (AREs) were first discovered in the 3' UTR of several cytokine and oncoprotein genes⁸³. In mammalian cells, the AREs were identified by their ability to target host mRNAs towards rapid degradation^{84, 85}. These AREs recruit tristetraprolin protein that facilitates binding of poly A ribonuclease that enables cleavage of poly A tail from the transcript. Specifically, genes that require a very precise control of their spatial and temporal expression patterns, in addition to a transcriptional control, harbors regulation of the translation by virtue of influencing stability of the mRNA and such genes employ AREs^{84, 85}. AREs are composed of a variable number of copies of the AUUUA pentamer or UUAUUUAUU nonamer⁸⁶. The list of mRNAs bearing such elements has since then greatly expanded, revealing that ARE-containing mRNAs encode a wide repertoire of functionally diverse proteins^{87,88}. Based on the number and distribution of the AUUUA pentamer they contain, AREs have been classified into three categories. Class I AREs are characterized by the presence of one to three pentamers that are distributed within a large part of the 3'UTR, coupled with a nearby U-rich region. Class II AREs have at least two overlapping copies of the nonamer UUAUUU(U/A)(U/A)U in a U- rich environment and class III AREs do not contain any

pentamers, but have U-rich stretches. In our case, HOSK belongs to class III AREs. This AU-rich area enables tristetraprolin, a CCCH tandem zinc finger protein that binds to ARE-containing transcripts and destabilizes them by promoting the removal of their poly (A) tails⁸⁹. Thus, presence of ARE in HOSK might cause the transient existence of alternatively spliced COL1A2 mRNA transcript. In fact earlier studies have shown that alternatively spliced COL1A2 mRNA transcript is transient in its existence⁴².

Recently studies have shown that the alternatively spliced COL1A2 mRNA in chondrocytes displayed a half-life of less than 3 hours, suggesting that it is intrinsically less stable than the authentic COL1A2 mRNA⁴² which can exist for days. This decreased stability could be due to the unique structure of the alternative transcript. Others postulated that exon A may contain sequences that decrease RNA stability⁴². Alternatively, the intrinsic instability of the alternative transcript may be due to the presence of the small open reading frame; the presence of an in-frame translation termination codon in exon 7 could be perceived as a premature stop codon, which may result in decreased RNA stability⁹⁰. However, it is our contention that it is the class III ARE-rich nature of the HOSK 3' untranslated region that accounts for the transient nature of the alternatively spliced mRNA transcript.

2.6.4 Summary

HOSK is a protein product of an alternatively spliced COL1A2 transcript (a gene that is already known to produce other proteins-albeit of unknown identity). The secondary structures of the alternative transcript expose IRES which, by causing a reading of the transcript out-of-frame from the collagen, leads to a translation that yields

HOSK. The heterogeneous tissue expression of HOSK might also be accounted by the IRES-based translational mechanism. This fact that alternatively spliced COL1A2 mRNA is short-lived appears to be due to its 3' AREs, which may cause rapid turnover of the HOSK.

2.7 REFERENCES

1. Ruvkun, G. & Hobert, O. The taxonomy of developmental control in *Caenorhabditis elegans*. *Science* 282, 2033-41 (1998).
2. Adams, M. D. et al. The genome sequence of *Drosophila melanogaster*. *Science* 287, 2185-95 (2000).
3. Baltimore, D. Our genome unveiled. *Nature* 409, 814-6 (2001).
4. Lander, E. S. et al. Initial sequencing and analysis of the human genome. *Nature* 409, 860-921 (2001).
5. Agrawal, A., Eastman, Q. M. & Schatz, D. G. Transposition mediated by RAG1 and RAG2 and its implications for the evolution of the immune system. *Nature* 394, 744-51 (1998).
6. Graveley, B. R. Alternative splicing: increasing diversity in the proteomic world. *Trends Genet* 17, 100-7 (2001).
7. Kornblihtt, A. R. Promoter usage and alternative splicing. *Curr Opin Cell Biol* 17, 262-8 (2005).
8. Levine, S. J. Mechanisms of soluble cytokine receptor generation. *J Immunol* 173, 5343-8 (2004).
9. Kozak, M. Alternative ways to think about mRNA sequences and proteins that appear to promote internal initiation of translation. *Gene* 318, 1-23 (2003).
10. Kozak, M. Pushing the limits of the scanning mechanism for initiation of translation. *Gene* 299, 1-34 (2002).

11. Ehrenfeld, E. & Semler, B. L. Anatomy of the poliovirus internal ribosome entry site. *Curr Top Microbiol Immunol* 203, 65-83 (1995).
12. Vagner, S., Galy, B. & Pyronnet, S. Irresistible IRES. Attracting the translation machinery to internal ribosome entry sites. *EMBO Rep* 2, 893-8 (2001).
13. Dasgupta, A., Das, S., Izumi, R., Venkatesan, A. & Barat, B. Targeting internal ribosome entry site (IRES)-mediated translation to block hepatitis C and other RNA viruses. *FEMS Microbiol Lett* 234, 189-99 (2004).
14. Pestova, T. V., Lomakin, I. B. & Hellen, C. U. Position of the CrPV IRES on the 40S subunit and factor dependence of IRES/80S ribosome assembly. *EMBO Rep* 5, 906-13 (2004).
15. Pestova, T. V. et al. Molecular mechanisms of translation initiation in eukaryotes. *Proc Natl Acad Sci U S A* 98, 7029-36 (2001).
16. Hellen, C. U. & Wimmer, E. Translation of encephalomyocarditis virus RNA by internal ribosomal entry. *Curr Top Microbiol Immunol* 203, 31-63 (1995).
17. Nanbru, C. et al. Alternative translation of the proto-oncogene c-myc by an internal ribosome entry site. *J Biol Chem* 272, 32061-6 (1997).
18. Park, E. H., Lee, J. M. & Pelletier, J. The Tie2 5' untranslated region is inhibitory to 5' end-mediated translation initiation. *FEBS Lett* 580, 1309-19 (2006).
19. Jang, G. M. et al. Structurally distinct elements mediate internal ribosome entry within the 5'-noncoding region of a voltage-gated potassium channel mRNA. *J Biol Chem* 279, 47419-30 (2004).
20. Butler, A., Wei, A. & Salkoff, L. Shal, Shab, and Shaw: three genes encoding potassium channels in *Drosophila*. *Nucleic Acids Res* 18, 2173-4 (1990).

21. Butler, A., Wei, A. G., Baker, K. & Salkoff, L. A family of putative potassium channel genes in *Drosophila*. *Science* 243, 943-7 (1989).
22. Pongs, O. et al. Shaker encodes a family of putative potassium channel proteins in the nervous system of *Drosophila*. *Embo J* 7, 1087-96 (1988).
23. Schwarz, T. L., Tempel, B. L., Papazian, D. M., Jan, Y. N. & Jan, L. Y. Multiple potassium-channel components are produced by alternative splicing at the Shaker locus in *Drosophila*. *Nature* 331, 137-42 (1988).
24. Tempel, B. L., Papazian, D. M., Schwarz, T. L., Jan, Y. N. & Jan, L. Y. Sequence of a probable potassium channel component encoded at Shaker locus of *Drosophila*. *Science* 237, 770-5 (1987).
25. Wei, A. et al. K⁺ current diversity is produced by an extended gene family conserved in *Drosophila* and mouse. *Science* 248, 599-603 (1990).
26. Chandy, K. G. et al. A family of three mouse potassium channel genes with intronless coding regions. *Science* 247, 973-5 (1990).
27. Douglass, J. et al. Characterization and functional expression of a rat genomic DNA clone encoding a lymphocyte potassium channel. *J Immunol* 144, 4841-50 (1990).
28. Swanson, R. et al. Cloning and expression of cDNA and genomic clones encoding three delayed rectifier potassium channels in rat brain. *Neuron* 4, 929-39 (1990).
29. Luneau, C. J. et al. Alternative splicing contributes to K⁺ channel diversity in the mammalian central nervous system. *Proc Natl Acad Sci U S A* 88, 3932-6 (1991).
30. Luneau, C., Wiedmann, R., Smith, J. S. & Williams, J. B. Shaw-like rat brain potassium channel cDNA's with divergent 3' ends. *FEBS Lett* 288, 163-7 (1991).

31. Perney, T. M., Marshall, J., Martin, K. A., Hockfield, S. & Kaczmarek, L. K. Expression of the mRNAs for the Kv3.1 potassium channel gene in the adult and developing rat brain. *J Neurophysiol* 68, 756-66 (1992).
32. Ohya, S. et al. Molecular cloning and tissue distribution of an alternatively spliced variant of an A-type K⁺ channel alpha-subunit, Kv4.3 in the rat. *FEBS Lett* 420, 47-53 (1997).
33. Attali, B. et al. Multiple mRNA isoforms encoding the mouse cardiac Kv1-5 delayed rectifier K⁺ channel. *J Biol Chem* 268, 24283-9 (1993).
34. Vullhorst, D., Jockusch, H. & Bartsch, J. W. The genomic basis of K(V)3.4 potassium channel mRNA diversity in mice. *Gene* 264, 29-35 (2001).
35. Bennett, V. D. & Adams, S. L. Characterization of the translational control mechanism preventing synthesis of alpha 2(I) collagen in chicken vertebral chondroblasts. *J Biol Chem* 262, 14806-14 (1987).
36. Bennett, V. D. & Adams, S. L. Identification of a cartilage-specific promoter within intron 2 of the chick alpha 2(I) collagen gene. *J Biol Chem* 265, 2223-30 (1990).
37. Bennett, V. D., Weiss, I. M. & Adams, S. L. Cartilage-specific 5' end of chick alpha 2(I) collagen mRNAs. *J Biol Chem* 264, 8402-9 (1989).
38. Bornstein, P. & Sage, H. Structurally distinct collagen types. *Annu Rev Biochem* 49, 957-1003 (1980).
39. Finer, M. H., Gerstenfeld, L. C., Young, D., Doty, P. & Boedtker, H. Collagen expression in embryonic chicken chondrocytes treated with phorbol myristate acetate. *Mol Cell Biol* 5, 1415-24 (1985).

40. Focht, R. J. & Adams, S. L. Tissue specificity of type I collagen gene expression is determined at both transcriptional and post-transcriptional levels. *Mol Cell Biol* 4, 1843-52 (1984).
41. Saxe, S. A., Lukens, L. N. & Pawlowski, P. J. Changes in the nuclear and cytoplasmic levels of type I and type II collagen RNAs during growth of chondrocytes in 5-bromo-2'-deoxyuridine. *J Biol Chem* 260, 3812-9 (1985).
42. Pallante, K. M. et al. The chick alpha2(I) collagen gene contains two functional promoters, and its expression in chondrocytes is regulated at both transcriptional and post-transcriptional levels. *J Biol Chem* 271, 25233-9 (1996).
43. Antoniv, T. T. et al. Identification of a repressor in the first intron of the human alpha2(I) collagen gene (COL1A2). *J Biol Chem* 280, 35417-23 (2005).
44. Schibler, U., Hagenbuchle, O., Wellauer, P. K. & Pittet, A. C. Two promoters of different strengths control the transcription of the mouse alpha-amylase gene *Amy-1a* in the parotid gland and the liver. *Cell* 33, 501-8 (1983).
45. Young, R. A., Hagenbuchle, O. & Schibler, U. A single mouse alpha-amylase gene specifies two different tissue-specific mRNAs. *Cell* 23, 451-8 (1981).
46. McGrogan, M., Simonsen, C. C., Smouse, D. T., Farnham, P. J. & Schimke, R. T. Heterogeneity at the 5' termini of mouse dihydrofolate reductase mRNAs. Evidence for multiple promoter regions. *J Biol Chem* 260, 2307-14 (1985).
47. Luo, X. C., Park, K., Lopez-Casillas, F. & Kim, K. H. Structural features of the acetyl-CoA carboxylase gene: mechanisms for the generation of mRNAs with 5' end heterogeneity. *Proc Natl Acad Sci U S A* 86, 4042-6 (1989).

48. Fraser, P., Cummings, P. & Curtis, P. The mouse carbonic anhydrase I gene contains two tissue-specific promoters. *Mol Cell Biol* 9, 3308-13 (1989).
49. Hanke, P. D. & Storti, R. V. The *Drosophila melanogaster* tropomyosin II gene produces multiple proteins by use of alternative tissue-specific promoters and alternative splicing. *Mol Cell Biol* 8, 3591-602 (1988).
50. Strehler, E. E., Periasamy, M., Strehler-Page, M. A. & Nadal-Ginard, B. Myosin light-chain 1 and 3 gene has two structurally distinct and differentially regulated promoters evolving at different rates. *Mol Cell Biol* 5, 3168-82 (1985).
51. Emerson, C. P., Jr. Embryonic signals for skeletal myogenesis: arriving at the beginning. *Curr Opin Cell Biol* 5, 1057-64 (1993).
52. Barnhart, K. M., Kim, C. G. & Sheffery, M. Purification and characterization of an erythroid cell-specific factor that binds the murine alpha- and beta-globin genes. *Mol Cell Biol* 9, 2606-14 (1989).
53. Wall, L., deBoer, E. & Grosveld, F. The human beta-globin gene 3' enhancer contains multiple binding sites for an erythroid-specific protein. *Genes Dev* 2, 1089-100 (1988).
54. Weiss, M. J. & Orkin, S. H. GATA transcription factors: key regulators of hematopoiesis. *Exp Hematol* 23, 99-107 (1995).
55. Akira, S. et al. A nuclear factor for IL-6 expression (NF-IL6) is a member of a C/EBP family. *Embo J* 9, 1897-906 (1990).
56. Umek, R. M., Friedman, A. D. & McKnight, S. L. CCAAT-enhancer binding protein: a component of a differentiation switch. *Science* 251, 288-92 (1991).

57. Houghlum, K., Buck, M., Adir, V. & Chojkier, M. LAP (NF-IL6) transactivates the collagen alpha 1(I) gene from a 5' regulatory region. *J Clin Invest* 94, 808-14 (1994).
58. Waterman, M. L., Fischer, W. H. & Jones, K. A. A thymus-specific member of the HMG protein family regulates the human T cell receptor C alpha enhancer. *Genes Dev* 5, 656-69 (1991).
59. Wasylyk, B., Hahn, S. L. & Giovane, A. The Ets family of transcription factors. *Eur J Biochem* 211, 7-18 (1993).
60. Yarmolinsky, M. B. & Haba, G. L. Inhibition By Puromycin Of Amino Acid Incorporation Into Protein. *Proc Natl Acad Sci U S A* 45, 1721-1729 (1959).
61. Morris, A. J. & Schweet, R. S. Release of soluble protein from reticulocyte ribosomes. *Biochim Biophys Acta* 47, 415-6 (1961).
62. Nathans, D. Puromycin Inhibition Of Protein Synthesis: Incorporation Of Puromycin Into Peptide Chains. *Proc Natl Acad Sci U S A* 51, 585-92 (1964).
63. Lodish, H. F. Alpha and beta globin messenger ribonucleic acid. Different amounts and rates of initiation of translation. *J Biol Chem* 246, 7131-8 (1971).
64. Fan, H. & Penman, S. Regulation of protein synthesis in mammalian cells. II. Inhibition of protein synthesis at the level of initiation during mitosis. *J Mol Biol* 50, 655-70 (1970).
65. Lee, G. T. & Engelhardt, D. L. Growth-related fluctuation in messenger RNA utilization in animal cells. *J Cell Biol* 79, 85-86 (1978).
66. Boedtker, H., Finer, M. & Aho, S. The structure of the chicken alpha 2 collagen gene. *Ann N Y Acad Sci* 460, 85-116 (1985).

67. Nah, H. D., Bennett, V. D., Niu, Z. & Adams, S. I. Alternative transcript of the chick alpha 2(I) collagen gene is transiently expressed during endochondral bone formation and during development of the central nervous system. *Dev Dyn* 206, 146-58 (1996).
68. Veeramachaneni, V., Makalowski, W., Galdzicki, M., Sood, R. & Makalowska, I. Mammalian overlapping genes: the comparative perspective. *Genome Res* 14, 280-6 (2004).
69. Scherer, S. W. et al. Human chromosome 7: DNA sequence and biology. *Science* 300, 767-72 (2003).
70. Ohmstede, C. A., Bland, M. M., Merrill, B. M. & Sahyoun, N. Relationship of genes encoding Ca²⁺/calmodulin-dependent protein kinase Gr and calspermin: a gene within a gene. *Proc Natl Acad Sci U S A* 88, 5784-8 (1991).
71. Strauss, A. W. et al. Molecular basis of human mitochondrial very-long-chain acyl-CoA dehydrogenase deficiency causing cardiomyopathy and sudden death in childhood. *Proc Natl Acad Sci U S A* 92, 10496-500 (1995).
72. Zhou, C. & Blumberg, B. Overlapping gene structure of human VLCAD and DLG4. *Gene* 305, 161-6 (2003).
73. Shiokawa, D. & Tanuma, S. I. Isolation and characterization of the DLAD/Dlad genes, which lie head-to-head with the genes for urate oxidase. *Biochem Biophys Res Commun* 288, 1119-28 (2001).
74. Saito, M., Takenouchi, Y., Kunisaki, N. & Kimura, S. Complete primary structure of rainbow trout type I collagen consisting of alpha1(I)alpha2(I)alpha3(I) heterotrimers. *Eur J Biochem* 268, 2817-27 (2001).

75. Dubois, G. M., Haftek, Z., Crozet, C., Garrone, R. & Le Guellec, D. Structure and spatio temporal expression of the full length DNA complementary to RNA coding for alpha2 type I collagen of zebrafish. *Gene* 294, 55-65 (2002).
76. Stefanovic, B., Hellerbrand, C. & Brenner, D. A. Regulatory role of the conserved stem-loop structure at the 5' end of collagen alpha1(I) mRNA. *Mol Cell Biol* 19, 4334-42 (1999).
77. Eddy, S. R. How do RNA folding algorithms work? *Nat Biotechnol* 22, 1457-8 (2004).
78. Reeder, J., Hochsmann, M., Rehmsmeier, M., Voss, B. & Giegerich, R. Beyond Mfold: recent advances in RNA bioinformatics. *J Biotechnol* 124, 41-55 (2006).
79. Chappell, S. A., Edelman, G. M. & Mauro, V. P. Biochemical and functional analysis of a 9-nt RNA sequence that affects translation efficiency in eukaryotic cells. *Proc Natl Acad Sci U S A* 101, 9590-4 (2004).
80. Dresios, J., Chappell, S. A., Zhou, W. & Mauro, V. P. An mRNA-rRNA base-pairing mechanism for translation initiation in eukaryotes. *Nat Struct Mol Biol* 13, 30-4 (2006).
81. Owens, G. C., Chappell, S. A., Mauro, V. P. & Edelman, G. M. Identification of two short internal ribosome entry sites selected from libraries of random oligonucleotides. *Proc Natl Acad Sci U S A* 98, 1471-6 (2001).
82. Negulescu, D., Leong, L. E., Chandy, K. G., Semler, B. L. & Gutman, G. A. Translation initiation of a cardiac voltage-gated potassium channel by internal ribosome entry. *J Biol Chem* 273, 20109-13 (1998).

83. Caput, D. et al. Identification of a common nucleotide sequence in the 3'-untranslated region of mRNA molecules specifying inflammatory mediators. *Proc Natl Acad Sci U S A* 83, 1670-4 (1986).
84. Bevilacqua, A., Ceriani, M. C., Capaccioli, S. & Nicolini, A. Post-transcriptional regulation of gene expression by degradation of messenger RNAs. *J Cell Physiol* 195, 356-72 (2003).
85. Espel, E. The role of the AU-rich elements of mRNAs in controlling translation. *Semin Cell Dev Biol* 16, 59-67 (2005).
86. Chen, C. Y. & Shyu, A. B. AU-rich elements: characterization and importance in mRNA degradation. *Trends Biochem Sci* 20, 465-70 (1995).
87. Bakheet, T., Frevel, M., Williams, B. R., Greer, W. & Khabar, K. S. ARED: human AU-rich element-containing mRNA database reveals an unexpectedly diverse functional repertoire of encoded proteins. *Nucleic Acids Res* 29, 246-54 (2001).
88. Shaw, G. & Kamen, R. A conserved AU sequence from the 3' untranslated region of GM-CSF mRNA mediates selective mRNA degradation. *Cell* 46, 659-67 (1986).
89. Lai, W. S., Kennington, E. A. & Blackshear, P. J. Tristetraprolin and its family members can promote the cell-free deadenylation of AU-rich element-containing mRNAs by poly(A) ribonuclease. *Mol Cell Biol* 23, 3798-812 (2003).
90. Dietz, H. C. et al. The skipping of constitutive exons in vivo induced by nonsense mutations. *Science* 259, 680-3 (1993).

TACCTCTGATCCTGGCAAAAACGGTGATAAAGGTCATGCTGGTCTTGTCTGGTCTCGGG
GTGCTCCAGGTCCTGATGGAAACAATGGTGTCTCAGGGACCTCCTGGACCACAGGGTG
TTCAAGGTGGAAAAGGTGAACAGGGTCCCGCTGGTCTCCAGGCTTCCAGGGTCTGC
CTGGCCCTCAGGTCCTCGCTGGTGAAGTTGGCAAACCAGGAGAAAGGGGTCTCCATG
GTGAGTTTGGTCTCCCTGGTCTGCTGGTCCAAGAGGGGAACGCGGTCCCCAGGTG
AGAGTGGTGTGCTGCCGGTCTACTGGTCTATTGGAAGCCGAGGTCCTTCTGGACCC
CAGGGCCTGATGGAAACAAGGGTGAACCTGGTGTGGTTGGTGTGCTGTGGCACTGCT
GGTCCATCTGGTCTAGTGGACTCCCAGGAGAGAGGGGTGCTGCTGGCATACTGGA
GGCAAGGGAGAAAAGGGTGAACCTGGTCTCAGAGGTGAAATTGGTAACCCTGGCAG
AGATGGTGTCTCGTGGTGTCTCTGGTGTCTAGGTGCCCTGGTCTGCTGGAGCCACAG
GTGACCGGGGCGAAGCTGGGGCTGCTGGTCTGCTGGTCTGCTGGTCTCGGGGAAGCCC
TGGTGAACGTGGTGAAGTCCGGTCTGCTGGCCCAATGGATTTGCTGGTCTGCTGGTGTCT
GCTGGTCAACCTGGTGTAAAGGAGAAAGAGGAGCCAAAGGGCCTAAGGGTGAACACGG
TGTGTTGGTCCCACAGGCCCGTTGGAGCTGCTGGCCAGCTGGTCCAAATGGTCCCCC
GGTCTGCTGGAAGTCGTGGTGTGATGGAGGCCCCCTGGTATGACTGGTTTCCCTGGTGTG
CTGGACGGACTGGTCCCCAGGACCCTCTGGTATTTCTGGCCCTCCTGGTCCCCCTGGTCT
GCTGGGAAAGAAGGGCTTCGTGGTCTCGTGGTGTGACCAAGGTCCAGTTGGCCGAACTGGA
GAAGTAGGTGCAGTTGGTCCCCCTGGCTTCGCTGGTGTGAGAAGGGTCCCTCTGGAGAGGCTG
GTACTGCTGGACCTCCTGGCACTCCAGGTCCTCAGGGTCTTCTTGGTGTCTCTGGTATTCTG
GGTCTCCCTGGTCTGAGAGGTGAACGTGGTCTACCAGGTGTTGCTGGTGTCTGTGGGTGAAC
CTGGTCTCTTGGCATTGCCGGCCCTCCTGGGGCCCGTGGTCTCCTGGTGTCTGTGGGTAGT
CCTGGAGTCAACGGTGTCTCCTGGTGAAGCTGGTCTGTGATGGCAACCCTGGGAACGATGGT
CCCCAGGTTCGCGATGGTCAACCCGGACACAAGGGAGAGCGCGGTTACCCTGGCAATATT
GGTCCCCTGGTGTGCTGCAGGTGCACCTGGTCTCATGGCCCCGTGGGTCTGCTGGCAAAC
ATGGAACCGTGGTGAACCTGGTCTTCTGGTCTGTTGGTCTGCTGGTGTCTGTTGGCCC
AAGAGGTCTAGTGGCCACAAGGCATTCGTGGCGATAAGGGAGAGCCCGGTGAAAAGG
GGCCAGAGGTCTTCTGGCTTAAAGGGACACAATGGATTGCAAGGTCTGCCTGGTATCGC
TGGTACCATGGTGTCAAGGTGTCTCCTGGTCCCGTGGGTCTGCTGGTCTAGGGGCCCT
GCTGGTCTTCTGGCCCTGCTGGAAAAGATGGTCTGCACTGGACATCCTGGTACAGTTGGAC
CTGCTGGCATTTCGAGGCCCTCAGGGTACCAAGGCCCTGCTGGCCCCCTGGTCCCCCTGG
CCCTCCTGGACCTCCAGGTGTAAGCGGTGGTGGTTATGACTTTGGTTACGATGGAGACTTC
TACAGGGCTGACCAGCCTCGCTCAGCACCTTCTCTCAGACCCAAGGACTATGAAGTTGATG
CTACTCTGAAGTCTCTCAACAACCAGATTGAGACCCTTCTTACTCCTGAAGGCTCTAGAAA
GAACCCAGCTCGCACATGCCGTGACTTGAGACTCAGCCACCCAGAGTGGAGCAGTGGTTA
CTACTGGATTGACCCTAACCAAGGATGCACTATGGATGCTATCAAAGTATACTGTGATTTCT
TCTACTGGCGAAACCTGTATCCGGGCCCAACCTGAAAACATCCCAGCCAAGAACTGGTAT
AGGAGCTCCAAGGACAAGAAACACGTCTGGCTAGGAGAAACTATCAATGCTGGCAGCCAG
TTTGAATATAATGTAGAAGGAGTGACTTCCAAGGAAATGGCTACCCAACCTTGCCTTCATGC
GCCTGCTGGCCAACCTATGCCTCTCAGAACATCACCTACCACTGCAAGAACAGCATTGCATA
CATGGATGAGGAGACTGGCAACCTGAAAAAGGCTGTCACTTCTACAGGGCTCTAATGATGT
TGAACCTGTTGCTGAGGGCAACAGCAGGTTCACTTACACTGTTCTTGTAGATGGCTGCTCT
AAAAAGACAAATGAATGGGGAAAGACAATCATTGAATACAAAACAAATAAGCCATCACG
CCTGCCCTTCTTGTATATTGCACCTTTGGACATCGGTGGTGTGCTGACCAGGAATTCTTTGTGG
ACATTGGCCCAGTCTGTTTCAAATAAATGAACTCAATCTAAATTAATAAAGAAAGAAATTT
GAAAAAATTTCTCTTTGCCATTTCTTCTTCTTTTAACTGAAAGCTGAATCCTTCCAT
TTCTTCTGCACATCTACTTGTAAATTGTGGGCAAAAAGAGAAAAAAGAAAGGATTGATCAGA
GCATTGTGCAATACAGTTTCATTAACCTTCCCCCTCTCCCCCAAAAATTTGAATTTTTTTT
TCAACACTCTTACACCTGTTATGGAAAATGTCAACCTTTGTAAGAAAACCAAAA

Figure 2.1: Full nucleotide sequence of HOSK. The bold identifies the HOSK coding sequence and the underlined area identifies the 1.4 kb coding sequence

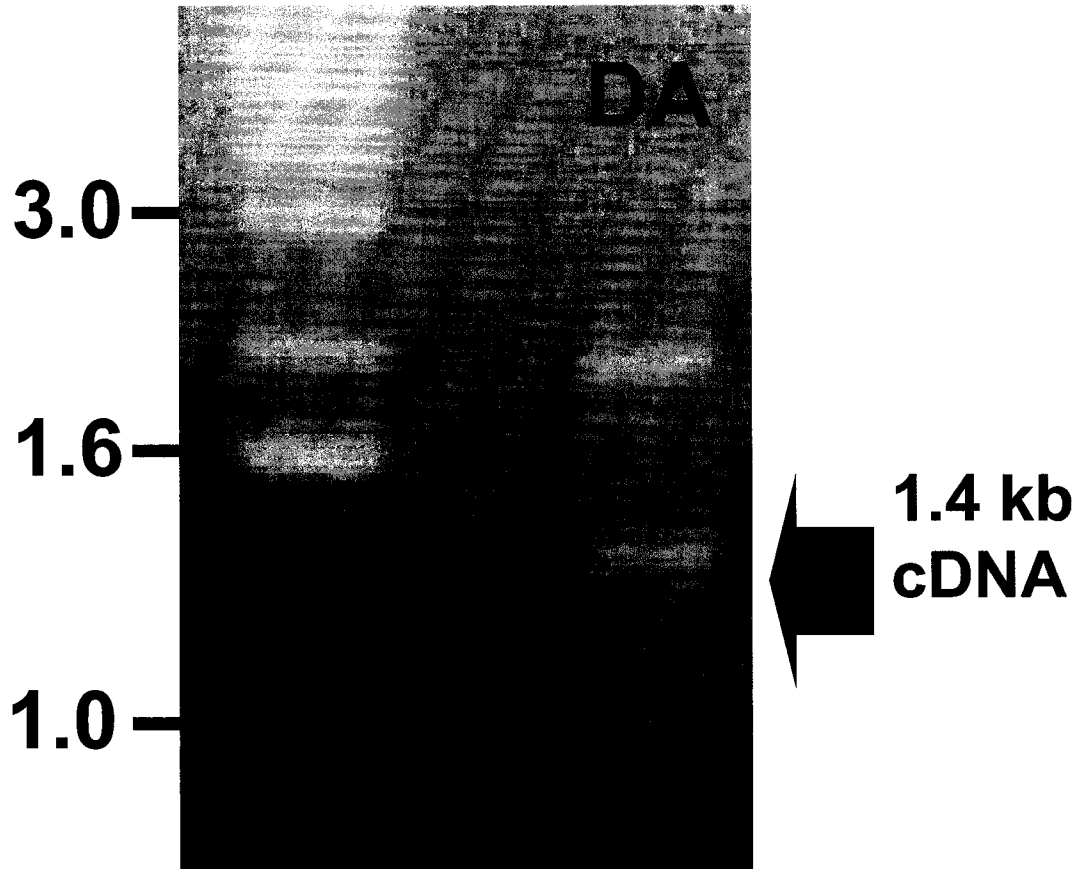


Figure 2.2: Isolation of 1.4 fragment with Kv1.5 from human ductus arteriosus (DA) with sense complement human Kv1.5 primers.

5' end of HOSK sequence

```
TACCTCTGATCCTGGCAAAAACGGTGATAAAGG
TCATGCTGGTCTTGCTGGTGGTCTCGGGGTGCTCCAGGTCCTGATGGAAACAATG
      5'.....TACCTCGGGACCACGGGGTG...3'
TGCTCAGGGACCTCCTGGACCACAGGGTGTTC AAGGTGGAAAAGGTGAACAGGG
TCCCGCTGGTCCTCCAGGCTTCCAGGGTCTGCCTGGCCCCTCAGGTCCCGCTGGTG
AAGTTGGCAAACCAGGAGAAAGGGGTCTCCATGGTGAGTTTGGTCTCCCTGGTCC
TGCTGGTCCAAGAGGGGAACGCGGTCCCCCAGGTGAGAGTGGTGCTGCCGGTCTCT
ACTGGTCCTATTGGAAGCCGAGGTCTTCTGGACCCCCAGGGCCTGATGGAAACA
AGGGTGAACCTGGTGTGGTTGGTGTGCTGTGGGCACTGCTGGTCCATCTGGTCCTAGT
GGA CTCCAGGAGAGAGGGGTGCTGCTGGCATACTGGAGGCAAGGGAGAAAAG
GGTGAACCTGGTCTCAGAGGTGAAATTGGTAACCCTGGCAGAGATGGTGCTCGTG
GTGCTCCTGGTGCTGTAG
```

3' end of HOSK sequence (Reversed and Complemented)

```
CCCAGGTCGCGATGGTCAACCCGGACACAAGGGAGAGCGCGGTTACCCTGGCAA
TATTGGTCCC GTTGGTGTGCTGCAGGTGCACCTGGTCTCCTCATGGCCCCGTGGGTCCTG
      5' ...TACCTCGGGACCACGGGGTG...3'
CTGGCAAACATGGAAACCGTGGTGA AACTGGTCCTTCTGGTCCTGTTGGTCCTGCT
GGTGCTGTTGGCCCAAGAGGTCTAGTGGCCACAAGGCATTTCGTGGCGATAAGG
GAGAGCCCCGGTGAAAAGGGGCCAGAGGTCTTCTGGCTTAAAGGGACACAATG
GATTGCAAGGTCTGCCTGGTATCGCTGGTCACCATGGTGATCAAGGTGCTCCTGG
CTCCGT
```

Figure 2.3: Primers of sense complement human Kv1.5 primers aligned with the HOSK sequence at 5' end and 3' end. Please note that 3' sequence is already reversed and complemented

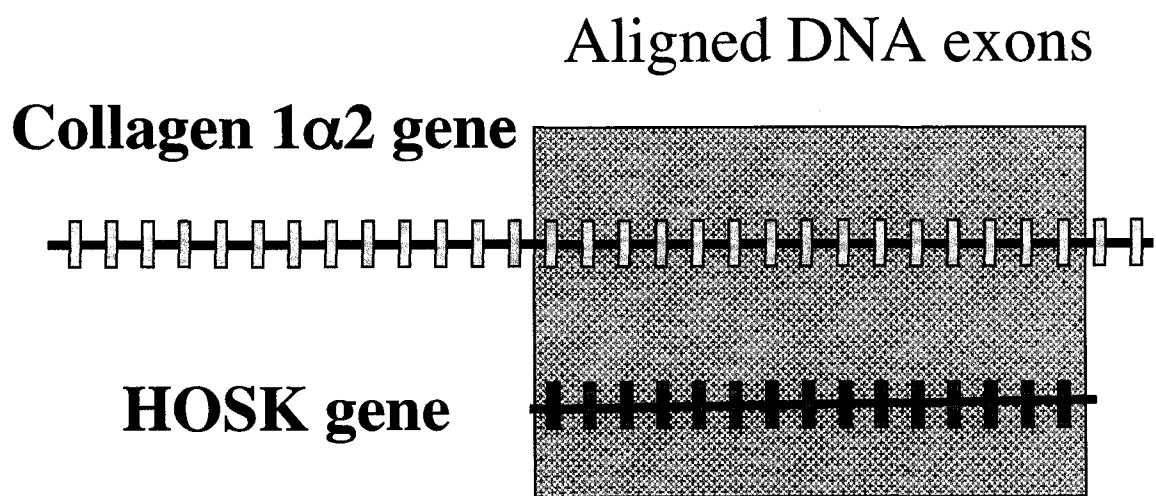


Figure 2.4: Schematic of DNA exons alignment of Collagen 1 α 2 with HOSK gene. Note the alignment is on the 3' end representing last 29 exons or 2869 bps.

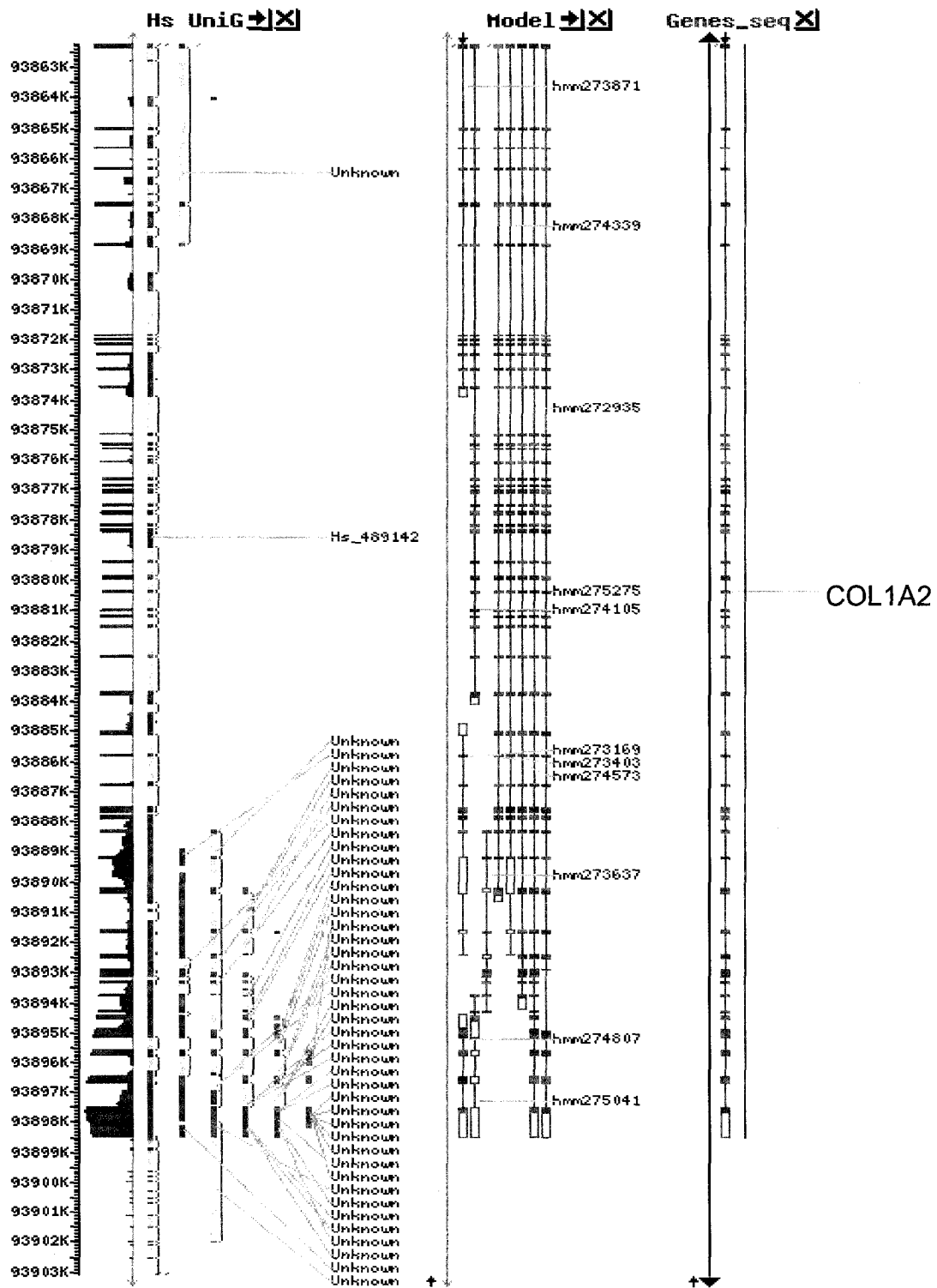
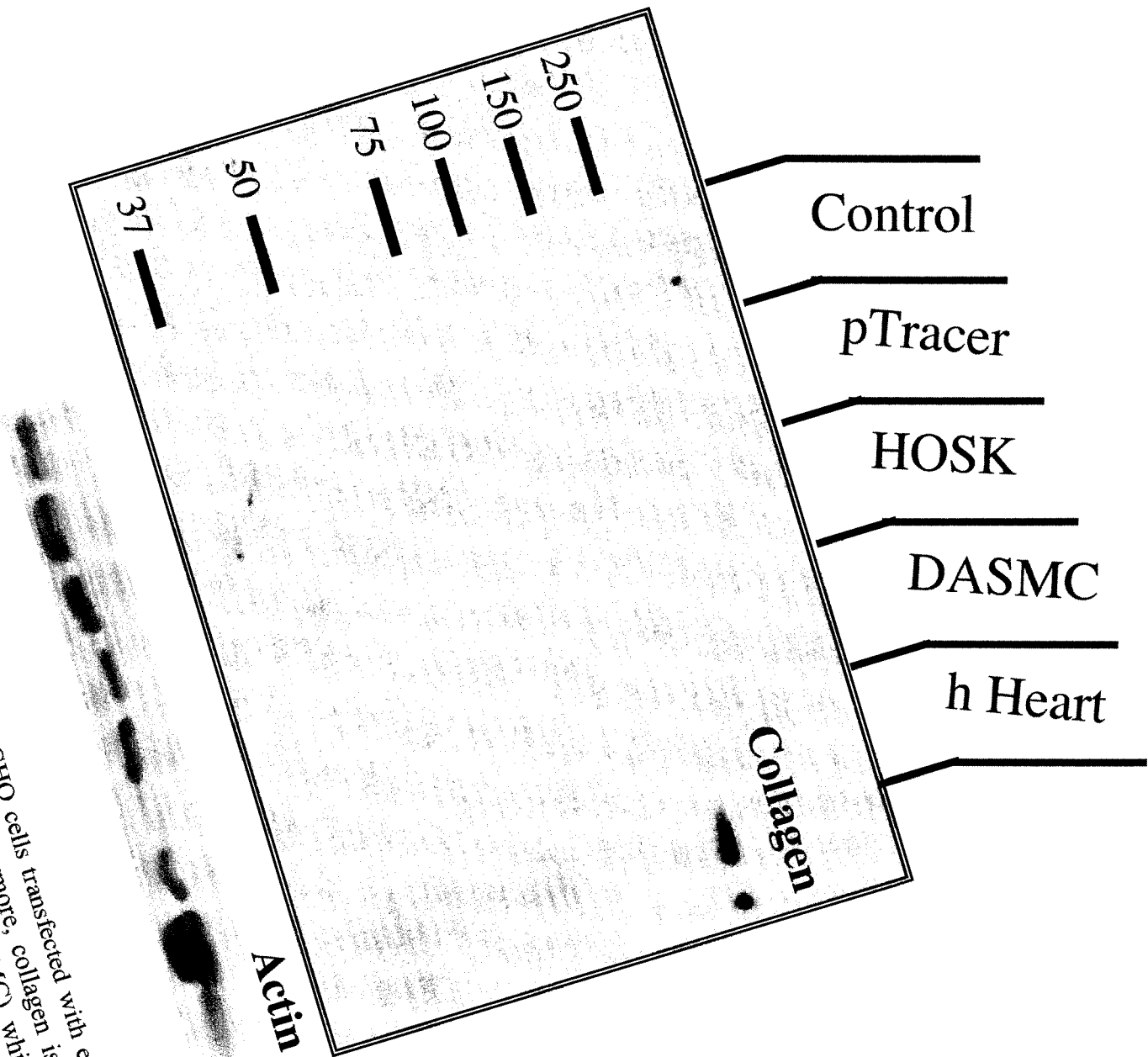


Figure 2.5: Location of COL1A2 in NCBI database. The histogram on the left denotes the number of genes being expressed on this 7q21-22 chromosome. Please note presence of various overlapping genes at 3' end of the segment with unknown function.

Reproduced with permission of the copyright owner. Further reproduction prohibited without permission.

Figure 2.6: Collagen protein is not present in CHO cells transfected with either empty vector (pTracer-CMV) or HOSK channel. Furthermore, collagen is also absent in human ductus arteriosus smooth muscle cells (DASMC) while the human heart served as a control.



TACCTCTGATCCTGGCAAAAACGGTGATAAAGGTCATGCTGGTCTTGCTGGTGCTCGGGGT
GCTCCAGGTCCTGATGGAAACAATGGTGCTCAGGGACCTCCTGGACCACAGGGTGTTCAA
GGTGGAAAAGGTGAACAGGGTCCCCTGGTCCCTCAGGCTTCCAGGGTCTGCCTGGCCCC
CAGGTCCCCTGGTGAAGTTGGCAAACCAGGAGAAAGGGGTCTCCATGGTGAGTTTGGTC
TCCCTGGTCTGCTGGTCCAAGAGGGGAACCGGGTCCCCAGGTGAGAGTGGTGCTGCCG
GTCCTACTGGTCTATTGGAAGCCGAGGTCCTTCTGGACCCCCAGGGCCTGATGGAAACAA
GGGTGAACCTGGTGTGGTGGTGCTGTGGGCACTGCTGGTCCATCTGGTCTAGTGGACTC
CCAGGAGAGAGGGGTGCTGCTGGCATACTGGAGGCAAGGGAGAAAAGGGTGAACCTGG
TCTCAGAGGTGAAATTGGTAACCCTGGCAGAGATGGTGCTCGTGGTGCTCCTGGTGCTGTA
GGTGCCCCCTGGTCTGCTGGAGCCACAGGTGACCGGGGCGAAGCTGGGGCTGCTGGTCT
GCTGGTCTGCTGGTCTCGGGGAAGCCCTGGTGAACGTGGTGAAGTCTGGTCTGCTGGCC
CCAATGGATTTGCTGGTCTGCTGGTGGTGGTCAACCTGGTGCTAAAGGAGAAAGAGG
AGCCAAAGGGCCTAAGGGTGA AAAACGGTGTGTTGGTCCCACAGGCCCGTTGGAGCTGC
TGGCCCAGCTGGTCCAATGGTCCCCCGGTCTGCTGGAAGTCGTGGTGAAGGCCCC
CCTGGTATGACTGGTTTCCCTGGTGGTGGTGGTCAACCTGGTGCTAAAGGAGAAAGAGG
TTTCTGGCCCTCCTGGTCCCCCTGGTCTGCTGGGAAAGAAGGGCTTCGTGGTCTCGTGGT
GACCAAGGTCCAGTTGGCCGAACCTGGAGAAGTAGGTGCAGTTGGTCCCCCTGGCTTCGCTG
GTGAGAAGGGTCCCTCTGGAGAGGCTGGTACTGCTGGACCTCCTGGCACTCCAGGTCTCA
GGGTCTTCTGGTGGTCTGCTGGTATTCTGGGTCTCCCTGGCTCGAGAGGTGAACGTGGTCTAC
CAGGTGTTGCTGGTGGTGGTGAACCTGGTCTCTGGCATTGCCGGCCCTCCTGGGGC
CCGTGGTCTCCTGGTGGTGGTGGTGGTGGTGGTGGTGGTGGTGGTGGTGGTGGTGGTGGT
CGTGATGGCAACCCTGGGAACGATGGTCCCCAGGTCGCGATGGTCAACCCGGACACAAG
GGAGAGCGCGGTTACCCTGGCAATATTGGTCCCGTTGGTGGTGGTGGTGGTGGTGGTGGT
ATGGCCCCCTGGGTCTGCTGGCAACATGGAAACCGTGGTGGTGGTGGTGGTGGTGGTGGT
TGTTGGTCTGCTGGTGGTGGTGGTGGTGGTGGTGGTGGTGGTGGTGGTGGTGGTGGTGGT
GATAAGGGAGAGCCCGGTGAAAAGGGGCCAGAGGTCTTCTGGCTTAAAGGGACACAAT
GGATTGCAAGGTCTGCCTGGTATCGCTGGTCAACATGGTGGTGGTGGTGGTGGTGGTGGTGGT
TGGGTCTGCTGGTCTAGGGGCCCTGCTGGTCTTCTGGCCCTGCTGGAAAAGATGGTGG
CACTGGACATCCTGGTACAGTTGGACCTGCTGGCATTGAGGGCCCTCAGGGTCACCAAGGC
CCTGCTGGCCCCCTGGTCCCCCTGGCCCTCCTGGACCTCCAGGTGTAAGCGGTGGTGGT
ATGACTTTGGTTACGATGGAGACTTCTACAGGGCTGACCAGCCTCGCTCAGCACCTTCTCT
CAGACCCAAGGACTATGAAGTTGATGCTACTCTGAAGTCTCTCAACAACCAGATTGAGACC
CTTCTTACTCCTGAAGGCTCTAGAAAAGAACCCAGCTCGCACATGCCGTGACTTGAGACTCA
GCCACCAGAGTGGAGCAGTGGTACTACTGGATTGACCCTAACCAAGGATGCACTATGG
ATGCTATCAAAGTATACTGTGATTTCTACTGGCGAAACCTGTATCCGGGCCCAACCTGA
AAACATCCCAGCCAAGAACTGGTATAGGAGCTCCAAGGACAAGAAAACAGTCTGGCTAGG
AGAAACTATCAATGCTGGCAGCCAGTTTGAATATAATGTAGAAGGAGTGACTTCCAAGGA
AATGGCTACCCAACCTTGCCTTCATGCGCCTGCTGGCCAACTATGCCTCTCAGAACATCACC
TACCACTGCAAGAACAGCATTGCATACATGGATGAGGAGACTGGCAACCTGAAAAAGGCT
GTCATTCTACAGGGCTCTAATGATGTTGAACTTGTGGTGGTGGTGGTGGTGGTGGTGGTGGT
ACACTGTTCTGTAGATGGCTGCTCTAAAAAGACAAATGAATGGGGAAAGACAATCATTG
AATACAAAACAATAAGCCATCACGCCTGCCCTTCTTGATATTGCACCTTTGGACATCGG
TGGT
ATCTAAATTA AAAAAGAAAAGAAATTTGAAAAACTTTCTCTTTGCCATTTCTTCTTCTT
CTTTTTTAACTGAAAGCTGAATCCTTCCATTTCTTCTGCACATCTACTTGCTTAAATTGTGG
GCAAAAAGAGAAAAAGAAGGATTGATCAGAGCATTGTGCAATACAGTTTCATTAACCTCTT
CCCCCTCTCCCCAAAAATTTGAATTTTTTTTCAACACTCTTACACCTGTTATGGAAAAT
GTCAACCTTTGTAAGAAAACCAAAA

Figure 2.8: Full cDNA nucleotide sequence of HOSK channel. Please note the bold underlined sequences mark the AU-rich regions.

Free Energy of Structure = -1323.7 kkal/mol

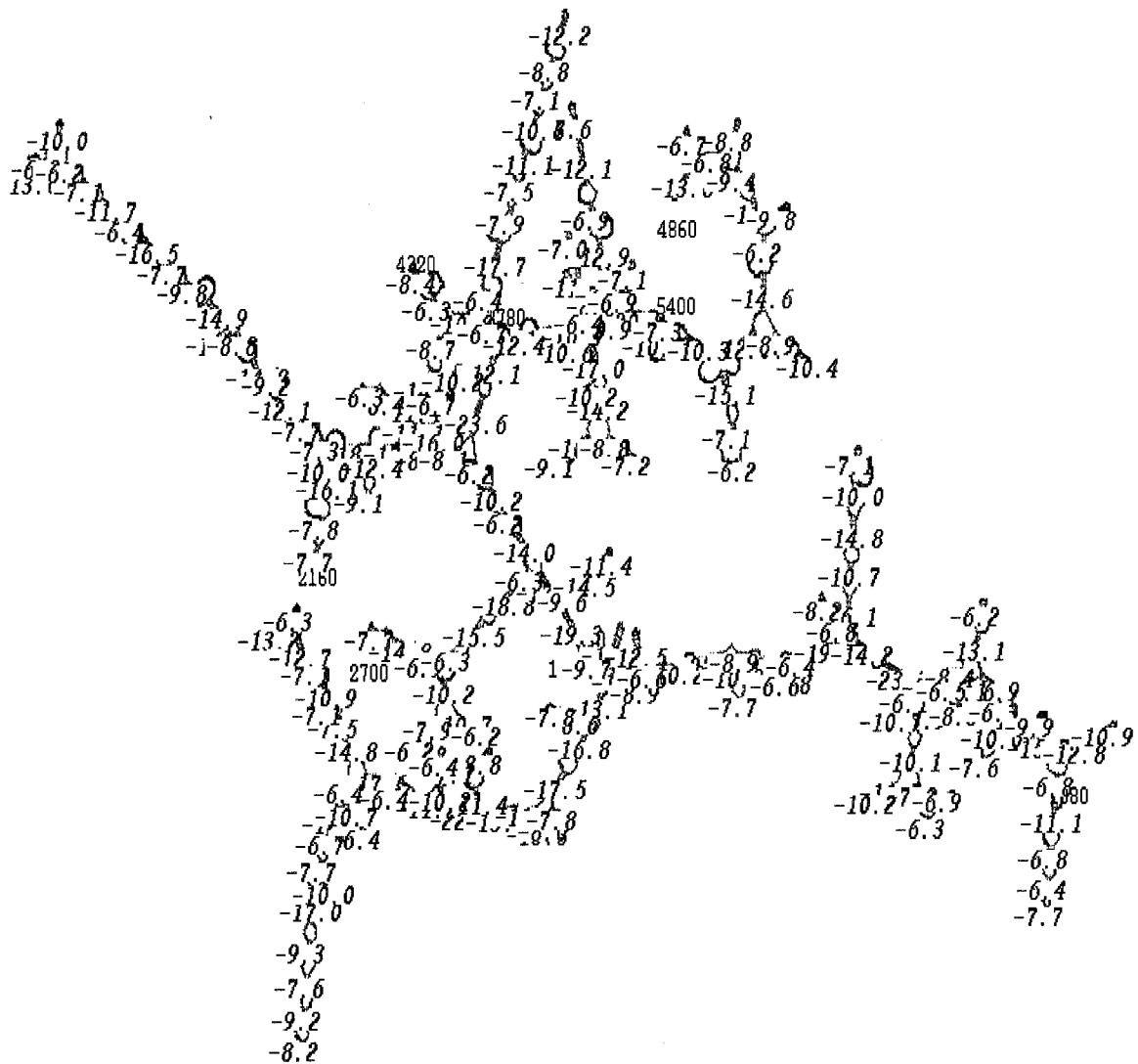


Figure 2.9: MFOLD of RNA structure of collagen 1α2 gene. Please note formation of various stems and loops.

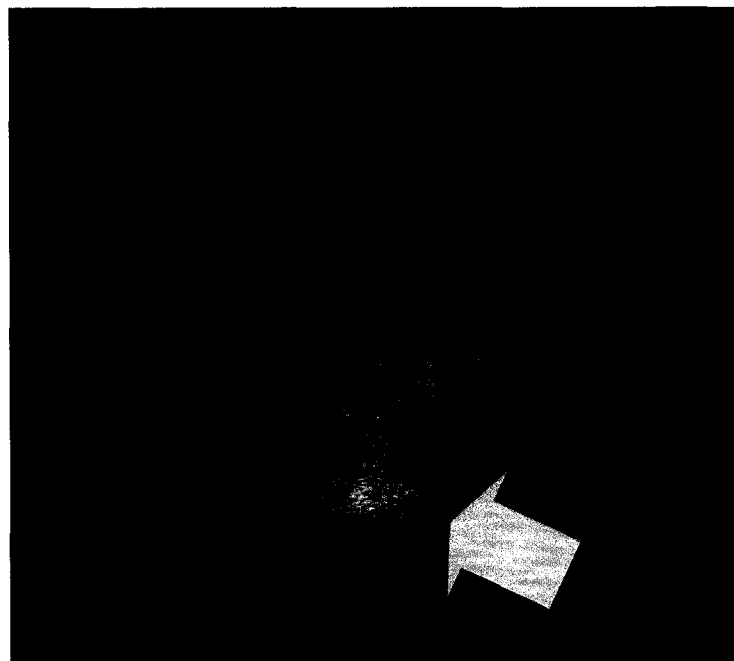
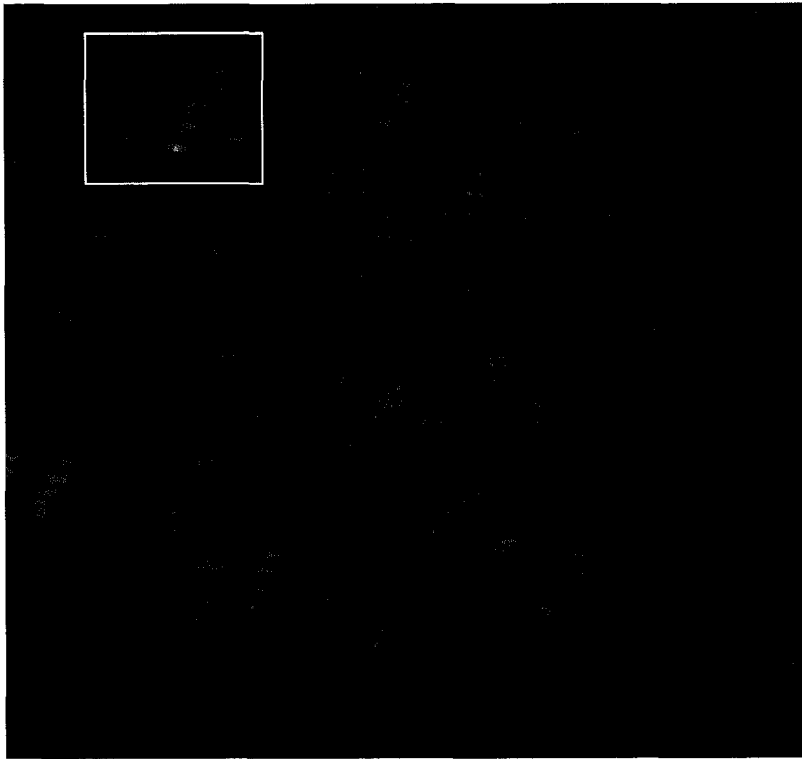


Figure 2.10: Fluorescent in-situ Hybridization (FISH) on human chromosomes. FISH analysis suggests localization on chromosome 7.

Reproduced with permission of the copyright owner. Further reproduction prohibited without permission.

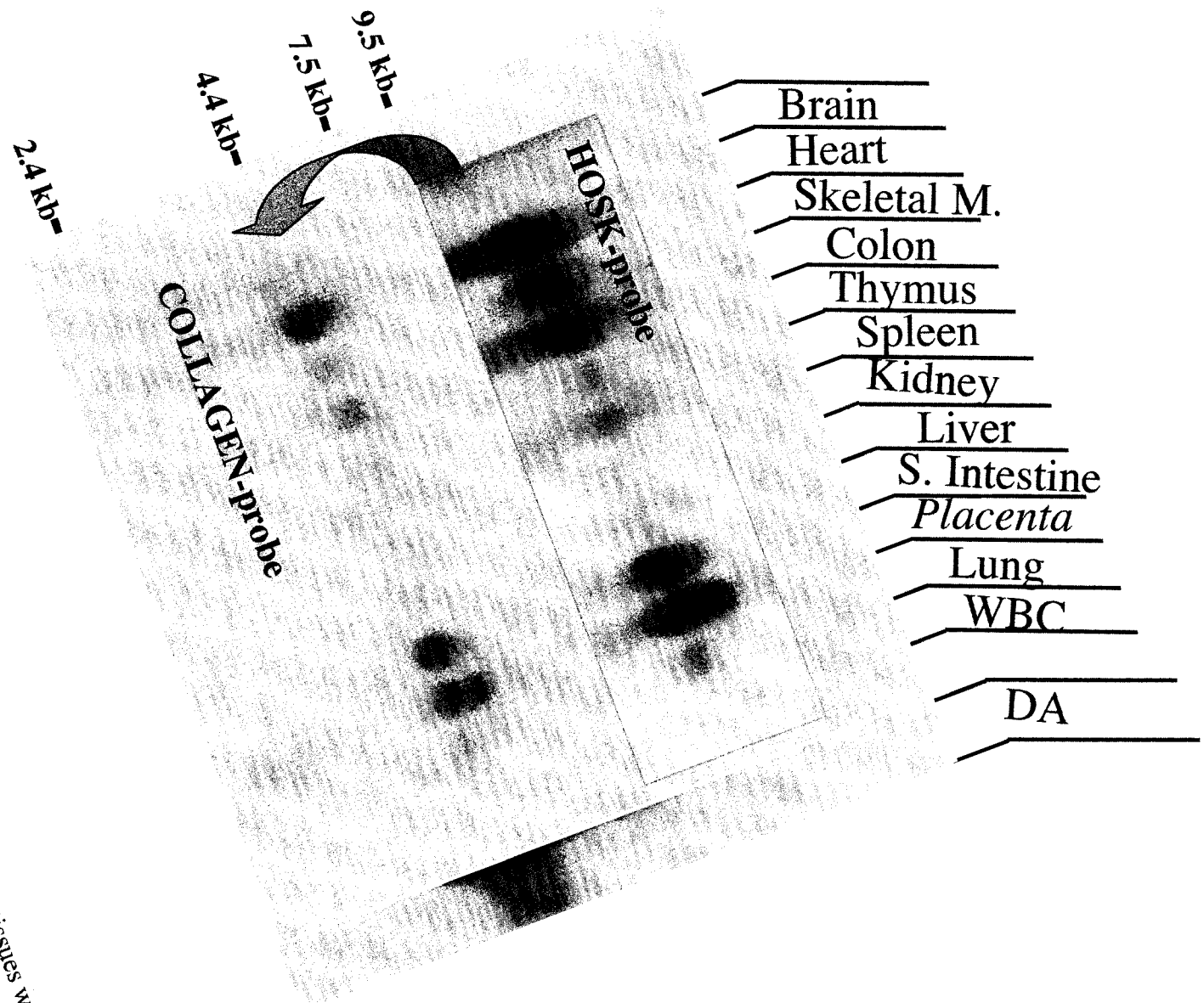


Figure 2.11: Northern Blot analysis on a panel of human tissues with HOSK and Collagen probes. Please note the expression of two transcripts in DA and placenta. Brain and WBC have do not express COL1A2 transcripts

Ductal Cells

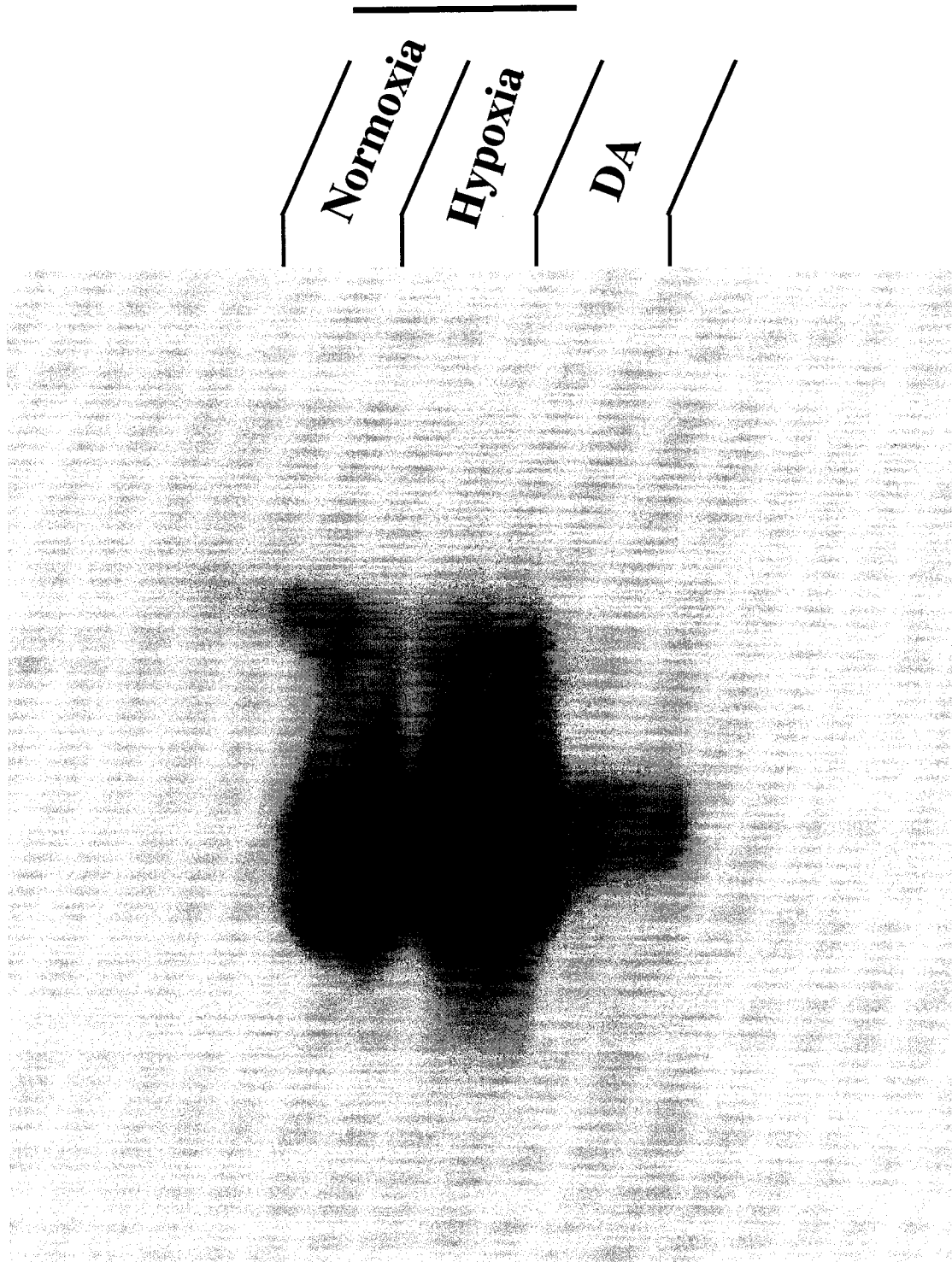


Figure 2.12: Northern Blot of hDASMC incubated for 48 hrs in either hypoxia or normoxia. There is an increase in mRNA level in hypoxic DASMC. Human DA served as positive control for HOSK probe.

3.1 INTRODUCTION

30% of the genes in the human genome¹ encode membrane proteins, of which ion channels are a major subgroup. Ion channels form pores in biological membranes through which selected inorganic ions pass rapidly (at near-diffusion rates, 10^8 ions s^{-1} through a single channel). Originally recognized as being central to function of excitable cells, for example the nervous system and the heart², ion channels are now known to be expressed and crucial to the function of non-excitable cells (e.g. smooth muscle cells and endothelium). Ion channels are found in most organisms, from primitive to advanced, from prokaryotes to mammals and often serve functions which are remarkably similar in organisms as diverse as bacteria, yeast and plants and humans. Mutations in ion channels are associated with numerous diseases of, the nervous system and the cardiac system² and therefore are also of interest for novel therapeutic targets³. More recently decreased expression of O₂-sensitive Kv channel has emerged as a hallmark of a vascular disease, pulmonary arterial hypertension (PAH), and decrease in O₂ sensitive Kv channels is also seen in preterm DA⁴.

Despite the large number of ion channels and their evident biological importance, the three-dimensional structures that underlie their functionality remained a mystery until recently. A landmark study done by Dr. Roderick Mackinnon's laboratory provided a stepping-stone for the membrane protein crystallization⁵ and today the membrane 3D database contains over 100 membrane protein including various Kv channels (http://blanco.biomol.uci.edu/membrane_proteins_xtal.html for a summary).

Empirical data spanning half a decade and recent crystallization of Kv channels in *Aeropyrum pernix* (KvAP)⁶ and Kv1.2⁷ have culminated into the following picture.

Delayed rectifier potassium channels can assemble as homotetramers⁸ with each of the four subunits composed of six transmembrane helices. Some voltage-gated potassium channels are also known to assemble as heterotetramers⁹. The S5 and S6 transmembrane helices and the interconnecting loop form the conduction pathway of the channel, also known as the pore^{5, 10}. The function of S1–S3 helices has not been yet clearly defined, but likely are important determinants of channel structure, gating¹¹⁻¹³ and the membrane targeting. The S4 helix is thought to be the voltage sensor in a wide variety of voltage-gated ion channels¹⁴⁻¹⁶. The S4 helix is composed of a regular array of positively charged amino acids with two hydrophobic residues between each positively charged amino acid¹⁷. The charged residues located within the transmembrane electric field are influenced by change in the membrane potential. Upon depolarization, the charge reversal on the membrane facilitates S4 movement, leading to channel opening¹⁸. The first four transmembrane helices (S1–S4) form the voltage-sensing domain, whereas the last two transmembrane helices (S5–S6), along with an intervening P loop, form the pore domain. The re-entrant loop contains a short pore helix and an extended polypeptide chain that contains the characteristic sequence motif TVGYG, which forms the selectivity filter¹⁹.

The TVGYG motif, located near the extracellular end of the pore, is highly (but not absolutely) conserved amongst K⁺ channels. The amino acid residues of this motif enable the filter to adopt a conformation in which the main chain carbonyl oxygen atoms point toward the center of the pore axis, generating six discrete binding sites for K⁺ ions flowing through the pore. The filter region exhibits a degree of flexibility which may be responsible for ‘fast gating’ of K⁺ channels²⁰. This chapter discusses the protein

identification and isolation of HOSK channel. HOSK has four hydrophobic domains (HD), which likely span the plasma membrane. HOSK has a variant voltage sensor between HD1 and HD2, characterized by the presence of positively charged amino acids, (arginine and lysine) spaced at every 3rd residue between non-cationic amino acids. Furthermore, HOSK predicts a re-entrant loop signifying a pore region but, unlike the prototypic Kv channel, the filter sequence appears to be GVL. Furthermore, the alignment of the amino acid sequence of HOSK in mammals and lack of alignment in non-amniotic species suggests that HOSK originated relatively late in evolution, in the amniotes.

3.2 MATERIAL AND METHODS

3.2.1 Generation of a HOSK Antibody

The pore sequence peptide H₂N-GVLLAYLEAREKRVN-COOH was used as an epitope for synthesis of an anti-pore, HOSK antibody. Keyhole limpet hemocyanin (KLH) was used with Freund's adjuvant (immunogen) for antibody synthesis. The bovine serum albumin conjugated with peptide was synthesized for the titration and subsequently affinity purification. The immunogen conjugated with peptide was injected in rabbits and the serum containing antibody was collected by Custom Hybridoma (Division of Pick Cell laboratories, Amsterdam, Netherlands).

3.2.2 Immunoblot

Immunoblotting was performed on PA and DA from patients, primary cultures of PSMCs and DASMCS and transfected CHO cells, as previously described in chapter 2. To assess the specificity of the HOSK band the immunogenic peptide was incubated with antibody in 10:1 ratio for 30 minutes and subsequently used as negative control primary antibody.

3.2.3 Plasmids

In an effort to isolate and purify HOSK channel a fusion of HOSK with myc protein was synthesized. Briefly, validated HOSK sense primer with modified antisense primer carrying the myc tag sequence was used to isolate HOSK transcript from human DA. The resultant cDNA transcript was used to synthesize HOSK channel fused with

myc protein. pTracer-CMV was used as the expression vector. The directional cloning was confirmed by Nru I restriction digest. Transfection in CHO cells and COS cells were performed with Fugene 6 transfection reagent (Roche, Indianapolis, Indiana) following the manufacturer's specifications.

3.2.4 Protein analysis with SELDI-TOF MS

To ensure that HOSK transfection yielded a protein of the sequence predicted in silico, based on a presumed ORF transcription, we performed SELDI-TOF MS (Surface Enhanced Laser Desorption Ionization/Time of Flight Mass Spectrometry: Ciphergen Fremont, California) with subsequent tryptic digestion. SELDI-TOF MS was used for protein identification. Enrichment of HOSK from transfected CHO cells was achieved by immunoprecipitation using the IPeX kit from GeBA (Kfar-Hanagid, Israel). The rabbit polyclonal, affinity-purified HOSK antibody was covalently coupled to agarose beads and HOSK was eluted according to the manufacturer's guideline. The eluted antigen was digested on-chip (NP20 array) with modified, sequencing-grade trypsin (Promega, Madison, WI). A 1:5 dilution of saturated alpha-cyano-4-hydroxy cinnamic acid in 50% Acetonitrile/0.5% trifluoroacetic acid was used as matrix. Tryptic peptides were then analyzed using a Ciphergen PBS II Protein Chip reader that had been externally calibrated with an all-in-one peptide standard from Ciphergen. Protein identification was performed by searching the ProFound database for identification of peptides of identical size.

3.2.5 *In silico* analysis

In silico analysis was performed to predict the probable open reading frame for HOSK. The Kyte-Doolittle Hydrophilicity plot (generated in MacVector (Accelrys, Inc, San Diego, CA) was used to identify the number of hydrophobic domains in HOSK. Entering the putative HOSK protein sequence this program predicted the number of transmembrane domains (using the criteria that a hydrophobic domain had to be at least 21 amino acid long to span the membrane). For this analysis, the hydrophobicity threshold was at 2, which is determined by the hydrophobic nature of the amino acid for the formation of hydrophobic transmembrane domain. Furthermore, various open reading frames in different species were generated starting from the first exon where the HOSK protein is translated. ClustalW alignment (<http://www.ebi.ac.uk/clustalw/>) was used to perform global progressive alignment of the resulting protein sequence amongst species. NetNglyc 1.0 server utility²¹ on the Center for Biological Sequence Analysis Prediction Servers (Technical University of Denmark; <http://www.cbs.dtu.dk/services/>) was used to predict HOSK glycosylation sites. Conserved domain analysis was done with conservative domain database (CDD) on NCBI database website (<http://www.ncbi.nlm.nih.gov/Structure/cdd/wrpsb.cgi>).

3.3 RESULTS

3.3.1 Analysis of the protein sequence

HOSK appears to a hydrophobic, cationic protein that contains 169 amino acid and has a predicted molecular weight of 18.8 kDa (although the immunoblot showed 21.3 kDa; discussed later: Figure 1). The Kyte-Doolittle hydrophilicity plot suggests 4 putative HDs with a hydrophilic reentrant loop (pore) between domains 3 and 4 (Figure 2). This suggests that HOSK has putative four transmembrane domains.

The features of the HOSK sequence that we believe confer voltage sensitivity includes the presence of positively charged amino acid between HD1 and HD2. These positive residues are interspaced with three non-polar amino acids, reminiscent of other Kv channels (Figure 1). Furthermore, the hydrophilicity plot also shows presence of a possible reentrant loop which is quite similar to other Kv channel. However, a closer inspection reveals that the pore sequence is unique (Figure 2). Our hypothesis is that the GVL sequence determines the K⁺ filter sequence for HOSK channel based on empirical data (see chapter 4). Conservative domain analysis suggests that HOSK has a myristoylation site (a post-translational modification that targets protein to the membrane²²) and a phosphorylation site for casein kinase II (Figure 3).

Subsequently *in silico* extension of 5' region of HOSK channel showed a putative upstream start codon in frame with the translation of HOSK channel. This putatively generates a HOSK protein of 270 amino acids. However, if the starting methionine of all the analyzed aminotic species is considered then the putative HOSK protein generated will be of 246 amino acids. (Figure 4). Although, our HOSK protein has 169 amino acids,

it represents the crux of the functional aspect of the channel (discussed in chapter 4 and 5).

3.3.2 Expression of HOSK channel

To identify the expression of HOSK protein in various tissues, a custom made antibody was synthesized targeted at the pore sequence. Immunoblots showed the presence of protein in 2 human DAs, 2 culture lines of human DASMCs and PSMCs (Figure 5). However, HOSK was absent in human PAs isolated from lung transplant patients. The custom-made antibody lacked the specificity as it isolated multiple bands in various tissue. Furthermore, we were unable to duplicate the blot. Therefore in an attempt to isolate HOSK channel from the HOSK transfected CHO cells, a fusion protein of HOSK with myc tag was synthesized. Despite the successful stable transfection (as indicated by the GFP fluorescence) and the corresponding HOSK current detected in electrophysiological recordings from the HOSK transfected CHO cells, we were unable to produce a viable immunoblot. Furthermore, immunochemistry was also preformed. The cells were fixed with paraformaldehyde and for the visualizing of the channel, secondary antibody were attached with Alexa 488 fluorophore (red). With the aid of 2-photon confocal microscopy we were unable to visualize the HOSK channel. Therefore, we used SELDI-TOF MS, a technology designed to detect small quantity protein.

3.3.3 Isolation of HOSK with SELDI-TOF MS

To further verify if HOSK transcript produces the proposed amino acid sequence, based on a presumptive ORF reading of the collagen 1A2 gene, HOSK protein was

isolated from transfected CHO cells. On the isolated cells SELDI-TOF MS was performed. Initial experimentation with the weak cation exchanger chip CM10 shows that HOSK produces a 21.3 kDa protein (larger protein than predicted), not seen in control and sham transfected CHO cells (Figure 6). This slightly larger size suggests that HOSK undergoes posttranslational modification that increases its mass from the predicted molecular of 18.8 kDa. Conservative domain analysis by NetNGly suggests presence of 2 putative glycosylation sites (NQEK at position 58 and NLVS at position 148). Antibody capture on protein chip using HOSK antibody also resulted in a singular peak of 21.3 kDa (Figure 7). Analysis of tryptic peptides after on-chip digestion did not correspond to any known protein in the ProFound database. However, the peaks (fragment sizes) were in agreement with the in silico digestion of the predicted HOSK protein sequence.

3.3.4 Evolutionary origination of HOSK

The HOSK protein is unique and is not homologous to known K⁺ channels or other ion channels. However, in silico sequence alignments show significant homology of HOSK across mammalian species, when the COL1A2 cDNA sequence is read in frame to create the HOSK protein. The analysis shows 84-95% similarity in pairwise comparison in predicted protein sequence amongst mammalian species; however, the *Xenopus* and zebrafish, non-amniotic species, lack HOSK (displaying only 30 and 42% similarity, respectively). Furthermore, functionally important elements of HOSK (the voltage sensing basic residues and the GVL putative pore sequence) are absent from the two non-amniotic organisms (Figure 8).

3.4 DISCUSSION

HOSK encodes a 169 amino acid protein with a molecular weight of 21.3 kDa. Although the empirical weight of HOSK is 21.3 kDa (based on SELDI-TOF MS), the estimated weight based on amino acid sequence suggests a protein of 18.8 kDa signifying a possible post-translational modification of HOSK. Conservative domain analysis of the HOSK channel suggests the presence of a putative myristoylation site. However, the fact that the myristoylation site is not at N-terminus raises questions as to whether it would be biologically active²³. We were unable to find any putative sites for palmitoylation or geranylgeranylation. However, putative glycosylation sites were sought with the NetNGlyc 1.0 Server. This analysis identified two putative glycosylation sites in HOSK.

Glycosylation has been reported to influence trafficking and/or function of other voltage-gated-like ion channels. These protein superfamilies include the transient receptor potential (TRP), voltage-gated sodium (Nav), voltage-gated calcium (Cav), hyperpolarization-activated cyclic nucleotide gated (HCN), cyclic nucleotide-gated (CNG), voltage-gated potassium (Kv), two-pore potassium (K2P), calcium-activated potassium (KCa), and inwardly rectifying potassium (Kir) channel families²⁴. In human ether-go-go (HERG) channels (also known as KV11.1), mutagenesis of this glycosylation site causes aberrant targeting to the membrane^{25, 26}. This has been associated with a naturally occurring human mutation which appears to be linked to a variant of the "long QT syndrome" which precipitates potentially lethal cardiac dysrhythmias²⁷. HCN2, a channel which has a mutation of the putative glycosylation site, similarly failed to traffic to the plasma membrane²⁸. Unlike these members of the voltage-gated-like channel²⁴, TRPV4 membrane trafficking is downregulated rather than facilitated by glycosylation²⁹.

Thus, glycosylation is important regulator of channel protein trafficking to the membrane and HOSK is equipped for this type of regulation.

Conservative domain analysis of the HOSK channel also indicates the presence of casein kinase II phosphorylation site. Casein kinase II is a ubiquitous second messenger-independent serine-threonine protein kinase consisting of two α catalytic and two regulatory β subunits and is believed to be constitutively active³⁰⁻³². Recently, casein kinase II is emerging as an enzyme that plays a key role in neuronal tissue. The highest level of casein kinase II activity is in the brain and substrates have been identified in both synaptic and nuclear compartments³³ and has been shown to increase NMDA channel activity in hippocampal neurons³⁴. Furthermore, studies indicate that a high level of constitutive phosphorylation of the Kv3.1 channel, consistent with casein kinase II -mediated phosphorylation, increases the activity of Kv3.1 channel when expressed in CHO cells or in medial nucleus of the trapezoid body (MNTB) neurons³⁵. The properties of Kv3.1 that are sensitive to casein kinase II (decreasing the threshold of activation and inactivation) are critical for the transmission of high-frequency signaling within the MNTB³⁵. Because of its role in high-frequency transmission, casein kinase II -mediated phosphorylation may play a role in conducting auditory information^{36, 37}. Furthermore, the unique property of activation and inactivation at relatively positive potentials ensures that Kv3.1 attenuates the amplitude of the action potential and is available to rapidly repolarize the membrane during high-frequency firing, as compared to other classic delayed rectifiers³⁷. Thus, casein kinase II contributes to the activation of Kv3.1 and rapid repolarization of the membrane.

More recently, casein kinase II has been shown to deactivate small conductance Ca^{2+} -activated K^+ channels (SK_{Ca} channels). SK_{Ca} channels couple the membrane potential to fluctuations in intracellular Ca^{2+} concentration in many types of cells³⁸⁻⁴⁰. SK_{Ca} channels are gated by Ca^{2+} ions via calmodulin, which is constitutively bound to the intracellular COOH terminus of the channel, where it serves as a Ca^{2+} sensor^{41, 42}. The cytoplasmic N and C termini of the SK_{Ca} channel protein form a polyprotein complex with the catalytic and regulatory subunits of protein kinase casein kinase II and protein phosphatase 2A⁴³. Within this complex, casein kinase II phosphorylates calmodulin at threonine 80, reducing by 5-fold the apparent Ca^{2+} sensitivity and accelerating channel deactivation⁴³. Thus, casein kinase II is involved in regulating SK_{Ca} channel activity. Due to the known role of casein kinase II in channel activation and deactivation the identification of targets for this kinase suggest it has the potential to regulate the open-state probability of HOSK channels.

3.4.1 Structural Biology of the HOSK Channel

3.4.1.1 Putative Hydrophobic Domains

The HOSK channel have four HDs with a re-entrant loop between HD3 and HD4, signifying a pore region. Although a similar profile of four HDs are also found in TASK. However, unlike one pore in HOSK, TASK channels have two pore. The two-pore-domain K^+ channels, or K2P channels, constitute a novel class of K^+ channel subunits. They have four transmembrane segments and are active as dimers. The tissue distribution of these channels is widespread, and they are found in both excitable and nonexcitable cells. K2P channels produce currents with unusual characteristics. They are quasi-

instantaneous and noninactivating, and they are active at all membrane potentials and insensitive to the classic K⁺ channel blockers⁴⁴. These properties designate them as background or “leak” K⁺ channels⁴⁵. Because of their activity at negative potential they have the potential to play a major role in setting the resting membrane potential^{46, 47}. Another salient feature of K₂P channels is the diversity of their regulatory mechanisms. The tandem of P domains in weak inward rectifiers (TWIK) -1 and TWIK-2 are stimulated by activators of protein kinase C and decreased by internal acidification. The baseline TWIK-related acid-sensitive K⁺ (TASK)-1 and TASK-2 channels are sensitive to external pH changes in a narrow range, near physiological pH. The TWIK-related (TREK)-1 and TWIK-related arachidonic acid-stimulated K⁺ (TRAAK) channels are the first polyunsaturated fatty acid-activated and mechano-gated K⁺ channels⁴⁸ to be cloned. Although, the HOSK has four HDs, it’s electrophysiology and pharmacology markedly differs from K₂P channels. HOSK is voltage-gated and is inhibited by drugs such as 4-aminopyridine (4-AP; inhibitor of K_v channels), correolide (inhibitor of K_v1.x channels) and margatoxin (K_v1.3 channel inhibitor). Furthermore, HOSK is also regulated by oxygen. Given these properties, HOSK represents a new class of channel characterized by four HDs, one-pore and sensitivity to K_v channel inhibitory drugs comparable to certain Shaker (K_v1.x) channels. (All the above mentioned properties such as response to 4-AP, correolide, margatoxin and response to oxygen is discussed in chapter 4).

3.4.1.2 Voltage sensing

HOSK’s putative voltage-sensing domain lies as a part of HD1, and is comprised of 2 arginine and 2 lysine residues, separated by 2 non-cationic amino acids. This

configuration has similarities to the S4 region (voltage sensor) of typical Kv channels; however HOSK's voltage sensor differs in length and in the properties of residues interposed between the cationic amino acids¹⁹. This similarity suggests that while HOSK and other Kv channels share similar voltage-sensing mechanisms there is a fundamental difference in sensor structure.

3.4.2.2 Gating of K⁺ channels

The charge moved during gating and required to open the channel presumably arises from contributions from several areas of the channel. In HOSK channel this might be achieved by 4 positively charged amino acids. In Kv channels the predominant contribution comes from the S4 helix with seven positively charged lysine and arginine residues. Partly because the breadth of the transmembrane voltage field is unknown and the seven charged S4 residues cover a large portion of the helix, it is thought that each residue will contribute different amounts to the total gating charge. This has been supported by mutational studies which look at total gating charge per channel following neutralization mutations of individual charged residues^{14, 15, 49, 50}. Neutralization of any one of the first four charged residues (those closest to the extracellular space in *Shaker*, specifically R362, R365, R368 and R371) significantly reduces total gating charge per channel^{15, 50} (Figure 3 in Chapter 1). The exact contribution of each of these residues is difficult to assess because the neutralizations may change the channel structure or influence the transmembrane region through which the field is focused. However, these four residues all seem to contribute to the total gating charge which moves upon during depolarization⁵¹. In *Shaker* channels there are an additional three charged residues (K374,

R377 and K380) which are located closer to the intracellular space. Neutralization of K374 to glutamine results in no functional expression of the channel^{49, 52-54} and therefore, its role is hard to interpret. The sixth charged residue, R377, shows no change in channel gating when mutated to the neutral glutamine^{49, 53, 54}. Moreover, histidine-scanning mutagenesis suggests that this residue does not participate in gating⁵¹. Neutralization of the seventh residue, K380, does not lead to a reduction in gating charge^{15, 54}. Thus, it seems that charged residues closer to the extracellular space (R362–R371) contribute more to total gating charge than residues closer to the intracellular space (K374–K380). Supporting the putative voltage sensor we identified four residues in HOSK channel which might be responsible for gating and is in agreement with these Kv data emphasizing that four charged residues are sufficient to create an intact voltage-sensor.

The positively charged amino acids in the sensor undergo conformational change when depolarization occurs. The conformational change is coupled to the K⁺ channel gating which induces channel opening. However, the precise mechanism of this pathway remains the subject of vigorous debate. Prior to the era of K⁺ channel crystallization, empirical data were used to formulate a voltage sensing domain model with following characteristics:

- (i) Each S4 segment is insulated from the surrounding hydrophobic environment of the bilayer by aqueous vestibules and a short, hydrophobic ‘gating pore’, formed largely by S1–S3 segments peripherally and the pore domain centrally. These vestibules allow the hydration of the S4 segment up to 20 Å from the intracellular, and 5 Å from the extracellular, space⁵⁵.
- (ii) The electric field is primarily focused across the 10 Å gating pore, which is much

thinner than the thickness of the bilayer⁵⁵.

(iii) The S2 is lined with 1-3 negative charges, strategically placed to lower the energy of the S4 charges while they are transiently docked within it⁵¹.

(iv) The S4 segment responds to changes in transmembrane voltage with relatively small movements, estimated to be $<15 \text{ \AA}$, whereas the S1–S3 segments remain more or less unperturbed by voltage. These S4 movements can involve one or more combinations of tilt, rotation, axial and lateral translation, and minor changes in secondary structure, thus giving rise to the several variations of the conventional model^{56, 57}. In all variants of the conventional model, however, there is an energetic problem of moving charged amino acids through a low dielectric environment. This problem can be solved in two ways: first, by placing a majority of S4 charges in a highly solvated aqueous environment; second, by stabilizing transitions through the gating pore with negative charges^{56, 57}. Thus, the S4 charges cross the membrane with minimal contact with the hydrophobic core of the bilayer. However, crystallization of KvAP suggested an alternative voltage-sensing model: the paddle model.

The paddle model of voltage sensing was recently introduced by members of the MacKinnon laboratory^{6, 58}. Based on high-resolution structures of the bacterial K⁺ channel KvAP and an accessibility study using tethered biotin, the paddle model of voltage sensing⁵⁸, is radically different from the conventional model. As its name implies, the critical component of this model is a paddle-like structure formed by S4 and the C-terminal half of S3 (S3b). One subunit of the KvAP structure is shown with the permeation pathway oriented vertically to its left side. Set apart from the pore domain, the voltage sensor paddle is a fixed unit that carries its charged cargo across the bilayer

with large >20 Å movements entirely through lipid. Perhaps the most appealing feature of the paddle model is its simplicity. The rigid helix–turn–helix structure that comprises the paddle takes the place of the shielded sliding helix, proposed in the conventional model, and translocates its gating charges across the entire bilayer *en masse* in response to changes of membrane potential.

The new results of Cuello *et al.*⁵⁹ indeed confirm that at least one face of the S4 segment is exposed to the lipid bilayer but that face does not contain the charged residues. In the paddle model, the charges move in the lipid bilayer, in contrast to the classical gating model, in which they are in a protected environment, presumably made of protein and water. The electron paramagnetic resonance (EPR) results show that most of the charged residues in S4 (Arg123, Arg126, Arg133 and Arg136), when replaced by an spin-labeled mutant, show low mobility and low accessibility to O₂ or Ni⁺⁺ chelate complex (NiEdda), which strongly suggests that they are not exposed to the lipid environment. Starting from the extracellular side, the second charged residue, Arg120, is partially protected and the first charged residue is mobile and exposed to water and lipid, which is consistent with a location in the transition-boundary layer of the lipid bilayer. The EPR results exhibit a phase change along the S4 segment, which suggests a break in the α -helical structure. One possible interpretation proposed by Cuello *et al.*⁵⁹ puts all the charged residues intracellularly, away from the lipid bilayer. In the *Shaker* K⁺ channel, only the four most-extracellular charges are part of the gating charges^{50, 52}, whereas the most intracellular charges are important for structural stability of the S4 segment¹³. It will be important to determine whether, in KvAP, Arg133 and Arg136 form part of the voltage sensor so that a detailed mechanism of gating charge movement can be proposed.

Thus, like Cuello et al. suggested HOSK voltage sensor might be intracellular and is part of HD1 domain. Moreover, HOSK is structurally unique and is unlike all known K⁺ channels, therefore, understanding its gating would also likely have great value.

3.4.1.4 Selectivity Filter

HOSK channel has a proposed re-entrant loop between the HD3 and the HD4 region. This topology is similar to other known Kv channels where the last two segments harbor the pore-forming loop. However, the residues present in HOSK's pore region are distinct from those in conventional Kv channels. The ionic selectivity and conduction of other Kv channels are determined by TVGYG sequence. These amino acids have been shown through mutagenesis, crystallization and computational analysis to be the prime determinant of the K⁺ ion selectivity. HOSK, on the other hand, has GVL as its K⁺ ion selectivity sequence. However, this break from convention is not without precedent. Variation in the conservative domain of pore sequence GYG are known. Channels such as Erg, Kv6.1 and the TASK family use variation of GYG domain such as GFG or GLG⁶⁰. Furthermore, Mackinnon's group has shown that substitution of GYG with GVG maintains K⁺ selectivity⁶¹. Recently, Salinas et al has cloned a subunit named KCNK7 which, although it does not form a functional channel alone (it requires another unidentified subunit), employs GLE as its selectivity filter⁶². Furthermore, various prokaryotes have alternative K⁺ recognition site. For example, *T. maritime*, an archaeobacteria, uses GYSI as a K⁺ filter sequence⁶³, while the bacterium *Chlorobi tepidum* uses GFSE as its filter sequence^{64, 65}. A complete list of 28 different bacteria with variant pore sequence is shown in Table 1. Thus, given the prior evidence in

prokaryotes and eukaryotes, HOSK's use of GVL as a K⁺ selectivity has biological plausibility (and is supported by our mutagenesis experiments Figure 22 in chapter 4).

Immunoblot analysis shows that the HOSK channel is present in human DA and DASMC and PASMC, although such expression was not evident in human PA. Admittedly, our HOSK antibody was imperfect for immunoblotting, tending to yield multiple bands. In an attempt to increase the specificity of isolation of HOSK channel from the transfected CHO cells we synthesized a fusion protein of HOSK with a myc tag. The HOSK transfected CHO cells showed significant expression of HOSK channel as determined by GFP expression, our reporter gene. This was further substantiated in CHO cell transfected with HOSK-myc transcript. However, once again, an anti-myc immunoblot failed to show the presence of any protein with use of HOSK and/or myc antibody (data not shown). This led to the conclusion that the protein was likely not abundant and required a more sensitive detection technique. Supporting this, transfection reliably revealed GFP immunofluorescence (indicating transgene expression).

Using SELDI-TOF MS which employs the sophistication of mass spectrometry coupled with isolation of protein on an chromatographic membrane, we were able to purify HOSK. This was possible as SELDI-TOF MS requires a very small amount of protein. Protein-Chip analysis showed that HOSK is a 21.3 kDa protein. On-chip tryptic digestion resulted in peaks that corresponded to no known protein in the ProFound database (This database has the entries of proteins with its corresponding trypsin digested spectrum). However, comparison of *in silico* tryptic digestion of HOSK resulted in peptide fragments that significantly corroborated with the peaks generated by the on-chip

tryptic digestion. This suggests that the putative sequence of HOSK as generated by in silico analysis is in agreement with the empirical data of the protein chip.

3.4.2 Evolutionary Perspective

Kv channels originated at a time when primordial organisms were establishing themselves as Earth's first inhabitants. Since their appearance in evolution, Kv channels have largely retained their structure, to the extent that *Drosophila* and *Homo sapiens* share very similar K⁺ channels. Therefore, Kv channels represent a conserved and ancient membrane protein essential to separating the inner self from the outside environment, while allowing selective communication.

The HOSK protein is unique and is not homologous to known K⁺ channels or other ion channels. However, in silico sequence alignments show significant similarity of HOSK across mammalian species, when the COL1A2 cDNA sequence is read in frame to create the HOSK protein. The analysis shows 84-95% similarity in pairwise comparison in the predicted protein sequence amongst mammalian species (Figure 4). However, *Xenopus* and zebrafish, non-amniotic species, lack HOSK (displaying an amino acid *in silico* match of 30 and 42%, respectively). Furthermore, functionally important elements of HOSK (the voltage sensing basic residues and the GVL putative pore sequence) are absent from the two non-amniotic organisms. A nucleotide BLAST search of genome sequences indicates that the nucleotide sequence corresponding to HOSK first appears in vertebrates, when the collagen $\alpha 2(I)$ arose (it is present in *Danio rerio* but absent from *Ciona intestinalis* a non-vertebrate chordate), but that the functional HOSK coding region originated as an overlapping coding region in animals that develop amnions. Since the

alignment doesn't show significant similarity with any other channels, and the phylogenetic tree doesn't group with any other family, we suggest that HOSK is a novel K^+ channel. However, question remains why HOSK came into existence late in the evolution.

Studies have shown that most genes specific to nervous system, emerged as a result of either activating dormant genes or due to *de novo* existence⁶⁶. Recent comparison of nervous system -specific genes from organisms ranging from metazoa to humans found that 14% of the nervous system -specific orthologous genes had emerged prior to the divergence between yeast and human⁶⁷. This suggests that a common ancestor, which had no nervous system, already possessed a portion of the genes homologous to human nervous system -specific genes. This further implies that 14% of the nervous system -specific genes changed their original function during evolution⁶⁸. The remainder of 86% of the 255 nervous system -specific human genes seemed to have emerged during evolution. These authors found that 24% of the 255 nervous system -specific genes emerged after divergence of urochordata and human but before divergence of fishes and human⁶⁷ (Figure 9). They concluded that the main cause of the nervous system evolution was the addition of new genes around the time of the emergence of vertebrates. Thus, HOSK may have originated when the nervous system was undergoing extensive evolutionary remodeling. The pressure of new proteins for nervous system might have resulted in evolutionary existence of HOSK (as EST for HOSK was found in dorsal root ganglia).

3.4.3 Summary

HOSK is a 21.3kDa protein which has putative sites for post-translational modification by glycosylation and CK2 phosphorylation. Although not yet crystallized, in silico analysis indicates that HOSK has four HD and one reentrant loop (pore). The voltage-sensing domain of the HOSK channel is distinct from that in other Kv channels, although there are similarities in the spaced deployment of charged amino acids. However, the kinship between Kv channels and the HOSK falters at the potassium filter sequence. Therefore, the protein structure of HOSK suggests a new class of K^+ channels. To facilitate future studies of electrophysiology and protein crystal structure, we have successfully incorporated the HOSK cDNA sequence in sync with the coding region of pQE-TriSystem vector for synthesis and purification of HOSK channels in mammalian cells. We plan to reconstitute the HOSK channel in artificial bilayer in hopes to measure the activity of nascent HOSK channels and also hope to acquire sufficient protein to perform crystallography.

3.5 REFERENCES

1. Capener, C. E., Kim, H. J., Arinaminpathy, Y. & Sansom, M. S. Ion channels: structural bioinformatics and modelling. *Hum Mol Genet* 11, 2425-33 (2002).
2. Ashcroft, F. M. From molecule to malady. *Nature* 440, 440-7 (2006).
3. Modell, S. M. & Lehmann, M. H. The long QT syndrome family of cardiac ion channelopathies: a HuGE review. *Genet Med* 8, 143-55 (2006).
4. Weir, E. K., Lopez-Barneo, J., Buckler, K. J. & Archer, S. L. Acute oxygen-sensing mechanisms. *N Engl J Med* 353, 2042-55 (2005).
5. Doyle, D. A. et al. The structure of the potassium channel: molecular basis of K⁺ conduction and selectivity. *Science* 280, 69-77 (1998).
6. Jiang, Y. et al. X-ray structure of a voltage-dependent K⁺ channel. *Nature* 423, 33-41 (2003).
7. Long, S. B., Campbell, E. B. & Mackinnon, R. Crystal structure of a mammalian voltage-dependent Shaker family K⁺ channel. *Science* 309, 897-903 (2005).
8. MacKinnon, R. New insights into the structure and function of potassium channels. *Curr Opin Neurobiol* 1, 14-9 (1991).
9. Sheng, M., Liao, Y. J., Jan, Y. N. & Jan, L. Y. Presynaptic A-current based on heteromultimeric K⁺ channels detected in vivo. *Nature* 365, 72-5 (1993).
10. Yellen, G., Jurman, M. E., Abramson, T. & MacKinnon, R. Mutations affecting internal TEA blockade identify the probable pore-forming region of a K⁺ channel. *Science* 251, 939-42 (1991).
11. Papazian, D. M. Potassium channels: some assembly required. *Neuron* 23, 7-10 (1999).

12. Tiwari-Woodruff, S. K., Lin, M. A., Schulteis, C. T. & Papazian, D. M. Voltage-dependent structural interactions in the Shaker K(+) channel. *J Gen Physiol* 115, 123-38 (2000).
13. Tiwari-Woodruff, S. K., Schulteis, C. T., Mock, A. F. & Papazian, D. M. Electrostatic interactions between transmembrane segments mediate folding of Shaker K⁺ channel subunits. *Biophys J* 72, 1489-500 (1997).
14. Liman, E. R., Hess, P., Weaver, F. & Koren, G. Voltage-sensing residues in the S4 region of a mammalian K⁺ channel. *Nature* 353, 752-6 (1991).
15. Logothetis, D. E., Movahedi, S., Satler, C., Lindpaintner, K. & Nadal-Ginard, B. Incremental reductions of positive charge within the S4 region of a voltage-gated K⁺ channel result in corresponding decreases in gating charge. *Neuron* 8, 531-40 (1992).
16. Noda, M. et al. Primary structure of *Electrophorus electricus* sodium channel deduced from cDNA sequence. *Nature* 312, 121-7 (1984).
17. Fedida, D. & Hesketh, J. C. Gating of voltage-dependent potassium channels. *Prog Biophys Mol Biol* 75, 165-99 (2001).
18. Catterall, W. A. Structure and function of voltage-sensitive ion channels. *Science* 242, 50-61 (1988).
19. MacKinnon, R. Potassium channels. *FEBS Lett* 555, 62-5 (2003).
20. Sands, Z., Grottesi, A. & Sansom, M. S. Voltage-gated ion channels. *Curr Biol* 15, R44-7 (2005).

21. Blom, N., Sicheritz-Ponten, T., Gupta, R., Gammeltoft, S. & Brunak, S. Prediction of post-translational glycosylation and phosphorylation of proteins from the amino acid sequence. *Proteomics* 4, 1633-49 (2004).
22. Farazi, T. A., Waksman, G. & Gordon, J. I. The biology and enzymology of protein N-myristoylation. *J Biol Chem* 276, 39501-4 (2001).
23. Boutin, J. A. Myristoylation. *Cell Signal* 9, 15-35 (1997).
24. Yu, F. H. & Catterall, W. A. The VGL-kanome: a protein superfamily specialized for electrical signaling and ionic homeostasis. *Sci STKE* 2004, re15 (2004).
25. Gong, Q., Anderson, C. L., January, C. T. & Zhou, Z. Role of glycosylation in cell surface expression and stability of HERG potassium channels. *Am J Physiol Heart Circ Physiol* 283, H77-84 (2002).
26. Petrecca, K., Atanasiu, R., Akhavan, A. & Shrier, A. N-linked glycosylation sites determine HERG channel surface membrane expression. *J Physiol* 515 (Pt 1), 41-8 (1999).
27. Satler, C. A., Vesely, M. R., Duggal, P., Ginsburg, G. S. & Beggs, A. H. Multiple different missense mutations in the pore region of HERG in patients with long QT syndrome. *Hum Genet* 102, 265-72 (1998).
28. Much, B. et al. Role of subunit heteromerization and N-linked glycosylation in the formation of functional hyperpolarization-activated cyclic nucleotide-gated channels. *J Biol Chem* 278, 43781-6 (2003).

29. Xu, H., Fu, Y., Tian, W. & Cohen, D. M. Glycosylation of the osmoreponsive transient receptor potential channel TRPV4 on Asn-651 influences membrane trafficking. *Am J Physiol Renal Physiol* 290, F1103-9 (2006).
30. Allende, C. C. & Allende, J. E. Promiscuous subunit interactions: a possible mechanism for the regulation of protein kinase CK2. *J Cell Biochem Suppl* 30-31, 129-36 (1998).
31. Allende, J. E. & Allende, C. C. Protein kinases. 4. Protein kinase CK2: an enzyme with multiple substrates and a puzzling regulation. *Faseb J* 9, 313-23 (1995).
32. Dobrowolska, G., Lozeman, F. J., Li, D. & Krebs, E. G. CK2, a protein kinase of the next millennium. *Mol Cell Biochem* 191, 3-12 (1999).
33. Blanquet, P. R. Casein kinase 2 as a potentially important enzyme in the nervous system. *Prog Neurobiol* 60, 211-46 (2000).
34. Lieberman, D. N. & Mody, I. Casein kinase-II regulates NMDA channel function in hippocampal neurons. *Nat Neurosci* 2, 125-32 (1999).
35. Macica, C. M. & Kaczmarek, L. K. Casein kinase 2 determines the voltage dependence of the Kv3.1 channel in auditory neurons and transfected cells. *J Neurosci* 21, 1160-8 (2001).
36. Brew, H. M. & Forsythe, I. D. Two voltage-dependent K⁺ conductances with complementary functions in postsynaptic integration at a central auditory synapse. *J Neurosci* 15, 8011-22 (1995).
37. Wang, L. Y., Gan, L., Forsythe, I. D. & Kaczmarek, L. K. Contribution of the Kv3.1 potassium channel to high-frequency firing in mouse auditory neurones. *J Physiol* 509 (Pt 1), 183-94 (1998).

38. Oliver, D. et al. Gating of Ca²⁺-activated K⁺ channels controls fast inhibitory synaptic transmission at auditory outer hair cells. *Neuron* 26, 595-601 (2000).
39. Stocker, M., Krause, M. & Pedarzani, P. An apamin-sensitive Ca²⁺-activated K⁺ current in hippocampal pyramidal neurons. *Proc Natl Acad Sci U S A* 96, 4662-7 (1999).
40. Tse, A. & Hille, B. GnRH-induced Ca²⁺ oscillations and rhythmic hyperpolarizations of pituitary gonadotropes. *Science* 255, 462-4 (1992).
41. Keen, J. E. et al. Domains responsible for constitutive and Ca(2+)-dependent interactions between calmodulin and small conductance Ca(2+)-activated potassium channels. *J Neurosci* 19, 8830-8 (1999).
42. Xia, X. M. et al. Mechanism of calcium gating in small-conductance calcium-activated potassium channels. *Nature* 395, 503-7 (1998).
43. Bildl, W. et al. Protein kinase CK2 is coassembled with small conductance Ca(2+)-activated K⁺ channels and regulates channel gating. *Neuron* 43, 847-58 (2004).
44. Lesage, F. et al. TWIK-1, a ubiquitous human weakly inward rectifying K⁺ channel with a novel structure. *Embo J* 15, 1004-11 (1996).
45. Duprat, F. et al. TASK, a human background K⁺ channel to sense external pH variations near physiological pH. *Embo J* 16, 5464-71 (1997).
46. Gurney, A. M. et al. Two-pore domain K channel, TASK-1, in pulmonary artery smooth muscle cells. *Circ Res* 93, 957-64 (2003).

47. Schmid, A., Feick, P. & Schulz, I. Inwardly rectifying, voltage-dependent and resting potassium currents in rat pancreatic acinar cells in primary culture. *J Physiol* 504 (Pt 2), 259-70 (1997).
48. Lesage, F. & Lazdunski, M. Molecular and functional properties of two-pore-domain potassium channels. *Am J Physiol Renal Physiol* 279, F793-801 (2000).
49. Perozo, E., Santacruz-Toloza, L., Stefani, E., Bezanilla, F. & Papazian, D. M. S4 mutations alter gating currents of Shaker K channels. *Biophys J* 66, 345-54 (1994).
50. Seoh, S. A., Sigg, D., Papazian, D. M. & Bezanilla, F. Voltage-sensing residues in the S2 and S4 segments of the Shaker K⁺ channel. *Neuron* 16, 1159-67 (1996).
51. Bezanilla, F. The voltage sensor in voltage-dependent ion channels. *Physiol Rev* 80, 555-92 (2000).
52. Aggarwal, S. K. & MacKinnon, R. Contribution of the S4 segment to gating charge in the Shaker K⁺ channel. *Neuron* 16, 1169-77 (1996).
53. Papazian, D. M. et al. Electrostatic interactions of S4 voltage sensor in Shaker K⁺ channel. *Neuron* 14, 1293-301 (1995).
54. Papazian, D. M., Timpe, L. C., Jan, Y. N. & Jan, L. Y. Alteration of voltage-dependence of Shaker potassium channel by mutations in the S4 sequence. *Nature* 349, 305-10 (1991).
55. Gandhi, C. S. & Isacoff, E. Y. Molecular models of voltage sensing. *J Gen Physiol* 120, 455-63 (2002).
56. Horn, R. How S4 segments move charge. Let me count the ways. *J Gen Physiol* 123, 1-4 (2004).

57. Yellen, G. The moving parts of voltage-gated ion channels. *Q Rev Biophys* 31, 239-95 (1998).
58. Jiang, Y., Ruta, V., Chen, J., Lee, A. & MacKinnon, R. The principle of gating charge movement in a voltage-dependent K⁺ channel. *Nature* 423, 42-8 (2003).
59. Cuello, L. G., Cortes, D. M. & Perozo, E. Molecular architecture of the KvAP voltage-dependent K⁺ channel in a lipid bilayer. *Science* 306, 491-5 (2004).
60. Shealy, R. T., Murphy, A. D., Ramarathnam, R., Jakobsson, E. & Subramaniam, S. Sequence-function analysis of the K⁺-selective family of ion channels using a comprehensive alignment and the KcsA channel structure. *Biophys J* 84, 2929-42 (2003).
61. Heginbotham, L., Lu, Z., Abramson, T. & MacKinnon, R. Mutations in the K⁺ channel signature sequence. *Biophys J* 66, 1061-7 (1994).
62. Salinas, M. et al. Cloning of a new mouse two-P domain channel subunit and a human homologue with a unique pore structure. *J Biol Chem* 274, 11751-60 (1999).
63. Nelson, K. E. et al. Evidence for lateral gene transfer between Archaea and bacteria from genome sequence of *Thermotoga maritima*. *Nature* 399, 323-9 (1999).
64. Kawarabayasi, Y. et al. Complete genome sequence of an aerobic thermoacidophilic crenarchaeon, *Sulfolobus tokodaii* strain 7. *DNA Res* 8, 123-40 (2001).
65. She, Q. et al. The complete genome of the crenarchaeon *Sulfolobus solfataricus* P2. *Proc Natl Acad Sci U S A* 98, 7835-40 (2001).

66. Holland, N. D. Early central nervous system evolution: an era of skin brains? *Nat Rev Neurosci* 4, 617-27 (2003).
67. Noda, A. O., Ikeo, K. & Gojobori, T. Comparative genome analyses of nervous system-specific genes. *Gene* 365, 130-6 (2006).
68. Sarnat, H. B. & Netsky, M. G. When does a ganglion become a brain? Evolutionary origin of the central nervous system. *Semin Pediatr Neurol* 9, 240-53 (2002).

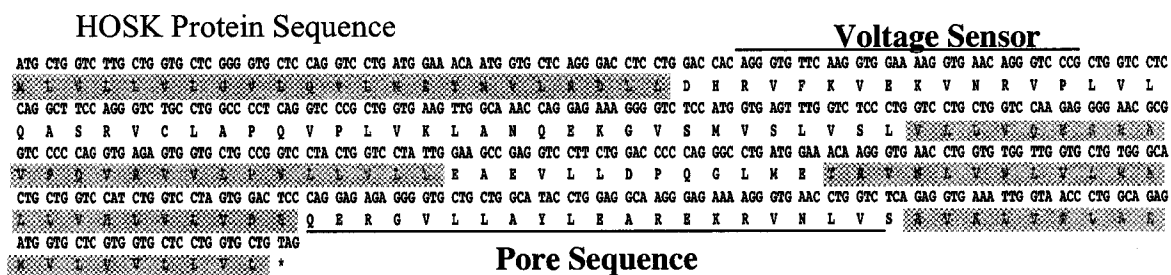


Figure 3.1: Amino acid sequence of the HOSK channel. The putative four hydrophobic domains are indicated by shaded regions. The underlined portion of the sequence signify the voltage-sensing domain and the pore sequence.

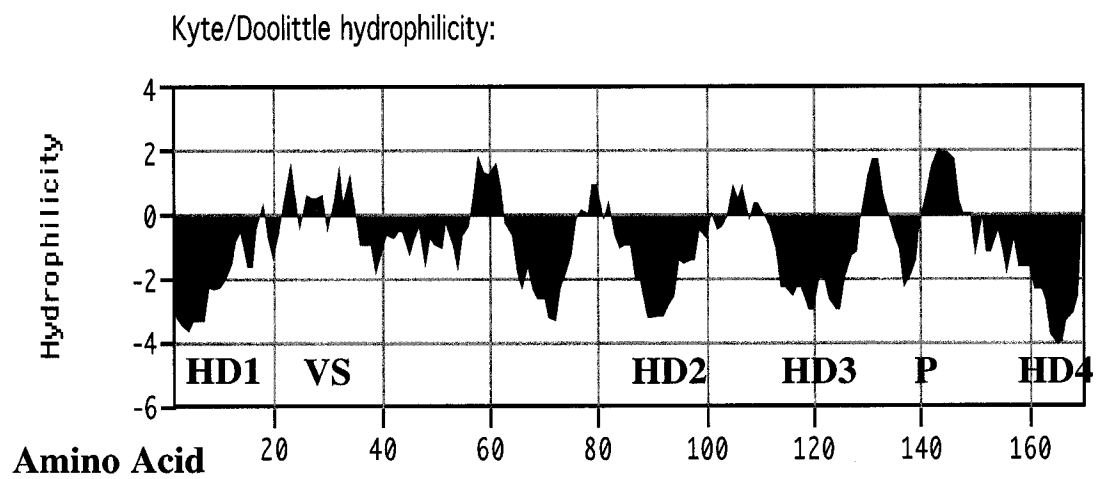


Figure 3.2: Kyte-Doolittle hydrophilicity plot of the HOSK channel. The putative Hydrophobic Domains are identified as HD1, HD2, HD3 and HD4. The P signifies the pore region and VS signifies voltage-sensing domain

MLVLLVLGVLQVLMETMVLRDLLDHRVFKVEKVNR
↓ ↓
VPLVLQASRVCLAPQVPLVKLANQEKGVSMVSLVSLV
LLVQEGNAVQVRVVLPLVLLVLEAEVLLDPQGLMET
RVNLVWLVLWALLVHLVLVDSQERGVLLAYLEAREK
↓
RVNLVSEVKLVTLAEMVLVLLVL

Figure 3.3: Amino acid sequence of the HOSK channel. The black arrows shows the putative site for glycosylation and the grey arrow marks the site for casein kinase II phosphorylation.

HOSK	1	-----		0
Human	1	MAELASWALLVVVVQVALLESEDI	MEMLVALGSLVSWDPEVFLVPLEISA	50
Macaca	1	MAELASWALLVVVVRVALLEFEAR	MEMLVALGSPVSWDPEVFLVPLEISA	50
Rat	1	-----	MEMPVALENLVSWDPEVFPGLLEMLA	26
Mice	1	-----	MEMPVDLGNLVSWDPEVFLGLLEMLA	26
Dog	1	MAQLVSWVLPALGVPPALLVSAV	MEILVALESLASWDPEVFLVPLVMLA	50
Cow	1	-----	MEILVALESLASWDPEVSVQVPLEISA	26
HOSK	1	-----		0
Human	51	PLEKKVLSASLASTAGLAQLAQLEQEESLATLDSLDPKAPLVILAKTVIK		100
Macaca	51	PLEKKVLSAFLASTAGLAQLAQLEQEESLATLDSLDPKAPLVILAKTVIK		100
Rat	27	QLVKKALWVSLASMADLAQLAQLDQEVKLATSDSLDPKAPLVILANLVRK		76
Mice	27	HLVKKALWVSLALMADLAQSAQLDQEVKLATSDSLDPKAPLVILANLVRE		76
Dog	51	QLVKKVPWVSLVLMAGLDQLAQREQEESPATSDSLDPKAPLVILAKMVIK		100
Cow	27	QLVKKVLWVSLVLTADLGPLAQREQEESLATLDSLDPKAPVVILAKLVKK		76
HOSK	1	-----		0
Human	101	VMLVLLVLGVLQVLMETMVLRLDLLDHRVFKVEKVNRPVPLVLQASRVCLAP		150
Macaca	101	VMLVLLVLGVLQVPMETMVLRLDLLDHRVSKVEKVNRPVPLVLQVSRVCLAP		150
Rat	77	APVSLVLGELQVPTATMVLRALDLRVFKVAKVNRALLVLQASRVSRVP		126
Mice	77	DPVLLVLGELQDPMATMELRAPLDRVFKVAKVNKALLVLLASRVSQVP		126
Dog	101	VMLVLLVLGVLQVLMETMVLRLDLLDHRVSKVEKVNRPVPLVLQASRVCLAP		150
Cow	77	VMLVLLVLGALQVPMATTVLRDPLDYRVSKVEKVNRPVLLVLQASRVCLAL		126
		* * * * *	* * * * *	
HOSK	50	QVPLVKLANQEKGVSMVSLVSLVLLVQEGNAVQVRVVLVPLVLLVLEAEV		99
Human	151	QVPLVKLANQEKGVSMVSLVSLVLLVQEGNAVQVRVVLVPLVLLVLEAEV		200
Macaca	151	QGQLVKLANQEKGVSLVSLVSLVLLVQEGNAVQVRVVLVPLVLLVLEAEV		200
Rat	127	LVPLEKLASREKGVFPVNSVSLVLLVQEEENVVQVRVELLVLVLLVLESEV		176
Mice	127	QVLEKLASPEKGVFLVNSVSLVLLVQEEENVVPRVVELLALLVLVLEAEV		176
Dog	151	QVQLVKLANQEKGVSLVNLVFLVLLVQEGSVVPLEKVLLVLLVLLVLEAEV		200
Cow	127	QAQLVKLANQEKGVSLVNLVSLALLVQEGSGGPQVKVLLGLLGLLEAEV		176
HOSK	100	LLDPQGLMETRVNLVWLVLWALLVHLVLDVDSQERGVLLAYLEAREKRVNL		149
Human	201	LLDPQGLMETRVNLVWLVLWALLVHLVLDVDSQERGVLLAYLEAREKRVNL		250
Macaca	201	LLDPQGLMETRVNLVWLVLQALLVHLVLDVDSQERGVLLAYLEAREKRVNL		250
Rat	177	PLEPQGLMGTRVKLVQSVLQALLVPLVVLVGFQERGVLLAYLEAKEKRVKL		226
Mice	177	PVEPQGLMETRVVKLVQSVLQAVLVLVPLGLVGFQERGVLLAYLGAKKRVKL		226
Dog	201	LLDPLGPMETRVNLAACLAPRAPLARPVPVDSQERGVLPAPLEAREKRVKP		250
Cow	177	LLDPQGLMETRVNRVWLALQALLAHLVLDVDSQERGVRLAFLEAREKRVKL		226
		. * * * * *	* * * * *	
HOSK	150	VSEVKLVTLAEMVLVLLVL-----		169
Human	251	VSEVKLVTLAEMVLVLLVL-----		270
Macaca	251	VSEVKLVTLAEMVLVLLVL-----		270
Rat	227	VSEVKSATLVEMVLEVLLVL-----		246
Mice	227	VSEVTLATLVEMVLVAFVL-----		246
Dog	251	VSEAKLVTAEMAPVELLVVPLVLPPEPLVTGVKLVLPVPLALLLVVVP		300
Cow	227	VSEVTLVALVEMVLVLLVLLVLLALLEPMTGVKLVPLALLALLLVVVA		276
		*** . ** **		

Figure 3.4: In silico analysis of 5' extension of collagen $\alpha 2(I)$ transcript from HOSK translational site suggest an in frame upstream methionine (as indicated by box). The shaded area denoted the starting translational methionine of the HOSK channel. * are the consensus sequence

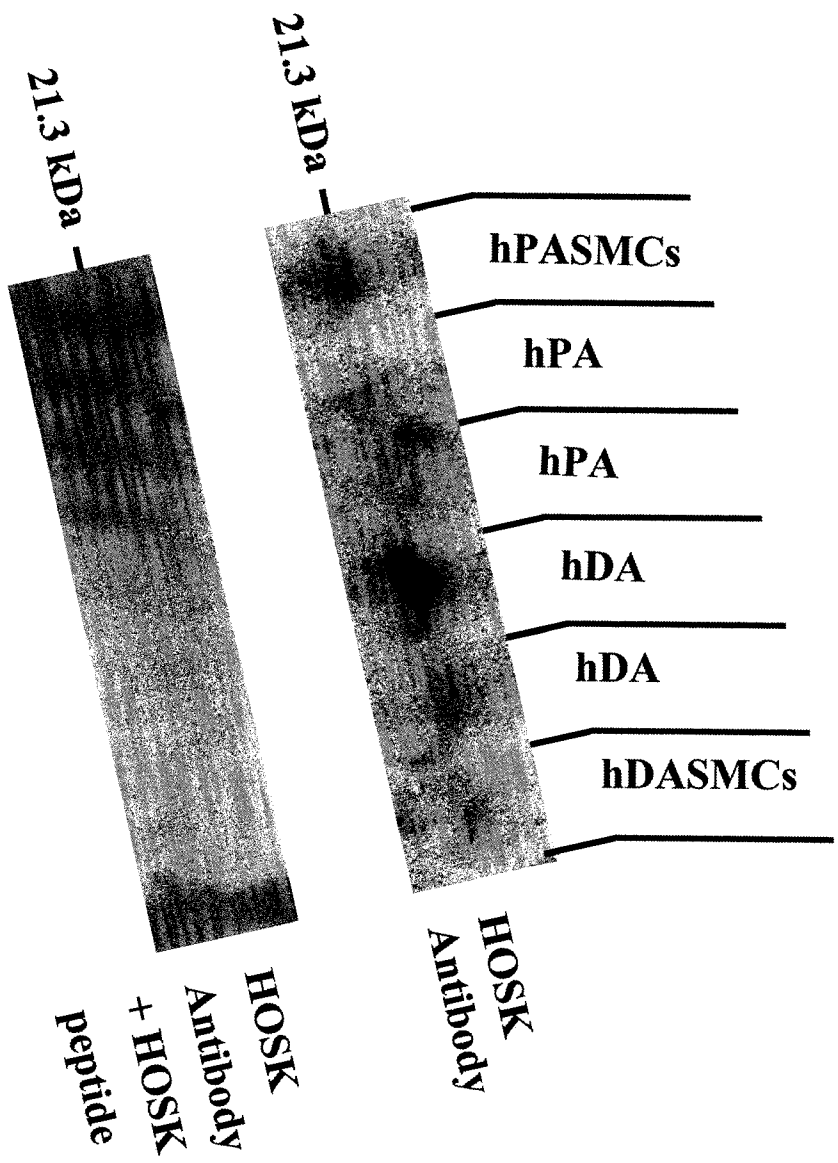


Figure 3.5: Immunoblot of various tissues show presence of HOSK in human DASM, human PASC and DA. The band disappears when antibody is pre-incubated with HOSK peptide.

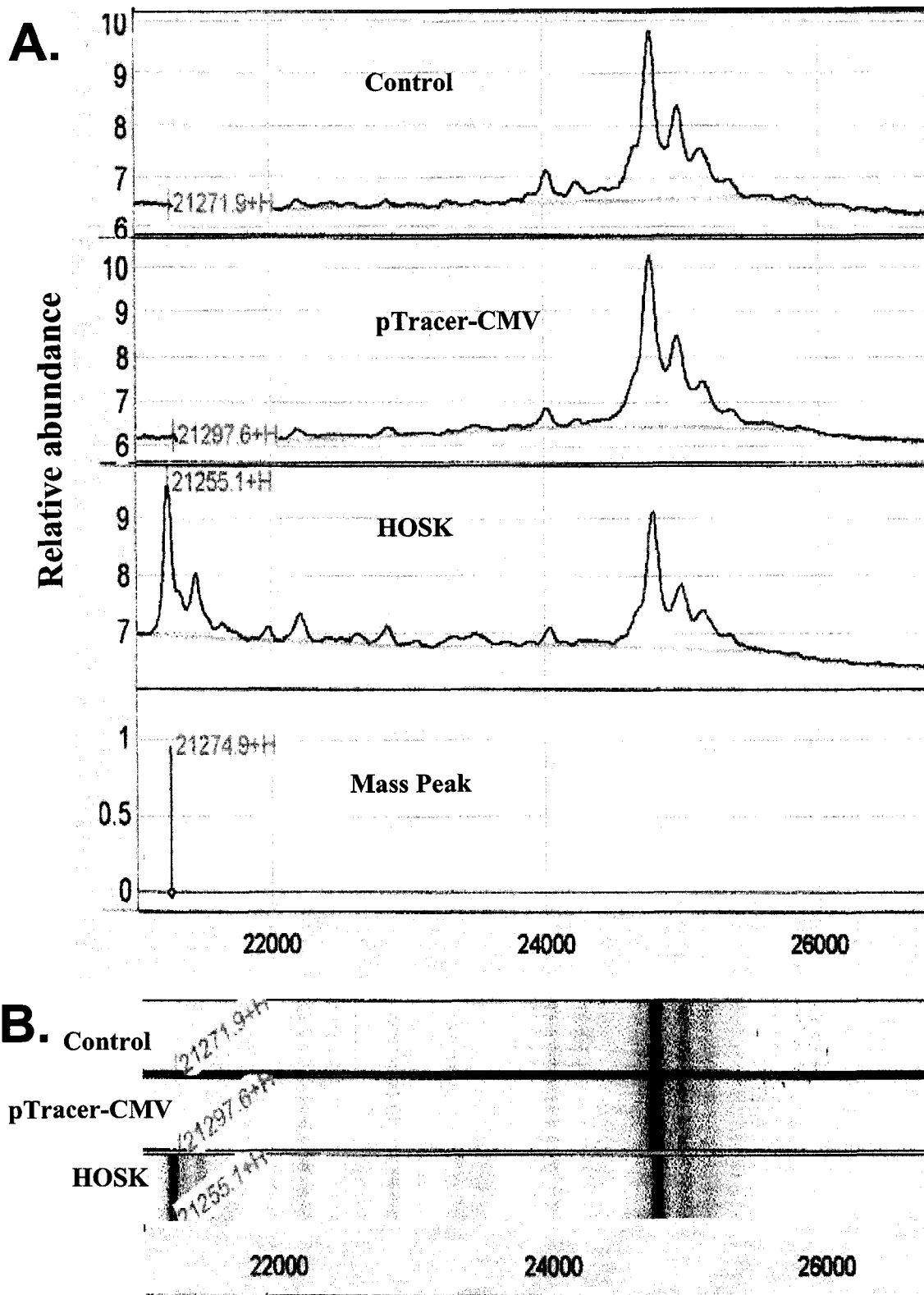
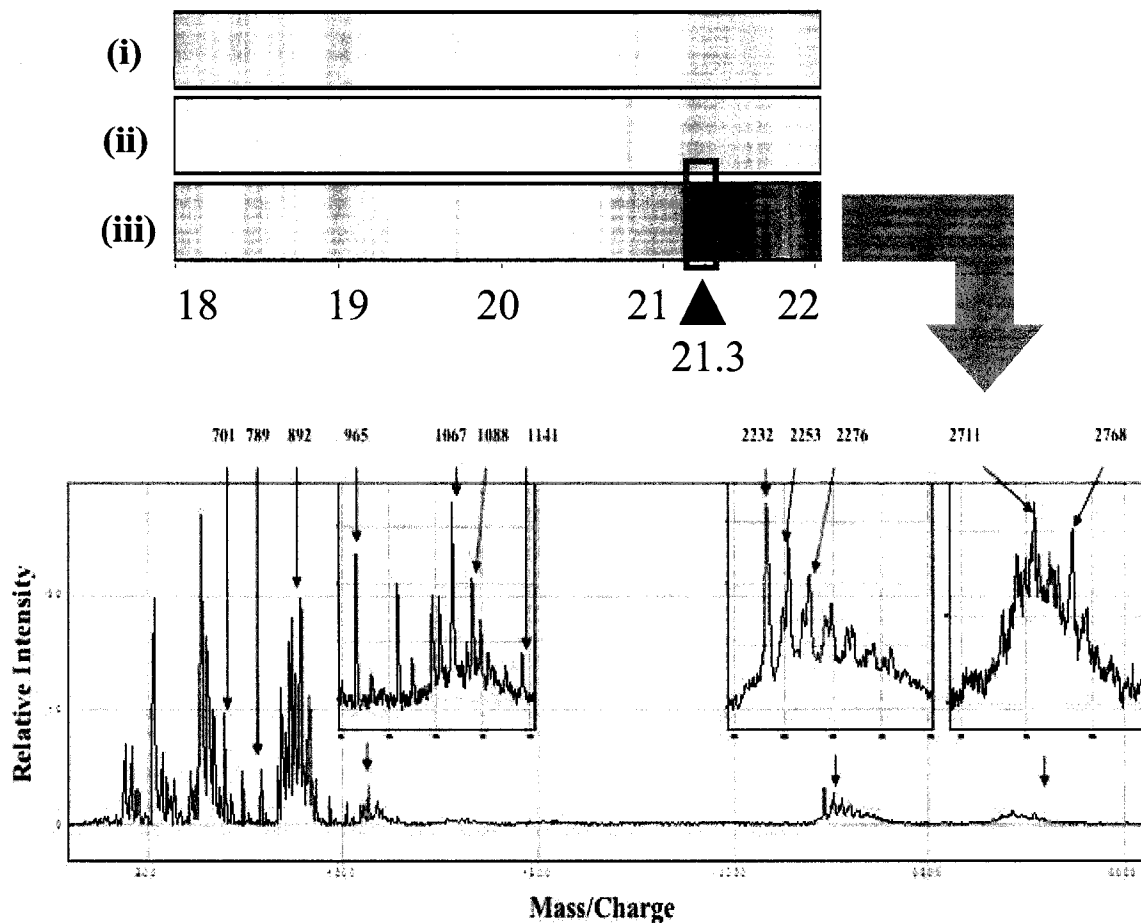


Figure 3.6: Isolation of HOSK channel using SELDI-TOF. The HOSK channel was identified at 21.3 kDa. The panel A shows the mass spectrometry and panel B shows the corresponding gel mode.



DLLDHR (768 Da) VPLVLQASR (982 Da) LANQEK (702 Da)
MLVLLVLGVL QVLMETMVL (2271 Da)
VLPVLLVLLAEVLLDPOG LMETR (2760 Da)
VNLVWLVLWALLVHLVLVDSQER (2714 Da) VNLVSEVK (887 Da)

Figure 3.7: On-chip antibody capture of HOSK and SELDI-TOF MS analysis shows the presence of a unique band in gel mode of (iii) HOSK transfected CHO cells when compared to (ii) pTracer transfected and (i) control CHO cells. On-chip tryptic digestion of the immunoprecipitated HOSK resulted in a spectrum that is unique to HOSK protein. Please note that some of the tryptic fragments that matched the identified peaks are listed below.

Formatted Alignments

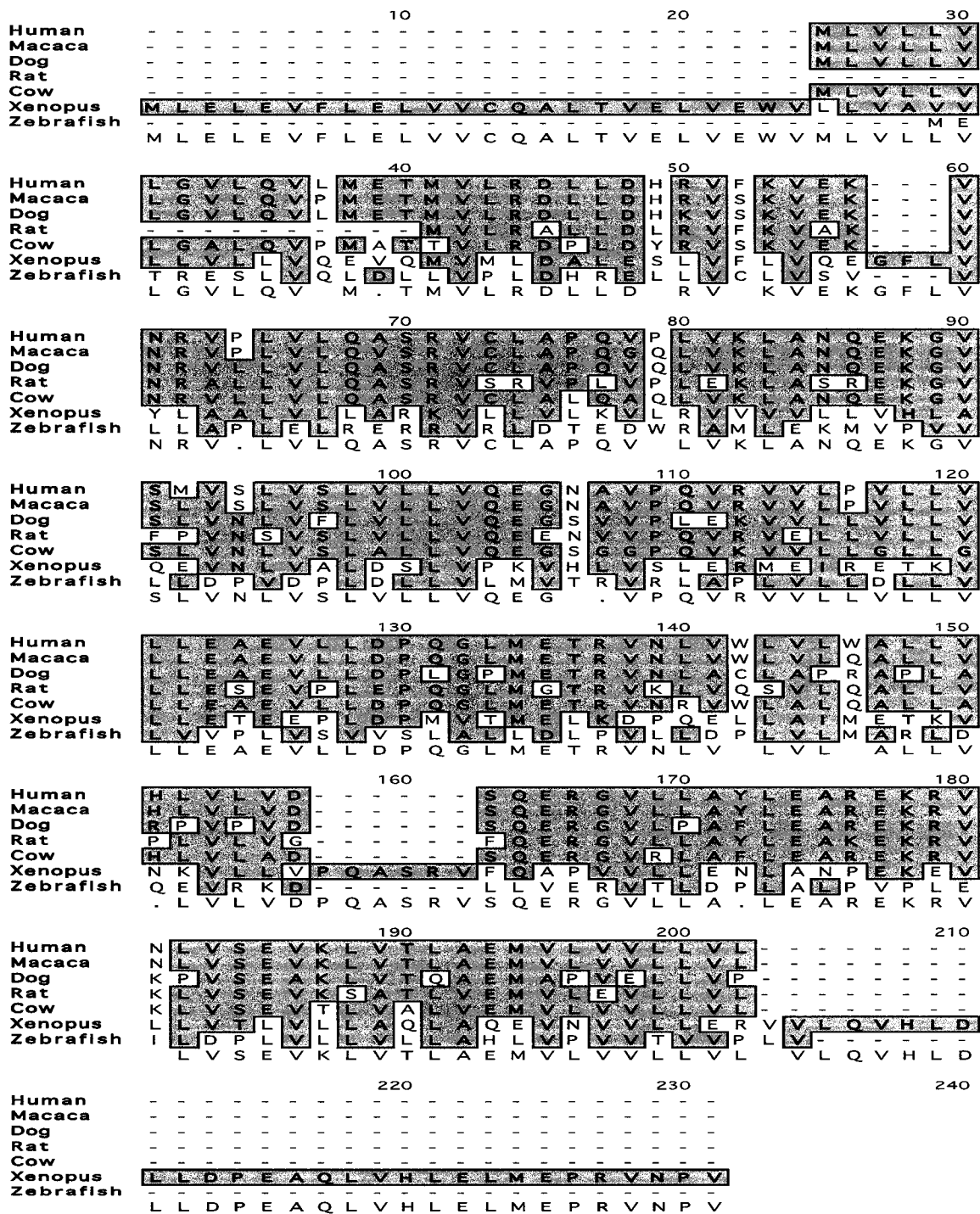


Figure 3.8: Species alignment of HOSK protein sequence using the open reading frame generated from the point where HOSK gene coincides with collagen $\alpha 2(I)$. HOSK channel will be expressed by human Macaca, Dog, Rat and Cows. However, the open reading frame of Xenopus and Zebrafish lacks similarity to the mammals. The last line in the alignments denotes the consensus sequence

The variations of K⁺-filter sequence (GYGD) among the prokaryotic K⁺ channels

Organisms	2TM			6TM		
	Channel core	RCK/KTN	unknown domain	Voltage gated	RCK	core only
<i>Archaea</i>						
<i>Crenarchaeota</i>						
<i>Su. solfataricus</i> P2		<u>GLYE</u>				
<i>Su. tokodai</i> str. 7		<u>GLYA</u>				
<i>Bacteria</i>						
<i>Chloroflexi</i>						
<i>Ckl. rapidum</i> TLS		<u>GFEE</u>				
<i>Cyanobacteria</i>						
<i>C. watsonii</i> WH 8501		<u>GFEE</u>				
<i>Prochlorococcus marinus</i> MIT 9313				<u>GHGD</u>		
<i>Synechocystis</i> sp. PCC 6803		<u>GYED</u>				
<i>Thermosynechococcus elongatus</i> BP-1		<u>GYEE</u>			<u>REIG</u>	
<i>Deinococcus-Thermus</i>						
<i>D. radiodurans</i> R1			<u>GLGD</u>			
<i>Firmicutes</i>						
<i>B. anthracis</i> (4 strains)	<u>GDAN</u>					
<i>Bacillus cereus</i> ATCC 10987	<u>GDAN</u>					
<i>Bacillus cereus</i> ATCC 14579	<u>GDAN</u>					
<i>Bacillus cereus</i> G9241	<u>GDGQ</u>					
<i>Bacillus cereus</i> ZK	<u>GDAN</u>					
	<u>GDGQ</u>					
<i>Bacillus halodurans</i> C-125	<u>GLGD</u>					
<i>Bacillus subtilis</i> str. 168			<u>GHGD</u>			
<i>Bacillus thuringiensis</i> str. 97-27	<u>GDAN</u>					
<i>Exiguobacterium</i> sp. 255-15	<u>GHET</u>					
<i>Ureaplasma parvum</i> ATCC 700970						<u>AYGD</u>
<i>Proteobacteria</i>						
<i>Magnezococcus</i> sp. MC-1		<u>GVGE</u>				
<i>Burkholderia cepacia</i> R18194	<u>GAEG</u>					
<i>Ralstonia eutropha</i> JMP134	<u>ELGD</u>					
<i>Ralstonia metallidurans</i> CH14	<u>ELGD</u>					
<i>Desulfosarcina psychrophila</i> LSv54	<u>GLAD</u>					
<i>D. desulfuricans</i> G20		<u>GFGE</u>				
<i>G. metallireducens</i> GS-15		<u>GFGE</u>				
<i>Microbulbifer degradans</i> 2-40	<u>GMEE</u>					
<i>Azotobacter vinelandii</i>					<u>GLGD</u>	
<i>Thermotogae</i>						
<i>T. maritima</i> MSB6		<u>GVET</u>				

The residues that deviate from the consensus, GYGD, are underlined.

Table 3.1: The variations of filter sequence (GYGD) among the prokaryotic K⁺ channels. (Adapted from ref 63)

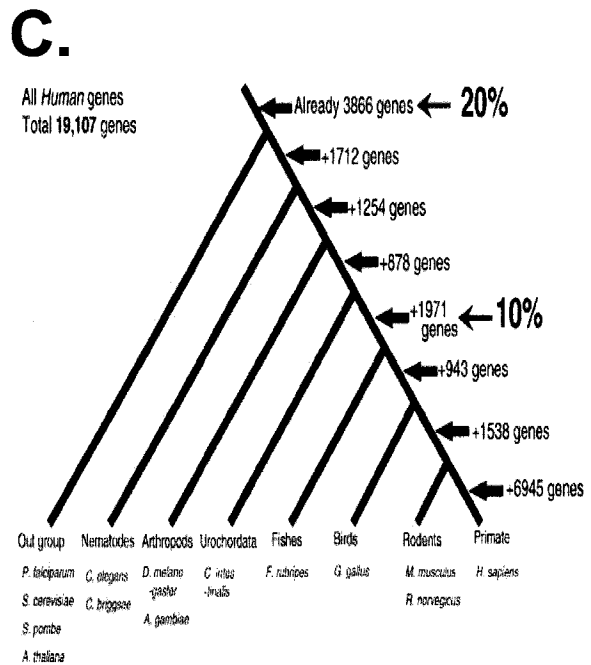
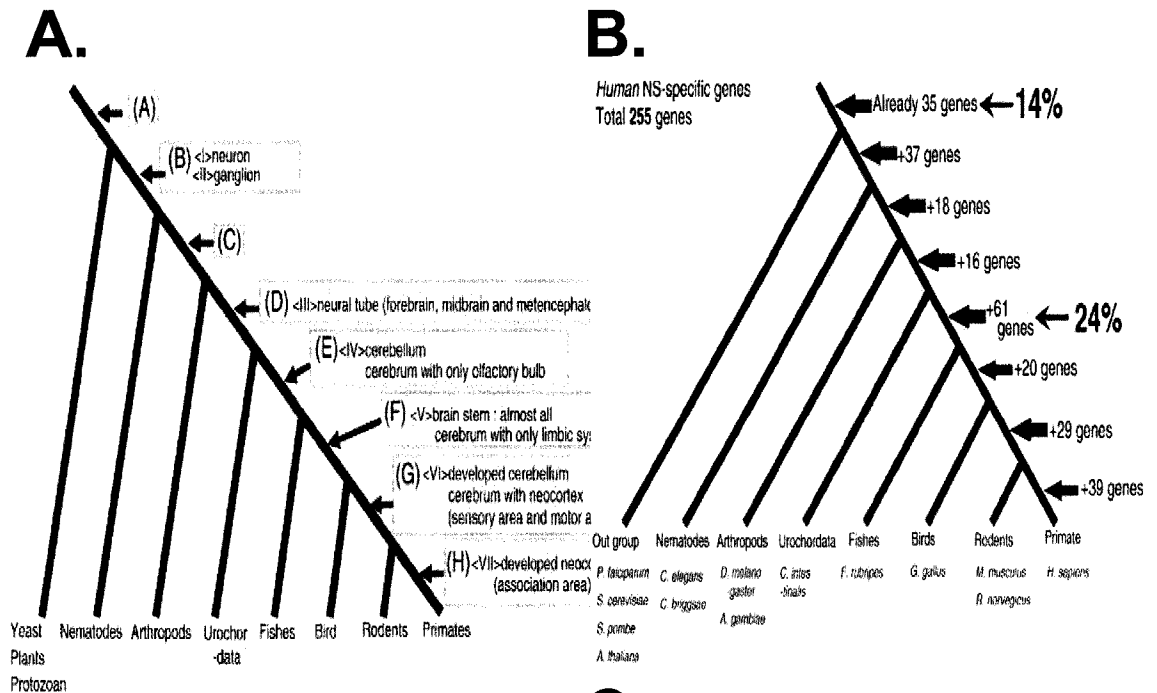


Figure 3.9: Schematic representation of evolution of NS. (A) Evolutionary process of the nervous system (NS). NS has evolved through at least seven evolutionary steps, I through VII, during eight periods, (A) through (H). (B) Emergence of the 255 human NS-specific genes during evolution. About quarter of the 255 human NS-specific genes emerged during period (E). The tree also illustrates (C) the emergence of the 19,107 human genes during evolution. (Adapted from ref 66)

4.1 INTRODUCTION

The ability to move, to perceive a colorful world or to process language relies on rapid communication among neurons. Such signaling, the fastest in our bodies, involves electrical messages produced by the ion channels in the cell membranes by virtue of the binary function of opening and closing. Elucidation of the fundamental role of ion channels in sensory transduction, electrical "computations," propagation of information over long distances, and synaptic transmission began only half a century ago¹.

Hodgkin and Huxley were the initial pioneers of the membrane biophysics¹. They used the giant squid axon as the model system and employed electrodes to record action potential and to study the effect of ionic substitution on electrical transmission which led to publication of series of five seminal papers (summarized in ref 1). These papers systematically developed the concept of selective ionic permeation and gating which is a property conferred by ion channels². They described the permeability changes as a set of chemical reaction whose rate constants were a function of voltage. Although they laid the conceptual foundation that foreshadowed the existence of ion channels, it was the advent of patch clamping that revolutionized cellular electrophysiology and helped identify ion channels as discrete protein pores. It was the combination of Erwin Neher's expertise in placing suction pipettes on the cell membranes and Bert Sakmann's experience with enzymatic isolation of cells that resulted in the first recording of the current from a single acetylcholine activated ion channel³. Subsequently the advent of molecular biology, in combination with patch clamping, has identified the channels which underlie the currents and resulted in today's understanding of the K⁺ channels.

Five distinct types of K⁺ channels have been identified: 1) voltage-dependent K⁺

(Kv) channels, 2) Ca²⁺-activated K⁺ (K_{Ca}) channels, 3) inward rectifier K⁺ (Kir) channels, 4) ATP-sensitive K⁺ (K_{ATP}) channels and, 5) two-pore K⁺ (K2P) channel. Each K⁺ channel is activated by different physicochemical stimuli. Arterial smooth muscle cells express Kv, K_{Ca}, Kir, and K_{ATP} channels. The estimates of channel number per cell range from 100-500 per cell for K_{ATP} and Kir channels to 1,000-10,000 Kv and K_{Ca} channels per cell⁴.

Kv channels are composed of four α -subunits, the principal pore-forming and voltage-sensing component of these channels. Each α -subunit contains six transmembrane helices and a pore (P-loop) within the membrane, which confers K⁺ conductivity and selectivity. Homotetrameric complexes of four identical α subunits generally form functional voltage-gated, K⁺-selective Kv channels. The prototypical Kv channel α subunits have been further divided into four families (Kv1-Kv4), based on sequence homology (Figure 1) and on their sequence similarity to single-gene orthologues in *Drosophila* (name given in italics): Kv1 (*Shaker*), Kv2 (*Shab*), Kv3 (*Shaw*), and Kv4 (*Shal*)⁵⁻⁹. Subunits can combine, within a family, to form heteromeric channels, with properties that reflect those of the originating α subunits (e.g. Kv1.2/Kv1.5).

The human genes encoding these α subunits are named KCN*, with the four gene families assigned the letters A–D (*i.e.*, Kv1 = KCNA, Kv2 = KCNB, Kv3 = KCNC, and Kv4 = KCND). Kv channels from 5-12 are involved in formation of heterotetrameric channels. They are assigned the letters from F-V (*i.e.*, Kv5 = KCNF, Kv6 = KCNG, Kv7 = KCNQ, Kv8 = KCNV, Kv9 = KCNS, and Kv10-12 = KCNH)¹⁰. Despite the differences in nomenclature, all the Kv channels share a common denominator of voltage

sensing

4.1.1 Voltage Dependence

The voltage dependence of channel activation and inactivation processes are described by a Boltzmann relationship, which relates the probability that a channel is activated or inactivated by the membrane potential^{12, 13}. The relationship between activation and membrane potential increases exponentially with voltage until a limiting value is reached. The probability that a channel is activated (P_{act}) at a given membrane potential (V_m) is given by

$$P_{act} = P_{act} \alpha \cdot 1 / (1 + \exp[(V_{0.5} - V_m) / K])$$

where $V_{0.5}$ is the membrane potential at which activation is one-half the maximum, and k is a slope factor that indicates the sensitivity of channel activation to changes in membrane potential¹³. The voltage dependence of channel inactivation is expressed by plotting the availability of channels to open [equal to $1 - P_{inact}$ (the probability that channels are inactivated)] against the membrane potential. The probability that a Kv channel is open in the steady state (P_o), is given by the product of the probability that channels are activated (P_{act}) and the probability that channels are not inactivated ($1 - P_{inact}$)¹³. Therefore, the total current (I) is measured by number of channels existing in open confirmation

$$I = P_o N_i \quad (\text{where } P_o = P_{act} (1 - P_{inact}))$$

Where N is the total number of channels involved

4.1.2 Functional Properties of Kv Channels

Kv channels are typically characterized by a $V_{0.5}$ activation range of -30mV to +19 mV, while the inactivation range ($V_{0.5}$) is -66 mV to +5 mV¹⁴. The single channel conductance is quite variable, ranging from 4.7 pS to 70 pS¹⁴. The Kv channels are inhibited by various toxins and drugs such as margatoxin, tityustoxin and correolide, with inhibition being quite specific to channel family (eg. margatoxin for Kv1.3 and tityustoxin for Kv1.2). However, all Kv channels are inhibited by 4-aminopyridine¹⁴, a pore-blocking agent. Kv channels are not inhibited by iberiotoxin, which blocks BK_{Ca} channels, or glyburide, which blocks K_{ATP} channels. Thus, electrophysiological and pharmacological properties can be used to identify the contribution of Kv channels to the ensemble current that most vascular smooth muscle cells display.

4.1.3 Physiological role of Kv channels in vasculature

4.1.3.1 Repolarization of the action potential

Despite the wide distribution of Kv channels, relatively few studies have been conducted on the physiological role of this channel in arterial smooth muscle. Because the channel is activated by depolarization, it may be involved in action potential repolarization in electrically excitable smooth muscle preparations such as the portal vein, and this is a principal function of the channel in other excitable cells, including neurons and cardiac muscle¹⁵. However, most arteries generally respond to stimuli with graded membrane potential changes, and therefore Kv channels are unlikely to be involved in action potential repolarization in these arteries¹⁶.

4.1.3.2 Regulation of membrane potential

In the healthy, normoxic pulmonary circulation, a tonic basal opening of K⁺ channels permits a constant efflux of K⁺ across the plasma membrane through K⁺ channels, driven by an electrochemical gradient. The fact that the resting E_M of PASMC is ~ -60mV is due, in large part, to the activity of K_v channels.

In vascular smooth muscle cells, K_v and Ca_L channels are tightly linked through E_M. This provides a general paradigm that explains how SMC E_M is coupled to arterial tone¹⁷. When K_v channels close, the tonic K⁺ efflux is decreased rendering the cell interior more positive (depolarized). At these potentials (i.e. positive to -30mV), the open probability of Ca_L channels increases, favoring calcium influx down a 10,000/1 extracellular/intracellular gradient, thereby raising cytosolic calcium concentrations and causing vasoconstriction.

There has been controversy as to whether K_v channels are open at sufficiently negative potentials to establish resting E_M. However, when patch clamp studies are conducted carefully, avoiding prolonged or repeated depolarizations that inactivate K_v channels, one can see K_{v1.x} activity at or near the PASMC's resting E_M¹⁸. The impression that K_v channels do not set E_M may be because that many investigators study cultured PASMC (in which E_M is already depolarized compared to fresh cells due to loss of K_{v1.x} channel expression)¹⁹. Therefore, even a small change in K_v activity at very negative potentials can have a significant effect on E_M and vascular tone^{20,21}.

The families and isoforms of K⁺ channels that determine E_M in PASMC vary somewhat by species, gender and developmental stage (fetus versus adult). For example, the resting E_M in the healthy adult PASMC is largely controlled by K_v channels²²⁻²⁴,

whereas BK_{Ca} channels contribute importantly in fetal PASMCs²⁵. Depending on the predominant K⁺ channels available, increases in intracellular Ca²⁺ may secondarily reinforce PASMC K_v closure, counteracting their predisposition to open at positive voltages²⁶. Likewise, agonists that activate protein kinase C and (increase intracellular calcium also inhibits K⁺ channels, thereby reinforcing the vasoconstriction²⁷.

The role of K⁺ channels in regulating vascular tone is complex, because channel function is regulated by numerous vasoactive substances (cGMP, endothelin, nitric oxide etc) and by calcium, pH and phosphorylation. Thus, diverse vasoactive peptides, including endothelin and serotonin, as well as a variety of drugs (pergolide²⁸ and dexfenfluramine²⁹) may cause pulmonary vasoconstriction in part by inhibiting PASMC K_v channels, directly or via protein kinase C and/or Ca²⁺-mediated inhibition of K_v channels^{28, 30, 31}. It is increasingly recognized that agents which acutely inhibit K_v channels, with prolonged exposure, inhibit transcription of K_v channel genes, leading to ionic remodeling. The selective loss of Kv1.5 and Kv2.1 is commonly seen in pulmonary arterial hypertension and may relate to elevated cytosolic calcium with activation of NFAT and/or normoxic activation of hypoxic inducing factor HIF-1 α ^{32, 33}.

TASK channels (TWIK-related acid sensitive K⁺ channel) may also or alternatively, as some believe, contribute to resting E_M. TASK is a K_{2P} channel which conducts a background, voltage-independent leak current³⁴. TASK-1 mediates a non-inactivating, background K⁺ current which contributes to resting E_M in rabbit PASMCs³⁵. Both the non-inactivating characteristic and the activation threshold of TASK channels are sensitive to extracellular pH, with acidosis inhibiting the current and causing depolarization³⁵. Moreover, changing extracellular pH from pH 7.4 to 6.4 or 8.4

respectively depolarizes or hyperpolarizes rat mesenteric and pulmonary arteries³⁶. The divergent findings regarding the relative roles of K_v vs TASK channels in setting the E_M might be due to study of PASMC from of different vascular segments (see section on diversity). The TASK investigators employed proximal pulmonary arteries for their studies³⁵ whereas our group has always focused on freshly dispersed resistance PASMC¹⁸. Although PAs express TASK-1, TASK-2, THIK-1, TREK-2 and TWIK-2, blockade of these channels (by non-selective anandamide or bupivacaine) generates only a small increase in pulmonary artery tone³⁶. This would be surprising if these channels determined E_M . In favor of the role of K_v channels in establishing E_M , anti- $K_v1.5$ or $K_v2.1$ antibodies substantially depolarize resistance PASMCs as does the K_v blocker 4-aminopyridine, which also causes vasoconstriction¹⁸. Moreover, in PAH (human or experimental) loss of $K_v1.5$ is associated with membrane depolarization³⁷⁻³⁹.

4.1.4 Hypoxic Pulmonary Vasoconstriction

Under physiological conditions, the pulmonary vessels deliver deoxygenated blood to the lungs, distributing it throughout the pulmonary capillary sheets where gas exchange takes place in alveoli. During hypoxic conditions, the pulmonary arterial beds undergo constriction thereby redistributing blood to more oxygenated areas. It is believed that it optimizes perfusion/ventilation matching.

At the smooth-muscle-cell membrane in the pulmonary artery, hypoxic inhibition of the outward potassium current causes depolarization of the membrane and entry of calcium through L-type voltage-gated calcium channels^{40, 41}. The membrane potential, and therefore control of voltage-gated calcium channels in the membrane of the smooth-muscle cell, is largely determined by the activation of K^+ channels from a high

concentration inside the cell (145 mM) to a low concentration outside the cell (5 mM). At the resting membrane potential (about -60 mV) these calcium channels are mostly closed. Hypoxia inhibits potassium current and depolarizes smooth-muscle cells in the pulmonary arteries, but it does not have these effects in smooth-muscle cells from vascular beds that dilate in response to hypoxia (e.g., those of the kidney or mesentery)^{40, 42}. Inhibition of potassium current is proportional to the severity of hypoxia⁴³ and is more prominent in small resistance pulmonary arteries (diameter, <500 μm) than in large extraparenchymal pulmonary arteries⁴⁴.

A variety of potassium channels in smooth-muscle cells of the pulmonary arteries are sensitive to acute changes in oxygen⁴⁵. In the fetus, the calcium-sensitive potassium channel (KCa) is the predominant oxygen-sensitive channel⁴⁶. After birth, a shift to several voltage-gated potassium channels (Kv; this nomenclature refers to K channel, voltage-dependent) occurs⁴⁷. For instance, hypoxia inhibits Kv1.5, cloned from human pulmonary arteries¹⁸, and hypoxic pulmonary vasoconstriction is diminished in mice that lack this channel⁴⁷. Acute hypoxic pulmonary vasoconstriction is blunted in rats previously exposed to chronic hypoxia⁴⁸ and chronic hypoxia decreases the oxygen-sensitive component of potassium current and the expression of Kv1.5 and Kv2.1 in smooth-muscle cells of the pulmonary arteries^{43, 49}. These findings, together with the observation that the diminution of hypoxic pulmonary vasoconstriction by chronic hypoxia in rats can be restored by intratracheal infection of human Kv1.5⁵⁰, have established a role for Kv channels, and particularly Kv1.5, in the mechanism of hypoxic pulmonary vasoconstriction. Kv2.1 and Kv3.1b and another potassium channel, two-pore acid-sensitive potassium channel type 1 (TASK-1), may also be involved^{18, 35, 51}.

4.1.5 Closure of DA

The ductus arteriosus (DA) is a fetal artery that allows blood ejected from the right ventricle to bypass the pulmonary circulation in utero. In utero, the ductus is a large vessel, roughly the size of the aorta and PA (Figure 1). At birth, functional closure of the DA is initiated by an O₂-induced, vasoconstrictor mechanism which, though modulated by endothelial-derived endothelin and prostaglandins, is intrinsic to the smooth muscle cell (DASMC)⁵². As PO₂ increases, a mitochondrial O₂-sensor (electron transport chain complexes I or III) is activated which generates a diffusible redox mediator (H₂O₂). H₂O₂ inhibits voltage-gated K⁺ channels (Kv) in DASMC. The resulting membrane depolarization activates L-type Ca²⁺ channels, thereby promoting vasoconstriction (Figure 2). Inhibiting mitochondrial ETC complexes I or III mimics hypoxia, depolarizing mitochondria, decreasing H₂O₂ levels, and increasing DASMC K⁺ current, thereby hyperpolarizing DASMCs and relaxing DA rings. We have developed two models for study of the DA's O₂-sensor pathway, both characterized by decreased O₂-constriction and Kv expression: a) preterm rabbit DA b) ionically-remodeled, human term DA. The O₂-sensitive channels Kv1.5 and Kv2.1 are important to O₂-constriction and overexpression of either channel enhances DA constriction.

We now believe that HOSK, a channel which is active at very negative membrane potentials, is very important to the functional closure of the DA and with Kv1.5 and Kv2.1 constitutes the effector arm of the DA's O₂-sensing system. The remainder of this chapter focuses on the electrophysiological properties of HOSK comparing it to other Kv channels expressed in human DA. The study suggests that all the electrophysiological

parameters of HOSK such as activation, inactivation conductance falls within the range of previously described Kv channels. Furthermore, responses to some of the pharmacology interventions such as 4-aminopyridine and correolide also show similarity to other known Kv channels. In addition perturbations with putative mediators of DA closure pathways such as hypoxic insult and hydrogen peroxide treatment of HOSK show results in concordance to the response observed in freshly isolated DASM. Thus, HOSK is among one of the channels that regulate DA membrane potential and perhaps the mainstay channel involved in O₂-mediated DA closure. This work has been submitted for peer-review to the journal *Nature*.

4.2 MATERIALS AND METHODS

4.2.1 Transfection of Chinese Hamster Ovary cells and Monkey Kidney (COS) cells

Heterologously expressed HOSK was studied in CHO and COS cells. Briefly, the HOSK transcript was ligated into pTracer-CMV (Invitrogen, Burlington, Ontario). pTracer-CMV is a vector that requires the presence of kozak sequence and putative start codon in the cDNA insert for the successful expression of the protein. The directional cloning was confirmed by Nru I restriction digest. Transfection in CHO cells and COS cells was performed with Fugene 6 transfection reagent (Roche, Indianapolis, Indiana) following the manufacturer's specifications.

4.2.2 Whole cell patch clamp solutions

Electrodes (resistance 1-5 M) were filled with a solution that contained (in mM) 140 KCl, 1.0 MgCl₂, 10 HEPES, 5 EGTA, and 10 glucose, pH 7.2. The chamber containing the cells was perfused (2 ml/min) with a solution containing (in mM) 145 NaCl, 5.4 KCl, 1.0 MgCl₂, 1.5 CaCl₂, 10 HEPES, and 10 glucose, pH 7.4 (extracellular solution). The cells were voltage clamped at a holding potential of 70 mV, and currents were evoked by steps from -100 to +50 mV with 0.1-Hz test pulses of 200 ms duration. Currents were filtered at 1 kHz and sampled at 2 or 4 kHz. Data were recorded and analyzed with pCLAMP 6.02 software (Axon Instruments, Foster City, CA).

Identification that HOSK is K⁺ channel, current were measured at increasing K⁺ concentration outside approaching 140 mM. The current-voltage relationship of HOSK

was measured in presence of cesium, barium, 4-AP and correolide. For the activation protocol the voltage was held at 0 mV potential and a stepwise protocol was followed from -100 mV to 70 mV. The tail currents were measured for activation. For inactivation protocol, the voltage step of +80 mV was held for 10s and then tail currents were measured for inactivation.

4.2.3 Single channel patch clamp (inside-out configuration)

Single channel electrophysiology of heterologously expressed HOSK was studied in the inside-out configuration in symmetrical KCL (140mM), as previously described¹. Pipettes (resistance 3-5 MΩ) were filled with a solution containing (mM) KCL 140; CaCl₂ 1.0; KH₂PO₄ 1.2, MgCl₂ 1.0; HEPES 10; glucose 5.0 (pH 7.4). Bath solution was identical with Pipettes solution except for the bath solution contained 5 mM Na₂ATP and pH was 7.2. For immunoelectropharmacology the antibody was added to the extracellular solution.

4.2.4 Immunoelectrophysiology

Experiments were performed comparing the effects on I_K and E_m of adding the antibodies into the patch pipette at a 1:125 dilution. In this configuration, the antibody rapidly diffuses into the cell and interacts with C-terminal epitope to which the antibody is directed. This technique has been validated as a means to dissect the molecular origins of whole-cell and single channel K⁺ currents in vascular smooth muscle cells^{18, 23} and has been validated by other groups^{28, 53, 54}. The baseline currents were allowed to stabilize before any recording was made (usually after 5 min). Vehicle controls provided time-

dependent controls to detect run-down or run-up of K⁺ currents (as well as to establish the effects of hypoxia and 4-AP on normal DA cells). Aliquoted antibodies were defrosted daily to avoid degradation.

4.2.5 Site-directed mutagenesis

To further validate the use of GVL as selective pore sequence, a HOSK antibody, generated against a pore epitope, was used to perform immunoelectropharmacology in CHO cells, a technique we have previously validated ¹⁸. For site-directed mutagenesis overlapping primers with targeted mutation sites (GVL to AAA) were synthesized. PCR was carried out and the parent methylated template was digested with Dpn I. Transformation was carried out in XL-1Blue cells (Invitrogen, Burlington, Ontario) and the mutation was confirmed by Automated DNA sequencer.

4.2.6 Quantitative real-time polymerase chain reaction

Quantitative real-time polymerase chain reaction (qRT-PCR) was used to quantify various Kv channels such as Kir1.2, Kv1.2, Kv1.5, Kv2.1, Kv3.1, BKCa, HOSK and 18S in human DASMC. The TaqMan one-step RT-PCR Master Mix reagent kit was used (Applied Biosystems, Foster City, CA). The reaction used 50ng RNA in 50 µl using relevant primer (500nM), and TaqMan probe (200nM), as designed by us. The assay was performed using ABI PRISM 7700 Sequence Detector System (Applied Biosystems Foster City, CA). Reverse transcription proceeded for 30 min at 48°C. AmpliTaq Gold activation occurred for 10 min at 95°C. Subsequently, 40 cycles of PCR were performed. Each cycle consisted of 15 seconds of denaturing (at 95°C) and 1 min of annealing and

extension (at 60°C). $2\Delta\Delta C_t$ is a ratio of the expression of Kv channel; HOSK; COL1A2 to 18S ribosome.

4.2.7 Immunoblot

Immunoblotting was performed on heterologously expressed HOSK in CHO cells, as previously described in chapter 2. Antibodies of Kv1.2, Kv1.5, Kv2.1, Kv3.1 and BKCa were incubated according to the manufacturer's specification.

4.2.8 Generation of a HOSK siRNA.

Silencer RNA was generated against the HOSK sequence. Initial experiments established the optimal dose for the gene knockdown. hDASMC were transfected with siRNA and scrambled RNA as our control. qRT-PCR showed no effect on other oxygen-sensitive Kv Channels expression in siRNA treated cells. Briefly, a 19-23 nucleotide area was identified which bears no resemblance to any other cDNA sequence as determined by BLAST. The siRNAs to the sequence were synthesized by Ambion Inc. (Austin, Texas).

4.2.9 Statistics

Two-way ANOVA was performed in all the experiments. The data is reported as mean \pm SEM. All the point denotes a data set of n=5-10, if not indicated. A p value was set at <0.05 for all the statistics.

4.3 RESULTS

Transfection of the EST (HOSK) fragment with a green fluorescent protein reporter (GFP)-each under a CMV promoter- into Chinese Hamster Ovary (CHO) or COS cells, generates a voltage-dependent current outward current (Figure 3). CHO cells have an endogenous ohmic current. Furthermore, to assess if the K⁺ current generated was due to transfection, CHO cells were transfected with increasing doses of HOSK channel cDNA. Dose-dependent increase in HOSK cDNA resulted in corresponding increases in the K⁺ current (Figure 4). To assess if the HOSK current had the properties of a typical of a K⁺ channel current, we assessed the reversal potential by increasing extracellular K⁺ concentration ($[K^+]_{out}$). The progressive increase in $[K^+]_{out}$ shifted the reversal potential to the right (Figure 5). In addition, in the symmetrical 140mM K⁺ ionic configuration, an equilibrium potential of 0 mV is achieved, typical of a K⁺ channel. We also performed ionic substitution experiments replacing solution inside and outside of the whole cell patch.. The ionic selectivity profile (Rb>K>>Cs>Na) is typical of K⁺ channels (Figure 6). Likewise, HOSK's sensitivity to inhibition by extracellular cesium chloride (Figure 7) and barium (Figure 8) also suggests that HOSK has properties similar to K⁺ channels. To further characterize the activation kinetics, HOSK tail currents were measured (Figure 9 and 10) Like a typical K_v channel, HOSK demonstrated an $V_{1/2}$ activation of -7.1 ± 2.0 mV and $V_{1/2}$ inactivation at -18.9 ± 1.4 mV (Figure 9 and 10). Two K_v channel blockers inhibit heterologous HOSK I_K 50% (4-AP (Figure 11); correolide, a K_v1.x inhibitor, (Figure 12)). This concept is also reflected in the fact that K_d for K_v1.3 is 5.7 nM⁵⁶ while for HOSK channel is 38 nM suggesting that a higher concentration of correolide is required to obtain same level of inhibition. Maximum concentration of

specific inhibitors of large conductance calcium-sensitive potassium (iberiotoxin 100 nM; Figure 13), small conductance calcium sensitive calcium channel (Charybdotoxin 100 nM; Figure 14) and Kv2.1 (retigabine 10 nM; Figure 15) and Kv4.2 (E4031 10 nM; Figure 16) channels, respectively had no effect on HOSK's current-voltage relationship. However, margatoxin (a Kv1.3 inhibitor; 10 nM) caused a 20% inhibition of HOSK current (Figure 17).

Hypoxia increases (Figure 18) and oxygen decreases HOSK current in CHO cells. Like oxygen, exogenous hydrogen peroxide (100 μ M) (Figure 19), the putative diffusible redox mediator involved in O₂-induced DA constriction,⁵² inhibits HOSK current. The response of heterologously expressed HOSK to hypoxia and H₂O₂ are consistent with the effects observed in freshly isolated human DASMC⁵². Single channel recordings, made in the inside-out configuration in symmetrical 140mM potassium, showed that HOSK has a mean conductance of 19.5 ± 0.82 pS (Figure 20).

To establish whether GVL was the pore, site-directed mutagenesis was used to create an AAA substitution, which was confirmed by sequencing. Voltage-clamp of mutated channel showed that although the GFP reporter was expressed, no Kv current was generated, only the basal ohmic current characteristic of non-transfected CHO cells (Figure 21). This is consistent with our *in silico* developed hypothesis that GVL is the determinant of the pore sequence.

HOSK antibodies (1:250 dilution) applied to the internal membrane surface of CHO cell expressing HOSK via the patch pipette solution decreased the P_o of heterologously expressed HOSK. Channel opening recovered after the washout of antibodies suggesting the antibody blocking the channel pore (Figure 22). Moreover,

incubation of the HOSK-expressing patch with cocktail of Kv channel antibodies directed against other putative O₂-sensitive Kv channels found in human DASMC (Kv1.5, Kv2.1, Kv 3.1 and BKCa) had no effect, suggesting HOSK current is not due to upregulation of other Kv channels (Figure 23). In addition, to assess if the transfection of HOSK may result increase in other channel expression, we performed qRT-PCR on CHO cells. To our surprise we found mRNA for most of the Kv channels. Furthermore, immunoblot on protein extracted from CHO cells of various O₂-sensitive Kv channels such as Kv1.2, Kv1.5, Kv2.1 Kv3.1 and BKCa also showed protein expression. However, these expressional profile did not translated into functional channels. Heterologous expression of HOSK shows no increase in expression of Kv1.2, Kv1.5, and BKCa channels immunoblots (Figure 24). A slight increase is evident in Kv2.1 and Kv3.1b channels. However, antibodies directed against these channels in heterologously expressed HOSK channel in single-channel patch again showed no change opening probability signifying that Kv2.1 and Kv3.1b do not become functional in presence of HOSK protein (Figure 23).

To establish the physiological role of endogenous HOSK in human DASMCs, immunoelectropharmacology was performed on cultured DASMC. The HOSK antibody, when dialyzed into the DASMC via the patch pipette, inhibited I_K, whereas the antibody preabsorbed with the antigenic peptide had no effect (Figure 25). A second, independent approach to establishing the contribution of HOSK to endogenous DASMC current involved the use of siRNA. siRNA designed against HOSK channel inhibited the K⁺ current in human DASMC (Figure 26)

All the aforementioned studies were conducted on the full length EST clone. To verify if the truncated counterpart i.e, 1.4 kb fragment have any differential electrophysiological properties we carried out identical experiments with 1.4 kb. The electrophysiological profile of 1.4 kb show a similar sensitivity to Cs and 4-AP. Furthermore, the reactivity to perturbation of hypoxia and H₂O₂ were comparable to the HOSK clone (Figure 27). Single-channel patch on CHO cells transfected with 1.4 kb also showed a similar profile of reactivity to different antibody incubation (Figure 28). Furthermore, the CHO cells transfected with 1.4 kb showed an inhibitory profile similar to the HOSK channel (Figure 29).

4.4 DISCUSSION

4.4.1 Electrophysiology

The HOSK channel represents a new class of potassium channel with electrophysiological similarities to other Kv channels, particularly to Shaker (Kv1.x channels). HOSK channel, when transfected in CHO cells or COS cells, causes an increase in current in voltage-dependent manner. This effect was robust, occurring in all green cells (our marker of transfection), both in CHO and COS cells and demonstrable with either the EST or the 1.4kb construct. On close examination this current-voltage relationship is curvilinear, suggesting progressive activation with positive potential, which is characteristic of Kv channels¹³. These newly recruited channels display increased probability of opening at a given depolarization. Therefore, with increasing depolarization there is almost an exponential increase in the HOSK current. Furthermore, we established that the current was due to K⁺ ions, using ionic substitution experiments which showed the typical K⁺ channel reversal potential of 0mV in symmetric K⁺ ion concentration. Substitution experiments suggest that the HOSK channel had the expected K⁺ specificity, demonstrated by the finding that HOSK was unable to conduct Na⁺ and Cs⁺ ions. Moreover, like the other known Kv channels, HOSK conducts Rb⁺ ion faster than K⁺ ion. This might be due to the fact that Kv channels including HOSK show a more energetically stable configuration of Rb⁺ ion binding at S2 site in the permeation pore⁵⁷. The HOSK channel $V_{1/2}$ activation of -7.1 ± 2.0 mV and $V_{1/2}$ inactivation at -18.9 ± 1.4 mV is also well within range of conventional Kv channels. The activation curve suggests a shallow profile of opening probability of HOSK channel. This increased slope

factor might be due the fact that our voltage sensor domain has lysine residues flanked by other amine residues that might cause the shallowness in the activation curve of HOSK channel. Importantly, HOSK is active at very negative membrane potentials (i.e. -70mV ; Figure 4, 6, 7, 8 and 9), demonstrating its potential to contribute to the resting membrane potential such that inhibition of HOSK by oxygen could serve as the initial trigger for DASMCM depolarization and vasoconstriction which creates the initial functional closure of the DA at birth, prior to obliteration of the lumen by vascular remodeling⁴³.

In order to verify that the HOSK current is due to increase in HOSK channel in CHO cells, we did a dose-response curve of the increasing HOSK transfection. Data showed that with increasing HOSK cDNA transfection, a concomitant increase in the HOSK activity was also observed. This shows a indirect evidence that HOSK current is due to its intrinsic activity. Conversely, if HOSK were a co-factor rather than a channel, the linear dose response would not have been expected, unless it was a limiting factors.

4.4.2 Pharmacology

Pharmacologically, the HOSK channel show sensitivity to 4-AP and correolide, achieving $\sim 50\%$ inhibition at maximum doses. The correolide response is instructive. Recently studies were carried out to identify the putative correolide binding sites^{55, 56}. Site-directed mutagenesis along S5 and S6 of Kv1.3 was employed to identify those residues that contribute to high affinity binding of correolide. Substitutions at Leu346 and Leu353 in S5, and Ala413, Val417, Ala421, Pro423, and Val424 in S6, cause the most dramatic effect on correolide binding to Kv1.3⁵⁵. Therefore, to assess if HOSK channel shares these amino acids on the either side of the pore, a global progressive Clustal W

alignment was done with HOSK and Kv1.3. This analysis identified the presence of one amino acid in S3 domain of HOSK and 3 amino acids in the S4 domain. Furthermore, margatoxin (a Kv1.3 inhibitor) caused a 20% inhibition of HOSK current. However HOSK showed insensitivity to other drugs and toxins (such as titystoxin and E4031). Thus, the pharmacology of HOSK is reminiscent of certain Shaker channels, notably Kv1.3 and 1.5.

4.4.3 Oxygen sensitivity

Exposure to hypoxia increased HOSK channel activity (Figure 19); whereas oxygen decreased the HOSK current. This oxygen profile is in direct contrast to oxygen-sensitivity observed in the other O₂-sensitive Kv channels. Channels such as Kv1.5, Kv2.1, Kv1.2/Kv1.5, Kv2.1/9.3 and Kv3.1b display oxygen-sensitivity⁵⁸. These channels, mostly studied in the context of understanding the mechanism of hypoxic pulmonary vasoconstriction in PASMC, close during hypoxic response triggering depolarization in the pulmonary vasculature. This depolarization causes pulmonary arteries to contract due to increased cytosolic Ca²⁺, triggered by opening of L-type Ca²⁺ channels. In case of HOSK channels, oxygen decreases the HOSK-mediated K⁺ current. Furthermore, H₂O₂, which is one of the mediators of oxygen-mediated DA closure⁵², also results in decrease HOSK activity. Cumulatively, this is consistent with the hypothesis that HOSK has a contributory role as the effector of O₂-mediated DA closure. This is consistent with prior work from our group showing a role of H₂O₂ as a mediator in Kv1.5 and Kv2.1 activation. This highlights the potential for HOSK to contribute to functional closure of the DA.

Single-channel patch indicates that HOSK has conductance of 19 pS, which is well within the range of known Kv channel conductance. Immunoblot analysis also showed that HOSK transfection did not up-regulate expression of other oxygen-sensitive channel in CHO cells. Although supportive of our view that HOSK is a K⁺ channel, it does not preclude the possibility that the translocation of other Kv channels to the membrane could be enhanced (yielding more functional protein, without altering total expressed protein). To exclude the possibility that HOSK might be increasing K⁺ current in CHO and COS cells via upregulation of latent Kv channels, we performed immunoelectropharmacology using antibodies against a panel of oxygen-sensitive channels such as Kv1.2, Kv1.5, Kv2.1 and Kv3.1. This antibody mixture did not reduce the P_o of HOSK. In contrast, incubation of anti-HOSK antibody targeted to the epitope of the pore sequence inhibited the HOSK current, suggesting that the transfection-induced increase in single-channel activity was solely due to the HOSK channel.

4.4.4 Pore sequence

To determine the pore sequence responsible for the K⁺ ion selectivity, GVL sequence present in the reentrant loop of HOSK was mutated to AAA. This resulted in complete obliteration of the HOSK current such that only the measurable current was the intrinsic ohmic current generated by CHO cells. This suggests that GVL is K⁺ filter sequence for the HOSK channel. As discussed before there is a precedence of the pore sequence variation in prokaryotes as well as eukaryotes (Chapter 1). Thus, it might be possible that HOSK represent a new class of K⁺ channels with a variant pore sequence. Additionally, studies have also shown that if the tyrosine residue in the GYG sequence is

mutated to valine, the K⁺ ion selectivity is still maintained⁵⁹. This suggests that valine can provide the necessary carbonyl group at a distance from the pore that enables HOSK to conduct K⁺ ion at near diffusion rate. While our mutagenesis data are supportive of our proposal for the HOSK pore we did not do random mutagenesis to exclude the possibility that the AAA substitution is acting through a mechanism unrelated to the pore.

4.4.5 Endogenous HOSK channel activity in human DASMC

The physiological role of HOSK in human DASMCs was tested using immunoelectrophysiology. The HOSK antibody, when dialyzed into the DASMC via the patch pipette, inhibited I_K, whereas the antibody preabsorbed with the antigenic peptide had no effect (Figure 4e). This suggests that HOSK contributes to the total K⁺ current of hDASMCs. In addition the inhibition was noted at more hyperpolarized potential. Anti-HOSK antibody inhibited HOSK current at -50 mV, consistent with our hypothesis that HOSK contributes to the DASMC's membrane potential. This is important as it illustrates that in presence of oxygen, HOSK channels close and depolarize the cell membrane. This in turn may contribute to the well-established activation of voltage-sensitive Ca²⁺ channels that occurs when DAs are exposed to PO₂^{60, 61}. Furthermore, siRNA designed against HOSK channel inhibited the K⁺ current in human DASMC at potentials similar to anti-HOSK antibody. The appropriate off-target/scrambled siRNA were without effect, indicating the specificity of the siRNA strategy. Cumulatively, the cellular electrophysiology experiments identify HOSK as a K⁺ channel.

4.4.6 Caveats

We performed experiments in an effort to express HOSK channel in *Xenopus* oocytes. We used pXT7 (a generous gift from Dr. Warren Gallin) to synthesize HOSK RNA in vitro. Subsequent RNA injection in *xenopus* oocytes (performed by Dr. Kyla Smith) resulted only in detection of background current. Furthermore, we fostered a collaborative effort where we provided Dr. James D. Young's laboratory with HOSK cDNA. Subsequent RNA synthesis and injections into *Xenopus* oocytes resulted in no K⁺ current. Although, the failure of heterologous expression is unusual, it is not unprecedented. Indeed experiments attempting to express KcsA channels in *Xenopus* oocytes, the subject of Rod McKinnon's Nobel Prize winning work, also showed no K⁺ current⁶².

4.4.7 Lessons from the minK story

In addition, we also carried out experiments to demonstrate if HOSK channel is a true channel or a co-factor. This initiative was deemed important because of prior errors in identification of the minimal K⁺ channel (minK), as a channel. minK was identified as a gene that encodes a protein that shares no structural similarity with any other potassium channel and when expressed in *Xenopus* oocytes and some cell lines, it induces a voltage-dependent potassium current, sometimes termed I_{Sk} ⁶³. Like many other K⁺ channels, minK showed monovalent cations, selectivity⁶⁴, inhibition to barium, cesium, and tetraethylammonium (TEA), and activating profile reminiscent of an inwardly rectifying K⁺ channel⁶⁵. It has, however, not been possible to detect the opening of single

minK channels using patch-clamp recording⁶⁶.

Using a synthetic gene for the cDNA sequence of rat minK predicted a protein of 130 amino acids with a single hydrophobic stretch of 23 amino acids that has been suggested to be a transmembrane segment^{67, 68, 69}. The finding that specific mutations of the minK protein influence the characteristics of the induced current strongly suggests that the minK protein is intimately associated with the channel pore, rather than being an indirect activator of some other endogenous channel protein^{70, 71 72}

Ultimately experiments showed that the major factor with which minK proteins associate is the KvLQTI channel protein^{73, 74}. When expressed in COS or CHO cells, KvLQTI produces a relatively rapidly activating and slowly deactivating voltage-dependent potassium current^{73, 74}. If minK alone is transfected into these cells, it fails to produce currents. When, however, minK and KvLQTI are coexpressed in COS or CHO cells, a current is expressed that differs from that produced by KvLQTI alone. The minK-KvLQTI current activates slowly, with a delay in activation that is similar to that of the minK current recorded in oocytes. Moreover, the amplitude of the current is several fold greater than that of KvLQTI alone. KvLQTI mRNA can also be expressed in *Xenopus* oocytes, where it produces relatively rapidly activating currents similar to those recorded in COS or CHO cells^{73, 74}. Coexpression with minK produces currents similar to minK alone. In contrast to injections of minK RNA alone, however, no saturation of currents was found with increasing amount of coinjected minK-KvLQTI RNA, and the resultant current could be 20-fold greater than that achieved by injections of minK RNA alone⁷³. There is evidence for a direct interaction between the minK and KvLQTI proteins. Barhanin et al.⁷³ modified the KvLQTI gene by the addition of an epitope tag to allow

immunoprecipitation of the KvLQT1 protein. minK and the modified KvLQT1 gene were then infected, either alone or together, into insect Sf9 cells, using recombinant baculoviruses. Potassium currents recorded in such infected cells generally matched those in COS cells. When the KvLQT1 protein was immunoprecipitated from Sf9 membranes, the presence of minK protein in the immunoprecipitated complex was confirmed by Western blotting using antibodies directed against minK. These findings suggest that minK currents in *Xenopus* oocytes result from the association of the minK protein with endogenous KvLQT1 proteins. Mutants of minK that fail to express, but which antagonize the expression of normal minK currents, have a similar effect on the currents produced by minK and KvLQT1 coexpression⁷³. Thus minK, which initially was regarded as a new K⁺ channel turned out to be a co-factor for a dormant KvLQT1 channel.

Lessons from the minK-KvLQT-1 story helped us plan experiments to assess the validity of the HOSK channel, which also appears to be a structurally unique, small K⁺ channel with preserved K⁺ channel permeability and selectivity properties. However, the fundamental difference between the HOSK and minK is that single-channel patch can be performed on the HOSK channel while such was not a case with minK. Despite this difference we performed the necessary experiments to prove that HOSK can itself form functional channels and does not require not an endogenous factor.

To that end, we performed a dose dependent response of HOSK transfection in CHO cells. Escalating doses of HOSK cDNA resulted in concomitant increase in K⁺ current suggesting that HOSK, in its nascent form is generating the K⁺ current. However, if HOSK channel were a co-factor, an increasing dose of HOSK would ultimately plateau, as the current generated would have been limited by the intrinsic expression of

the innate channel. Furthermore, studies involving incubation of anti-HOSK antibody with single-channel patch, the dialysis of anti-HOSK antibody in human DASMCs and design of siRNA against HOSK provided substantial evidence in favor of HOSK being a channel. The fact that the conductance of HOSK was constant in two different expression systems would be surprising if the HOSK were a co-factor. Likewise the inhibitory effects of a pore-targeted antibody would be surprising if HOSK were a co-factor. Furthermore, to address this issue we have ligated HOSK into a protein-synthesizing vector. Future experiments that we have planned include the synthesis and purification of HOSK using bacterial expression systems with reconstitution of the channel protein itself in artificial bilayers, which would permit direct measurement of K⁺ current in a pure system, free from the possibility of observing effects of co-factors or chaperones.

4.4.8 HOSK Channel gene sequence

Subsequent to the electrophysiological analysis, examination of the 5' region of the HOSK gene, using *in silico* analysis, revealed a putative upstream start codon in frame with the translation of HOSK channel (Chapter 3). However, the fact that anti-HOSK antibodies and siRNA against HOSK resulted in attenuated K⁺ current suggests that crux of the channel activity lies in the analyzed HOSK sequence. Furthermore, the finding that a truncated version of HOSK (the 1.4 kb fragment) generated a remarkably similar electrophysiological signature (Figures 28-29) and pharmacological profile (Figure 30) suggests that the functional aspect of HOSK lies in the clone that we have examined in this thesis.

4.4.9 Summary

This chapter highlights several key aspects of HOSK's structure and function. The HOSK channel does appear to be unique (it is not homologous to existing Kv channels or other proteins in the Swiss database). HOSK also has a response to oxygen which is consistent with the observed response of endogenous whole cell K⁺ current in DASMC. Furthermore, by virtue of its activity at negative potential may determine the membrane potential. This may be important in initiating the functional closure of the DA. In conclusion, HOSK is a new type of K⁺ channel, of great interest to evolutionary scientists and those interested in structural biology. HOSK may play a pivotal role in O₂-mediated DA closure.

4.5 REFERENCES

1. Hodgkin, A. L. & Huxley, A. F. A quantitative description of membrane current and its application to conduction and excitation in nerve. 1952. *J. Physiol* 117, 500-544 (1990).
2. Armstrong, C. M. & Hille, B. Voltage-gated ion channels and electrical excitability. *Neuron* 20, 371-80 (1998).
3. Sakmann, B. Nobel Lecture. Elementary steps in synaptic transmission revealed by currents through single ion channels. *Embo J* 11, 2002-16 (1992).
4. Nelson, M. T. & Quayle, J. M. Physiological roles and properties of potassium channels in arterial smooth muscle. *Am J Physiol* 268, C799-822 (1995).
5. Butler, A., Wei, A. & Salkoff, L. Shal, Shab, and Shaw: three genes encoding potassium channels in *Drosophila*. *Nucleic Acids Res* 18, 2173-4 (1990).
6. Butler, A., Wei, A. G., Baker, K. & Salkoff, L. A family of putative potassium channel genes in *Drosophila*. *Science* 243, 943-7 (1989).
7. Pongs, O. et al. Shaker encodes a family of putative potassium channel proteins in the nervous system of *Drosophila*. *Embo J* 7, 1087-96 (1988).
8. Schwarz, T. L., Tempel, B. L., Papazian, D. M., Jan, Y. N. & Jan, L. Y. Multiple potassium-channel components are produced by alternative splicing at the Shaker locus in *Drosophila*. *Nature* 331, 137-42 (1988).
9. Tempel, B. L., Papazian, D. M., Schwarz, T. L., Jan, Y. N. & Jan, L. Y. Sequence of a probable potassium channel component encoded at Shaker locus of *Drosophila*. *Science* 237, 770-5 (1987).

10. Gutman, G. A. et al. International Union of Pharmacology. LIII. Nomenclature and molecular relationships of voltage-gated potassium channels. *Pharmacol Rev* 57, 473-508 (2005).
11. Robertson, B. E. & Nelson, M. T. Aminopyridine inhibition and voltage dependence of K⁺ currents in smooth muscle cells from cerebral arteries. *Am J Physiol* 267, C1589-97 (1994).
12. Volk, K. A., Matsuda, J. J. & Shibata, E. F. A voltage-dependent potassium current in rabbit coronary artery smooth muscle cells. *J Physiol* 439, 751-68 (1991).
13. Volk, K. A. & Shibata, E. F. Single delayed rectifier potassium channels from rabbit coronary artery myocytes. *Am J Physiol* 264, H1146-53 (1993).
14. Coetzee, W. A. et al. Molecular diversity of K⁺ channels. *Ann N Y Acad Sci* 868, 233-85 (1999).
15. Beech, D. J. & Bolton, T. B. Two components of potassium current activated by depolarization of single smooth muscle cells from the rabbit portal vein. *J Physiol* 418, 293-309 (1989).
16. Hirst, G. D., Silverberg, G. D. & van Helden, D. F. The action potential and underlying ionic currents in proximal rat middle cerebral arterioles. *J Physiol* 371, 289-304 (1986).
17. Weir, E. K. & Archer, S. L. The mechanism of acute hypoxic pulmonary vasoconstriction: the tale of two channels. *Faseb J* 9, 183-9 (1995).
18. Archer, S. L. et al. Preferential expression and function of voltage-gated, O₂-sensitive K⁺ channels in resistance pulmonary arteries explains regional

- heterogeneity in hypoxic pulmonary vasoconstriction: ionic diversity in smooth muscle cells. *Circ Res* 95, 308-18 (2004).
19. Navarro-Antolin, J., Levitsky, K. L., Calderon, E., Ordonez, A. & Lopez-Barneo, J. Decreased expression of maxi-K⁺ channel beta1-subunit and altered vasoregulation in hypoxia. *Circulation* 112, 1309-15 (2005).
 20. Jackson, W. F. Ion channels and vascular tone. *Hypertension* 35, 173-8 (2000).
 21. Standen, N. B. & Quayle, J. M. K⁺ channel modulation in arterial smooth muscle. *Acta Physiol Scand* 164, 549-57 (1998).
 22. Archer, S. L., Huang, J., Henry, T., Peterson, D. & Weir, E. K. A redox-based O₂ sensor in rat pulmonary vasculature. *Circ Res* 73, 1100-12 (1993).
 23. Archer, S. L. et al. Molecular identification of the role of voltage-gated K⁺ channels, Kv1.5 and Kv2.1, in hypoxic pulmonary vasoconstriction and control of resting membrane potential in rat pulmonary artery myocytes. *J Clin Invest* 101, 2319-30 (1998).
 24. Yuan, X.-J. Voltage gated K⁺ currents regulate resting membrane potential and [Ca²⁺]_i in pulmonary artery myocytes. *Circ Research* 77, 370-378 (1995).
 25. Cornfield, D., Reeve, H., Tolarova, S., Weir, E. & Archer, S. Oxygen causes fetal pulmonary vasodilation through activation of a calcium-dependent potassium channel. *Proc Natl Acad Sci USA* 93, 8989-8094 (1996).
 26. Post, J. M., Gelband, C. H. & Hume, J. R. [Ca²⁺]_i inhibition of K⁺ channels in canine pulmonary artery: Novel mechanism for hypoxia-induced membrane depolarization. *Circ Res* 77, 131-139 (1995).

27. Goirand, F. et al. ETA, mixed ETA/ETB receptor antagonists, and protein kinase C inhibitor prevent acute hypoxic pulmonary vasoconstriction: influence of potassium channels. *J Cardiovasc Pharmacol* 41, 117-25 (2003).
28. Hong, Z. et al. Pergolide is an inhibitor of voltage-gated potassium channels, including Kv1.5, and causes pulmonary vasoconstriction. *Circulation* 112, 1494-9 (2005).
29. Weir, E. et al. Anorexic agents aminorex, fenfluramine, and dexfenfluramine inhibit potassium current in rat pulmonary vascular smooth muscle and cause pulmonary vasoconstriction. *Circulation* 94, 2216-2220 (1996).
30. Imbrici, P., Tucker, S. J., D'Adamo, M. C. & Pessia, M. Role of receptor protein tyrosine phosphatase alpha (RPTPalph) and tyrosine phosphorylation in the serotonergic inhibition of voltage- dependent potassium channels. *Pflugers Arch* 441, 257-62. (2000).
31. Shimoda, L. A., Sylvester, J. T. & Sham, J. S. Inhibition of voltage-gated K⁺ current in rat intrapulmonary arterial myocytes by endothelin-1. *Am J Physiol* 274, L842-53 (1998).
32. Bonnet, S. et al. NFAT regulates Kv1.5, a voltage-gated K⁺ channel which is downregulated in both human and animal pulmonary hypertension. (abstract). *Canadian Journal of Cardiology* 21, 57 (2005).
33. Bonnet, S. et al. An abnormal mitochondrial-HIF-1-Kv channel pathway disrupts oxygen-sensing and triggers pulmonary arterial hypertension (PAH) in fawn-hooded rats: similarities to human PAH. *Circulation* (in press) (2006).

34. Duprat, F. et al. TASK, a human background K⁺ channel to sense external pH variations near physiological pH. *Embo J* 16, 5464-71 (1997).
35. Gurney, A. M. et al. Two-pore domain K channel, TASK-1, in pulmonary artery smooth muscle cells. *Circ Res* 93, 957-64 (2003).
36. Gardener, M. J. et al. Functional evidence of a role for two-pore domain potassium channels in rat mesenteric and pulmonary arteries. *Br J Pharmacol* 142, 192-202 (2004).
37. Reeve, H. L., Nelson, D. P., Archer, S. L. & Weir, E. K. Effects of fluoxetine, phentermine, and venlafaxine on pulmonary arterial pressure and electrophysiology. *Am J Physiol* 276, L213-9 (1999).
38. Yuan, X. J. Voltage-gated K⁺ currents regulate resting membrane potential and [Ca²⁺]_i in pulmonary arterial myocytes. *Circ Res* 77, 370-8 (1995).
39. Yuan, X. J., Wang, J., Juhaszova, M., Gaine, S. P. & Rubin, L. J. Attenuated K⁺ channel gene transcription in primary pulmonary hypertension. *Lancet* 351, 726-7 (1998).
40. Post, J., Hume, J., Archer, S. & Weir, E. Direct role for potassium channel inhibition in hypoxic pulmonary vasoconstriction. *Am J Physiol* 262, C882-C890 (1992).
41. Yuan, X.-J., Goldman, W., Tod, M., Rubin, L. & Blaustein, M. Hypoxia reduces potassium currents in cultured rat pulmonary but not mesenteric arterial myocytes. *Am J Physiol* 264, L116-L123 (1993).

42. Yuan, X.-J., Goldman, W., Tod, M., Rubin, L. & Blaustein, M. Ionic currents in rat pulmonary and mesenteric arterial myocytes in primary culture and subculture. *Am J Physiol* 264, L107-L115 (1993).
43. Weir, E. K., Lopez-Barneo, J., Buckler, K. J. & Archer, S. L. Acute oxygen-sensing mechanisms. *N Engl J Med* 353, 2042-55 (2005).
44. Archer, S. L. et al. Differential distribution of electrophysiologically distinct myocytes in conduit and resistance arteries determines their response to nitric oxide and hypoxia. *Circ Res* 78, 431-442 (1996).
45. Michelakis, E. D., Thebaud, B., Weir, E. K. & Archer, S. L. Hypoxic pulmonary vasoconstriction: redox regulation of O₂-sensitive K⁺ channels by a mitochondrial O₂-sensor in resistance artery smooth muscle cells. *J Mol Cell Cardiol* 37, 1119-36 (2004).
46. Cornfield, D. N., Reeve, H. L., Tolarova, S., Weir, E. K. & Archer, S. L. Oxygen causes fetal pulmonary vasodilation through activation of a calcium-dependent potassium channel. *Proc. Natl. Acad. Sci.* 93, 8089-8094 (1996).
47. Michelakis, E. D., Thebaud, B., Weir, E. K. & Archer, S. L. Hypoxic pulmonary vasoconstriction: redox regulation of O(2)-sensitive K(+) channels by a mitochondrial O(2)-sensor in resistance artery smooth muscle cells. *J Mol Cell Cardiol* 37, 1119-36 (2004).
48. McMurtry, I. F., Petrun, M. D. & Reeves, J. T. Lungs from chronically hypoxic rats have decreased pressor response to acute hypoxia. *Am J Physiol* 235, H104-9 (1978).

49. Reeve, H. L., Michelakis, E., Nelson, D. P., Weir, E. K. & Archer, S. L. Alterations in a redox oxygen sensing mechanism in chronic hypoxia. *J Appl Physiol* 90, 2249-56 (2001).
50. Pozeg, Z. I. et al. In vivo gene transfer of the O₂-sensitive potassium channel Kv1.5 reduces pulmonary hypertension and restores hypoxic pulmonary vasoconstriction in chronically hypoxic rats. *Circulation* 107, 2037-44 (2003).
51. Osipenko, O. N., Tate, R. J. & Gurney, A. M. Potential role for kv3.1b channels as oxygen sensors. *Circ Res* 86, 534-40 (2000).
52. Michelakis, E. D. et al. O₂ sensing in the human ductus arteriosus: regulation of voltage-gated K⁺ channels in smooth muscle cells by a mitochondrial redox sensor. *Circ Res* 91, 478-86 (2002).
53. Hogg, D. S., McMurray, G. & Kozlowski, R. Z. Endothelial cells freshly isolated from small pulmonary arteries of the rat possess multiple distinct k⁺ current profiles. *Lung* 180, 203-14 (2002).
54. West, J. et al. Suppression of type II bone morphogenic protein receptor in vascular smooth muscle induces pulmonary arterial hypertension in transgenic mice. *Chest* 128, 553S (2005).
55. Hanner, M. et al. Binding of correolide to the K(v)1.3 potassium channel: characterization of the binding domain by site-directed mutagenesis. *Biochemistry* 40, 11687-97. (2001).
56. Hanner, M. et al. Binding of correolide to K(v)1 family potassium channels. Mapping the domains of high affinity interaction. *J Biol Chem* 274, 25237-44. (1999).

57. Sansom, M. S. et al. Potassium channels: structures, models, simulations. *Biochim Biophys Acta* 1565, 294-307 (2002).
58. Coppock, E. A., Martens, J. R. & Tamkun, M. M. Molecular basis of hypoxia-induced pulmonary vasoconstriction: role of voltage-gated K⁺ channels. *Am J Physiol Lung Cell Mol Physiol* 281, L1-12 (2001).
59. Heginbotham, L., Lu, Z., Abramson, T. & MacKinnon, R. Mutations in the K⁺ channel signature sequence. *Biophys J* 66, 1061-7 (1994).
60. Michelakis, E. et al. Voltage-gated potassium channels in human ductus arteriosus. *Lancet* 356, 134-7 (2000).
61. Tristani-Firouzi, M., Reeve, H. L., Tolarova, S., Weir, E. K. & Archer, S. L. Oxygen-induced constriction of rabbit ductus arteriosus occurs via inhibition of a 4-aminopyridine-, voltage-sensitive potassium channel. *J Clin Invest* 98, 1959-65 (1996).
62. Schrempf, H. et al. A prokaryotic potassium ion channel with two predicted transmembrane segments from *Streptomyces lividans*. *Embo J* 14, 5170-8 (1995).
63. Kaczmarek, L. K. Voltage-dependent potassium channels: minK and Shaker families. *New Biol* 3, 315-23 (1991).
64. Hausdorff, S. F., Goldstein, S. A., Rushin, E. E. & Miller, C. Functional characterization of a minimal K⁺ channel expressed from a synthetic gene. *Biochemistry* 30, 3341-6 (1991).
65. Blumenthal, E. M. & Kaczmarek, L. K. Inward rectification of the minK potassium channel. *J Membr Biol* 136, 23-9 (1993).

66. Kaczmarek, L. K. & Blumenthal, E. M. Properties and regulation of the minK potassium channel protein. *Physiol Rev* 77, 627-41 (1997).
67. Takumi, T., Ohkubo, H. & Nakanishi, S. Cloning of a membrane protein that induces a slow voltage-gated potassium current. *Science* 242, 1042-5 (1988).
68. Liu, Q. R. et al. A very short peptide makes a voltage-dependent ion channel: the critical length of the channel domain of colicin E1. *Proteins* 1, 218-29 (1986).
69. Pragnell, M. et al. Estrogen induction of a small, putative K⁺ channel mRNA in rat uterus. *Neuron* 4, 807-12 (1990).
70. Oiki, S., Takumi, T., Okada, Y. & Nakanishi, S. Alterations of gating parameters by neutral substitutions of transmembrane Leu52 of slow potassium channel. *Ann N Y Acad Sci* 707, 402-6 (1993).
71. Takumi, T. et al. Alteration of channel activities and gating by mutations of slow ISK potassium channel. *J Biol Chem* 266, 22192-8 (1991).
72. Wilson, G. G., Sivaprasadarao, A., Findlay, J. B. & Wray, D. Changes in activation gating of IsK potassium currents brought about by mutations in the transmembrane sequence. *FEBS Lett* 353, 251-4 (1994).
73. Barhanin, J. et al. K(V)LQT1 and IsK (minK) proteins associate to form the I(Ks) cardiac potassium current. *Nature* 384, 78-80 (1996).
74. Sanguinetti, M. C. et al. Coassembly of K(V)LQT1 and minK (IsK) proteins to form cardiac I(Ks) potassium channel. *Nature* 384, 80-3 (1996).



Figure 4.1: Ductus arteriosus is a conduit blood vessel that connects pulmonary artery to aorta. (Netters, Frank H. Atlas of Human Anatomy Second Edition)

Ductus Arteriosus

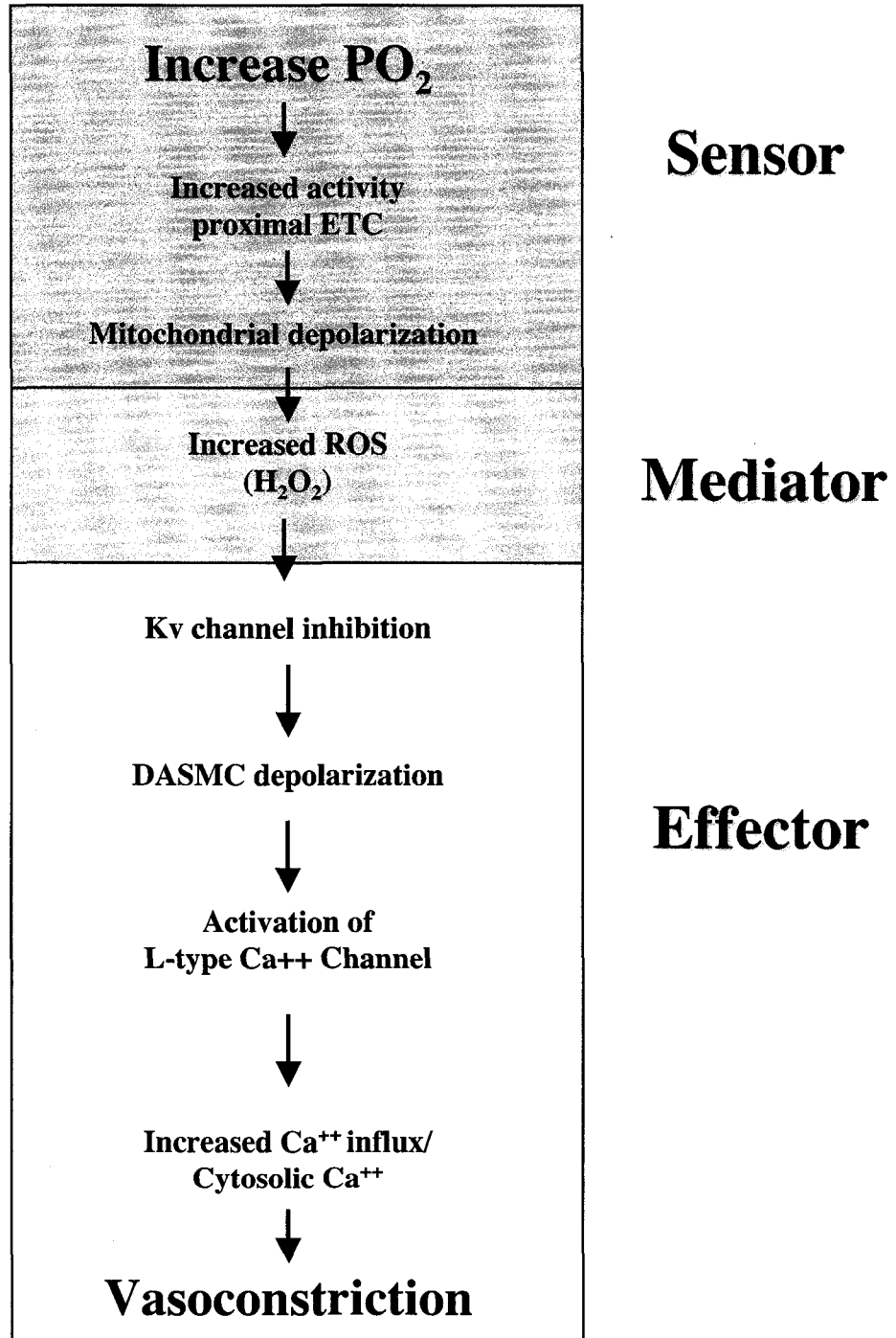


Figure 4.2: Increase in PO₂ results in mitochondrial membrane depolarization. This leads to increased reactive oxygen species (ROS). This increase causes inhibition of Kv channels leading to vasoconstriction.

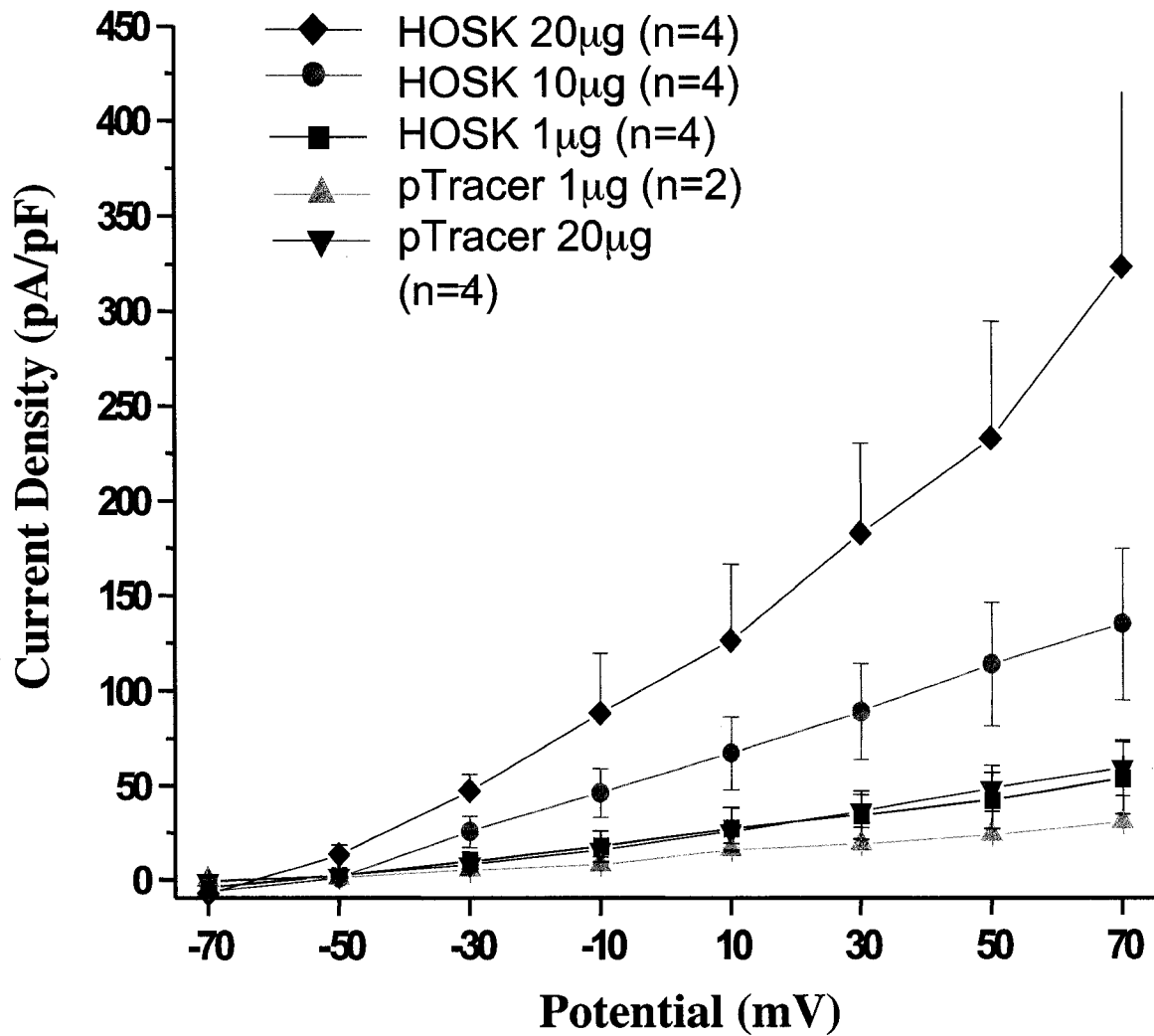


Figure 4.4: Dose-dependent increase in HOSK cDNA results in concomitant increase in current density in CHO cells.

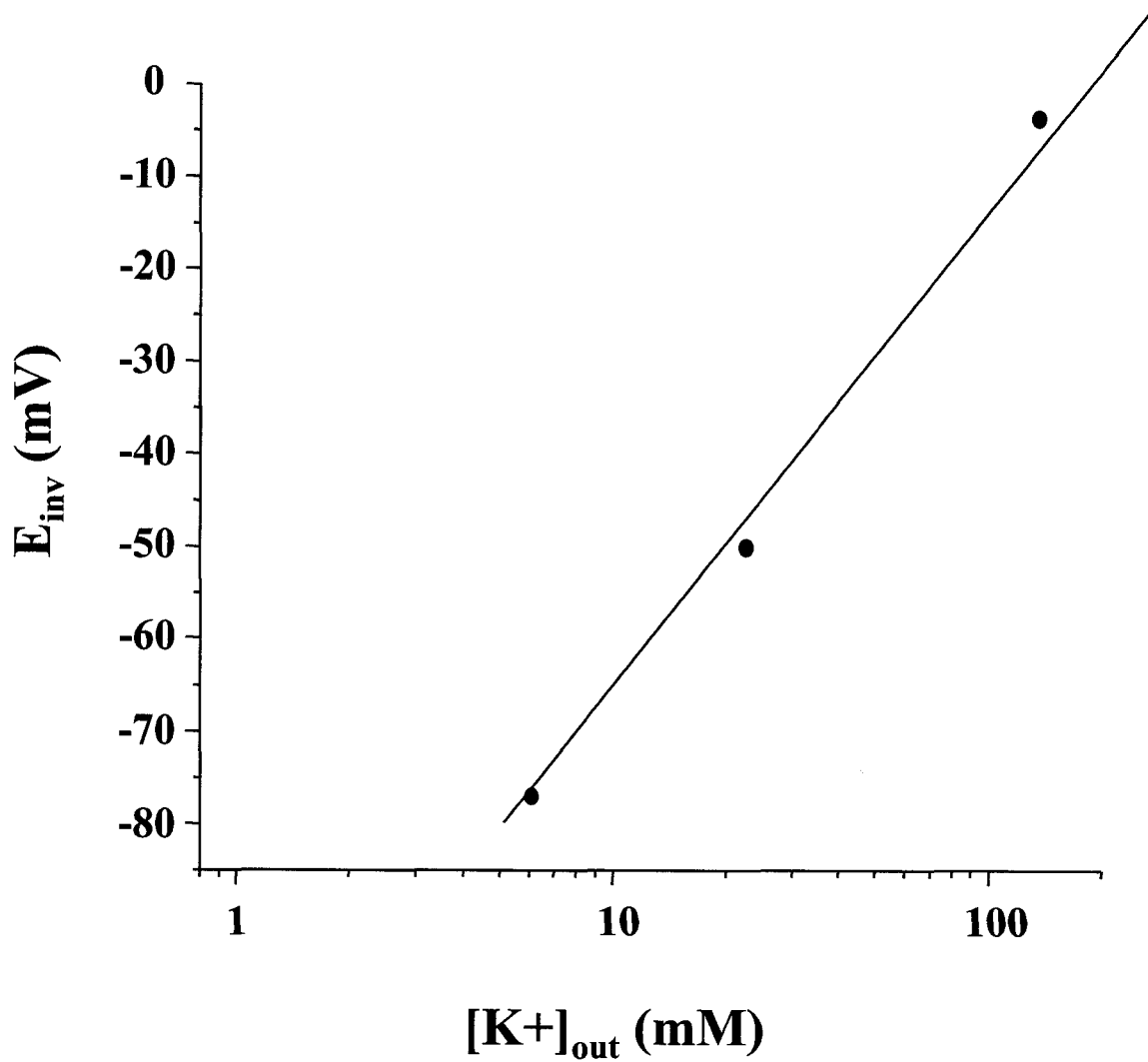


Figure 4.5: Logarithm curve shows that progressive increase in $[K^+]_{out}$ results in reversal potential approaching zero.

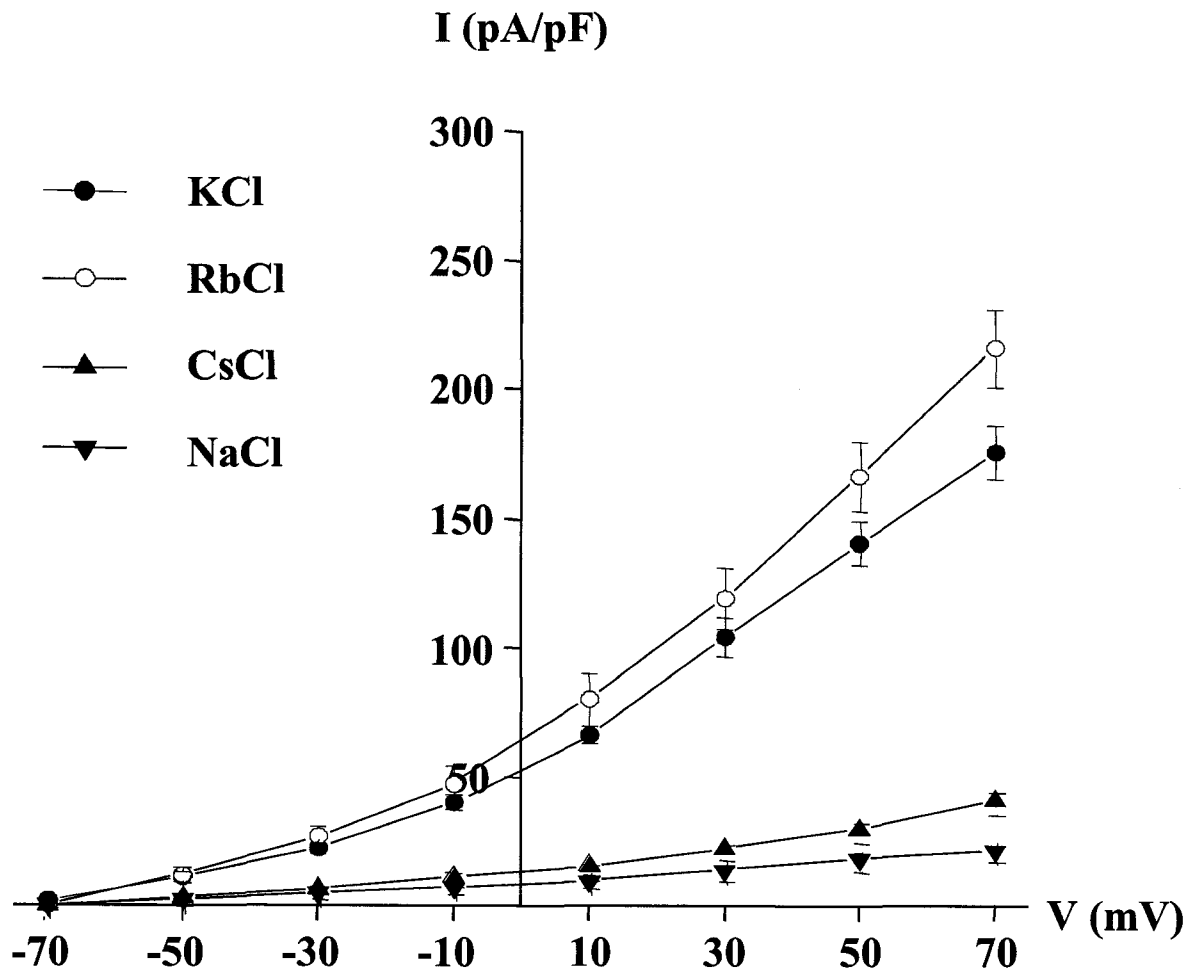


Figure 4.6: Ionic substitution experiments show that HOSK channel cannot conduct cesium chloride (CsCl) and sodium chloride (NaCl). However, it is permeable for rubidium chloride, a property reminiscent of other Kv channels

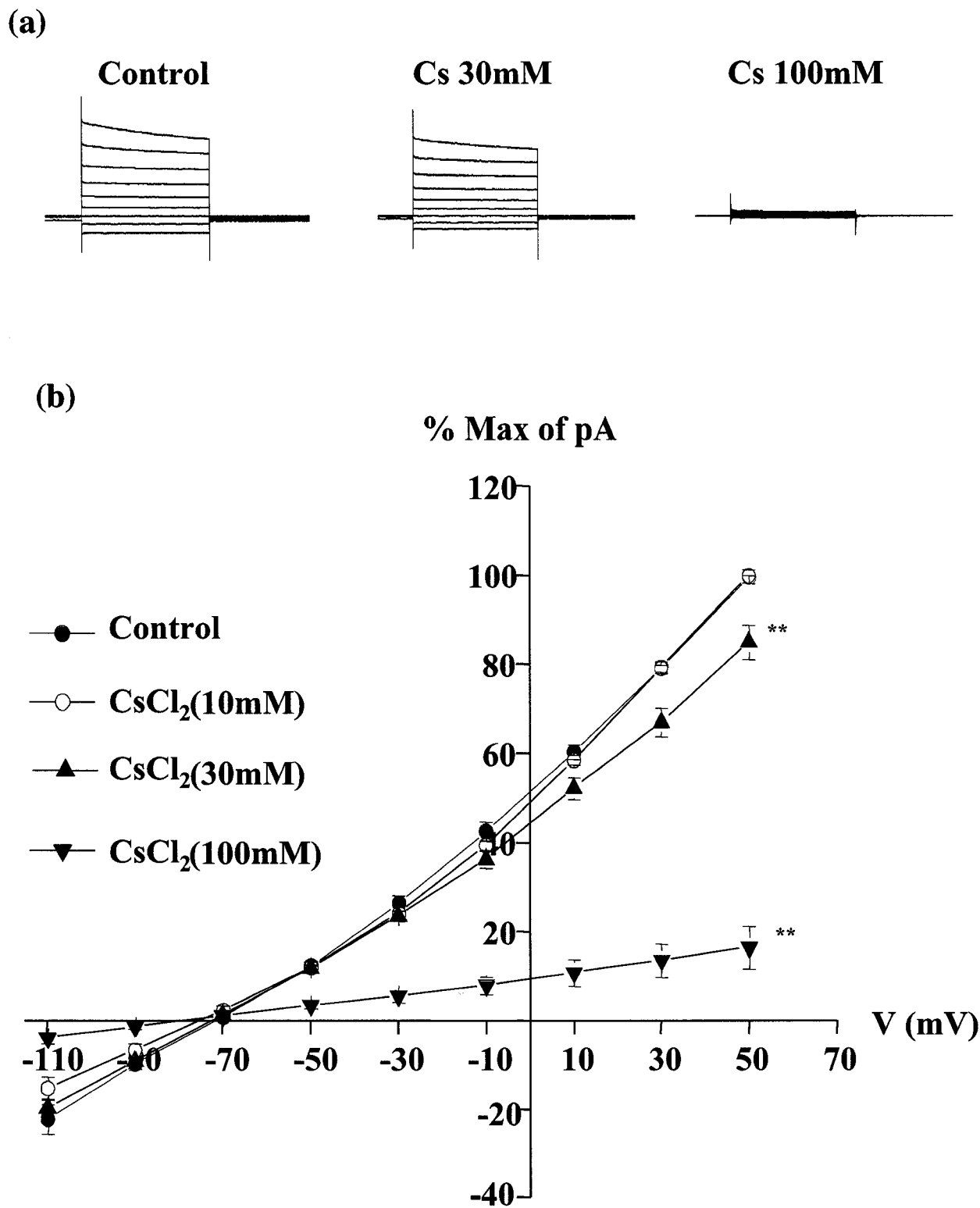


Figure 4.7: Ionic substitution experiments show that HOSK channel can be inhibited by cesium chloride (CsCl) in a dose-dependent manner. (a) Representative traces and (b) mean \pm SEM current-voltage (I-V) plots

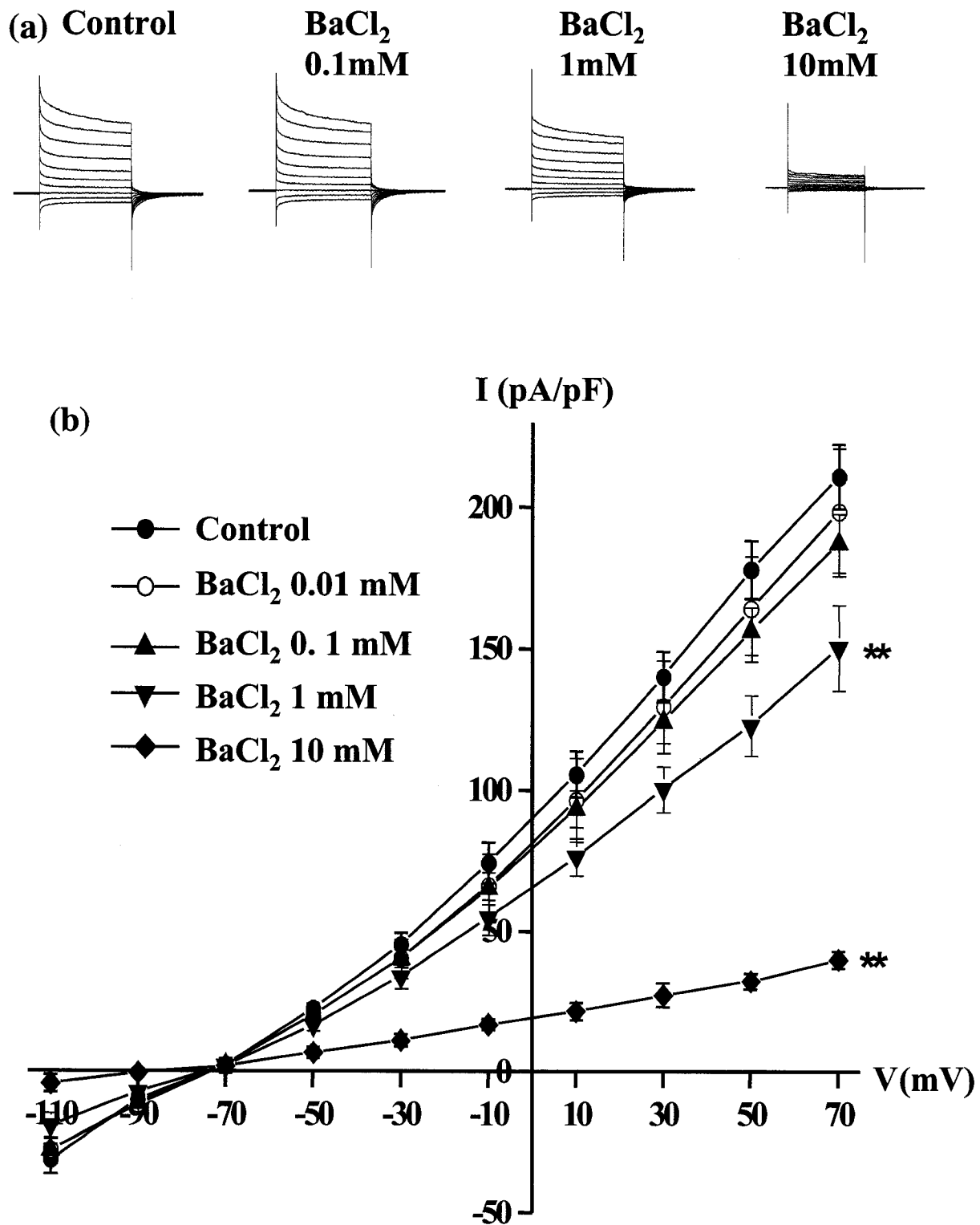


Figure 4.8: Ionic substitution experiments show that HOSK channel can be inhibited by barium chloride (BaCl₂) in a dose-dependent manner. (a) Representative traces and (b) mean±SEM current-voltage (I-V) plots

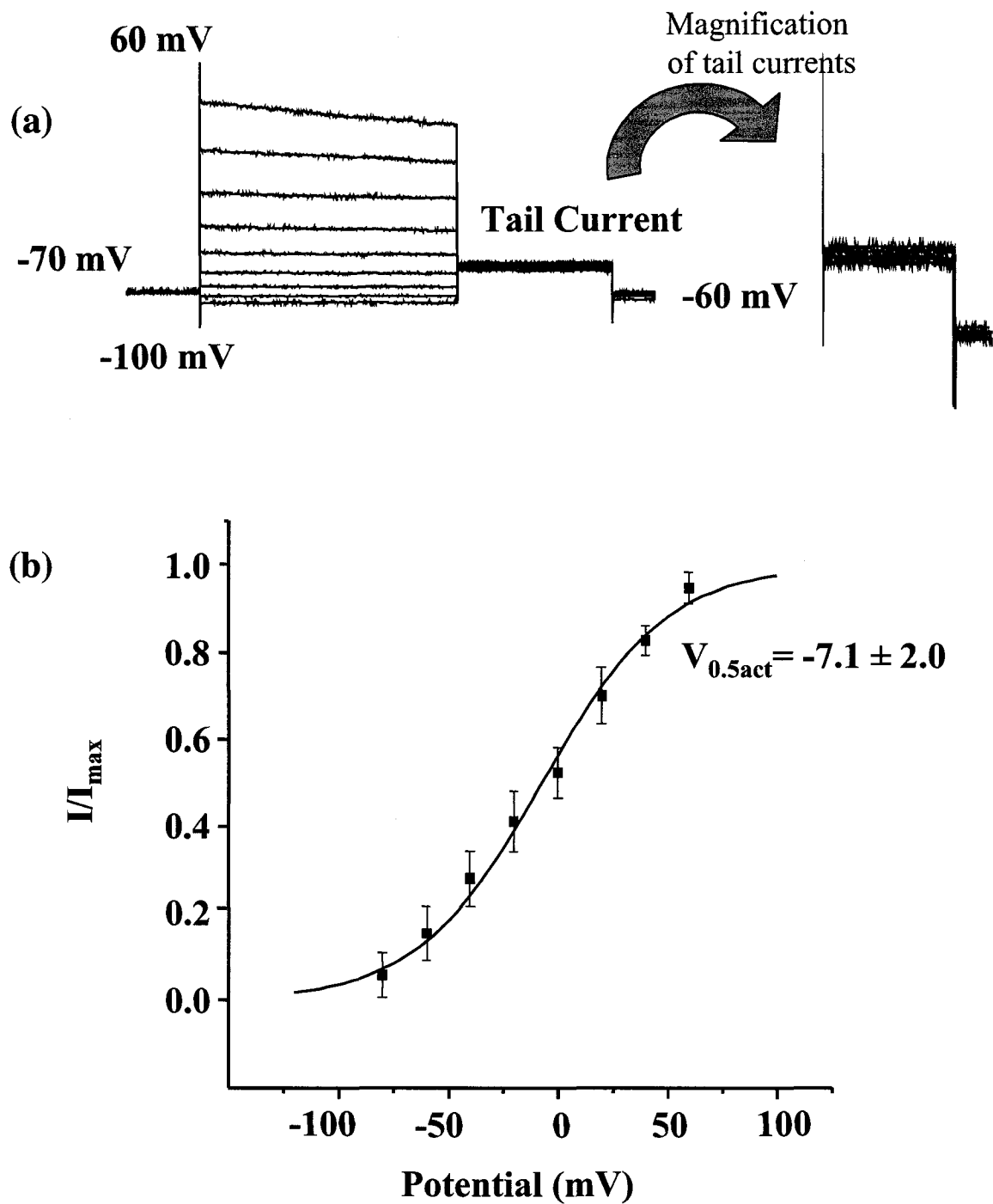


Figure 4.9: (a) Activation protocol entailed measurement of tail current after the stepwise increase in voltage was brought down to -60 mV. (b) The current-voltage relationship is reported as a mean \pm SEM

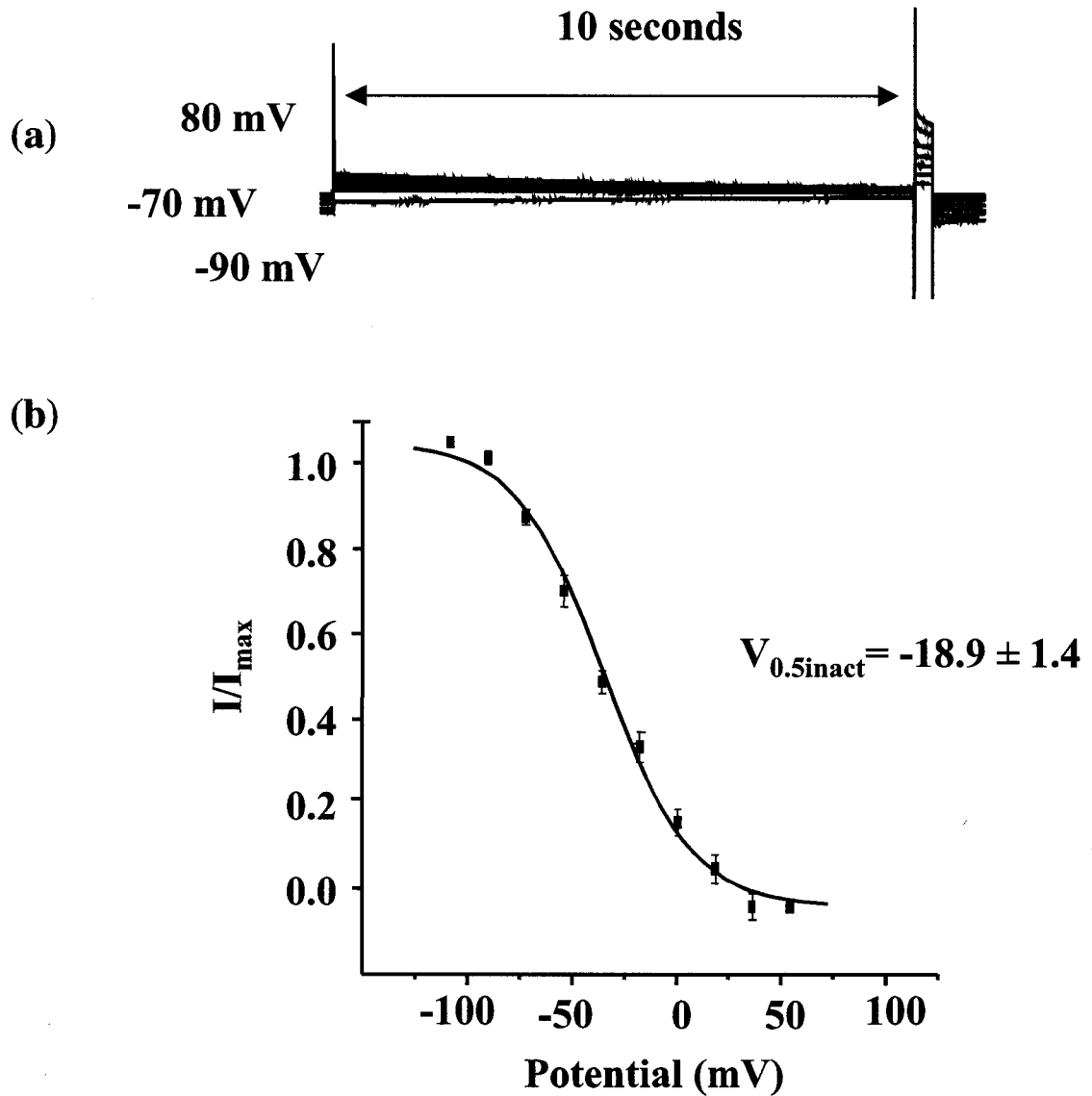


Figure 4.10: (a) Inactivation protocol entailed measurement of tail current after inactivating the HOSK channel by holding it at +80 mV for 10 seconds. (b) The current-voltage relationship of inactivation is reported as a mean \pm SEM

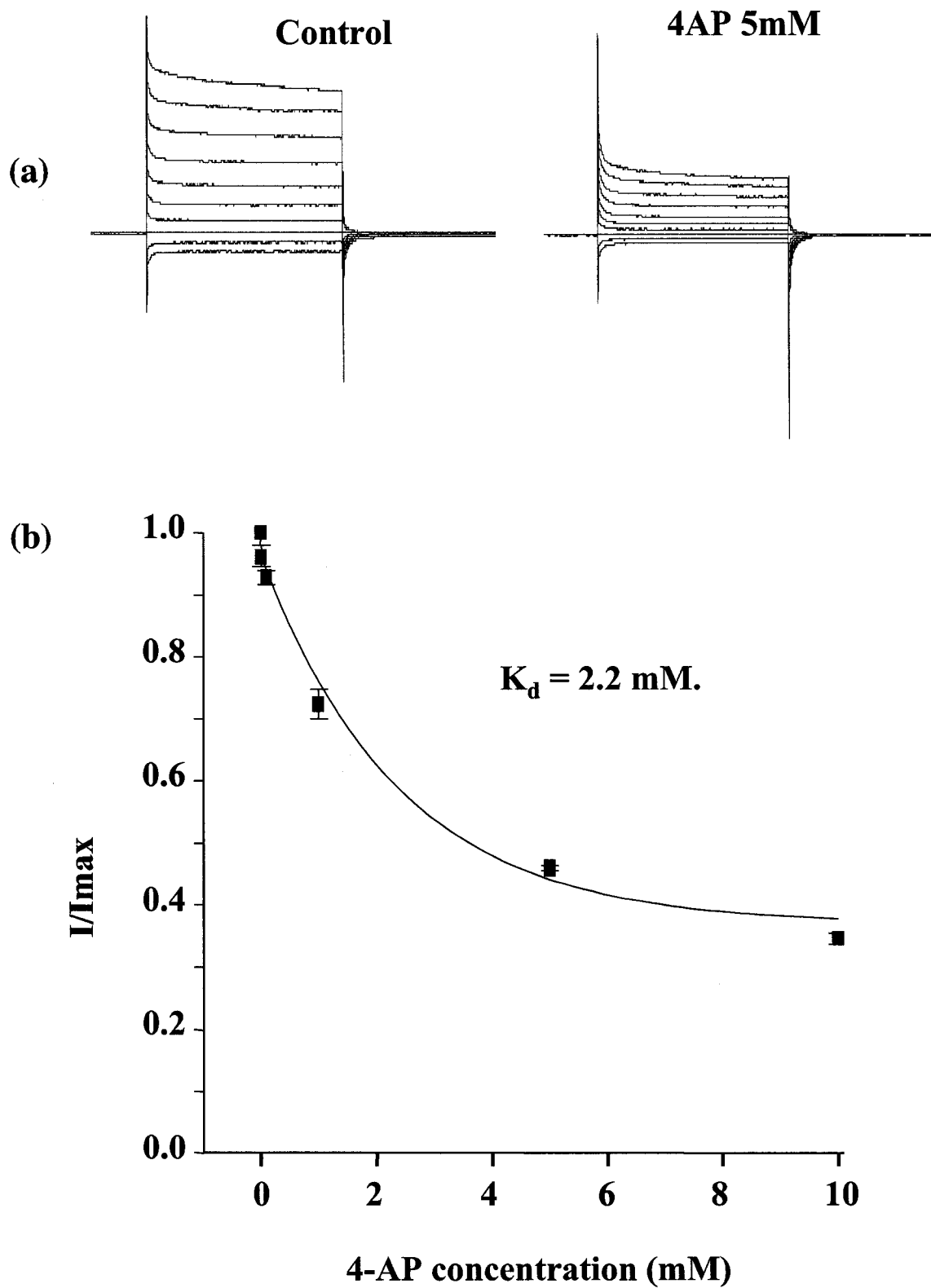


Figure 4.11: Inhibition of HOSK channel by the Kv blocker 4-aminopyridine (4-AP) (a) Representative traces and (b) current inhibition at various 4-AP concentration

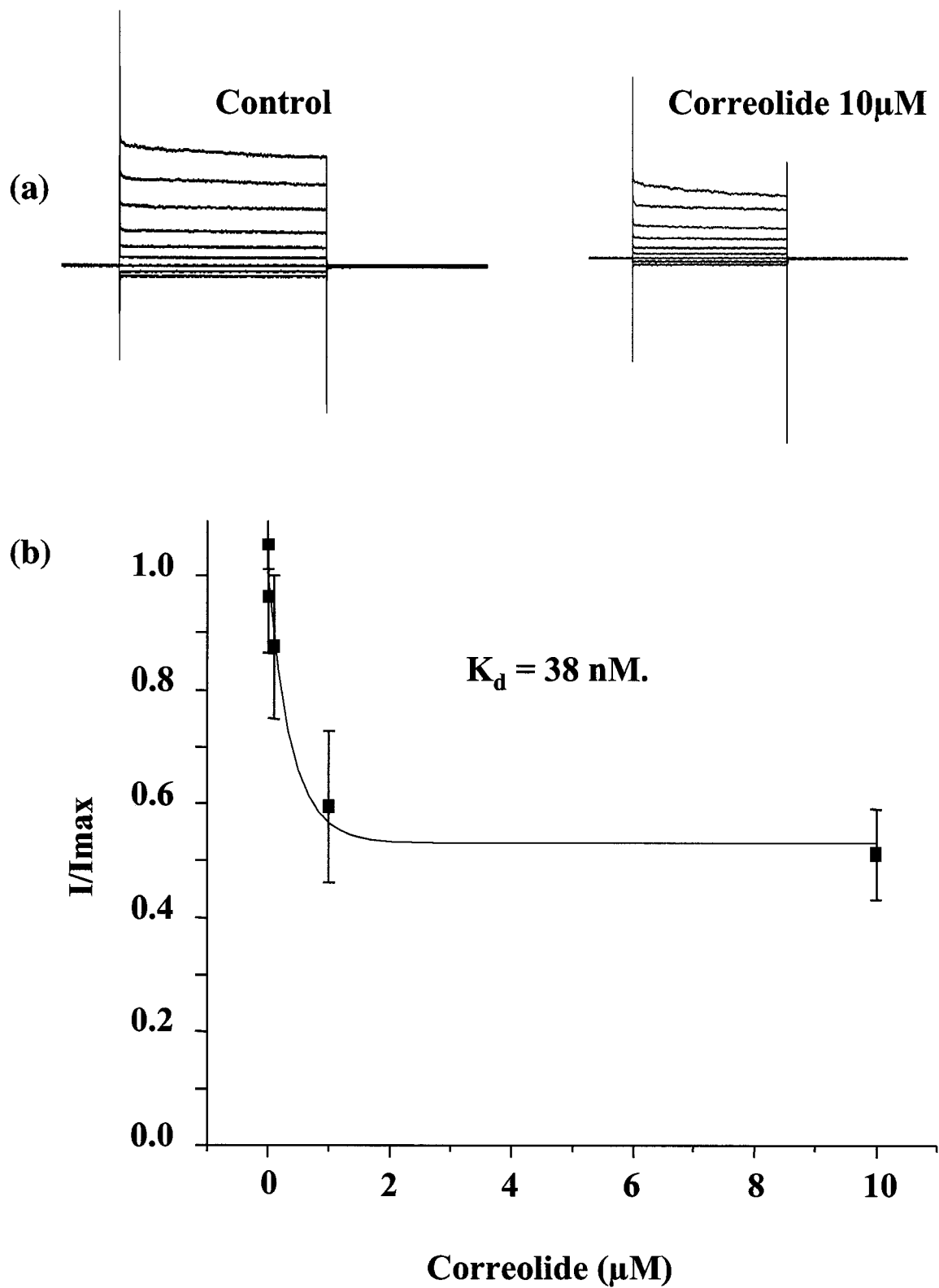


Figure 4.12: Inhibition of HOSK channel by the Kv1.x blocker correolide (a) Representative traces and (b) current inhibition at different correolide concentrations.

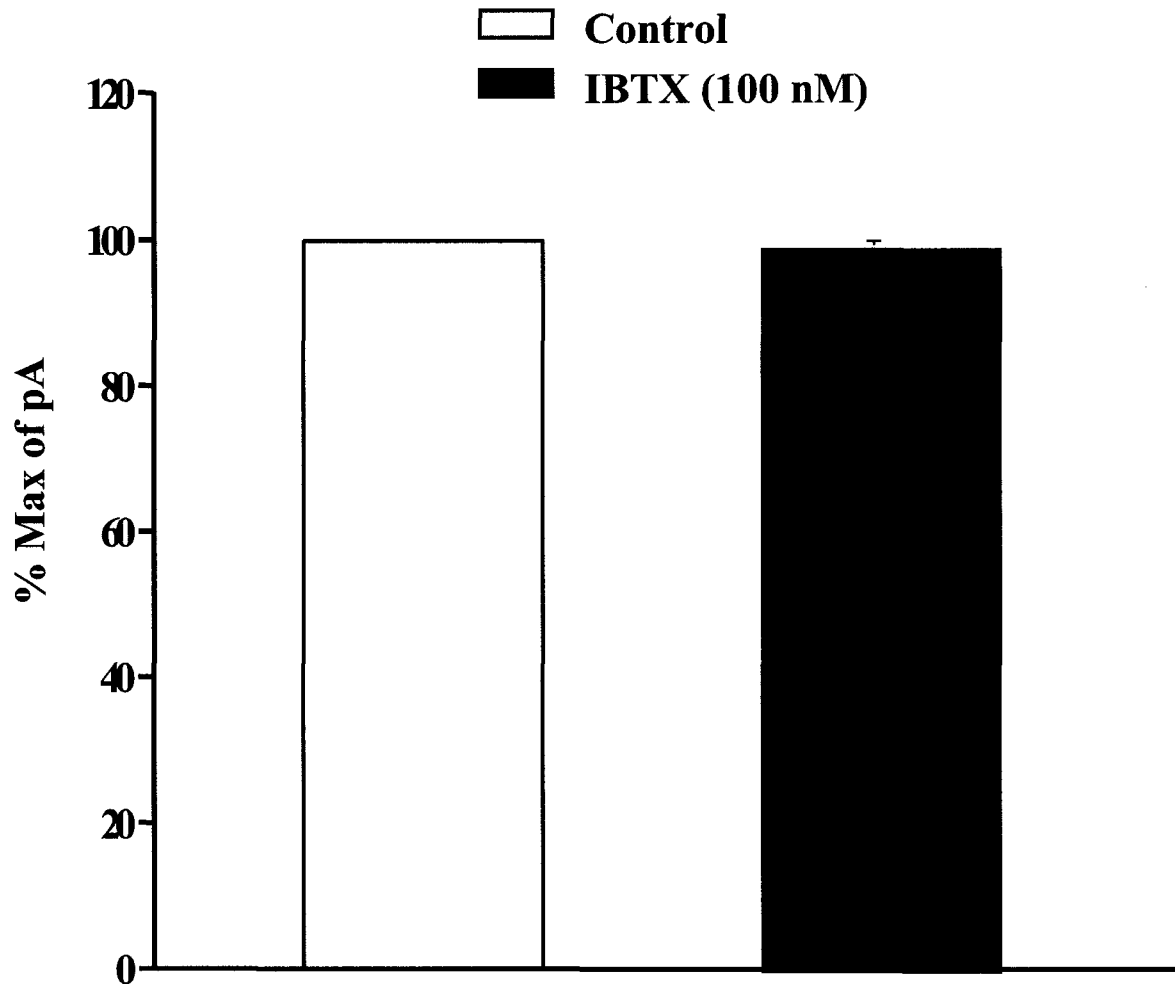


Figure 4.13: HOSK channel is not inhibited by big conductance calcium sensitive K^+ channel inhibitor, Iberitoxin (IBTX) in transfected CHO cells. The bar represents mean \pm SEM

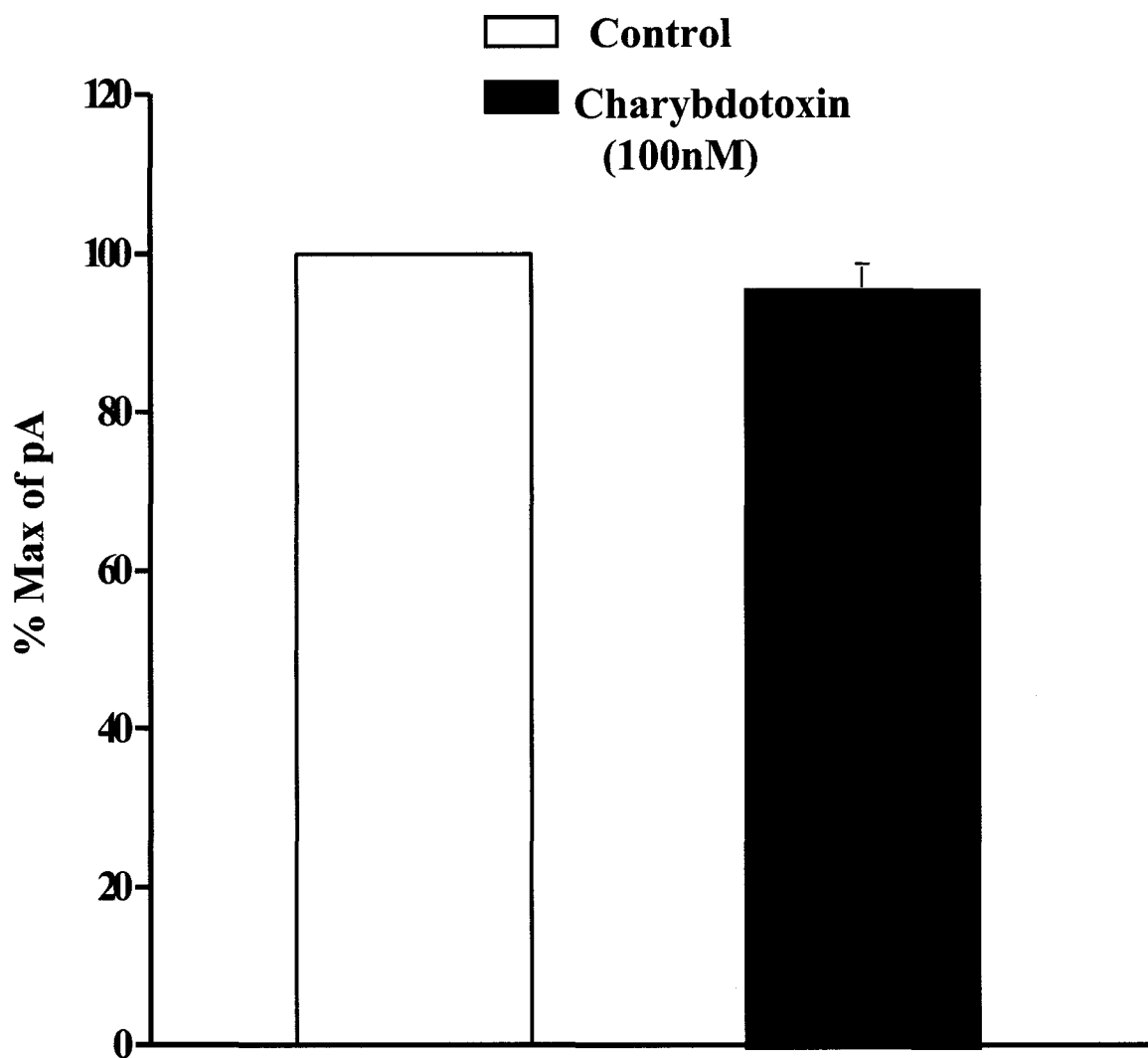


Figure 4.14: HOSK channel is not inhibited by small conductance calcium sensitive K^+ channel inhibitor, Charybdotoxin in transfected CHO cells. The bar represents mean \pm SEM

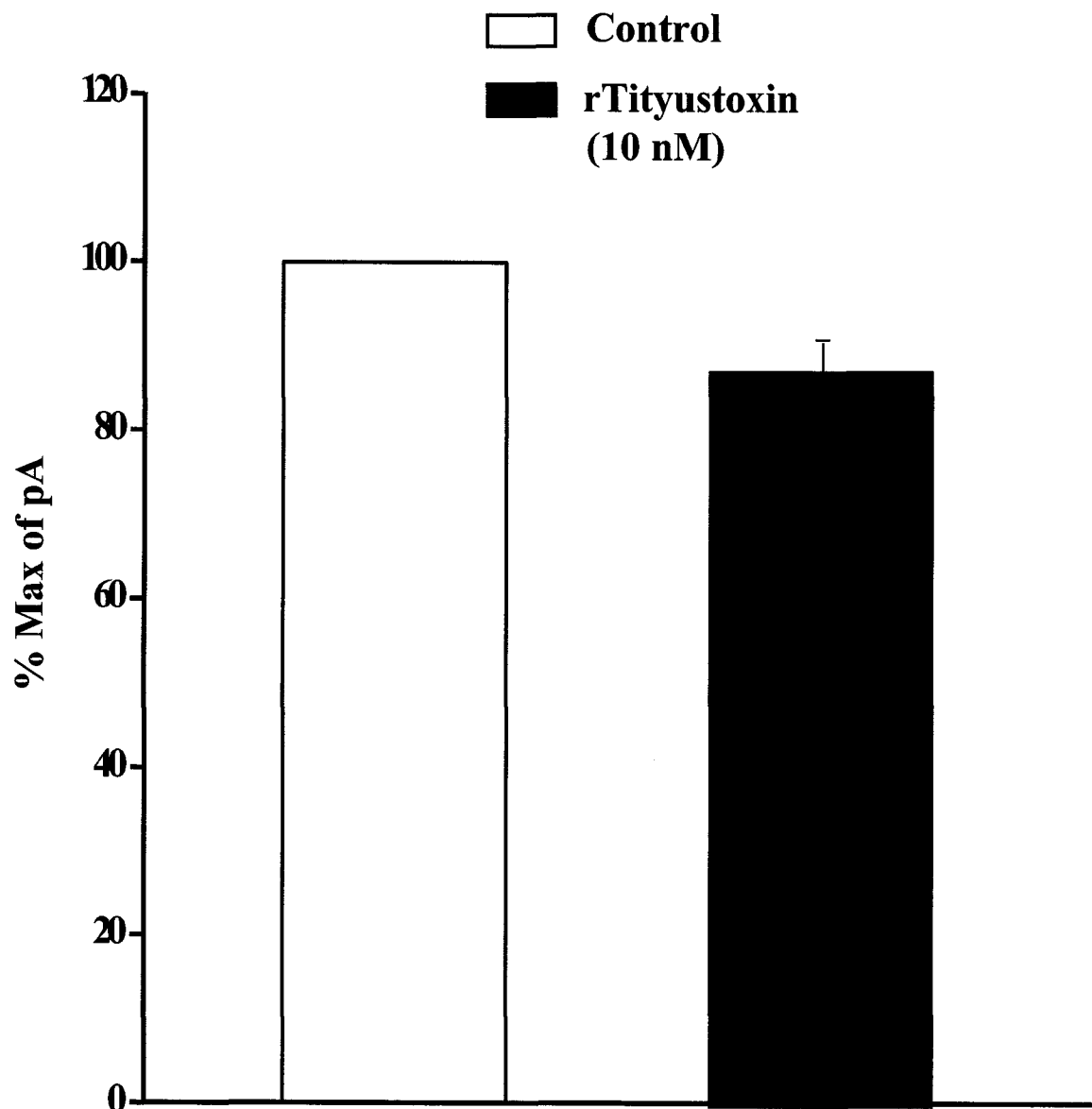


Figure 4.15: HOSK channel is not inhibited by Kv1.2 and Kv2.1 channel inhibitor, rityustoxin in transfected CHO cells. The bar represents mean \pm SEM

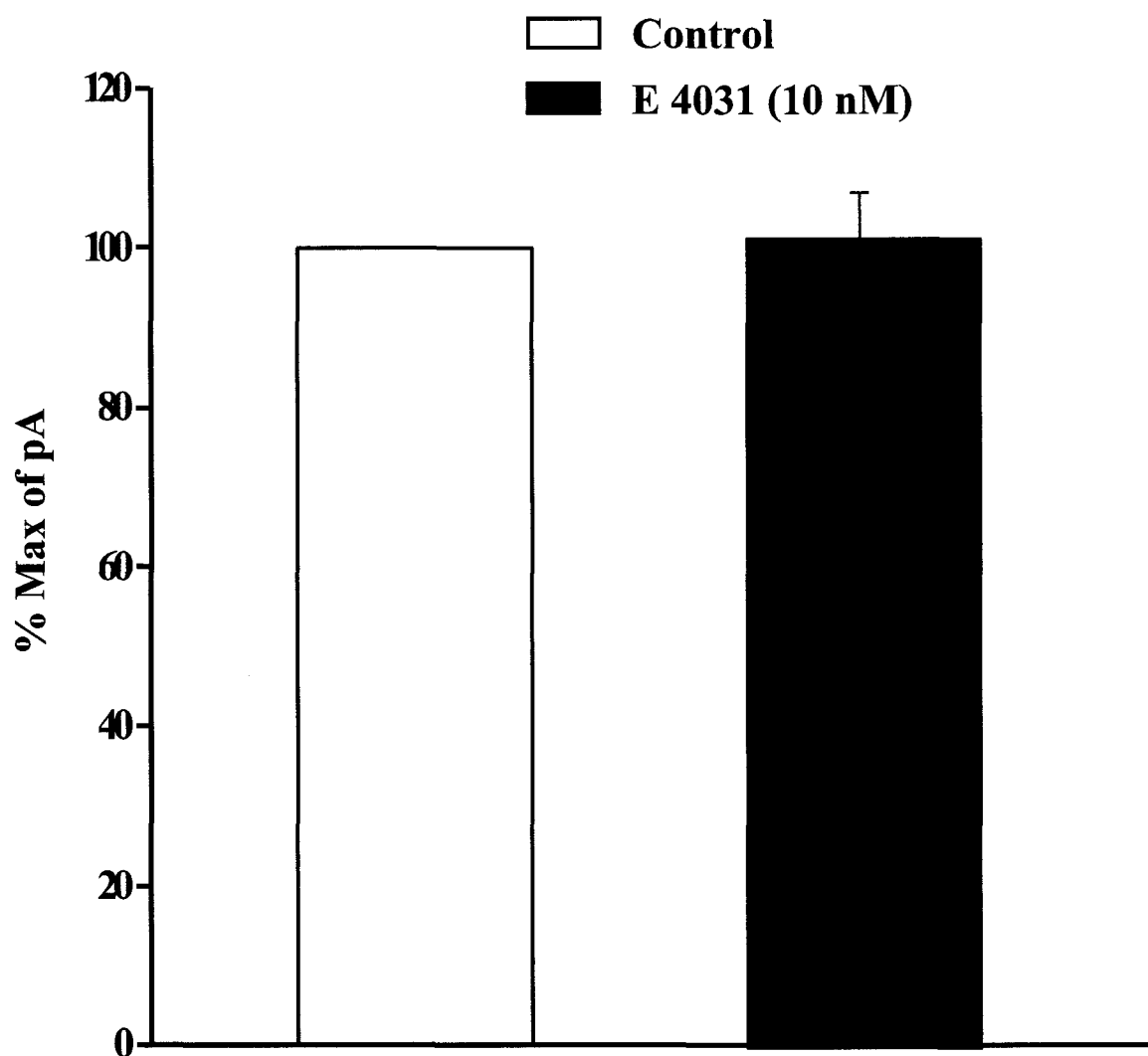


Figure 4.16: HOSK channel is not inhibited by Kv4.2 channel inhibitor, E 4031 in transfected CHO cells. The bar represents mean \pm SEM

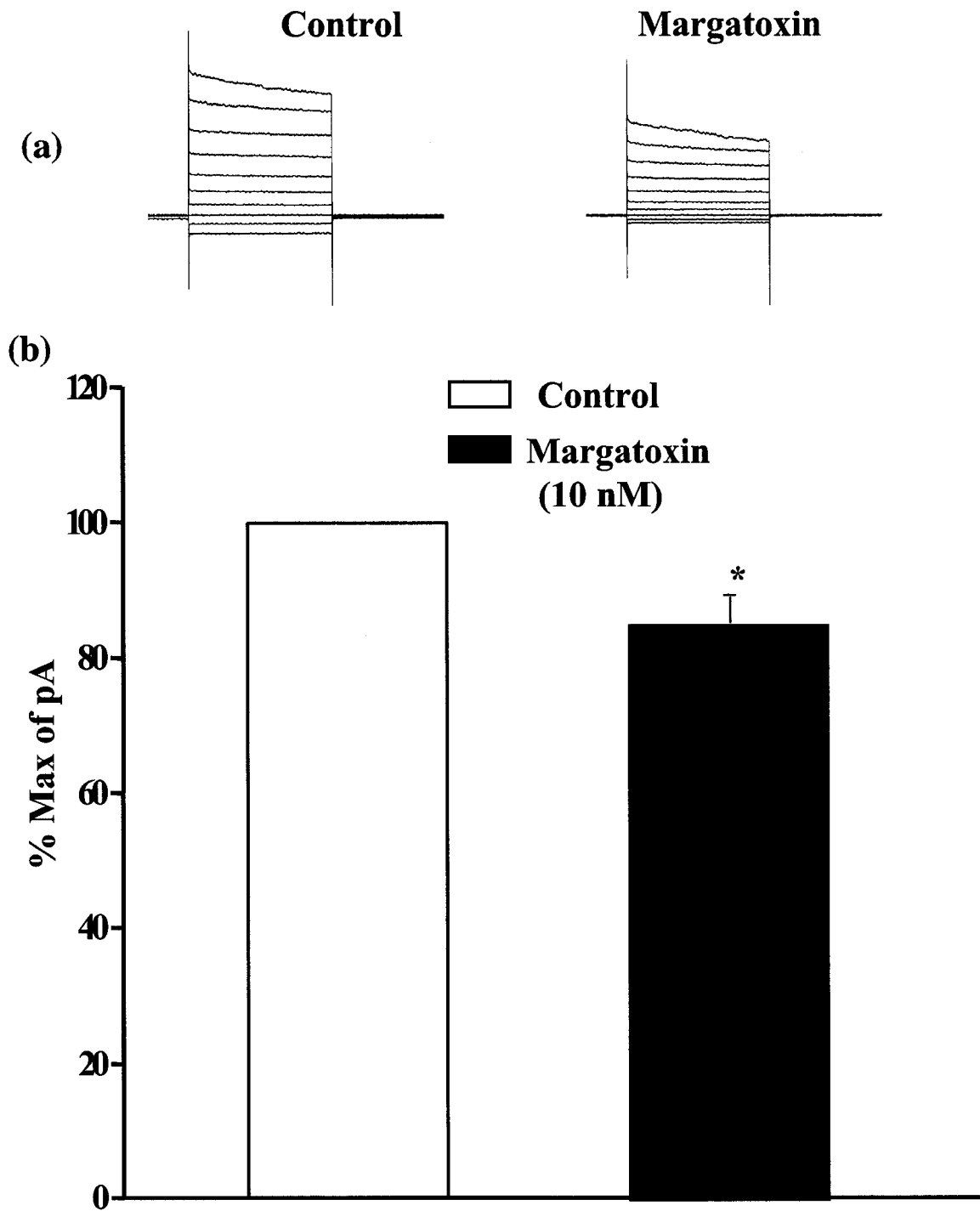


Figure 4.17: HOSK channel is sensitive to Kv1.3 channel inhibitor, margatoxin. (a) Representative trace and (b) Box plot showing margatoxin significantly inhibits the percent maximum current of HOSK transfected CHO cells. The bar represents mean \pm SEM

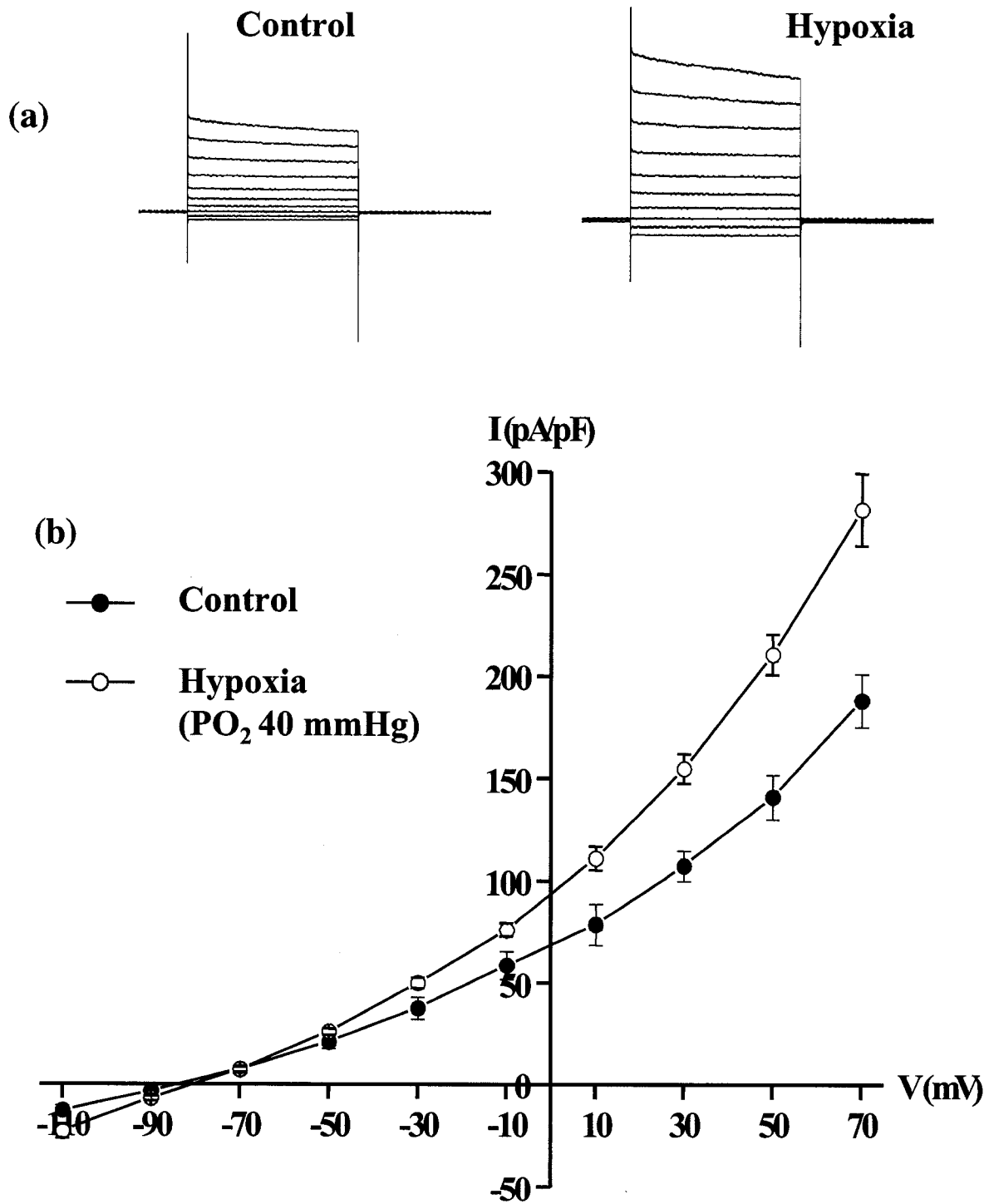


Figure 4.18: Current-voltage relationship of CHO cells transfected with HOSK show that HOSK current is activated by hypoxia. (a) Representative traces and (b) mean \pm SEM current-voltage (I-V) plots

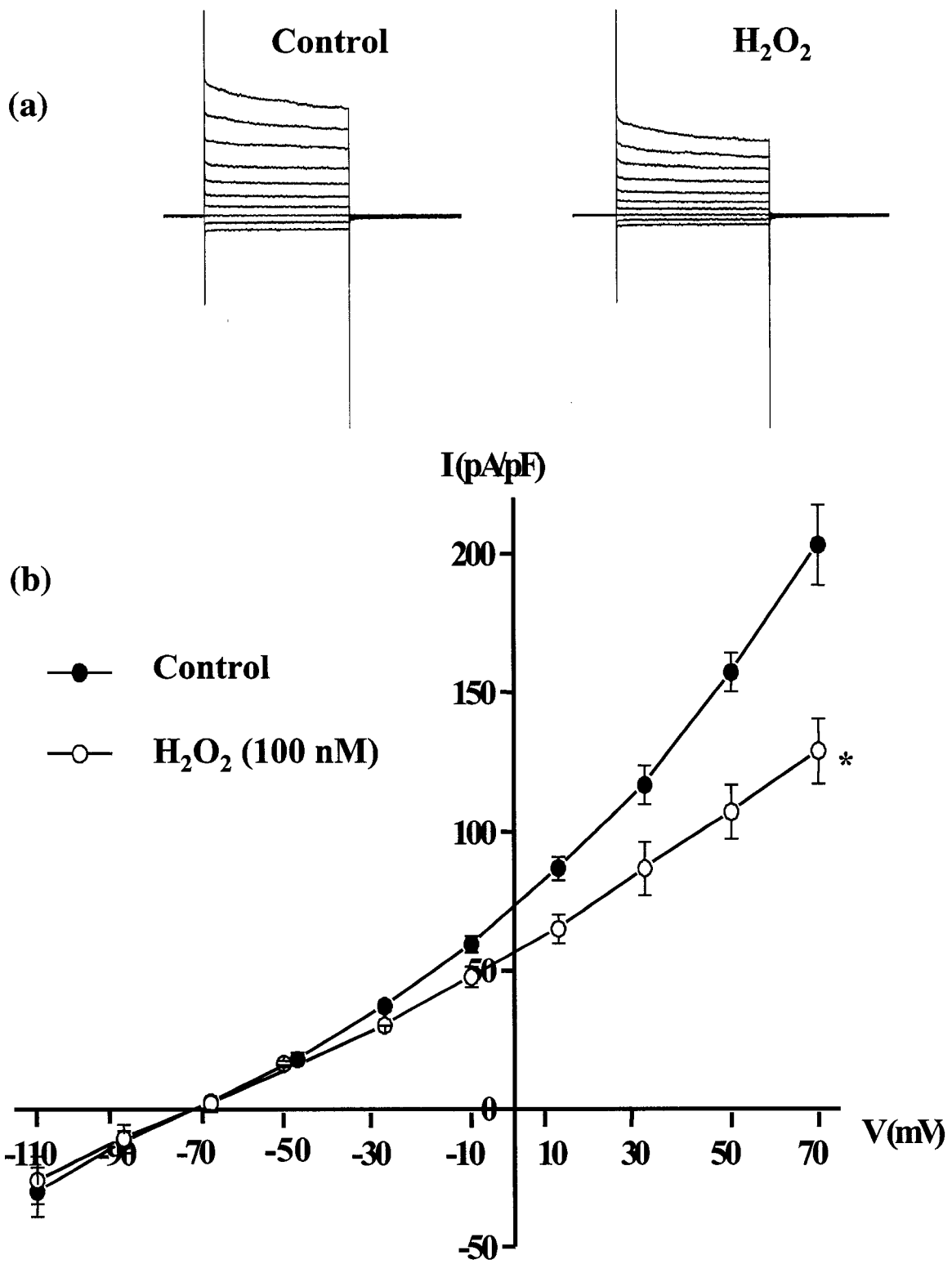


Figure 4.19: Current-voltage relationship of CHO cells transfected with HOSK show that HOSK current is inhibited by H_2O_2 . (a) Representative traces and (b) mean \pm SEM current-voltage (I-V) plots

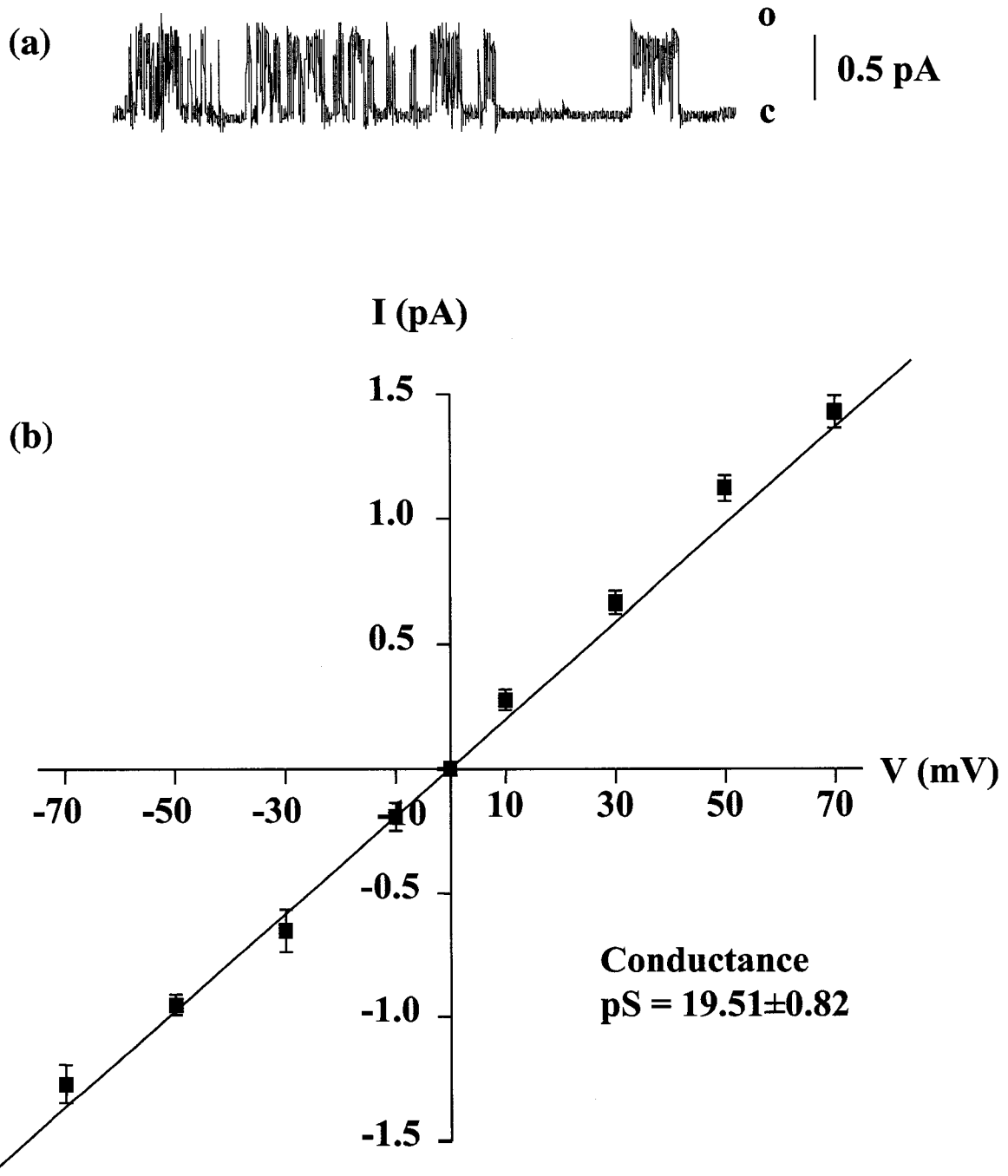


Figure 4.20: Single channel conductance by HOSK in the inside-out configuration. (a) Representative single channel recording demonstrating opening (o) and closing (c) of the 19.5 pS HOSK channel. (b) mean \pm SEM current-voltage (I-V) plots

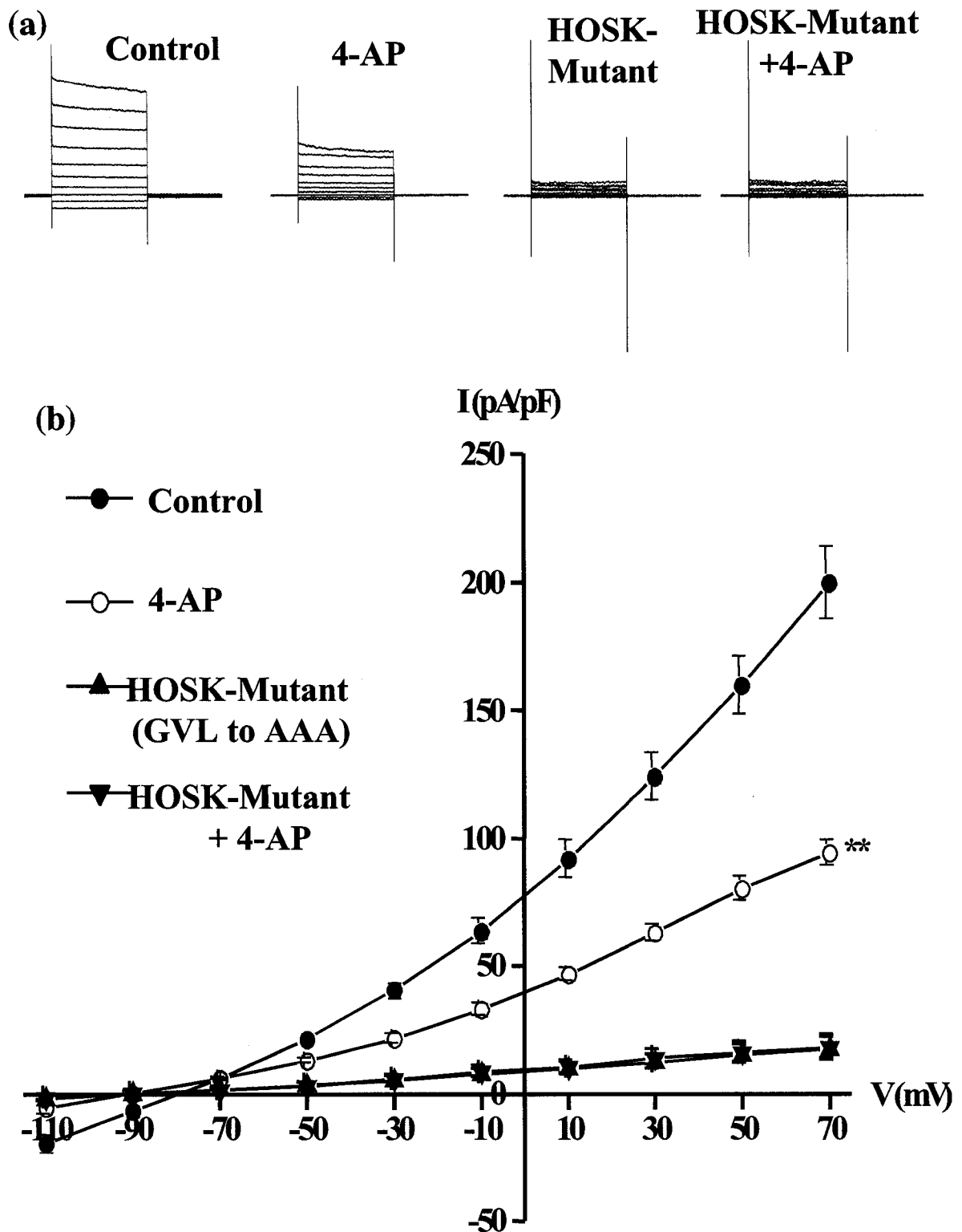


Figure 4.21: Mutagenesis of the HOSK pore (substitution of GVL with AAA) eliminates the voltage-dependent current and 4-aminopyridine sensitivity. (a) Representative traces and (b) mean \pm SEM current-voltage (I-V) plots

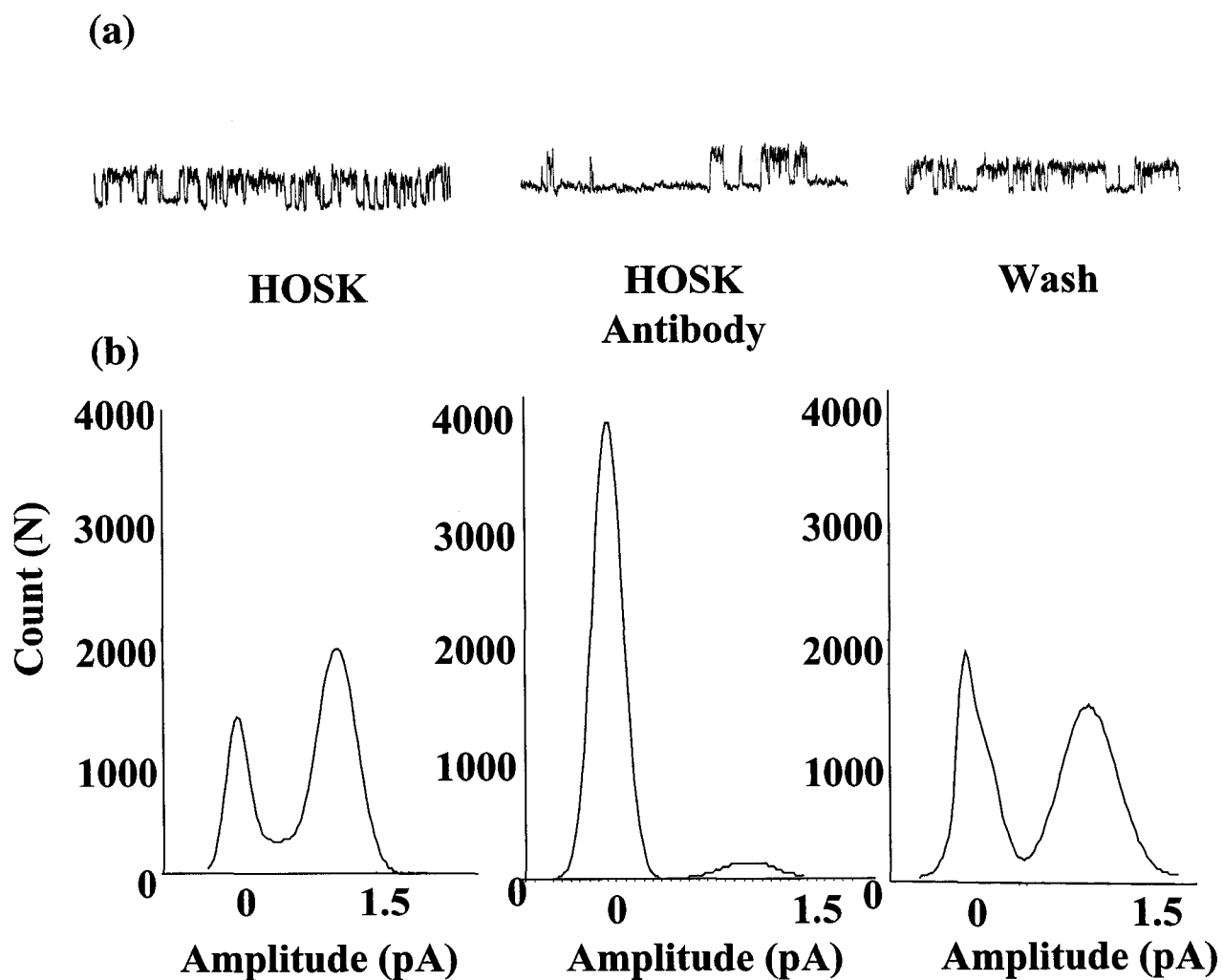


Figure 4.22: Immunoelectropharmacology was performed in HOSK expressing CHO cells. HOSK opening (at 1.5 pA amplitude) is reversibly inhibited by anti-HOSK antibody. (a) Representative traces and (b) the total number of channels in closed (0 pA) or in open configuration (1.5 pA).

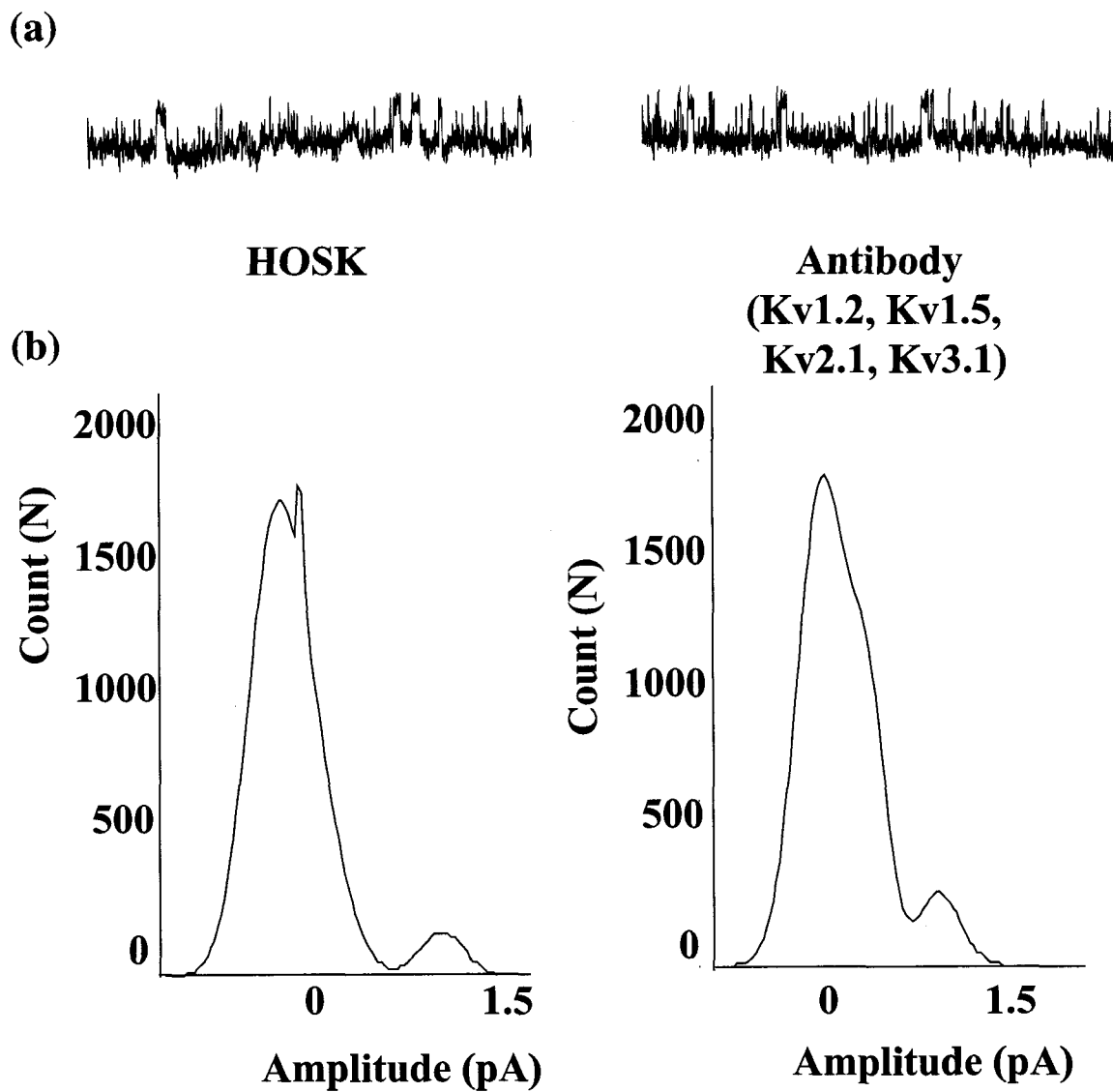


Figure 4.23: Immunoelectropharmacology was performed in HOSK expressing CHO cells. HOSK opening (at 1.5 pA amplitude) is unaffected by a cocktail of Kv antibodies. (a) Representative traces and (b) the total number of channels in closed (0 pA) or in open configuration (1.5 pA).

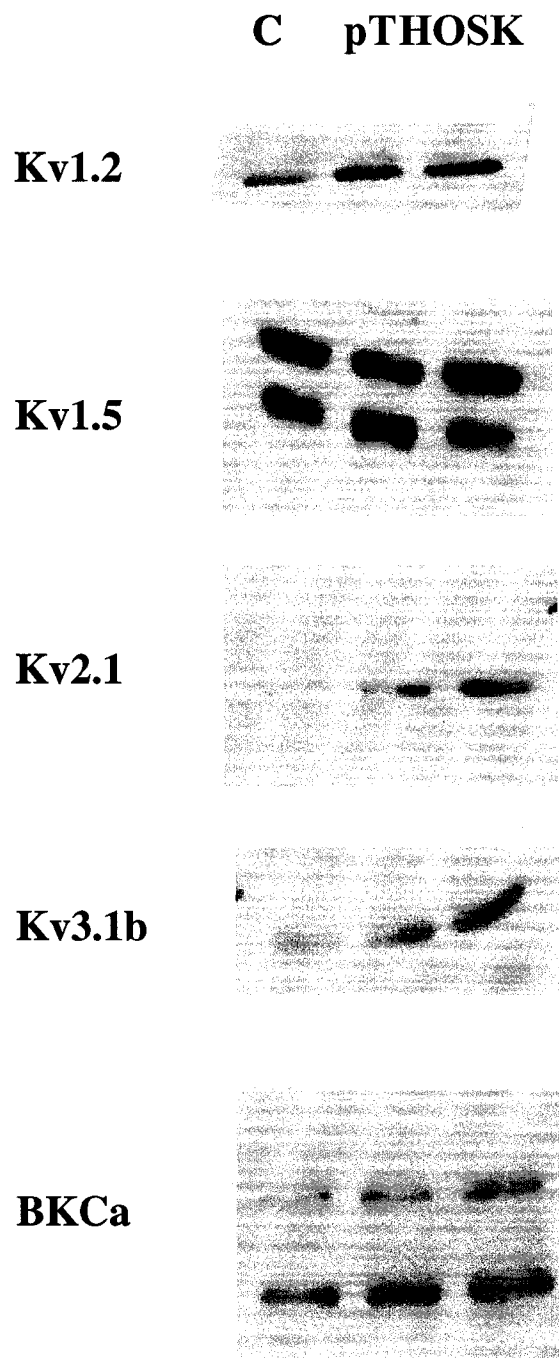


Figure 4.24: Immunoblot of various channels shows no change HOSK transfected CHO cells when compared to non-transfected CHO cells (C; control) and pTracer-CMVC transfected CHO cells in Kv1.2, Kv1.5 and big conductance calcium sensitive K⁺ channel (BKCa). However, slight increase in protein expression is evident in Kv2.1 and Kv3.1b channels.

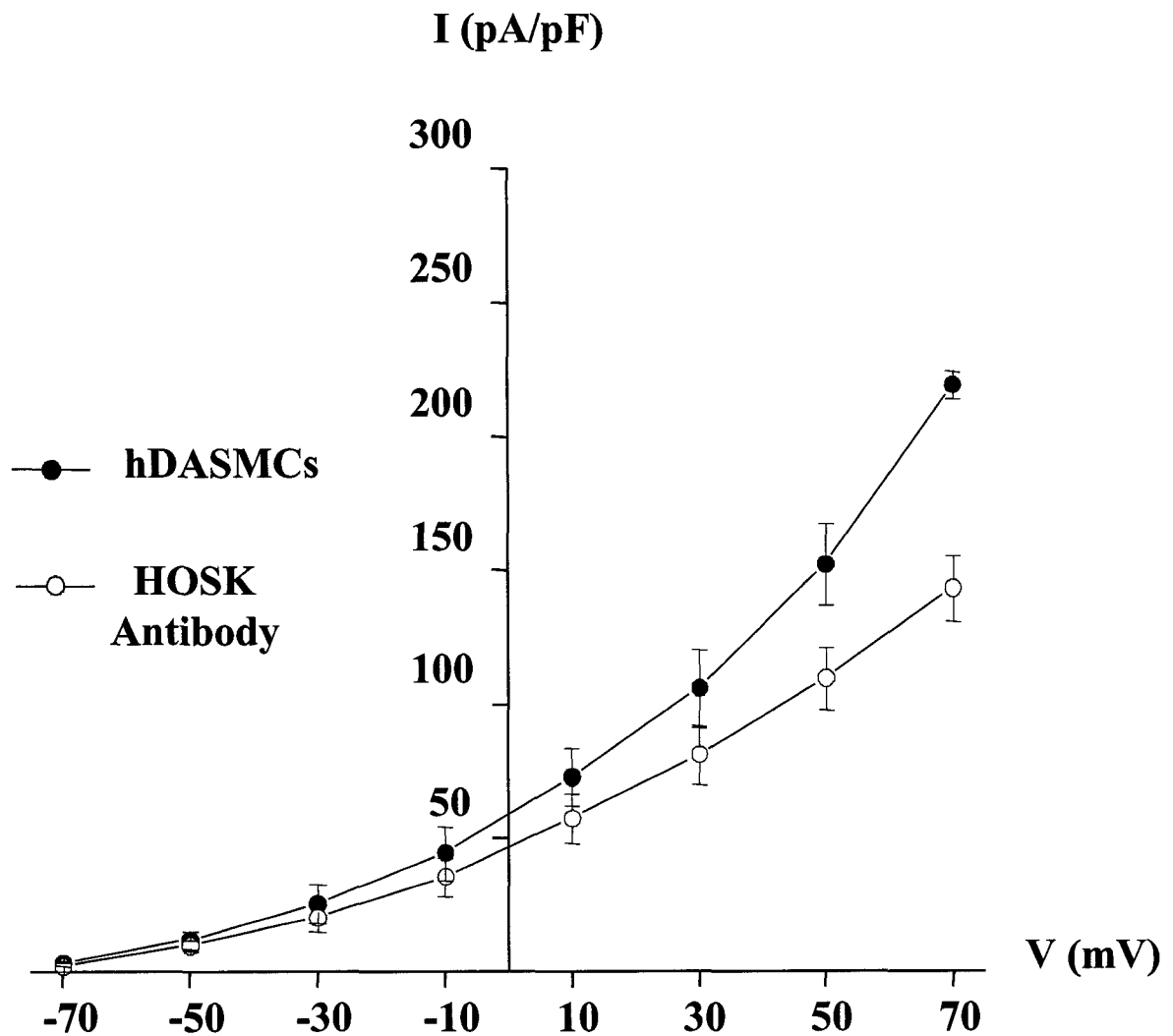
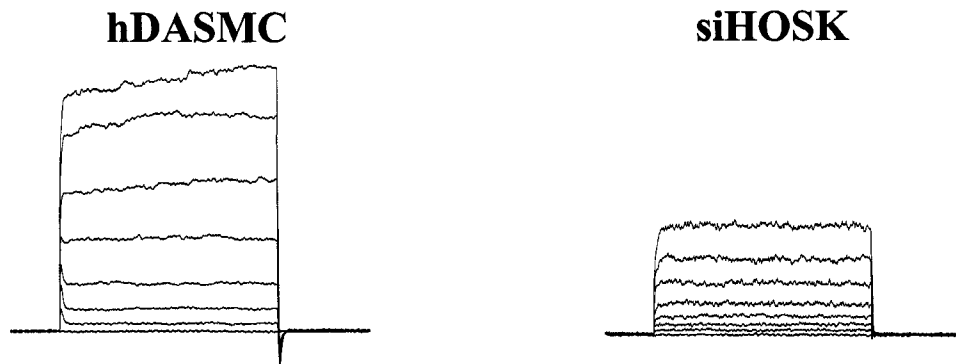


Figure 4.25: The HOSK antibody, when dialyzed into the DASMC via the patch pipette, inhibited K⁺ current, whereas the antibody preabsorbed with the antigenic peptide had no effect. The graph shows mean \pm SEM current-voltage (I-V) plot.

(a)



(b)

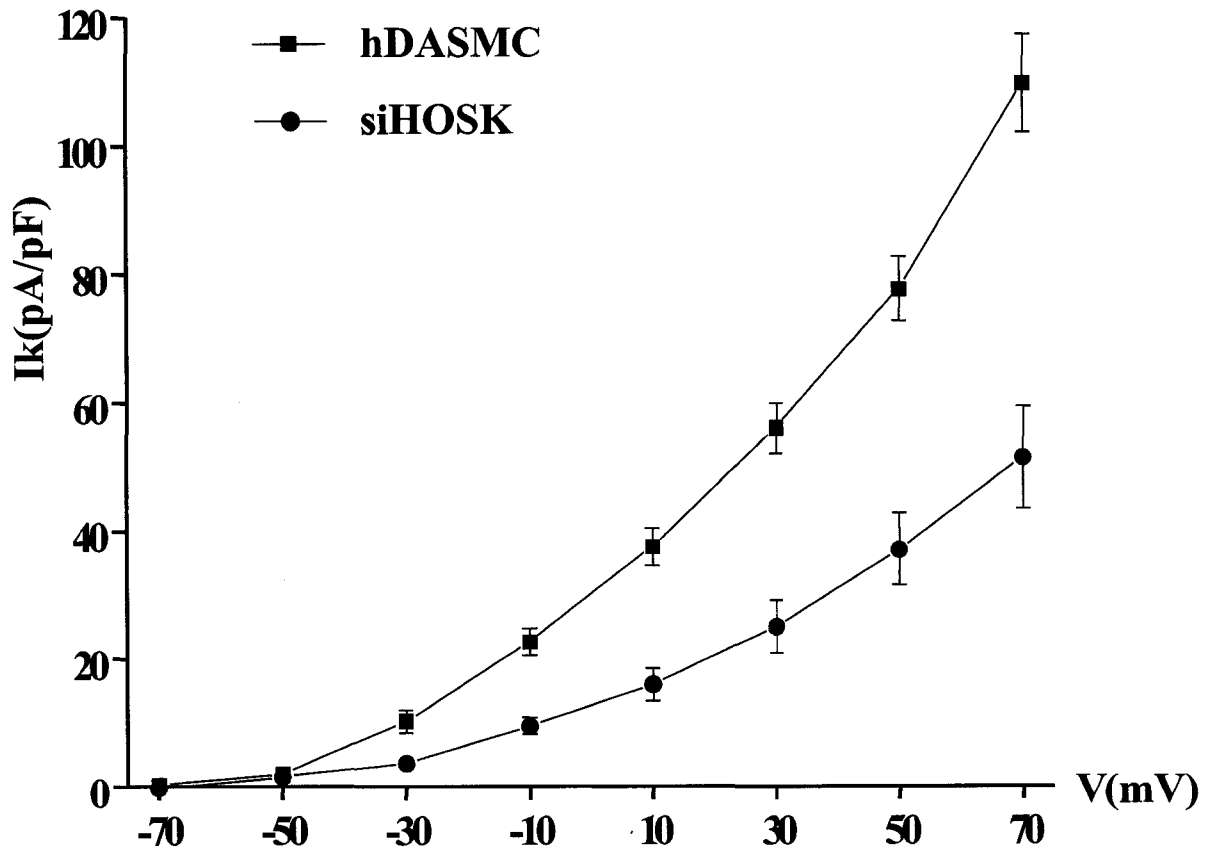


Figure 4.26: HOSK siRNA attenuates whole-cell K^+ current in hypoxic human DASMCs.(a) Representative trace and (b) is a graph showing mean \pm SEM in a current-voltage (I-V) plot.

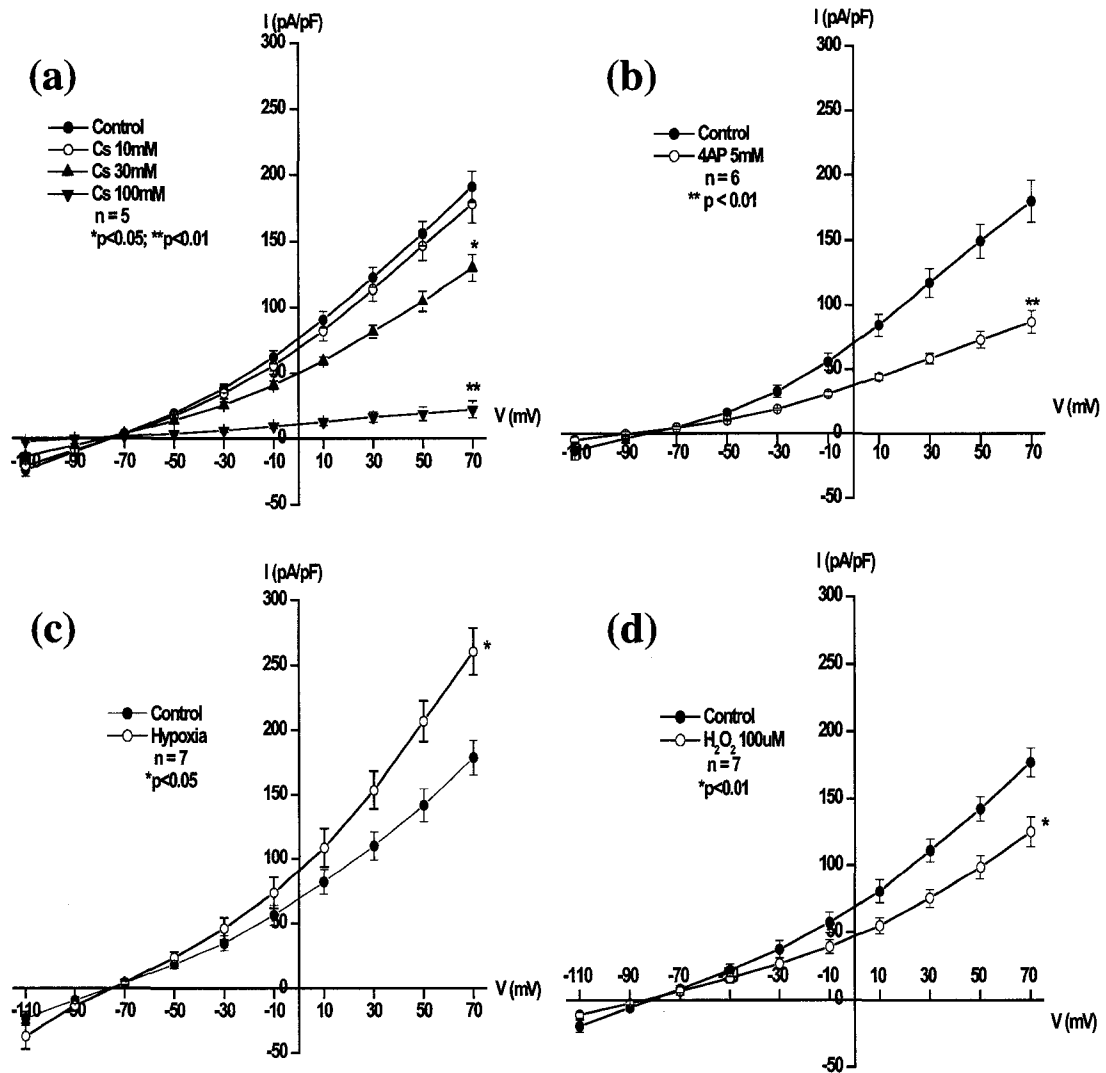
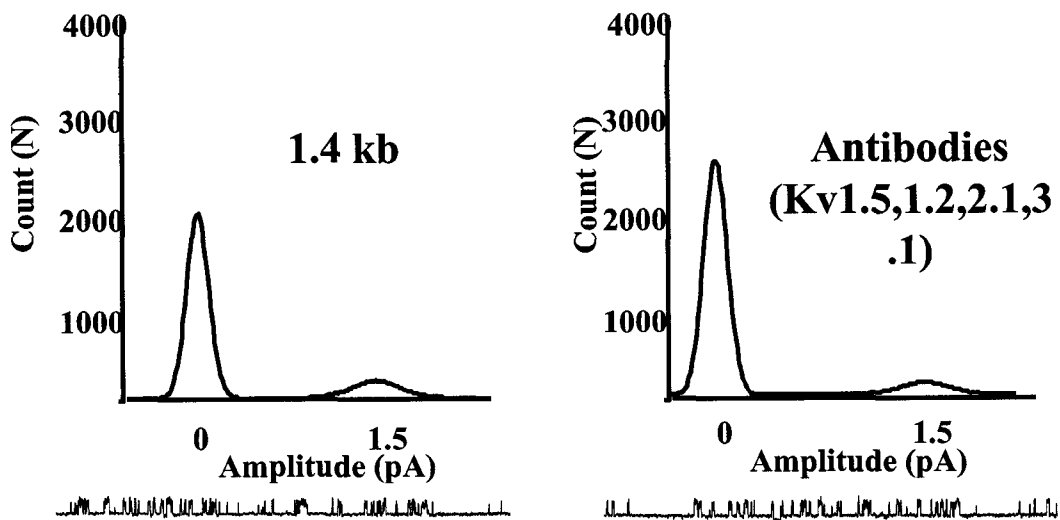


Figure 4.27: Transfection of pTracer-CMV carrying 1.4 kb fragment in CHO cells resulted in a current that was virtually identical to that created by expressing the EST clone. The 1.4kb product had current that showed (a) dose-dependent decrease of K⁺ current by extracellular cesium. (b) sensitivity to the Kv blocker 4-AP (c) activation by hypoxia and (d) inhibition by H₂O₂ (reminiscent of endogenous DASMC current)

(a)



(b)

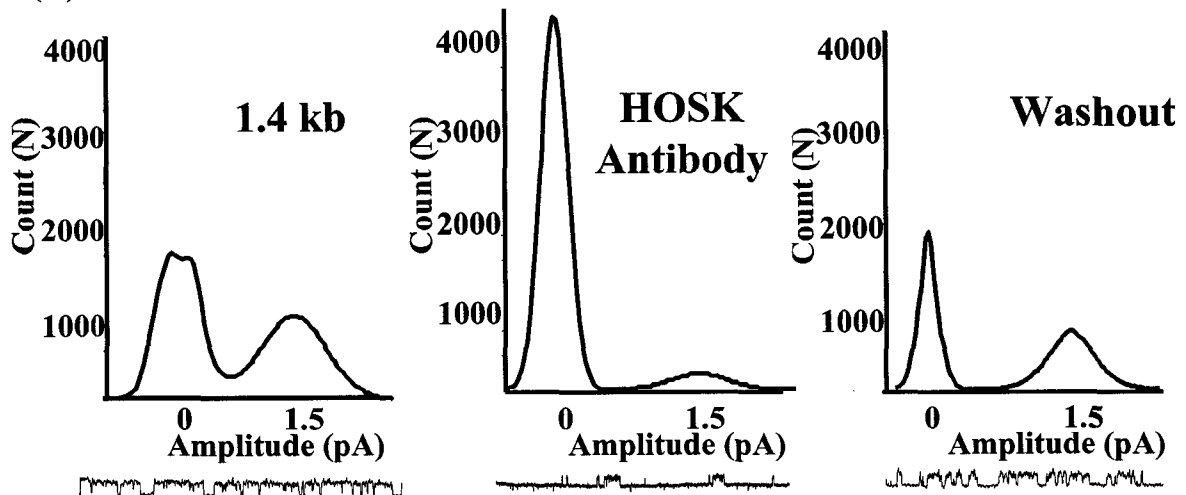


Figure 4.28: Immunoelectropharmacology was performed in 1.4 kb expressing CHO cells. (a) 1.4kb generated an openings (at 1.5 pA amplitude) are unaffected by a cocktail of Kv antibodies. (b) However, HOSK specific antibody reversibly inhibited 1.4 kb generated K^+ current. These findings are the same as for the EST expressing CHO cells.

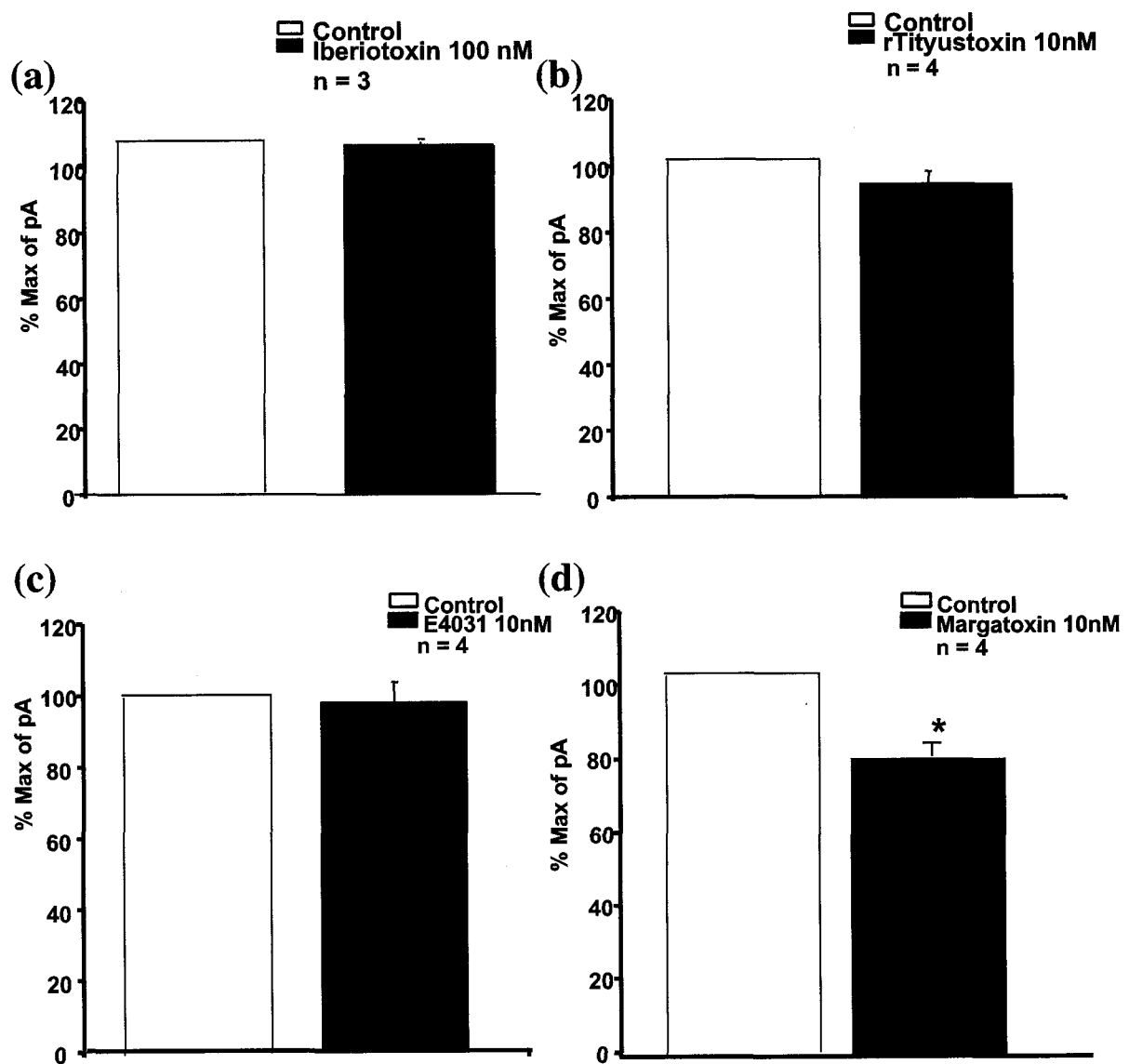


Figure 4.29: K⁺ current in HOSK Transfected CHO cells was not inhibited by (a) Iberiotoxin (IBTX), an inhibitor of big conductance calcium sensitive K⁺ channels (b) rTityustoxin, a Kv1.2 and Kv2.1 channel inhibitor or (c) the Kv4.2 channel inhibitor, E 4031. However, (d) Kv1.3 inhibitor, margatoxin, inhibited K⁺ current in HOSK transfected CHO cells by 20%..

5.1 INTRODUCTION

Potassium Channels mediate the hypoxic response of most specialized oxygen-sensitive tissues, including the ductus arteriosus, resistance pulmonary arteries, neuroepithelial bodies and the carotid body¹. Because K⁺ channels are the major determinants of membrane potential, they regulate the gating of other types of ion channels, notably the voltage-gated L-type calcium channel and establish the driving gradients for many ions². Through this indirect control of cytosolic calcium, K⁺ channels control activation of the contractile apparatus and thus vascular tone and regulate cell proliferation and activation of calcium-sensitive transcription factors (such as NFAT³). More recently it has been recognized that the direct control of cytosolic Ca²⁺ that K⁺ channels exert regulates vascular remodeling by regulating the activity of caspases and thus apoptosis⁴.

Although the DA and PA are contiguous, their response to O₂ is reversed. In the normal fetal state, hypoxia keeps the ductus dilated, while the PA constricts (a response that contributes to the high pulmonary vascular resistance of the fetal lung in utero and which mediates ventilation-perfusion matching during hypoxic pulmonary vasoconstriction, HPV⁵). At the moment of birth, the rise in PO₂ causes simultaneous DA constriction (Figure 1) and relaxation of the contiguous PA. Most of the Kv channel α -subunits that have been implicated in O₂ sensing are found in the VSMC in these two oxygen-sensitive arteries and the expression profile is similar in PA and DA SMCs⁶. The electrophysiological profile of the DASMC O₂-sensitive K⁺ current (an outward current that is rapidly activating, slowly inactivating) is 4-AP sensitive, iberiotoxin resistant, voltage-dependent and inhibited by hydrogen peroxide or oxygen⁶. Homo-or

heterotetramers of Kv1.5 or Kv2.1 account for some of the DASMC O₂-sensitive current. A maturational deficiency in these two channels in preterm DA appears to contribute to the high prevalence of patency and weak O₂ constriction, as demonstrated by the ability of Kv gene transfer to partially restore O₂ constriction to ionically remodeled human DA and preterm rabbit DA⁶. Despite the opposing effects of O₂ on vascular tone, Kv2.1 and Kv1.5 are also crucial to establishing E_M in PASMC and their inhibition leads to HPV⁷. However in PASMC, H₂O₂, like O₂ increase K⁺ current and hyperpolarizes the SMC. This suggests that the differential response of the tissues may relate *either* to differences in either the O₂ sensor or the unique occurrence of a new O₂ sensitive K⁺ channel in the ductus.

5.1.1 Hypothesis

Because there is evidence of a common redox sensor in both tissues (mitochondria generating reactive O₂ species, in proportion to PO₂ we hypothesized that the human DA expresses either a ductus-specific splice variant of Kv1.5 or a unique O₂-sensitive α -subunit. Therefore, polymerase chain reactions (PCR) were carried out to isolate Kv1.5 fragment from cDNA of several human DA, taken from neonates suffering from congenital heart defect and undergoing palliative surgical repair involving aortic arch.

We report the characterization of a novel human oxygen-sensitive K⁺ channel (HOSK), initially identified as a 1.4 kb fragment isolated from term human DA cDNA. Sequencing of this fragment and in silico analysis identified a 3.0 kb expressed sequence tag isolated from the dorsal root ganglia of a 36-year old adult male. Subsequent rapid amplification of 5' cDNA ends from human DA produced a presumed full-length

transcript that we cloned into a mammalian expression plasmid with a green fluorescent protein reporter (GFP).

5.1.2 Biophysical characterization of the HOSK channel

Transfection of HOSK into the Chinese Hamster Ovary (CHO) or Monkey Kidney (COS) cells, which normally have only an endogenous ohmic current, generates a voltage-dependent outward current (figure 2a and b). To assess whether this HOSK current was a typical K^+ channel current, we assessed its reversal potential and also performed ionic substitution experiments. Heterologously expressed HOSK displays a typical K^+ channel reversal potential of 0 mV in symmetrical 140mM K^+ configuration. HOSK's ionic selectivity profile ($Rb > K >> Cs > Na$) is also typical of a K^+ channel (Figures 2c-d), as is HOSK's inhibition by extracellular cesium chloride (Figure 2e). Both the 3.0 kb EST-derived cDNA and the originally isolated 1.4kb cDNA yielded similar Kv currents in CHO cells (Figure 7, 11, 14-20, 24, 28-30 in chapter 4).

To further characterize the HOSK channel, the activation kinetics and tail currents were measured. HOSK demonstrated $V_{1/2}$ activation of -7.1 ± 2.0 mV and $V_{1/2}$ inactivation at -18.9 ± 1.4 mV (Figure 2f), values that are within the range of typical Kv channels⁸. Two Kv channel blockers inhibit heterologous HOSK current (4-aminopyridine, a Kv channel inhibitor; correolide, a Kv1.x inhibitor, Figure 2g). HOSK's response to correolide is reminiscent of certain Shaker channels⁹.

Single channel recordings, made in the inside-out configuration in symmetrical 140mM potassium, showed that HOSK has a mean conductance of 19.5 ± 0.82 pS (Figure 3b), consistent with conductances of other known Kv channels (range from 4-70 pS⁸).

5.1.3 Oxygen sensitivity of HOSK channel

Hypoxia increases and oxygen decreases HOSK current in CHO cells. Like oxygen, exogenous hydrogen peroxide (100 μ M), the putative diffusible redox mediator involved in O₂-induced DA constriction¹⁰, inhibits HOSK current (Figure 3a). The response of heterologously expressed HOSK to hypoxia and H₂O₂ are consistent with the effects of these redox stimuli on whole cell K⁺ current in freshly-isolated human DASMC¹⁰. HOSK is active at very negative membrane potentials (i.e. -70mV; Figure 2b, d, e and f), demonstrating its potential to contribute to the resting membrane potential such that inhibition of HOSK by oxygen could serve as the initial trigger for DASMC depolarization and vasoconstriction⁵.

To prove that the single-channel activity identified in HOSK transfected CHO cells was due to HOSK, we used appropriate controls of nontransfected CHO cells and CHO cells transfected with an empty plasmid with a GFP reporter. We also used a HOSK antibody to perform immunoelectropharmacology, a technique we have previously validated⁹. Transfected CHO cells were selected for patch clamp study if they fluoresced green, indicating that they had been transfected and expressed GFP protein. Sham transfected and GFP only transfected CHO cells showed no Kv current and had minimal single channel activity. HOSK antibodies (1:250 dilution) applied to the single channel patch decreased HOSK open probability. Channel opening recovered after the washout of antibodies suggesting the antibody blocked the channel pore. Moreover, incubation of the HOSK-expressing patch with cocktail of Kv channel antibodies directed against other O₂-

sensitive Kv channels found in human DASMC (Kv1.5, Kv2.1, Kv 3.1 and BKCa) had no effect on channel open probability (Figure 3d).

5.1.4 Identification of HOSK's Pore

To establish whether the sequence that we identified as HOSK's pore (based on in silico analysis) was indeed GVL, we used site-directed mutagenesis to create an AAA substitution. Voltage-clamp of mutated channel showed that although the GFP reporter was expressed, no Kv current was generated; only the basal ohmic current characteristic of non-transfected CHO cells (Figure 3c). This is consistent with our hypothesis that GVL is the potential K⁺ filter sequence for HOSK.

The novelty of HOSK's filter sequence (from GYG to GVL) is not without precedence. Channels such as Erg, Kv6.1 and TASK family members (which like HOSK have 4-transmembrane domains) use variations of the GYG domain such as GFG or GLG¹¹. Furthermore, substitution of GYG with GVG maintains K⁺ selectivity¹². Recently, a subunit named KCNK7 has been cloned which employs GLE as its selectivity filter (although it requires another unidentified subunit to form a functional channel)¹³. Furthermore, various prokaryotes have alternative K⁺ recognition site. For example, *Thermotoga maritime* uses GYSI as a K⁺ filter sequence¹⁴. Likewise, both *Sulfolobus solfataricus* and *Sulfolobus tokodaii*, encode potassium channels with putative pore sequences of GLYS and GLYA, respectively^{15, 16}. Other species with variant filter sequences include a GFQE in *Desulfovibrio desulfuricans* and a GFKE in *Geobacter metallireducens*, an underground bacterium associated with iron corrosion. *Synechocystis* sp. PCC6803, a fresh water cyanobacterium utilizes GYSD, whilst a GYQE pore

sequence is found in *Magnetococcus* sp. MC-1¹⁷.

5.1.5 Is endogenous HOSK active in human DASMCM?

To establish the physiological role of HOSK in human DASMCMs, immunoelectropharmacology was performed⁷. HOSK antibody, when dialyzed into the DASMCM via the patch pipette, inhibited whole-cell K⁺ current (Figure 3e). Furthermore, siRNA designed against the HOSK channel inhibited the human DASMCM's K⁺ current (Figure 3f). Thus, endogenous HOSK active in human DASMCM.

5.1.6 In silico modeling of HOSK structure

The cDNA of HOSK encodes a putative 169 amino acid protein (Figure 4a), with four hydrophobic domains. The voltage sensor of HOSK is characterized by a set of 4 basic residues, with each third residue being the arginine or lysine (Figure 4a and c). This arrangement of basic residues at every third position of a transmembrane helix is also found in the S4 (the voltage sensing) region of Kv channels.

The HOSK gene is located on chromosome 7, as confirmed by fluorescence in-situ hybridization (FISH) (Figure 4d). Surprisingly, the cDNA sequence of HOSK is 100% identical with a region of the mRNA encoding collagen α 2(I). However HOSK has an alternative translational start site and the resultant largest open reading frame (ORF) of the collagen α 2(I) transcript produces HOSK channel making this protein derived from a "gene within a gene". Northern blot analysis performed on a panel of human tissues, using the 1.4 kb HOSK and collagen α 2(I) (COL1A2) cDNA as a probe, identified two transcripts in human DA, DASMCMs, and placenta (Figure 5a). However, the other human

tissues/cells examined only contained either one transcript or no transcript at all (brain and white blood cells). Moreover, incubation of human DASMCs for 48 hrs at PO₂ 120mmHg decreased HOSK transcript levels, signifying the oxygen-sensitive regulation of transcript expression (Figure 5a).

Our finding of a Kv gene within a gene is consistent with the discovery that the genome contains almost 800 overlapping genes¹⁸ of which ~100 are present on chromosome 7¹⁹. In fact region of 7q21-22 (where the collagen and HOSK genes are located) is a hotspot for overlapping genes, as determined by NCBI BLAST-2-Seq¹⁹.

There is precedent for the notion that alternative splicing of COL1A2 generates a transcript that does not code for the collagen; having been noted in chickens²⁰⁻²² and humans²³. Instead these authors suggested that alternative splicing COL1A2 acts as a template for the production of at least one protein other than collagen²⁰⁻²². We postulate that HOSK results from internal translation of alternative splicing COL1A2 (Figure 5e). We suggest that this alternative transcript acts as a template for the HOSK synthesis. Indeed, in silico analysis showed presence of 4 internal ribosomal entry sites (IRES²⁴) upstream of the HOSK channel. Furthermore, in human DASMC and in HOSK-transfected CHO cells, no COL1A2 protein was detected (Figure 5c). In addition, alternative splicing COL1A2 was expressed in early stages of embryogenesis in neuroectodermal-derived tissues²⁵, at a time and in a location where collagen expression would be unlikely. Subsequent to the electrophysiological analysis, in silico extension of 5' region of HOSK channel showed an upstream start codon in frame with the translation of HOSK channel. However, the fact that anti-HOSK antibodies and siRNA against

HOSK resulted in attenuated K^+ current suggests that crux of the channel activity lies in the analyzed HOSK sequence.

To verify that HOSK transcript produces the proposed protein sequence, HOSK protein was isolated from transfected CHO cells and SELDI-TOF MS was performed. HOSK capture on protein chip was enhanced using adherent beads coated with HOSK antibody, resulted in a singular peak of 21.3 kDa. Analysis of MS spectrum, after on-chip tryptic digestion, did not correspond to any known protein in the ProFound database, suggesting HOSK is a new protein (Figure 5d).

The HOSK protein is unique and is not homologous to known K^+ channels or other ion channels. However, in silico sequence alignments show significant homology of HOSK across mammalian species, when the COL1A2 cDNA sequence is read in frame to create the HOSK protein. The analysis shows 84-95% similarity in pairwise comparison in predicted protein sequence amongst mammalian species; however, both *Xenopus* and zebrafish, which are non-amniotic species, lack HOSK (manifesting only 30-42% similarity, as assessed by in silico sequence alignment studies; Figure 4f). Furthermore, functionally important elements of HOSK (the voltage sensing basic residues and the GVL putative pore sequence) are absent from the two non-amniotic organisms. A nucleotide BLAST search across genomic sequence indicates that HOSK first appears in vertebrates, with *Danio rerio* being the most ancient divergence; whereas we found no match for HOSK in *Ciona intestinalis*, which is a non-vertebrate chordate. Since the alignment doesn't show significant similarity with any other channels, and the phylogenetic tree doesn't group with any other family, we conclude that HOSK is a novel K^+ channel.

5.2 HOSK AS A NEW TYPE OF K⁺ CHANNEL

5.2.1 Similarities and differences with other K⁺ channels

Although HOSK is a new type of K^v channel, it displays structural and functional properties reminiscent of K^v channels. Looking at the structure closely one can appreciate that HOSK has multiple transmembrane domains, a re-entrant loop that signifies the pore structure and voltage-sensing domain comparable to other K^v channels.

To achieve the diverse functions that K⁺ channel mediate (cell volume regulation, hormone secretion, and electrical impulse formation in electrically excitable cells²⁶), using only ion conduction, K⁺ channel needs a universal configuration of pore region that can not only be highly selective to K⁺ ions but also conduct K⁺ ion at near diffusion rate. Each subunit contains at least two fully transmembrane α -helices and a pore that runs half way through the membrane, pointing its C-terminal negative end-charge toward the ion pathway. Near the midpoint of the membrane the ion pathway is nearly 10 Å in diameter, forming a central water-filled cavity. By allowing the K⁺ ion to remain hydrated at the membrane center, and by directing the C-terminal negative end-charge of α -helices toward the ion pathway, a K⁺ ion is stabilized at the membrane center²⁷. This orientation is important as the funnel structure created by the pore enables the K⁺ ion to strip off its hydration shell, progressively and concomitantly stabilized by the carbonyl groups of the residues constituting the pore²⁸. Therefore, it is essential that a K⁺ channel has a re-entrant loop, which by virtue of tetramerization or dimerization (in K₂P channels) forms this inverted teepee structure (Figure 6).

HOSK channel, as suggested by the hydrophobicity plot, forms a re-entrant loop (Figure 2 in chapter 3). Since, this loop is a signature structure of K⁺ ion conductivity, we postulate that HOSK follows a similar conduction reaction, like other Kv channels. Since each subunit has one pore, we suggest that HOSK form a tetramer that enables the loop region of HOSK to combine and provide necessary conical structure that will enable the HOSK channel to select and subsequently pass K⁺ ions with high specificity and conductivity. These features, if confirmed by crystallography, would make HOSK quite like other K⁺ channels, despite its novel sequence and encoding mechanism.

5.2.2 The HOSK voltage sensor

Some kinship between HOSK and other Kv channels is evident in the voltage-sensing domain. The voltage-gated channels have a common domain of six helical transmembrane segments (S1–S6). The fourth segment, S4, has a symmetrical arrangement of charged residues, with each third residue being arginine or lysine (figure, 4a). This S4 sequence motif, a basic residue at every third position, followed by two hydrophobic residues in a sequence with 4–8 repeats, is conserved across a large superfamily of voltage-gated channels. Movement of the basic residues generates the gating current. Wild-type Shaker channels displace 3.2–3.4 charges per subunit as the channel gates from the resting to the activated state²⁹⁻³¹. Neutralizations of the S2/S3 negative charges and S4-positive charges have identified the residues that carry the gating charge. Studies from the MacKinnon and Bezanilla labs showed that charge neutralizations reduce the gating charge and that S4 carries most of it^{29, 31}. In one study neutralization of arginine (R)-R2, R3, R4, and lysine (K)-K5 reduced the gating charge by 1.2, 1.7, 1.5,

and 1.4 charges per subunit³¹; in the other study neutralization of R1, R2, R3, R4, and K5 reduced gating charge by 1, 1, 1, 1, and 0.5 per subunit²⁹. Both studies found a contribution for K5, the fifth charge, although the gating charge associated with this residue was less critical. In support of these observations, a histidine substituted for R2, R3, or R4 transports a proton across the membrane^{32, 33}. Together, the three studies lead to the conclusion that the majority of the gating charge is carried by R1-R4.

However, the residues between the positive charges also play a distinct role in gating. Scanning perturbation analysis of various channels have shown that S4 contains a high impact positive charge (+), followed by a high-impact hydrophobic residue (X1) and a low-impact hydrophobic residue (X2)^{34, 35}. High impact residues are thought to lie at a protein-protein interface, where their mutation can disrupt protein packing and thus impact gating. Low impact residues are thought to face lipid or water. Within the short length of the gating canal, the low impact residues would lie on one face of an α -helix and face lipid³⁴. Thus, the repeat [+ , X1, X2...] act as a building blocks for the voltage-sensing domain.

The HOSK channel has such a segment with repeats of +, X1, X2, created by four basic, positively-charged residues interspaced with 2 non-cationic amino acids (+ is an arginine or lysine and X₁; in HOSK its always a valine). Since previous studies have suggested that four residue are sufficient for sensing voltage, thus the 4 repeats in HOSK are theoretically sufficient to account for its voltage-sensing. This suggests that HOSK's putative voltage-sensing domain is a variant of the sensor in other known Kv channels but one which follows the common rules that allow voltage sensing. Hence, the HOSK channel, like other Kv channels utilizes the same sequence motif for voltage-sensing. By

extension, the movement of voltage-sensing domain of the HOSK channel might follow a similar behaviour as other Kv channels. Currently the movement of voltage-sensing domain is a subject of much debate in literature, as we discussed in Chapter 1³⁶.

As mentioned previously, HOSK is sensitive to correolide and marginally sensitive to margatoxin. It is intriguing that while HOSK and Kv sequences do not align, the amino acid residues that are instrumental in binding correolide in Kv channels are also present in the expected locations in HOSK channels, signifying the presence of a common mechanism of binding correolide between HOSK and other Kv channels^{37, 38}. This is analogous to HOSK's variant but "rule compliant" voltage sensor. However, HOSK is insensitive to tityustoxin, iberiotoxin and E4031. Collectively, this suggests that HOSK sensitivity is similar to Kv1.x family. While, the some of the structural features and most of the electrophysiological and pharmacological properties ties HOSK and Kv channels in one class, fundamental differences exist in other structural areas.

One feature that separates HOSK from rest of the K⁺ channels is the presence of GVL as its K⁺ ion filter sequence. This feature alone makes the HOSK channel unique. The novelty of HOSK's structure is not totally without precedent. Variations in the conserved pore sequence GYG are known. As mentioned before numerous prokaryotes and eukaryotes carry K⁺ channel pore sequence different from the conventional GYG or GFG^{11, 12, 13, 14, 15, 16, 17}.

Moreover it is not surprising there are also important variations in the number of transmembrane domains amongst K⁺ channels. While the Kir channels have two transmembrane domains and the Kv channels six transmembrane domains, there have been K⁺ channels isolated that have 8 and 12 transmembrane domains^{17, 39}. The most

recently discovered K⁺ channels, the TASK family of two-pore K⁺ channels, have 4 transmembrane domains⁴⁰, like HOSK. However, unlike HOSK, the TASK channels have two-pores and physiological and pharmacological profiles are quite distinct from HOSK. HOSK belongs to its own class in this regard; it is a prototype for K⁺ channels with four transmembrane domains but only one pore. If confirmed by others the K⁺ channel nomenclature will need to be modified to add HOSK class channels.

HOSK also shows sensitivity in oxygen that differs from most of the O₂ sensitive K_v channels. Homomeric and heteromeric recombinant K_v channel subunits include K_v1.2, K_v1.5, K_v2.1, K_v3.1b and K_v2.1/ K_v9.3 channels⁴¹ can form “O₂-sensitive” channels. In pulmonary artery SMC, hypoxia rapidly and reversibly inhibits the K_v channels that maintain the resting membrane potential of the oxygen-sensitive tissue. This is in direct contrast to the activity of HOSK channel which shows increased conduction during hypoxic conditions.

5.3 PHYSIOLOGICAL IMPLICATIONS OF HOSK

5.3.1 Closure of DA during pregnancy

The DA is a fetal artery that connects pulmonary artery to aorta thereby shunting the right ventricular blood to the systemic vasculature bypassing the non-ventilated lungs (Figure 1 in chapter 4). At birth, increased PO₂ initiates O₂-induced sequelae which causes functional closure (in few minutes) followed by anatomical obliteration of DA (over a few days)⁴²⁻⁴⁴. The response of the term DA to O₂ rarely fails however in preterm human DAs, particularly small infants <1800 g, patent DA occurs with a prevalence of ~

50%, despite adequate oxygenation⁴². Although the cause of patent DA is multifactorial, failure of initial O₂ constriction appears to play a role and the core of the constrictor mechanism exists in DASMCs, as studies have shown that O₂-induced vasoconstriction persists in denuded DA vessels. Although crucial role of endothelium-derived relaxing (NO⁴⁵ and prostacyclin^{42, 46, 47}) and constricting (endothelin)⁴⁸⁻⁵¹ factors in regulating DA tone is well established, these factors play more of a modulating role. The key mechanistic factor involved in O₂-induced vasoconstriction of DA is voltage-gated K⁺ (K_v) channels^{6,10}.

Studies done by our laboratory and others have delineated a putative pathway of O₂-mediated DA constriction. This pathway involves DASMC mitochondria acting as redox sensors, producing reactive oxygen species (ROS) in proportion to PO₂, which serve as diffusible mediators that modulate the activity of several O₂-sensitive K⁺ channel^{6, 10}. Nonetheless, in both the DA and PA a rise in PO₂ increases mitochondrial derived H₂O₂ and yet in the DA K⁺ current is inhibited (with membrane depolarization and vasoconstriction) whilst in the PA the reverse is true. This points to a conserved sensor but a different ion channel-with opposing redox responses to a common stimulus^{7, 9, 52-58}. Before delving into the interaction of all three factors as a “functional oxygen-sensing unit”, the characteristics of each component will be examined.

5.3.2 Mitochondria as an oxygen sensor

The mitochondria's role as the predominant site for O₂ consumption and ATP synthesis makes it an obvious candidate site for an O₂ sensor. Indeed mitochondrial electron transport chain (ETC) inhibitors cause pulmonary vasoconstriction, DA

dilatation and carotid body activation, a set of response that mimics hypoxia with a precision not achieved by other stimuli ⁵⁹.

Proximal ETC inhibition targeting complex I (rotenone) or complex III (antimycin) inhibitors, but not distal ETC inhibition, using the complex IV inhibitor (cyanide), selectively inhibits O₂ constriction in the human DA and reverses O₂-induced inhibition of whole cell K⁺ current (I_K) in DASMCs⁶. Indeed, both rotenone and antimycin cause DA constriction, and their ability to inhibit O₂ constriction is additive, with the combination completely prevents O₂ constriction. In addition, the magnitude of DA constricts to O₂ predicts the magnitude of the dilators response to rotenone. These findings are a mirror image of those in the pulmonary circulation, where ETC inhibitors, also mimic hypoxia, causing pulmonary vasoconstriction⁶⁰⁻⁶³ and inhibition of I_K.

The O₂ sensing function of DASMC mitochondria is tied to the redox cascade within the ETC. Electrons from intramitochondrial reduced nicotinamide adenine dinucleotide (NADH) and flavin adenine dinucleotide (FADH₂), are transferred down a redox gradient, from NADH/NAD (-0.35mV) to O₂/H₂O (+0.82mV)⁵⁹. Four multicomponent megacomplexes accomplish the transfer of electrons. In the course of electron flux, a small amount of ROS (superoxide) is formed at complexes I and III and H⁺ ions are pumped across the inner mitochondrial membrane establishing the mitochondria's extremely negative membrane potential ($\Delta\Psi_m$). The superoxide is rapidly converted to H₂O₂ (serving as a signaling molecule) whilst the $\Delta\Psi_m$ provides the potential energy which is coupled to ATP synthesis by the mitochondrial ATP synthase⁶⁴. Terminal electron transfer to O₂ forms water. Thus there is a link between electron donors, electron flux and production of ROS. It appears that Complex I and III and

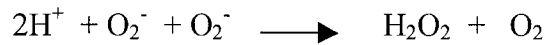
particularly important in O₂ sensing mechanisms because it is at these sites that ROS are generated^{65, 66}. The peroxides can then diffuse to the plasma membrane while it may be that superoxide anion can move through diisothiocyano-2,2 disulfonic acid stilbene (DIDS)-sensitive voltage sensitive anion channels, validating mitochondria as sources of cytosolic superoxide anion⁶⁷.

5.3.3 Reactive Oxygen Species (ROS) as a mediator of O₂-induced DA constriction

ROS from mitochondria and other cellular sources have been traditionally regarded as toxic by-products of metabolism with the potential to cause damage to lipids, proteins and DNA. To protect against the potentially damaging effects of ROS, cells possess several antioxidant enzymes such as superoxide dismutase (SOD; which reduces O₂⁻ to H₂O₂). These antioxidants are highly compartmentalized, with SOD2 being the key mitochondrial antioxidant that protects the ETC, converting superoxide anion to diffusible H₂O₂⁶⁸.

One of the primary ROS is O₂⁻. Superoxide itself can be toxic, especially through inactivation of proteins that contain Fe-S centers such as aconitase, succinate dehydrogenase and mitochondrial NADH-ubiquinone oxidoreductase⁶⁸. Fortunately, O₂⁻ in aqueous solution is short-lived. This instability in aqueous solution is based on rapid dismutation of O₂⁻ to H₂O₂, a reaction facilitated by higher concentrations of the protonated form of O₂⁻ (HO₂•) in more acidic pH conditions⁶⁸. Superoxide is also rapidly converted to peroxynitrite by interaction with nitric oxide (which is also present in the mitochondria)⁶⁸. Superoxide is also eliminated by enzymes that have been evolved with the task of detoxifying this particular species of ROS, collectively named the superoxide

dismutases. There are three of them in mammalian systems: a cytosolic CuZn superoxide (SOD1; CuZnSOD), an intramitochondrial manganese superoxide dismutase (SOD2; MnSOD) and extracellular CuZn superoxide dismutase (SOD3). Collectively, they catalyse the following reaction:



The dismutation reaction has an overall rate constant of $5 \times 10^5 \text{ M}^{-1} \text{ s}^{-1}$ at pH 7.0. SOD speeds up this reaction almost 10^4 fold (rate constant = $1.6 \times 10^9 \text{ M}^{-1} \text{ s}^{-1}$). Thus, although not as fast as the O_2^- interaction with NO^{68} , SOD, particularly SOD2 in the mitochondria, rapidly converts superoxide to a more stable, diffusible molecule H_2O_2 ^{69,70}.

Using chemiluminescence measurements with luminol for the detection of oxidative radicals, our laboratory showed significantly higher levels of ROS in normoxic, compared to hypoxic DA¹⁰. This increase in chemiluminescence was completely reversed by catalase¹⁰. Removal of endogenous H_2O_2 with intracellular catalase increased normoxic I_K and hyperpolarized membrane potential while extracellular t-butyl H_2O_2 decreased I_K and depolarized membrane potential. More rapid metabolism of O_2^- with CuZn superoxide dismutase had no significant effect on normoxic K^+ currents¹⁰, implying that extracellular superoxide was not the signaling molecule. Moreover, reducing agents such as *N*-Mercaptopropionylglycine (NMPG), duroquinone and dithiothreitol dilated normoxic-constricted DA rings, while the oxidizing agent 5,5'-dithiobis-(2-nitrobenzoic acid) constricted hypoxia-dilated rings⁷¹. In human DAs, H_2O_2 production increases as PO_2 rises and H_2O_2 inhibits I_K , causing membrane depolarization¹. Thus, increase in PO_2 at birth results in concomitant increase in H_2O_2 production in DASMC.

In this thesis we show that HOSK activity is reversibly inhibited by increasing PO₂ from the normal fetal levels (40mmHg) to levels seen postnatally (PO₂ ~100mmHg). Furthermore, H₂O₂ mimicked oxygen, indicating the parallel that exists between the HOSK channel and the response of endogenous K⁺ currents in the DA, reported in previous studies done in the laboratory. In addition, HOSK has been shown to contribute to the membrane potential of the DA (Figure 3e and 3f). This is evident in mutagenesis studies and studies involving anti-HOSK antibody and anti-HOSK siRNA treated hDASMC. Since, HOSK sets the membrane potential in hDASMC, it is plausible that HOSK is a major effector for oxygen-mediated DA closure during birth. Therefore, when oxygen is increased this is sensed by mitochondria that results in concomitant increase in ROS. This increased in ROS or H₂O₂ results in HOSK closure, which initiates a sequence of events culminating into DA constriction.

5.4 POTENTIAL PATHOLOGICAL RAMIFICATION OF HOSK

5.4.1 Speculation

This hypothesis is also particularly attractive because the transcript of HOSK exists transiently and its expression at the mRNA level is dynamically regulated by PO₂ (Figure 5a). Therefore, when an infant is born the alternative splice variant of COL1A2 (AS COL1A2) could be activated to produce HOSK. The DA physiological closure happens in a matter of minutes; perhaps subsequently, AS COL1A2 expression decreases and a rise in the full length COL1A2 produces collagen, which is essential for the

anatomical obliteration of DA lumen. Although this is speculative, it is probable that HOSK is an important contributor to DA closure.

5.4.2 Patent DA (PDA)

A common complication for very preterm (premature) infants is PDA (patent ductus arteriosus). A patent ductus arteriosus (PDA) complicates the clinical course of preterm infants, increasing their risks of developing chronic lung disease, necrotizing enterocolitis, and intraventricular hemorrhage and therefore, can lead to life-threatening complications⁷². The usual treatment for PDA is indomethacin, a drug that will successfully close the PDA in the majority of cases, but remains ineffective virtually 66% of times in infants born at 28 weeks gestation⁴². Current intervention of such cases is the surgical intervention.

Perhaps, one of the reasons for decreased oxygen-sensitivity in these infants is due to decreased expression and/or activity of HOSK (although we have not yet examined this possibility). Interventions that increase HOSK channel expression and/or activity might present itself as a new potential avenue of intervention.

5.5 STUDY LIMITATIONS AND FUTURE DIRECTIONS

One of the limitations of the study relates to the identification of the alternative transcript of COL1A2. Chapter 2 describes the role of AS COL1A2 as the template for HOSK. One way to identify the AS COL1A2 that we did not use was a probe specific to the exon A that differentiate between full length collagen transcript and its alternative form. Identification would have showed which of the two transcripts acts as a template

for HOSK. Perhaps *in vitro* translation and subsequent purification of protein and sequencing would have given the empirical evidence necessary for our claims. However, this might be one of the future projects to be done to substantiate that in fact AS COL1A2 does act as a template for the HOSK. Furthermore, this thesis was short on studies on looking at the regulation of HOSK at the transcriptional level. We found that oxygen has an inhibitory effect on the transcript. However, the mechanism behind the oxygen-mediated decrease in AS COL1A2 transcript remains to be elucidated.

Another area where the study is limited is in protein isolation. We synthesized HOSK-specific antibody with the use of putative pore of HOSK as the epitope. However, the antibody proved to be unsuccessful in immunoblotting. To further our initiative of isolating protein we synthesized a fusion protein of HOSK with myc tag. However, the myc antibody was not effective either. We were able to isolate the protein in SELDI-TOF and were able to perform “on-chip” tryptic digestion that resulted in spectrum, in agreement with HOSK *in silico* tryptic digestion fragments. Although we endeavored to isolate protein and perform amino acid sequencing, we were only able to have an indirect confirmation of amino acid sequence.

Furthermore, this thesis did not look at the voltage-sensing domain of the HOSK channel. Although the characteristics of amino acid sequence are in accordance with the previously established voltage-sensing domain of other Kv channels, this thesis lacks the protein sequence and crystallization data.

One area that requires further elucidation is the functional oxygen-sensing axis in DA. This thesis claims that perhaps HOSK is one of the effectors for O₂-mediated DA closure.

Furthermore, this thesis has used various computer-generated models to predict the functioning and regulation of the HOSK channel. Although, those claims are based on the programs which are governed by the rules predetermined by other channels or proteins, these claims by no means suggests that HOSK will act or be regulated in precisely that manner. For those studies, we have to conduct experiments to substantiate those claims. However, these computer-generated models do provide one with a fortified hypothesis and guidance to conduct experiments and realize if such functional characteristic or regulation does occur in the HOSK channel.

Finally, one of the limitations of this study is that we are claiming HOSK is a potassium channel. Earlier studies conducted on minK have shown that the initial claims of minK as a K⁺ channel were rejected later on⁷³. To this end, we have conducted these experiments with rigor to identify that in fact HOSK is a co-factor. We have progressively increased the dose of HOSK DNA in CHO cells and found a concomitant increase in the K⁺ current. In fact, this very protocol identified minK as a co-factor. Experiments with minK showed that the progressive increase in cDNA injections in *Xenopus* oocyte led to an increase in protein expression, however, the resultant current generated was plateau. Furthermore, we performed single-channel patch on heterologously expressed HOSK channel and showed that cocktail of oxygen-sensitive Kv channel antibody did not inhibited the K⁺ current. However, anti-HOSK antibody was able to completely abolish the channel opening probability in single-channel patch of HOSK transfected CHO cells. In addition, we knocked down HOSK in hDASMC and found with qRT-PCR that no changes in expression level were detected in various native oxygen-sensitive K⁺ channels. Despite of these experiments, it is possible, but unlikely,

that HOSK might be a cofactor and is acting in conjunction with another Kv channel. In this regards, we have ligated HOSK in protein synthesizing vector. Future studies might entail the use of this vector to synthesize and purify HOSK channels from mammalian cells and reconstitute the resulting protein in artificial lipid bilayer. If the create a “HOSK current” there would be no question that HOSK is a channel, not a co-factor or chaperone.

5.6 CONCLUSION

We have identified, isolated and characterized a new class of potassium channel hidden within the COL1A2 gene. HOSK derives from a collagen mRNA template that is transcribed out of frame. HOSK cDNA, isolated from human DA, corresponds to a 3.0 kb neuronal, expressed sequence tag (EST). Heterologously expressed HOSK creates a voltage-gated current that displays K^+ specificity ($Rb > K >> Cs > Na$) and is inhibited by 4-aminopyridine and the Kv1.x inhibitor, correolide. HOSK is active at the resting membrane potential of human DA smooth muscle cells (DASMC) and, consistent with its role in O_2 -sensing, the open-state probability of this 19pS channel is increased by hypoxia and decreased by oxygen or H_2O_2 . Anti-HOSK antibodies or HOSK siRNA inhibit human DASMC K^+ current, consistent with endogenous activity of HOSK. In silico modeling suggests that HOSK has four hydrophobic domains (HD) with a unique K^+ selectivity filter, established by GVL, rather than the typical GYG amino acid sequence. Its putative voltage-sensing domain lies within HD1, and is comprised of 2 arginine and 2 lysine residues, separated by 2 non-cationic amino acids. The voltage sensor of the HOSK channel differs from Kv channels in length and in the properties of

residues interspacing the cationic amino acids of the voltage sensor region. HOSK has an unusual coding mechanism. It is translated from an alternative open reading frame within the collagen $\alpha 2(I)$ mRNA transcript. Phylogenetic analysis indicates that HOSK is only present in amniotes. HOSK, hidden by its complex “gene within a gene” encoding mechanism and unique structure, is a novel K^+ channel, arising independent of the canonical K^+ channel family. If confirmed by crystallography, HOSK, with its 4 hydrophobic domain Kv channel and unusual pore sequence may be useful in further understanding the structural biology of ionic selectivity. Physiologically HOSK appears important to the initial functional closure of the DA.

5.7 REFERENCES

1. Archer, S. L. et al. O₂ sensing in the human ductus arteriosus: redox-sensitive K⁺ channels are regulated by mitochondria-derived hydrogen peroxide. *Biol Chem* 385, 205-16 (2004).
2. Michelakis, E. D. & Weir, E. K. The pathobiology of pulmonary hypertension. Smooth muscle cells and ion channels. *Clin Chest Med* 22, 419-32 (2001).
3. Bonnet, S. et al. NFAT regulates Kv1.5, a voltage-gated K⁺ channel which is downregulated in both human and animal pulmonary hypertension. (abstract). *Canadian Journal of Cardiology* 21, 57 (2005).
4. Remillard, C. V. & Yuan, J. X. Activation of K⁺ channels: an essential pathway in programmed cell death. *Am J Physiol Lung Cell Mol Physiol* 286, L49-67 (2004).
5. Weir, E. K., Lopez-Barneo, J., Buckler, K. J. & Archer, S. L. Acute oxygen-sensing mechanisms. *N Engl J Med* 353, 2042-55 (2005).
6. Thebaud, B. et al. Oxygen-sensitive Kv channel gene transfer confers oxygen responsiveness to preterm rabbit and remodeled human ductus arteriosus: implications for infants with patent ductus arteriosus. *Circulation* 110, 1372-9 (2004).
7. Archer, S. L. et al. Molecular identification of the role of voltage-gated K⁺ channels, Kv1.5 and Kv2.1, in hypoxic pulmonary vasoconstriction and control of resting membrane potential in rat pulmonary artery myocytes. *J Clin Invest* 101, 2319-30 (1998).

8. Coetzee, W. A. et al. Molecular diversity of K⁺ channels. *Ann N Y Acad Sci* 868, 233-85 (1999).
9. Archer, S. L. et al. Preferential expression and function of voltage-gated, O₂-sensitive K⁺ channels in resistance pulmonary arteries explains regional heterogeneity in hypoxic pulmonary vasoconstriction: ionic diversity in smooth muscle cells. *Circ Res* 95, 308-18 (2004).
10. Michelakis, E. D. et al. O₂ sensing in the human ductus arteriosus: regulation of voltage-gated K⁺ channels in smooth muscle cells by a mitochondrial redox sensor. *Circ Res* 91, 478-86 (2002).
11. Shealy, R. T., Murphy, A. D., Ramarathnam, R., Jakobsson, E. & Subramaniam, S. Sequence-function analysis of the K⁺-selective family of ion channels using a comprehensive alignment and the KcsA channel structure. *Biophys J* 84, 2929-42 (2003).
12. Heginbotham, L., Lu, Z., Abramson, T. & MacKinnon, R. Mutations in the K⁺ channel signature sequence. *Biophys J* 66, 1061-7 (1994).
13. Salinas, M. et al. Cloning of a new mouse two-P domain channel subunit and a human homologue with a unique pore structure. *J Biol Chem* 274, 11751-60 (1999).
14. Nelson, K. E. et al. Evidence for lateral gene transfer between Archaea and bacteria from genome sequence of *Thermotoga maritima*. *Nature* 399, 323-9 (1999).

15. Kawarabayasi, Y. et al. Complete genome sequence of an aerobic thermoacidophilic crenarchaeon, *Sulfolobus tokodaii* strain 7. *DNA Res* 8, 123-40 (2001).
16. She, Q. et al. The complete genome of the crenarchaeon *Sulfolobus solfataricus* P2. *Proc Natl Acad Sci U S A* 98, 7835-40 (2001).
17. Kuo, M. M., Haynes, W. J., Loukin, S. H., Kung, C. & Saimi, Y. Prokaryotic K(+) channels: from crystal structures to diversity. *FEMS Microbiol Rev* 29, 961-85 (2005).
18. Veeramachaneni, V., Makalowski, W., Galdzicki, M., Sood, R. & Makalowska, I. Mammalian overlapping genes: the comparative perspective. *Genome Res* 14, 280-6 (2004).
19. Scherer, S. W. et al. Human chromosome 7: DNA sequence and biology. *Science* 300, 767-72 (2003).
20. Bennett, V. D. & Adams, S. L. Characterization of the translational control mechanism preventing synthesis of alpha 2(I) collagen in chicken vertebral chondroblasts. *J Biol Chem* 262, 14806-14 (1987).
21. Bennett, V. D. & Adams, S. L. Identification of a cartilage-specific promoter within intron 2 of the chick alpha 2(I) collagen gene. *J Biol Chem* 265, 2223-30 (1990).
22. Pallante, K. M. et al. The chick alpha2(I) collagen gene contains two functional promoters, and its expression in chondrocytes is regulated at both transcriptional and post-transcriptional levels. *J Biol Chem* 271, 25233-9 (1996).

23. Antoniv, T. T. et al. Identification of a repressor in the first intron of the human alpha2(I) collagen gene (COL1A2). *J Biol Chem* 280, 35417-23 (2005).
24. Chappell, S. A., Edelman, G. M. & Mauro, V. P. Biochemical and functional analysis of a 9-nt RNA sequence that affects translation efficiency in eukaryotic cells. *Proc Natl Acad Sci U S A* 101, 9590-4 (2004).
25. Nah, H. D., Bennett, V. D., Niu, Z. & Adams, S. I. Alternative transcript of the chick alpha 2(I) collagen gene is transiently expressed during endochondral bone formation and during development of the central nervous system. *Dev Dyn* 206, 146-58 (1996).
26. Armstrong, C. M. & Hille, B. Voltage-gated ion channels and electrical excitability. *Neuron* 20, 371-80 (1998).
27. Roux, B. & MacKinnon, R. The cavity and pore helices in the KcsA K⁺ channel: electrostatic stabilization of monovalent cations. *Science* 285, 100-2 (1999).
28. MacKinnon, R. Potassium channels. *FEBS Lett* 555, 62-5 (2003).
29. Aggarwal, S. K. & MacKinnon, R. Contribution of the S4 segment to gating charge in the Shaker K⁺ channel. *Neuron* 16, 1169-77 (1996).
30. Schoppa, N. E., McCormack, K., Tanouye, M. A. & Sigworth, F. J. The size of gating charge in wild-type and mutant Shaker potassium channels. *Science* 255, 1712-5 (1992).
31. Seoh, S. A., Sigg, D., Papazian, D. M. & Bezanilla, F. Voltage-sensing residues in the S2 and S4 segments of the Shaker K⁺ channel. *Neuron* 16, 1159-67 (1996).
32. Starace, D. M. & Bezanilla, F. Histidine scanning mutagenesis of basic residues of the S4 segment of the shaker k⁺ channel. *J Gen Physiol* 117, 469-90 (2001).

33. Starace, D. M., Stefani, E. & Bezanilla, F. Voltage-dependent proton transport by the voltage sensor of the Shaker K⁺ channel. *Neuron* 19, 1319-27 (1997).
34. Li-Smerin, Y., Hackos, D. H. & Swartz, K. J. A localized interaction surface for voltage-sensing domains on the pore domain of a K⁺ channel. *Neuron* 25, 411-23 (2000).
35. Schonherr, R., Mannuzzu, L. M., Isacoff, E. Y. & Heinemann, S. H. Conformational switch between slow and fast gating modes: allosteric regulation of voltage sensor mobility in the EAG K⁺ channel. *Neuron* 35, 935-49 (2002).
36. Ahern, C. A. & Horn, R. Stirring up controversy with a voltage sensor paddle. *Trends Neurosci* 27, 303-7 (2004).
37. Hanner, M. et al. Binding of correolide to the K(v)1.3 potassium channel: characterization of the binding domain by site-directed mutagenesis. *Biochemistry* 40, 11687-97. (2001).
38. Hanner, M. et al. Binding of correolide to K(v)1 family potassium channels. Mapping the domains of high affinity interaction. *J Biol Chem* 274, 25237-44. (1999).
39. Ketchum, K. A., Joiner, W. J., Sellers, A. J., Kaczmarek, L. K. & Goldstein, S. A. A new family of outwardly rectifying potassium channel proteins with two pore domains in tandem. *Nature* 376, 690-5 (1995).
40. Lesage, F. & Lazdunski, M. Molecular and functional properties of two-pore-domain potassium channels. *Am J Physiol Renal Physiol* 279, F793-801 (2000).
41. Moudgil, R., Michelakis, E. D. & Archer, S. L. Hypoxic pulmonary vasoconstriction. *J Appl Physiol* 98, 390-403 (2005).

42. Casalaz, D. Ibuprofen versus indomethacin for closure of patent ductus arteriosus. *N Engl J Med* 344, 457-8. (2001).
43. Coceani, F. & Olley, P. M. The response of the ductus arteriosus to prostaglandins. *Can. J. Physiol.* 51, 220-223 (1973).
44. Heymann, M. A., Rudolph, A. M. & Silverman, N. H. Closure of the ductus arteriosus in premature infants by inhibition of prostaglandin synthesis. *N. Engl. J. Med.* 295, 530-533 (1976).
45. Momma, K. & Toyono, M. The role of nitric oxide in dilating the fetal ductus arteriosus in rats. *Pediatr Res* 46, 311-5 (1999).
46. Coceani, F., Ackerley, C., Seidlitz, E. & Kelsey, L. Function of cyclo-oxygenase-1 and cyclo-oxygenase-2 in the ductus arteriosus from foetal lamb: differential development and change by oxygen and endotoxin. *Br J Pharmacol* 132, 241-51. (2001).
47. De Carolis, M. P. et al. Prophylactic ibuprofen therapy of patent ductus arteriosus in preterm infants. *Eur J Pediatr* 159, 364-8 (2000).
48. Coceani, F., Armstrong, C. & Kelsey, L. Endothelin is a potent constrictor of the lamb ductus arteriosus. *Can J Physiol Pharmacol* 67, 902-4 (1989).
49. Coceani, F. & Kelsey, L. Endothelin-1 release from the lamb ductus arteriosus: are carbon monoxide and nitric oxide regulatory agents? *Life Sci* 66, 2613-23. (2000).
50. Coceani, F., Kelsey, L. & Seidlitz, E. Occurrence of endothelium-derived relaxing factor-nitric oxide in the lamb ductus arteriosus. *Can. J. Physiol. Pharmacol.* 72, 82-88 (1994).

51. Coceani, F. et al. Endothelin A receptor is necessary for O₂ constriction but not closure of ductus arteriosus. *Am J Physiol* 277, H1521-31 (1999).
52. Yuan, X.-J., Goldman, W., Tod, M., Rubin, L. & Blaustein, M. Ionic currents in rat pulmonary and mesenteric arterial myocytes in primary culture and subculture. *Am J Physiol* 264, L107-L115 (1993).
53. Yuan, X. J., Wang, J., Juhaszova, M., Golovina, V. A. & Rubin, L. J. Molecular basis and function of voltage-gated K⁺ channels in pulmonary arterial smooth muscle cells. *Am J Physiol* 274, L621-35 (1998).
54. Aaronson, P. I. Hypoxic pulmonary vasoconstriction is/is not mediated by increased production of reactive oxygen species. *J Appl Physiol* 101, 1000; author reply 1004-5 (2006).
55. Ward, J. P. Last Word: Point:Counterpoint authors respond to commentaries on "Hypoxic pulmonary vasoconstriction is/is not mediated by increased production of reactive oxygen species". *J Appl Physiol* 101, 1004 (2006).
56. Ward, J. P. Point: Hypoxic pulmonary vasoconstriction is mediated by increased production of reactive oxygen species. *J Appl Physiol* 101, 993-5; discussion 999 (2006).
57. Weir, E. K. & Archer, S. L. Counterpoint: Hypoxic pulmonary vasoconstriction is not mediated by increased production of reactive oxygen species. *J Appl Physiol* 101, 995-8; discussion 998 (2006).
58. Weir, E. K. & Archer, S. L. Last Word: Point:Counterpoint authors respond to commentaries on "Hypoxic pulmonary vasoconstriction is/is not mediated by

- increased production of reactive oxygen species". *J Appl Physiol* 101, 1005 (2006).
59. Archer, S. & Michelakis, E. The mechanism(s) of hypoxic pulmonary vasoconstriction: potassium channels, redox O₂ sensors, and controversies. *News Physiol Sci* 17, 131-7 (2002).
 60. Waypa, G. B. & Schumacker, P. T. Hypoxic pulmonary vasoconstriction: redox events in oxygen sensing. *J Appl Physiol* 98, 404-14 (2005).
 61. Waypa, G. B. & Schumacker, P. T. O₂ sensing in hypoxic pulmonary vasoconstriction: the mitochondrial door re-opens. *Respir Physiol Neurobiol* 132, 81-91 (2002).
 62. McMurtry, I., Stanbrook, B. & Rounds, S. Studies of the mechanisms of hypoxic pulmonary vasoconstriction. *Advances Shock Res.* 8, 21-23 (1981).
 63. Michelakis, E. D. et al. Diversity in mitochondrial function explains differences in vascular oxygen sensing. *Circ Res* 90, 1307-15 (2002).
 64. Devin, A. & Rigoulet, M. Mechanisms of mitochondrial response to variations in energy demand in eukaryotic cells. *Am J Physiol Cell Physiol* (2006).
 65. Barja, G. Mitochondrial oxygen radical generation and leak: sites of production in states 4 and 3, organ specificity, and relation to aging and longevity. *J Bioenerg Biomembr* 31, 347-66 (1999).
 66. Archer, S. L., Huang, J., Henry, T., Peterson, D. & Weir, E. K. A redox-based O₂ sensor in rat pulmonary vasculature. *Circ Res* 73, 1100-12 (1993).

67. Han, D., Antunes, F., Canali, R., Rettori, D. & Cadenas, E. Voltage-dependent anion channels control the release of superoxide anion from mitochondria to cytosol. *J Biol Chem* (2002).
68. Fridovitch, I. Superoxide and superoxide dismutase. *Annu Rev Biochem* 64, 97-112 (1995).
69. Burke, T. & Wolin, M. Hydrogen peroxide elicits pulmonary arterial relaxation and guanylate cyclase activation. *Am. J. Physiol.* 252, H721-H732 (1987).
70. Wolin, M. S. Interactions of oxidants with vascular signaling systems. *Arterioscler Thromb Vasc Biol* 20, 1430-42. (2000).
71. Reeve, H. L., Tolarova, S., Nelson, D. P., Archer, S. & Weir, E. K. Redox control of oxygen sensing in the rabbit ductus arteriosus. *J Physiol* 533, 253-61 (2001).
72. Shah, S. S. & Ohlsson, A. Ibuprofen for the prevention of patent ductus arteriosus in preterm and/or low birth weight infants. *Cochrane Database Syst Rev*, CD004213 (2006).
73. Kaczmarek, L. K. & Blumenthal, E. M. Properties and regulation of the minK potassium channel protein. *Physiol Rev* 77, 627-41 (1997).

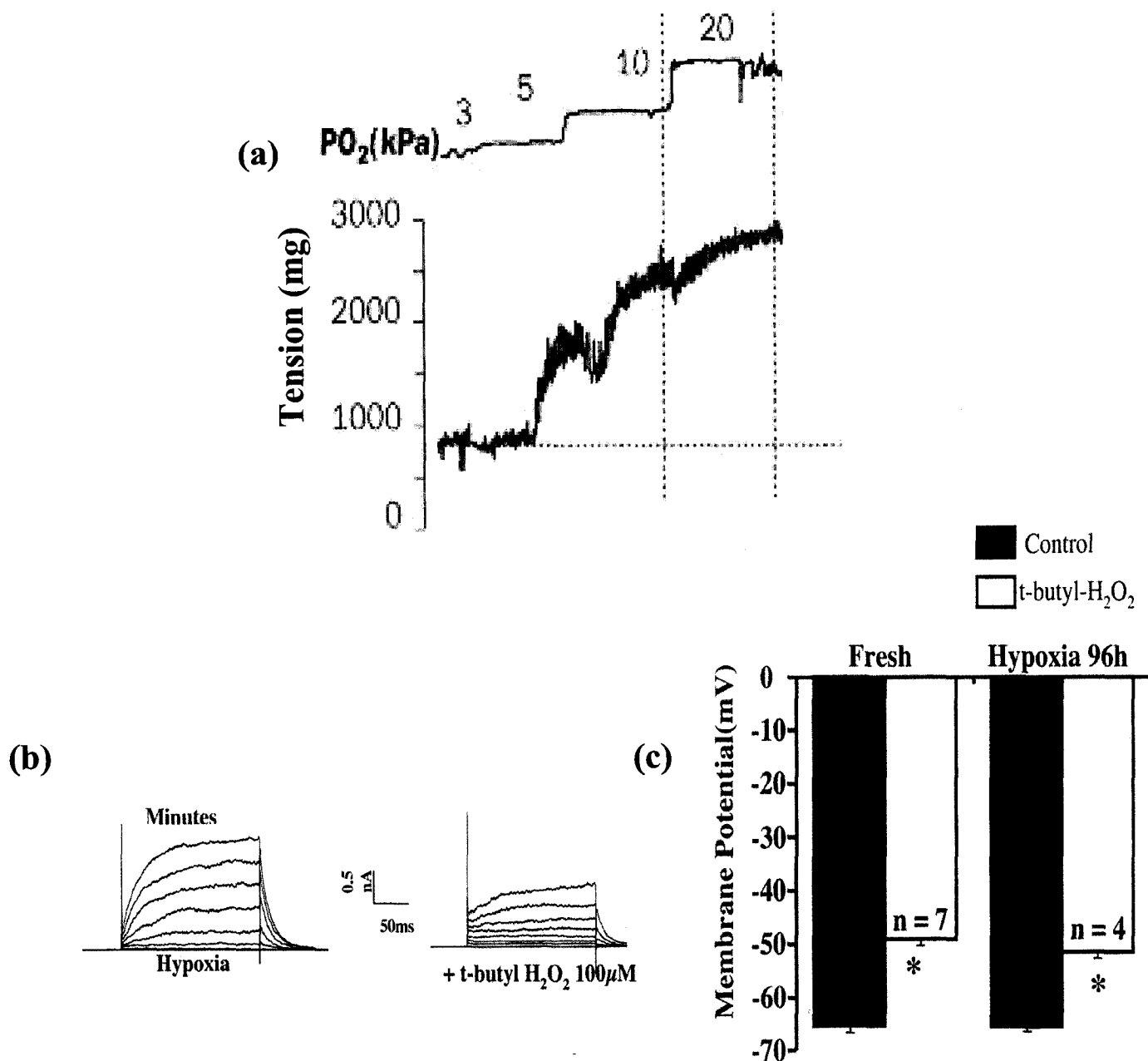


Figure 5.1: (a) Human ductus arteriosus constricts with increasing amount of oxygen. (b) Oxygen effect is mimicked by hydrogen peroxide (H₂O₂). (c) Increase in H₂O₂ concentration results in membrane depolarization that will lead to vasoconstriction via L-type calcium channels. This response is preserved even after 96h. (Adapted from ref 15)

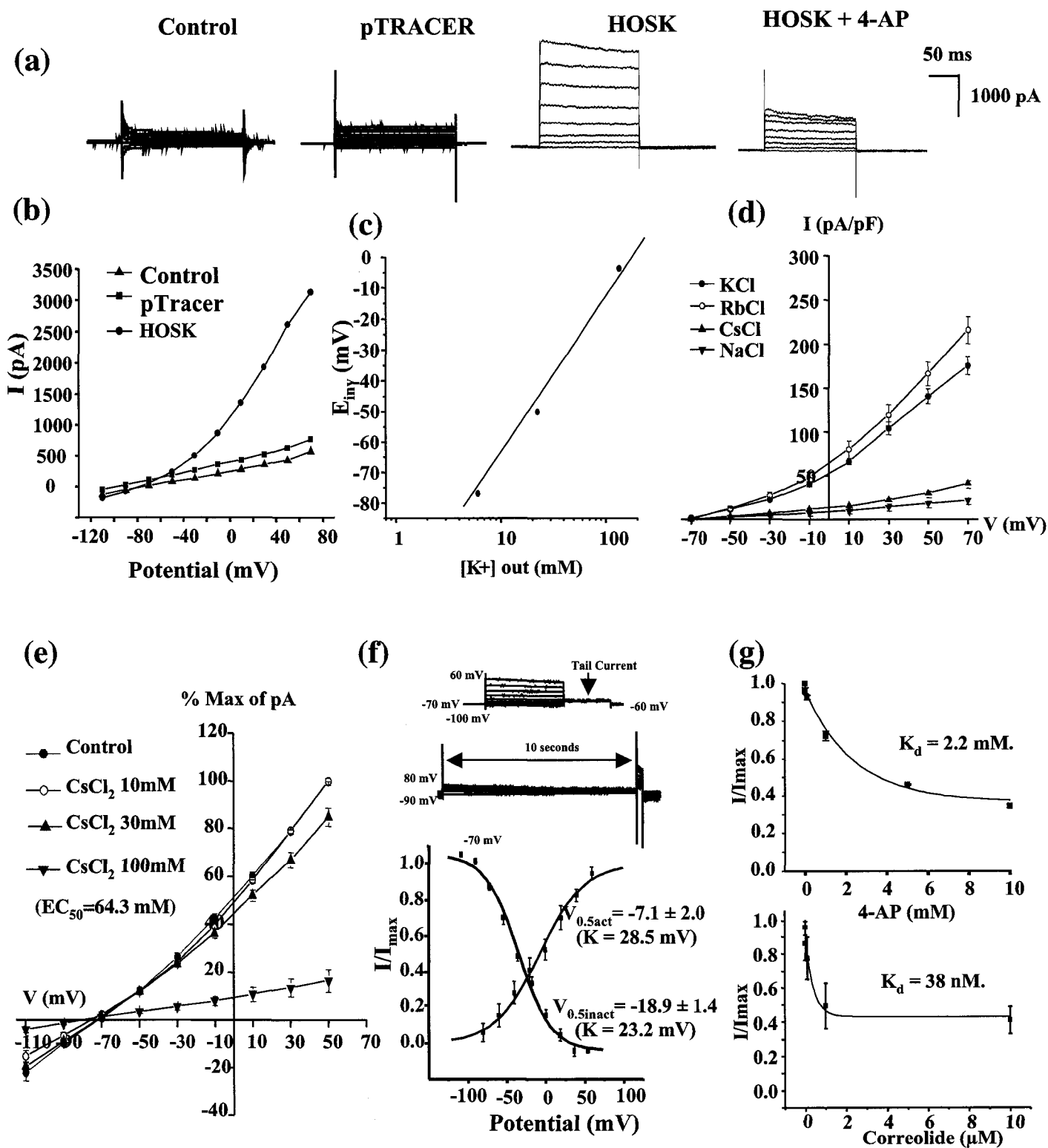


Figure 5.2: (a & b) Representative traces and mean \pm SEM current-voltage (I-V) plots showing that HOSK-transfection produces a voltage-dependent, 4-AP-inhibited current in CHO cells which otherwise have an ohmic current. (c) Equilibrium potential approaches zero in symmetrical K^+ (d) Ionic selectivity of HOSK is $Rb > K >> Cs > Na$. (e) Dose-dependent inhibition of HOSK current by extracellular cesium. (f) Voltage-sensitive activation and inactivation of HOSK channel (inset shows protocol) (g) Inhibition of HOSK by the Kv blocker 4-AP and Kv1.x specific inhibitor correolide.

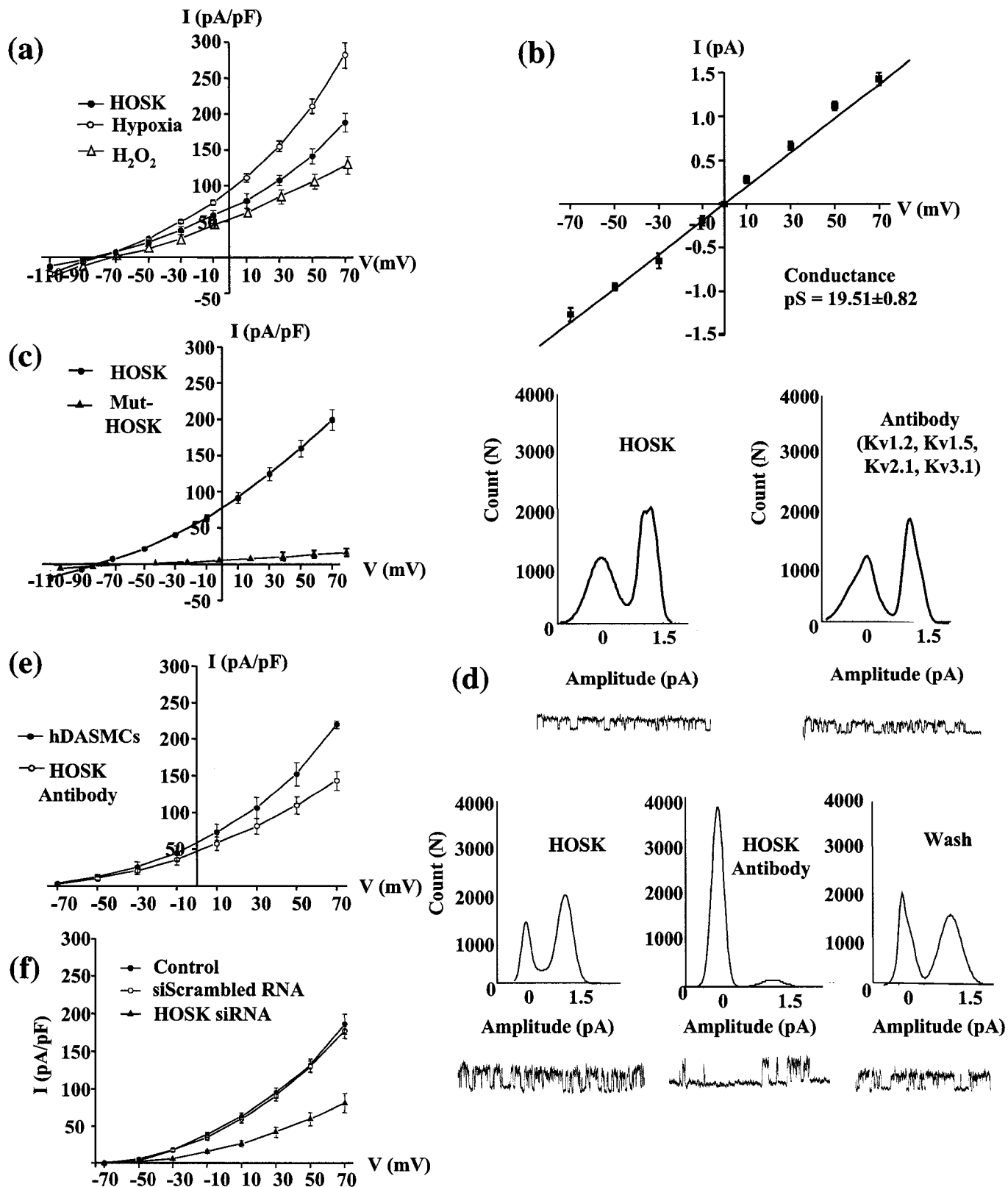


Figure 5.3:(a) HOSK current is activated by hypoxia and inhibited by H₂O₂. (b) Single channel conductance of HOSK is 19.5 pS. (c) Mutagenesis of the HOSK pore eliminates the voltage-dependent current. (d) Immunoelectropharmacology suggest that HOSK openings (at 1.5 pA amplitude) are unaffected by a cocktail of Kv antibodies (upper portion of panel) but are reversibly inhibited by anti-HOSK antibody. (e) Anti-HOSK antibody inhibit whole-cell current in human DASMCS. (f) HOSK siRNA attenuates whole-cell K⁺ current in hypoxic human DASMCS.